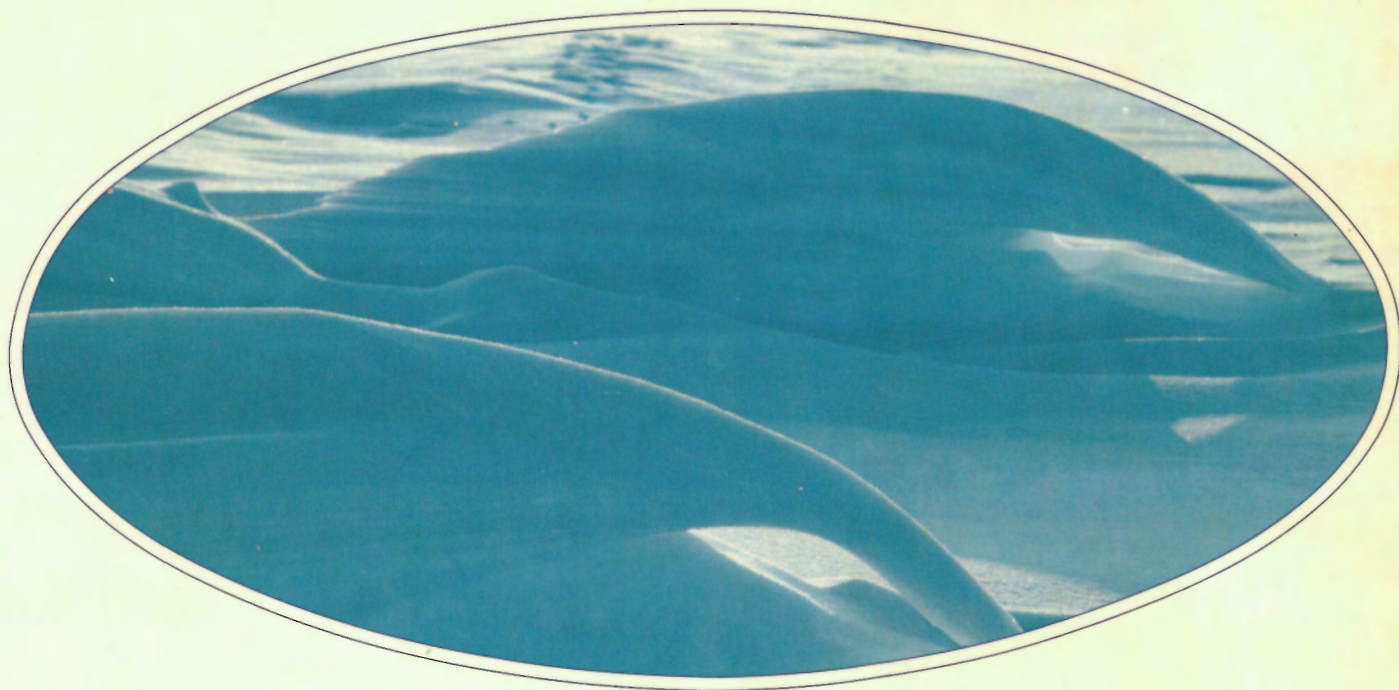


---

# Initial Geological Report on CESAR

---



This document was produced  
by scanning the original publication.

Ce document est le produit d'une  
numérisation par balayage  
de la publication originale.

---

## The Canadian Expedition to Study the Alpha Ridge, Arctic Ocean

---

Geological Survey of Canada  
Commission géologique du Canada  
Paper 84-22

INITIAL GEOLOGICAL REPORT ON CESAR —  
THE CANADIAN EXPEDITION TO STUDY  
THE ALPHA RIDGE, ARCTIC OCEAN

edited by

H.R. Jackson, P.J. Mudie and S.M. Blasco

1985





© Minister of Supply and Services Canada 1985

Available in Canada through

authorized bookstore agents and other bookstores

or by mail from

Canadian Government Publishing Centre  
Supply and Services Canada  
Ottawa, Canada K1A 0S9

and from

Geological Survey of Canada offices:

601 Booth Street  
Ottawa, Canada K1A 0E8

3303-33rd Street N.W.,  
Calgary, Alberta T2L 2A7

100 West Pender Street  
Vancouver, British Columbia V6R 1R3  
(mainly B.C. and Yukon)

A deposit copy of this publication is also available  
for reference in public libraries across Canada

Cat. No. M44-84/22E	Canada: 18.85
ISBN 0-660-11807-6	Other Countries: 22.60

Price subject to change without notice

**Scientific Editor**

W.C. Morgan

**Design and layout**

M.J. Kiel

# CONTENTS

1	Introduction
3	Summary/Sommaire <i>P.J. Mudie and H.R. Jackson</i>
11	Knowledge of the Alpha Ridge prior to CESAR <i>H.R. Jackson</i>
15	CESAR bathymetry <i>J.R. Weber and H.R. Jackson</i>
19	Seismic reflection results from CESAR <i>H.R. Jackson</i>
25	Bottom photography and sediment analyses on CESAR <i>C.L. Amos</i>
47	Petrology and geochemistry of a CESAR bedrock sample: implications for the origin of the Alpha Ridge <i>N.A. Van Wagoner and P.T. Robinson</i>
59	Lithostratigraphy of the CESAR cores <i>P.J. Mudie and S.M. Blasco</i>
101	Paleomagnetic stratigraphy of the CESAR cores <i>A.E. Aksu</i>
115	Planktonic foraminiferal and oxygen isotopic stratigraphy of CESAR cores 102 and 103: preliminary results <i>A.E. Aksu</i>
125	Correlation of Late Cretaceous Arctic silicoflagellates from Alpha Ridge <i>D. Bukry</i>
137	Diatom biostratigraphy of the CESAR 6 core, Alpha Ridge <i>J.A. Barron</i>
149	Palynology of the CESAR cores, Alpha Ridge <i>P.J. Mudie</i>
175	Piston coring on CESAR <i>F. Jodrey and D. Heffler</i>





## Introduction

This volume describes geological material obtained on the Canadian Expedition to Study the Alpha Ridge, abbreviated as CESAR. The Alpha Ridge is one of the Arctic Ocean's major features, and is particularly interesting to Canadians because it terminates on the North American side of the ocean off the continental shelf northwest of Ellesmere Island. The ridge takes its name from Ice Station Alpha, which drifted over it. This ice station was one of the two scientific camps in the Arctic established by the U.S. Air Force, in its project Skate, as a contribution to the Arctic Ocean Study Program of the International Geophysical Year of 1957-1958. Alpha Ridge was known before this from observations made during the drift of the U.S.S.R. Ice Station NP-4, and from soundings made by the High Latitude Aerial Expeditions of the U.S.S.R.

Good ideas come from individuals, not bureaucracies. J.R. Weber, J.F. Sweeney and A.S. Judge of the Earth Physics Branch proposed the expedition to celebrate the centenary of the First International Polar Year of 1882-1883. Good ideas also get followers. Eventually on the ice, staff congregated from a whole host of organizations: Earth Physics Branch, Geological Survey of Canada (Atlantic Geoscience Centre and Resource Geophysics and Geochemistry Division), Canadian Hydrographic Service, Atlantic Oceanographic Laboratory, Marine Ecology Laboratory; Universities — Dalhousie, Washington, Miami, Columbia (Lamont-Doherty), and Wisconsin. The logistics support was provided by the Polar Continental Shelf Project and the Department of National Defence.

Ice camp CESAR was established on the drifting sea ice and from it a variety of experiments were conducted from 31 March and 23 May (day 90 to 143) of 1983. This report is concerned with the experiments and observations relating to the geology, bathymetry, seismic reflection, bedrock, and sediment samples collected from the ice camp. The principal goal of the sampling programs was to collect data to improve the knowledge and understanding of the Alpha Ridge. Core material that provided constraints on the origin and the history of the ridge would be used for this. If the samples were not destroyed while recovering this information, or if insufficient material was available, it would be used to clarify questions on the sedimentary history and paleoenvironment of the Arctic Ocean. To enable the achievement of these goals a piston coring facility was erected at the main camp and gravity cores were collected at the main camp and at two remote camp sites.

## Introduction

Le présent volume décrit les matériaux géologiques prélevés au cours de l'expédition canadienne d'étude de la dorsale Alpha (CESAR). Dans l'océan Arctique, un accident important, la dorsale Alpha, intéresse tout particulièrement les Canadiens puisqu'il aboutit sur le côté nord américain de l'océan, au large du plateau continental gisant au nord-ouest de l'île Ellesmere. La dorsale tire son nom de la station sur glace Alpha, qui l'a complètement franchie. Établie sur la glace en dérive, la station Alpha était l'une des deux stations scientifiques installées dans l'Arctique par la U.S. Air Force dans le cadre du projet Skate, à titre de contribution au Programme d'étude de l'océan Arctique pour l'Année géophysique internationale de 1957-1958. Cette dorsale avait déjà été découverte grâce à des observations effectuées par des chercheurs russes lors de la dérive de leur station sur glace NP-4 et à des sondages effectués par l'URSS lors d'expéditions aériennes à haute latitude.

À l'origine d'un projet, il y a des individus tels MM. J.R. Weber, J.F. Sweeney et A.S. Judge de la Direction de la physique du globe. Ils ont en effet proposé de faire une expédition pour fêter le centenaire de la Première Année polaire internationale de 1882-1883. Il y a toujours des partisans pour les bons projets. Au bout de quelque temps, l'expédition a regroupé sur la glace du personnel provenant d'une foule d'organismes: la Direction de la physique du globe, la Commission géologique du Canada (Centre géoscientifique de l'Atlantique et Division de la géophysique et de la géochimie appliquées), le Service hydrographique du Canada, le Laboratoire océanographique de l'Atlantique, le Laboratoire d'écologie marine; les universités de Dalhousie, de Washington, de Miami, de Columbia (Lamont-Doherty) et du Wisconsin. Le personnel de l'Étude du plateau continental polaire et le ministère de la Défense nationale ont fourni le soutien logistique.

Diverses expériences ont été effectuées du 31 mars au 23 mai (jour 90 à 143) 1983 à partir du camp CESAR, établi sur la glace de mer en dérive. Le présent rapport traite des expériences et des observations portant sur la géologie, la bathymétrie, la sismique réflexion, le socle rocheux et les échantillons sédimentaires prélevés à partir du camp. Les programmes d'échantillonnage avaient comme objectif principal de recueillir des données en vue de contribuer à une meilleure connaissance de la dorsale Alpha. Les carottes qui fournissaient des renseignements sur l'origine et l'histoire de la dorsale devaient d'abord servir à cette fin. Si les échantillons n'étaient pas détruits lors de la récupération de ces données ou si le matériel était insuffisant, les carottes seraient utilisées pour expliquer l'histoire de la sédimentation et le paléoenvironnement de l'océan Arctique. Pour réaliser ces objectifs, une carotteuse à piston a été installée au camp principal et des carottes ont été prélevées au moyen de carotteuses à chute libre au camp principal et à deux camps éloignés.

The offshore Arctic Ocean is probably the least well explored of the global marine environments because of the difficulty of access by ship due to permanent ice. Consequently, the geological samples obtained represent a unique and irreplaceable source of data. Many different studies of the samples were undertaken and the results are described in this report as papers written by various authors. The authors have had little opportunity to exchange information on their findings because we wanted to make the data public quickly.

We aim here, to present accurate descriptions of the cores and other geological samples so that the original field and laboratory data are easily available to others. Differences in interpretation between authors of papers in this volume will be found, and no attempt has been made to try to reconcile these differences. We hope that the disagreements in interpretation will stimulate dialogues that shed more insight on the scientific problems regarding the geological origin and paleo-ecological history of the Arctic Ocean.

All the papers presented here were reviewed by J.S. Bell, G.L. Johnson and D.J.W. Piper. Individual papers were reviewed by I. Reid, G.P. Piper, D. Buckley, E. Irving, J. Hall, C. Isaacs, W. Berger, A. Sautar, P.J. Mudie, H.R. Jackson, P.J. Quinterma and J.A. Barron. To them all, many thanks.

On behalf of the Atlantic Geoscience Centre, we want to end by acknowledging the enormous help of the participants; our own and other technical staff, on and off the ice, and in particular the staff of the Polar Continental Shelf Project and the staff of the Earth Physics Branch. The work described in this report could not have been done without them. The success that CESAR was, should make them feel very proud.

*M.J. Keen and H.R. Jackson*  
Geological Survey of Canada

La partie littorale de l'océan Arctique est sans doute le milieu marin global le moins bien exploré étant donné la difficulté d'y accéder par navire ou par une voie sur la glace permanente. Par conséquent, les échantillons géologiques prélevés représentent une source unique et irremplaçable de données. Maintes études différentes des échantillons ont été faites et les résultats sont présentées ici sous forme de rapports rédigés par divers auteurs. Ces derniers n'ont eu que très peu l'occasion de se consulter au sujet des résultats puisque nous cherchions à publier les données le plus tôt possible.

Dans le présent document, les auteurs tenteront de décrire avec précision les carottes et autres échantillons géologiques afin de mettre à la disposition des intéressés les données originales provenant du terrain et du laboratoire. Les interprétations peuvent varier d'un auteur à l'autre et aucune tentative n'a été faite pour reconcilier ces différences. Nous espérons que les différences d'interprétations encourageront des échanges qui éclaireront davantage les questions scientifiques ayant trait à l'origine géologique et à l'histoire paléoécologique de l'océan Arctique.

Tous les rapports présentés ici ont été relus par MM. J.S. Bell, G.L. Johnson et D.J.W. Piper. Les rapports individuels ont été relus par MM. I. Reid, G.P. Piper, D. Buckley, E. Irving, J. Hall, C. Isaacs, W. Berger, A. Sautar, P.J. Mudie, H.R. Jackson, P.J. Quinterma et J.A. Barron. Grand merci à tous.

Au nom du Centre géoscientifique de l'Atlantique, nous désirons souligner l'aide considérable que nous avons reçue des participants: tous les employés techniques qui ont travaillé sur la glace et au laboratoire, et notamment le personnel de l'Étude du plateau continental polaire et de la Direction de la physique du globe. La réalisation des travaux décrits dans le présent rapport n'auraient pu se faire sans leur collaboration. Ils devraient être très fiers du succès de CESAR.

*M.J. Keen et H.R. Jackson*  
Commission géologique du Canada

## SUMMARY/SOMMAIRE

P.J. Mudie<sup>1</sup> and H.R. Jackson<sup>1</sup>  
Geological Survey of Canada

*Mudie, P.J. and Jackson, H.R., Summary/Sommaire; in Initial Geological Report on CESAR — the Canadian Expedition to Study the Alpha Ridge, Arctic Ocean, ed. H.R. Jackson, P.J. Mudie and S.M. Blasco; Geological Survey of Canada, Paper 84-22, p. 3-10, 1985.*

The geological origin and age of the Alpha Ridge and its sedimentary cover have long been the subject of controversy regarding the tectonic evolution of the Arctic Ocean and its paleoenvironmental history. This volume describes sediment cores, bedrock samples and related geological and geophysical data obtained during CESAR, the Canadian Expedition to Study the Alpha Ridge. The geological aims of CESAR were to collect data which would elucidate the following scientific problems.

- 1) The tectonic origin and age of the Alpha Ridge.
- 2) The lithostratigraphy and depositional history of the overlying sediments.
- 3) The paleoceanographic and paleoclimatic evolution of the Arctic Ocean.

Paper 1 summarizes the history of geological and geophysical data collected from the Alpha Ridge prior to CESAR. It has been shown that the Alpha Ridge is a major magnetic feature on a global scale, but the irregular magnetic anomaly patterns and heat flow values are not typical of an ocean crustal spreading centre. Gravity, magnetics and bathymetric data also indicate that the Alpha Ridge is not connected to the Canadian continental shelf, and the ridge is therefore not likely to be founded on continental crust. Seismic reflection data show that basement topography is mountainous with traces of normal faults extending to the surface, indicating that the ridge is under tension. Prior to CESAR, limited seismic refraction data revealed a sedimentary layer of 0.3-0.5 km thickness overlying a layer 2.8 km thick and a deeper layer of undetermined thickness. From 1957 to 1979, approximately 700 sediment cores, up to 5.5 m long, were collected from the Arctic Ocean, but only 3 of these penetrated pre-Neogene sediments. These three cores were from the southern part of the Alpha Ridge. One of the cores contained biosiliceous ooze, which provided a minimum Late Cretaceous age for the ridge and suggested an ice-free, nutrient-rich, warm Mesozoic Arctic Ocean environment.

Paper 2 records the detailed bathymetry (100 m contour intervals) of the Alpha Ridge in the region covered during CESAR (85°15'-86°00'N; 115°00'-105°00'W). The CESAR ice camp drifted over two ridge crests separated by a large, steep-sided valley referred to as a graben by J.K. Hall in 1970. The bottom

L'origine géologique et l'âge de la dorsale Alpha et de sa couverture sédimentaire sont depuis longtemps sujets d'une vive controverse à l'égard de l'évolution tectonique de l'océan Arctique et de son histoire paléoenvironnementale. Le présent document décrit les carottes sédimentaires, les échantillons rocheux et les données géologiques et géophysiques connexes obtenues au cours de l'expédition canadienne d'étude de la dorsale Alpha (CESAR). Cette expédition avait pour objectif géologique de prélever des données susceptibles d'élucider les problèmes scientifiques suivants:

- 1) l'origine tectonique et l'âge de la dorsale Alpha;
- 2) la lithostratigraphie et l'histoire sédimentaire des matériaux sus-jacents;
- 3) l'évolution paléocéanographique et paléoclimatique de l'océan Arctique.

La première contribution résume l'histoire des données géologiques et géophysiques sur la dorsale Alpha qui avaient été obtenues avant l'expédition. Les recherches ont démontré que la dorsale est un accident magnétique majeur à l'échelle globale, mais les motifs irréguliers des anomalies magnétiques ainsi que les valeurs du flux thermique ne sont pas typiques d'un centre d'expansion de la croûte océanique. Les données gravimétriques, magnétiques et bathymétriques indiquent également que cette dorsale n'est pas reliée au plateau continental canadien et donc ne se compose vraisemblablement pas de croûte continentale sombrée. Quant aux données recueillies par sismique réflexion, elles révèlent une topographie du socle montagneuse que caractérise des traces de failles normales se prolongeant jusqu'à la surface; la présence de ces failles indique qu'une tension s'exerce présentement sur la dorsale. Avant l'expédition, des données limitées de sismique réfraction avaient révélé la présence d'une couche sédimentaire de 0,3 à 0,5 km d'épaisseur recouvrant une couche de 2,8 km d'épaisseur, ainsi qu'une couche plus profonde d'épaisseur inconnue. Environ 700 carottes de sédiments d'une longueur maximale de 5,5 m ont été prélevées du fond de l'océan Arctique entre 1957 et 1979. Parmi les carottes prélevées dans la partie sud de la dorsale Alpha trois seulement avaient pénétré des sédiments pré-Néogène. Une des carottes contenait de la boue siliceuse organogène, matériau à l'aide duquel on a pu établir que la dorsale date au moins du Crétacé récent et que les eaux chaudes de l'océan Arctique mésozoïque étaient libre de glace et riche en éléments nutritifs.

La deuxième étude présente la bathymétrie détaillée (équidistance de 100 m) de la dorsale Alpha dans la région étudiée au cours de l'expédition CESAR (85°15'-86°00'N; 115°00'-105°00'O). Le camp de l'expédition, établi sur la glace flottante, avait dérivé au-

<sup>1</sup>Atlantic Geoscience Centre, Bedford Institute of Oceanography, Box 1006, Dartmouth, Nova Scotia B2Y 4A2



topography of the Alpha Ridge generally ranges from 2536 to 1087m, but many smaller-scale peaks and valleys dissect the ridges and valley slopes. For the purpose of consistent reference in this report, informal geographical names have been assigned to the major ridge axes and the graben-like valley. The northern and southern ridge belts are called the northern Alpha Ridge crest and the southern Alpha Ridge crest, respectively; the intervening major valley is referred to as the Alpha Ridge graben.

Paper 3 describes the seismic reflection data obtained during CESAR which provide the first relatively high-resolution acoustic-stratigraphic record of the sedimentary environments from which Alpha Ridge cores and dredge samples were obtained. The CESAR seismic reflection records show that the sediment cover on the ridges is layered and is mostly flat-lying or conformable to basement structures. Sediment thickness varies from ca. 0.2-0.5s on the ridges. A thicker sequence of less regularly bedded sediments occurs in the Alpha Ridge graben; much of this sediment was probably deposited by slumping. Faulting of the ridge sediments suggests present tension on the Alpha Ridge. Sediments in the Alpha Ridge graben, however, onlap the basement, thereby indicating that the tectonic formation of this valley predated the sediments. Basement structure is rough and irregular on the ridges, and the graben-like major valley is bounded by scarps. The high-intensity magnetic anomalies, the refraction velocities and rocks dredged from a basement outcrop all indicate that the acoustic basement is oceanic layer 2. The proportional relationship of the Alpha Ridge topography and magnetics suggest that the ridge was formed during the Cretaceous quiet period (Aptian to Santonian, 119-84 Ma BP).

Paper 4 describes the appearance and composition of the seabed on the northern Alpha Ridge crest and adjacent graben slope, as determined from bottom photographs and dredge samples. Most sites show bioturbation features and a strong bimodality of sediment texture which reflects two main sediment sources: 1) a compact matrix of well-sorted clayey mud derived from local bedrock weathering and advective water transport, and 2) a poorly sorted coarse fraction of fine sand to boulder-sized material which could only be transported to the Alpha Ridge by ice. The sediment is well compacted throughout the area, suggesting a very low deposition rate. This interpretation is substantiated by a sediment budget calculated from suspended sediment concentrations in water samples collected during CESAR, which yield a deposition rate of ca.  $3 \times 10^{-3} \text{ mm} \cdot \text{a}^{-1}$ . Bottom currents below 1600m water depth are weak ( $2 \text{ cm} \cdot \text{s}^{-1}$ ) as indicated by drift rates of plumes generated during camera drops. Percentage gravel increases upslope, however, and the shoalest site (1160m) showed starved ripples of sand-size material and scouring around cobbles. These bedforms suggest periodic erosion by storm-generated bottom currents.

Bottom mud, bedrock, ice and water samples were analyzed for grain size, particle shape, biogenic content

dessus de deux crêtes de dorsale séparées par une large vallée à versants raides identifiée par M. J.K. Hall en 1970 comme un graben. En règle générale, la topographie de la dorsale varie de 2 536 m à 1 087 m, mais de nombreux pics et vallées plus petits se découpent sur les crêtes et les versant de la vallée. À des fins d'uniformité, des noms géographiques officiels sont utilisés dans le présent rapport pour désigner les axes principaux de la dorsale ainsi que la vallée en forme de graben. Les axes nord et sud de la dorsale sont désignés crête nord de la dorsale Alpha et crête sud de la dorsale Alpha respectivement; on a donné à la grande vallée qui les sépare le nom de graben de la dorsale Alpha.

La troisième étude décrit les données prélevées par sismique réflexion au cours de l'expédition; ces données fournissent le premier enregistrement acoustique-stratigraphique à résolution relativement élevée des milieux sédimentaires d'où proviennent les carottes et les échantillons. Les enregistrements de sismique réflexion révèlent que la couverture sédimentaire des dorsales est stratifiée et surtout horizontale ou concordante avec les structures du socle. L'épaisseur des sédiments varie d'environ 0,2 à 0,5s sur les crêtes. Une séquence plus épaisse de sédiments moins régulièrement stratifiés se manifeste dans le graben de la dorsale Alpha; une grande partie de ces matériaux a vraisemblablement été mis en place suite à des glissements. La présence de failles dans les sédiments semble indiquer que la dorsale Alpha est présentement soumise à des tensions. Toutefois, la présence de sédiments recouvrant le socle dans le graben atteste du fait que la formation tectonique de cette vallée a précédé l'accumulation des sédiments. La structure du socle est accidentée et irrégulière sur les crêtes et la grande vallée en forme de graben est limitée par des escarpements. Les anomalies magnétiques à haute intensité, les vitesses de réfraction et les échantillons prélevés sur un affleurement révèlent que le socle acoustique est formé par la couche océanique 2. Le rapport proportionnel de la topographie et du magnétisme semble indiquer que la formation de la dorsale Alpha a eu lieu au cours de la période calme du Crétacé (Aptien à Santonien, 119 à 84 Ma B.P.).

La quatrième étude décrit l'apparence et la composition, déterminées à partir de photographies du fond et d'échantillons dragués, du fond océanique sur la crête nord de la dorsale Alpha et sur le versant contigu du graben. Presque tous les emplacements présentent des structures formées par bioturbation ainsi qu'une bimodalité marquée de la texture sédimentaire qui reflète deux sources principales de matériaux: 1) une matrice compacte de boue argileuse bien triée dérivée de l'altération de la roche en place locale et du transport par advection dans l'eau et 2) une fraction grossière mal triée dont les dimensions varient du sable fin aux blocs et que seule la glace aurait pu transporter jusqu'à la dorsale. Les sédiments sont bien tassés partout dans la région, phénomène qui semble indiquer que la mise en place s'est faite lentement; cette hypothèse est appuyée par le bilan sédimentaire calculé à partir des concentrations de sédiments en suspension dans les échantillons d'eau prélevés au cours de l'expédition dont l'analyse a établi une vitesse de sédimentation de l'ordre de  $3 \times 10^{-3} \text{ mm} \cdot \text{a}^{-1}$ . Les vitesses de dérive des panaches produits par la chute d'appareils photo révèlent que les courants de fond sont lents ( $2 \text{ cm} \cdot \text{s}^{-1}$ ) à des profondeurs supérieures à 1 600 m. Par contre, le pourcentage de gravier augmente à mesure que l'on remonte la pente et l'emplacement le moins profond (1 160 m) présente des indices d'affouillement autour des gros cailloux ainsi que des rides incomplètes composées de matériaux de la grosseur du sable. Ces structures semblent indiquer qu'il y a érosion périodique par les courants de fond produits par des tempêtes.

and chemical composition. Comparison of the chemistry and quantity of sedimentary components in these different sources reveals that most of the fine sediment on the Alpha Ridge and flank is probably derived from winnowing of weathered local bedrock and not from sea ice as reported in other studies. Some coarse silt-to sand-size material, however, probably reflects eolian transport onto the sea ice and subsequent melt-out. Ice-rafted dropstones are present over the entire seabed; their dolomitic or limestone composition indicates a source on the coast of Ellesmere Island, North Greenland or Axel Heiberg Island. Biogenic debris consists almost entirely of calcareous tests; these are more abundant in deeper water, suggesting some downslope transport following winnowing of the ridge crest areas. Postdepositional erosion in deeper water, however, is rare as indicated by well-preserved delicate sponge spicules.

Paper 5 discusses the rock samples dredged from the scarp of the major valley of the Alpha Ridge. The rocks are highly altered, vesicular, fragmental volcanics. The high vesicularity and very fine grained nature of the clasts suggest a shallower water environment for the ridge than its present bathymetric expression. No minerals have been found in the rocks that might be used to obtain a radiometric age for the bedrock. Therefore, dating of the Alpha Ridge bedrock must rely on biostratigraphic age correlation of the basal overlying sediments.

Paper 6 documents the methods used to obtain 16 piston cores and 12 gravity cores during CESAR, and the results of initial lithostratigraphic studies are reported. The core sites range from 2000m depth in the Alpha Ridge graben to ca. 1175m on the northern Alpha Ridge crest. All except CESAR core 6, from a fault block on the north scarp of the Alpha Ridge graben, contain hemipelagic and glaciogenic brown muds similar to those recorded for other parts of the Arctic Ocean ridge systems. Thirteen lithological units are described for these CESAR cores, based on dominant sediment texture, colour, carbonate content, sediment structure, and several distinctive clastic marker beds that can be correlated with those of previously described Alpha Ridge cores. Paleomagnetic and palynological data from several CESAR cores indicate that the age of the longest cores is Early Pliocene, and that a continuous sequence of Early Pliocene-Recent sediments covers most of the northern Alpha Ridge crest and adjacent graben.

Eleven of the late Cenozoic lithological units in the CESAR cores (units AB, C, DE, F, G, H, I, J, K, L and M) have siliciclastic and carbonate lithologies, calcareous and arenaceous biotas very similar to those previously recorded for the southeastern Alpha Ridge, and they can also be correlated with lithofacies in cores from the western Alpha Ridge-Chukchi Rise. Such widespread lithological correlation, which varies little over a wide range of topographic settings, strongly indicates that sea ice and local bedrock erosion must have been the main sources of sediment supply during the past 4-5 Ma BP. In most CESAR piston cores,

Des échantillons de boue, de roche en place, de glace et d'eau ont été étudiés afin d'en déterminer la granulométrie, la forme des particules, les matériaux organogènes et la composition chimique. Une comparaison de la chimie et de la quantité de composantes sédimentaires dans ces diverses sources révèle que la plus grande partie des sédiments fins sur la dorsale Alpha et le versant provient vraisemblablement du vannage de la roche en place locale altérée et non de la glace de mer comme l'avaient déjà signalé d'autres rapports. Toutefois, une certaine proportion des matériaux dont les dimensions varient du limon grossier au sable a probablement été transportée sur la glace de mer par le vent et ensuite déposée au moment de la fonte de la glace. On trouve des «dropstones» glaciels partout sur le fond océanique; leur composition dolomitique ou calcaire indique qu'ils proviennent de la côte de l'île Ellesmere, du nord du Groenland ou de l'île Axel Heiberg. Les débris organogènes se composent presque entièrement de tests calcaires; ceux-ci sont plus abondants en eau plus profonde, phénomène qui semble indiquer qu'il y a eu transport vers le bas de la pente suivant le vannage des crêtes de la dorsale. La présence de spicules d'éponges fragiles et bien conservés indique qu'il y a très peu d'érosion après la sédimentation dans les eaux plus profondes.

La cinquième étude présente une étude des échantillons rocheux provenant de l'escarpement de la vallée principale de la dorsale Alpha. Il s'agit de roches volcaniques détritiques fortement altérées et caractérisées par la présence de vacuoles. Les nombreuses vacuoles et la finesse des grains semblent indiquer que la formation de la dorsale a eu lieu dans un milieu aquatique moins profond que le milieu actuel. Aucun minéral n'a été trouvé qui permettrait de déterminer l'âge absolu de la roche en place. La datation du socle rocheux de la dorsale Alpha doit donc se fonder sur une corrélation avec l'âge biostratigraphique des sédiments de fond sus-jacents.

La sixième étude décrit les méthodes utilisées pendant l'expédition pour prélever 16 échantillons au moyen d'une carotteuse à piston et 12 échantillons au moyen d'une carotteuse à chute libre, ainsi que les résultats des premières études lithostratigraphiques. Les carottes ont été prélevées à des profondeurs variant de 2 000 m dans le graben à environ 1 175 m sur la crête nord de la dorsale. Tous les échantillons sauf la carotte CESAR 6, qui provient d'un bloc faillé sur l'escarpement nord du graben, contiennent des boues brunes hémipélagiques et glaciaires similaires à celles qui ont été trouvées ailleurs dans le réseau de dorsales de l'océan Arctique. Treize unités lithologiques identifiées dans les carottes sont décrites en fonction de la texture sédimentaire prédominante, la couleur, la teneur en matériau carbonaté, la structure des sédiments et la présence de plusieurs lits repères clastiques caractéristiques susceptibles d'être mis en corrélation avec des lits identifiés dans des carottes de la dorsale Alpha prélevées antérieurement. Les données paléomagnétiques et palynologiques obtenues de plusieurs carottes CESAR indiquent que les carottes les plus longues datent du Pliocène ancien et qu'une séquence continue de sédiments du Pliocène ancien-Holocène recouvre la plus grande partie de la crête nord de la dorsale et le graben contigu.

Onze des unités lithologiques du Cénozoïque récent (unités AB, C, DE, F, G, H, I, J, K, L et M) identifiées dans les carottes CESAR présentent des lithologies silicoclastiques et carbonatées et des biotes calcaires et arénacés très semblables à ceux qui ont déjà été identifiés dans la partie sud-est de la dorsale Alpha; elles peuvent être mises en corrélation avec les lithofaciès identifiées dans les carottes provenant de la partie ouest de la dorsale Alpha et

however, one to three new lithofacies (units A1, A2 and A3) are present at the base of the cores. These arenaceous units contain fewer ice-rafted clasts than the overlying sediments, and carbonate lithologies appear to be absent, suggesting a lack of iceberg transport from the eastern Canadian Arctic and Greenland. Work is in progress to determine the probable sources of sand (eolian, glaciogenic or local bedrock) in arenaceous beds within these oldest units.

CESAR core 6 penetrated about 2m of laminated diatom ooze covering the top of the north scarp of the Alpha Ridge graben. This porous biosiliceous ooze (unit 4) is overlain by two thin (ca. 10-20cm) semiconsolidated mudstone units: a brown sandy mud (unit 3) and a grey claystone (unit 2). The top 2m of CESAR core 6 contained brown siliciclastic mud similar to that of units A2 and A3 in the Late Cenozoic cores.

Biostratigraphic age estimates for unit 4 range from middle or late Campanian (diatoms) to middle or late Maastrichtian (silicoflagellates) or late Campanian-Paleocene (palynomorphs). Paleomagnetic data support a Maastrichtian-Paleocene age. The biosiliceous ooze contains perfectly preserved microfossil assemblages similar to those found in Fletcher Ice Island core FL437 from the southern Alpha Ridge crest. However, the CESAR biosiliceous sediment is unique in containing well-preserved rhythmic laminations which resemble annual varves. Initial biostratigraphic, sedimentological and geochemical studies of light and dark lamina couplets, however, failed to reveal features that normally characterize varved sediments. It is concluded that: 1) the fine structure of the lamina beds most closely resembles the complex sequences recorded in Triassic cherts of the Japanese Island forearc basins; 2) light and dark laminae reflect lesser or greater amounts of Fe-rich particulates which may be authigenic or due to bedrock erosion; and 3) slow biogenic sediment deposition in a fluctuating oxygen minimum zone best accounts for the biosiliceous rhythmites. The overlying mudstone units in CESAR core 6 appear to be derived from highly weathered volcanic rock; their age is uncertain, but palynomorph assemblages resemble those in siliceous sediment from Fletcher Ice Island core FL422 which has a Middle or Late Eocene age.

Paper 7 documents the paleomagnetic stratigraphy for two gravity cores, CESAR core 103 and 102, and two piston cores, CESAR core 14 and 6. The cores were continuously sampled at 2cm intervals. The intensities of natural remanent magnetization (NRM) in the Cenozoic sediments (CESAR cores 103, 102 and 14) ranged from  $0.1 \times 10^{-5} \text{emu.cm}^{-3}$  in normally magnetized samples to  $0.5 \times 10^{-6} \text{emu.cm}^{-3}$  in reverse magnetized samples. Plots of stable inclination versus depth for these cores show distinctive normal and reverse polarity chrons which can be correlated with the established Late Cenozoic stratigraphy. The gravity cores include the Bruhnes-Matuyama transition (0.73 Ma) and Jaramillo subchron; the piston core

de la crête Tchouktche. Une corrélation lithologique si répandue, caractérisée par une très faible variation sur une vaste gamme de milieux topographiques, indique qu'au cours des 4 ou 5 derniers millions d'années, la source de la plus grande partie des sédiments a été la glace de mer et l'érosion locale du socle rocheux. Toutefois, on trouve d'un à trois nouveaux lithofaciès (unités A1, A2 et A3) à la base de la plupart des carottes CESAR prélevées au moyen de carotteuses à piston. Ces unités arénacées contiennent moins de fragments glaciels que les sédiments sus-jacents et l'absence de lithologies carbonatées semble indiquer qu'elles n'ont pas été transportées du Groenland et de l'est de l'Arctique canadien par les icebergs. Des travaux en cours tenteront de déterminer les sources probables du sable (transport éolien ou glaciaire, ou socle rocheux) dans les couches arénacées à l'intérieur de ces unités les plus anciennes.

La carotte CESAR 6 a pénétré environ 2 m de boue à diatomées laminaire qui recouvre le haut de l'escarpement nord du graben de la dorsale Alpha. Cette boue siliceuse à la fois poreuse et de nature organogène (unité 4) repose sous deux unités minces (de 10 à 20 cm) de pélite semiconsolidée: une boue sableuse brune (unité 3) et une pélite argileuse grise (unité 2). Les 2 m supérieurs de la carotte 6 contiennent une boue silicoclastique brune similaire à celle des unités A2 et A3 dans les carottes du Cénozoïque récent.

L'âge biostratigraphique estimatif de l'unité 4 varie du Campanien moyen ou récent (diatomés) au Maastrichtien moyen ou récent (silicoflagellés) ou au Campanien récent-Paléocène (microfossiles organiques). Les données paléomagnétiques confirment l'âge maastrichtien-paléocène de l'unité. La boue siliceuse de nature organogène contient des assemblages de microfossiles parfaitement conservés s'apparentant aux assemblages trouvés dans la carotte FL437 de l'île de glace Fletcher, qui a été prélevée dans la crête sud de la dorsale Alpha. Toutefois, le sédiment siliceux organogène CESAR est le seul qui contienne des lamines rythmiques bien conservées s'apparentant à des varves annuelles. Toutefois, les études biostratigraphiques, sédimentologiques et géochimiques préliminaires des couples de lamines claires et sombres n'ont pas identifié d'éléments normalement caractéristiques des sédiments varvés. On conclut donc que: 1) la structure fine des couches laminaires s'apparente étroitement aux séquences complexes identifiées dans des cherts triasiques provenant des bassins d'avant-arc des îles japonaises; 2) le ton clair ou sombre des lamines est fonction d'un contenu accru ou réduit en particules ferugineuses authigènes ou produites par l'érosion du socle rocheux; et 3) la présence de dépôts lités de nature siliceuse et organogène serait due à l'accumulation lente de sédiments organogènes dans une zone à teneur minimale en oxygène variable. Les unités pélitiques sus-jacentes dans la carotte CESAR 6 semblent provenir de roches volcaniques fortement altérées; leur âge est incertain mais les assemblages de microfossiles organiques s'apparentent aux assemblages trouvés dans les sédiments siliceux de la carotte FL422 (Éocène moyen ou récent) de l'île de glace Fletcher.

La septième étude présente la stratigraphie paléomagnétique de deux carottes prélevées au moyen d'une carotteuse à chute libre, soit les carottes CESAR 103 et 102, et de deux carottes prélevées par carotteuse à piston, soit les carottes CESAR 14 et 6. Ces carottes ont été échantillonnées en continu à des intervalles de 2 cm. L'intensité de l'aimantation rémanente naturelle (A.R.N.) des sédiments cénozoïques (carottes CESAR 103, 102 et 14) varie de  $0,1 \times 10^{-5} \text{uem.cm}^{-3}$  dans les échantillons à aimantation directe à  $0,5 \times$



extends this magnetostratigraphy to the Gilbert chron (3.40 Ma). An average sedimentation rate of 1.00mm. 1000a<sup>-1</sup> is calculated based on the Brunhes-Matuyama and Matuyama-Gauss transitions, and it is estimated that the oldest sediment in most of the piston cores was deposited between ca. 4.5-4.0 Ma.

In CESAR core 6, the NRM ranged from  $2.9 \times 10^{-7}$  emu.cm<sup>-3</sup> to  $9.9 \times 10^{-6}$  emu.cm<sup>-3</sup> for the siliceous ooze (unit 4) and volcanic ash units (3 and 2), and from  $2.3 \times 10^{-6}$  emu.cm<sup>-3</sup> to  $9.8 \times 10^{-6}$  emu.cm<sup>-3</sup> in the hemipelagic mud of unit 1. Unit 4 is characterized by two reversed chrons (A- and C-) and a shorter positive chron (B+). This establishes that the siliceous ooze was deposited after the Late Campanian long positive chron; hence, B+ may be correlated with either anomaly 29 or anomaly 30 plus 31. Correlation with anomaly 29 provides a late Maastrichtian-Danian age for the siliceous ooze, which is supported by palynological data; correlation with anomaly 30 + 31 provides a late Maastrichtian age which agrees with the silicoflagellate biostratigraphy. Correlation of magnetic data from units 3, 2 and 1 is uncertain because of the absence of established guide microfossils. However, a reversed polarity interval at the top of unit 1 indicates a minimum age of 0.73 Ma for the surface sediment at the site of CESAR core 6.

Paper 8 documents the foraminiferal, <sup>18</sup>O and <sup>13</sup>C stratigraphies of the Late Pliocene-Holocene sediments (units I-M), and the first part of Paper 11 describes the palynostratigraphy of these sediments. Planktonic foraminifera are the dominant component of the biogenic skeletal debris in the 63µm sediment fraction from most samples of units I-M, with pteropods, benthic foraminifera, ostracods and pelocypods not exceeding 2%. *Neogloboquadrina pachyderma* and *Neogloboquadrina cryophila* are the major planktonic foraminifera; *Neogloboquadrina polusi*, *Globigerina quinqueloba*, *Globigerina egelida* and *Globigerina bulloides* are secondary in abundance. Parts of units L and I, however, are almost barren of planktonic foraminifera; in these intervals, dinoflagellates and other acid-resistant algal spores provide some paleoceanographic information although their total numbers are consistently low (100.g<sup>-1</sup>). Late Cenozoic pollen and spores are also present throughout units I-M; their abundance is too low to provide reliable paleoclimatic data, but the stratigraphic distribution of genera with known age ranges in circumpolar Arctic regions can be used to confirm the Pliocene-Holocene age of the sediments.

The planktonic foraminifer *Neogloboquadrina pachyderma* (sinistral) was used to measure changes in the <sup>18</sup>O and <sup>13</sup>C values of the Arctic Ocean surface water during the past 1 Ma. A strong correlation between <sup>18</sup>O and <sup>13</sup>C (r=0.92) indicates that the isotopic values of the foraminifera closely reflect the gross productivity of the surface water layer. Starting at the top of the cores, the carbonate-rich Late Pleistocene units M to upper L are characterized by four light and three heavy isotopic intervals which are also directly

10<sup>-6</sup> uem.cm<sup>-3</sup> dans les échantillons à aimantation inversée. Des graphiques de l'inclinaison stable par rapport à la profondeur des échantillons présentent des chrons distinctifs à polarité directe et à polarité inversée que l'on peut mettre en corrélation avec la stratigraphie établie du Cénozoïque récent. La transition entre les époques de Brunhes et de Matuyama (0,73 Ma) et le sous-chron de Jaramillo est représentée dans les carottes prélevées par carotteuse à chute libre; cette magnétochronologie s'étend jusqu'au chrone de Gilbert (3,40 Ma) dans les carottes prélevées par carotteuse à piston. La vitesse moyenne de sédimentation est évaluée à 1,00 mm. 1 000a<sup>-1</sup> d'après les transitions entre les époques de Brunhes et de Matuyama et celles de Matuyama et de Gauss; dans la plupart des carottes prélevées au moyen de l'appareil à piston, le matériau le plus ancien a vraisemblablement été mis en place il y a entre 4,5 et 4,0 Ma.

Dans la carotte CESAR 6, l'A.R.N. varie de  $2,9 \times 10^{-7}$  uem.cm<sup>-3</sup> à  $9,9 \times 10^{-6}$  uem.cm<sup>-3</sup> pour la boue siliceuse (unité 4) et les unités de cendres volcaniques (unités 3 et 2) et de  $2,3 \times 10^{-6}$  uem.cm<sup>-3</sup> à  $9,8 \times 10^{-6}$  uem.cm<sup>-3</sup> pour la boue hémipélagique de l'unité 1. Deux chrons inversés (A- et C-) et un chrone positif plus court (B+) caractérisent l'unité 4. La boue siliceuse a donc été mise en place après le long chrone positif du Campanien récent; le chrone B+ peut ainsi être mis en corrélation avec l'anomalie 29 ou l'anomalie 30 plus 31. Une mise en corrélation avec l'anomalie 29 indique que la boue siliceuse date du Maastrichtien récent-Danien; cette hypothèse concorde d'ailleurs avec les données palynologiques. La mise en corrélation avec l'anomalie 30 plus 31 donne un âge Maastrichtien récent, comme le confirme la biostratigraphie des silicoflagellés. Étant donné l'absence de microfossiles stratigraphiques, il n'est pas possible de corréler avec certitude les données magnétiques provenant des unités 3, 2 et 1. Toutefois, l'existence d'un intervalle à polarité inversée au sommet de l'unité 1 indique que le sédiment de surface à l'emplacement de l'échantillon CESAR 6 date au moins de 0,73 Ma.

La huitième étude présente la stratigraphie des sédiments du Pliocène récent-Holocène (unités I-M), laquelle est fondée sur le contenu en foraminifères, en O<sup>18</sup> et en C<sup>13</sup>, et la première partie de la onzième étude décrit la palynostratigraphie de ces sédiments. Les foraminifères planctoniques représentent la composante dominante des débris squelettiques de nature organogène dans la fraction sédimentaire de 63 µm de la plupart des échantillons des unités I-M, la quantité de ptéropodes, de foraminifères benthiques, d'ostracodes et de pélecypodes ne dépassant pas 2%. *Neogloboquadrina pachyderma* et *Neogloboquadrina cryophila* sont les espèces principales de foraminifères planctoniques; parmi les espèces moins abondantes, on compte *Neogloboquadrina polusi*, *Globigerina quinqueloba*, *Globigerina egelida* et *Globigerina bulloides*. Toutefois, certaines parties des unités L et I ne contiennent presque pas de foraminifères planctoniques; les dinoflagellés et d'autres spores d'algues résistantes à l'acide fournissent alors certaines informations paléocéanographiques, bien que la quantité totale d'individus soit toujours faible (100.g<sup>-1</sup>). Des pollens et des spores du Cénozoïque récent se manifestent également partout dans les unités I-M; leur abondance est trop faible pour fournir des données paléoclimatiques fiables, mais la répartition stratigraphique des genres d'âge connu dans les régions circumpolaires de l'Arctique permet de confirmer l'âge pliocène-holocène des sédiments.

Le foraminifère planctonique *Neogloboquadrina pachyderma* (sinestre) a servi à mesurer les changements de la teneur en O<sup>18</sup> et

related to total foraminiferal abundances. In most of the arenaceous unit L, there were not enough planktonic foraminifera to obtain isotopic data. The carbonate-rich units K and J include two isotopically light and two heavy intervals. The early Pleistocene sediments (lower J-upper I) contain too few foraminifera for isotopic analysis. Although the isotopic record of the Alpha Ridge cores is incomplete, the chronology established by the paleomagnetic and palynological data can be used to show that major changes from light to heavy  $^{18}\text{O}$  values have a periodicity of about 100 000 years, i.e. they appear to correspond primarily to global ice volume fluctuations driven by orbital variations in insolation. Evidence of a predicted 41 000 year periodicity is weak, however, perhaps reflecting bioturbational mixing of up to 5 cm which would integrate the isotopic record over 50 000 year intervals.

Quantitative studies of the relation between foraminiferal assemblages, temperature and salinity are required before firm conclusions can be drawn regarding the Late Cenozoic paleoceanographic history of the Arctic Ocean. However, the CESAR core data suggest the following salient features: 1) contrary to the Ewing-Donn theory of Arctic glaciation, there is no evidence for ice-free intervals in the central Arctic Ocean during the past 1 Ma; 2) Late Pleistocene decreases in total foraminifera probably reflect dilution of surface water salinity by increased runoff, as also indicated by the occurrence of the freshwater palynomorph *Pediastrum* in unit L; and 3) low total abundances and high ratios of benthic to planktonic foraminifera in the Late Pliocene sediments probably reflect increased carbonate dissolution on the seafloor. Reduction in carbonate influx from iceberg calving is also suggested by the absence of Paleozoic carbonate clasts and their characteristic palynomorphs. A combination of reduced carbonate influx and more sluggish Arctic Ocean water exchange could account for more corrosive bottom water conditions, hence the less frequent preservation of microfossil deposits.

Papers 9, 10 and 11 report on biostratigraphic studies of the age and paleoenvironment of the laminated biosiliceous sediments in unit 4 of CESAR core 6. These sediments consist almost entirely of diatoms and archeomonads (ca. 80% by volume) admixed with ca. 10% of silicoflagellates. The excellent preservation state of these microfossils, including fragile spined taxa, strongly indicates that the siliceous sediment in CESAR core 6 is in place and is not a slump block or gravity flow deposit. The silicoflagellates (Paper 9) are mostly dominated by *Vallacerta siderea*, with *Lyrarnula deflandrei* and *Lyrarnula burchardae* being subdominant. At the base of unit 4, however, a small variety of *Lyrarnula deflandrei* is dominant and several other *Lyrarnula* species have range tops just above this basal zone. One of these species, *Lyrarnula furcula*, also disappears in the upper part of the siliceous sediment in core FL437 from the southern Alpha Ridge crest. *Lyrarnula furcula* is a widespread, abundant silicoflagellate which is known from the Santonian-Cam-

en C<sup>13</sup> dans la couche superficielle de l'eau dans l'océan Arctique au cours du dernier million d'années. Une corrélation marquée entre l'O<sup>18</sup> et le C<sup>13</sup> ( $r=0,92$ ) indique que les valeurs isotopiques des foraminifères reflètent étroitement la productivité brute de la couche superficielle d'eau. En commençant du haut des carottes, les unités M à L supérieure du Pléistocène récent, riches en carbonate, sont caractérisées par la présence de quatre intervalles d'isotopes légers et trois d'isotopes lourds qui sont directement liés à l'abondance totale des foraminifères. Dans la plus grande partie de l'unité L arénacée, la quantité de foraminifères planctoniques est insuffisante pour fournir des données isotopiques. Les unités K et J riches en carbonate présentent deux intervalles d'isotopes légers et deux d'isotopes lourds. Les sédiments du Pléistocène ancien (unités J inférieure et I supérieure) contiennent trop peu de foraminifères pour permettre la séparation isotopique. Bien que les données isotopiques provenant des échantillons prélevés sur la dorsale soient incomplètes, la chronologie fondée sur les données paléomagnétiques et palynologiques montre que les changements majeurs de la teneur en isotopes légers et en isotopes lourds (O<sup>18</sup>) ont une périodicité d'environ 100 000 ans; ils semblent donc correspondre principalement aux fluctuations du volume global des glaces qui contrôlent les variations de l'insolation dues aux variations orbitales. On n'a pas confirmé l'existence de la périodicité prévue de 41 000 ans; la faiblesse des indications pourrait être due au mélange par bioturbation d'un maximum de 5 cm de sédiments qui aurait détruit les données isotopiques sur des intervalles de 50 000 ans.

Il faudra entreprendre des études quantitatives du lien entre les assemblages de foraminifères, la température et la salinité avant de pouvoir reconstituer l'histoire paléocéanographique de l'océan Arctique au cours du Cénozoïque récent. Toutefois, l'étude des données provenant des carottes CESAR permet de tirer certaines conclusions: 1) contrairement à la théorie d'Ewing-Donn sur la glaciation de l'Arctique, il n'y a aucune indication de l'existence d'intervalles libres de glace dans l'océan Arctique central au cours du dernier million d'années; 2) la réduction du nombre total de foraminifères au cours du Pléistocène récent est vraisemblablement due à la dilution de la salinité des eaux de surface par un accroissement du ruissellement, comme l'indique aussi la présence du microfossile organique d'eau douce *Pediastrum* dans l'unité L et, 3) les faibles abundances totales et les proportions élevées de foraminifères benthiques par rapport aux foraminifères planctoniques dans les sédiments du Pliocène récent sont vraisemblablement dues à une dissolution accrue des carbonates sur le fond océanique. L'absence de fragments carbonatés d'âge paléozoïque et de leurs microfossiles organiques caractéristiques porte également à croire qu'il y a eu réduction de l'apport de carbonates dû au vêlage des icebergs. La réduction de l'apport de carbonates et le ralentissement de l'échange d'eau dans l'océan Arctique auraient eu pour effet de rendre plus corrosives les eaux de fond, phénomène qui aurait nuit à la conservation des dépôts de microfossiles.

Les neuvième, dixième et onzième études décrivent les analyses biostratigraphiques entreprises afin de déterminer l'âge et le paléoenvironnement des sédiments laminaires de nature siliceuse et organogène de l'unité 4 de la carotte CESAR 6. Ces sédiments se composent presque entièrement de diatomées et d'archéomonades (environ 80 % au volume) et d'environ 10 % de silicoflagellés. L'excellent état de conservation de ces microfossiles, y compris des taxons épineux fragiles, indique fortement que le sédiment siliceux dans la carotte 6 a été mis en place et ne représente pas un bloc

panian to the Late Maastrichtian in the circum-Arctic, Pacific, and Indian oceans. The disappearance of this species in CESAR core 6 is the main basis for assigning a probable Middle or Late Maastrichtian age to unit 4. Precise correlation and paleoenvironmental interpretation are constrained, however, by the unique character of the Alpha Ridge silicoflagellate assemblages. The low diversity of species and absence of radiolarians suggests that the provincial character of the Alpha Ridge assemblages is the result of ecological factors such as low sunlight and possibly salinity. Unusual nutrient conditions may also be a limiting ecological factor and there is no evidence of compositional changes between light and dark laminae which would support the interpretation of annual varves.

Palynological data (Paper 11) from CESAR core 6 are mostly too sparse to provide detailed paleoenvironmental data but dinoflagellate assemblages from the core-cutter sample also suggest strong provincialism in the presence of previously unknown variants of species similar to *Spongodinium delitiense* and *Paleoperidinium pyrophorum*. These species characterize Late Campanian-Danian dinoflagellate assemblages of the Canadian Arctic Islands and Atlantic margin. The paucity of dinoflagellates in the laminated sediments also suggests unusual salinity or nutrient conditions, and there are no differences between pollen or microplankton in light and dark laminae which would suggest that they represent annual varves. Pollen are present in most samples from unit 4 as well as samples from the overlying volcanic ash units 3 and 2. The assemblages at the base of unit 4 are similar to those in Campanian-Danian sediments of the Canadian Arctic but the taxa in the top of unit 4 and in units 3-2 are more similar to those found in the Eocene siliceous ooze from Alpha Ridge core FL422 and they can be correlated with Late Paleocene to Eocene assemblages in the Canadian Arctic.

Diatoms from CESAR core 6, unit 4, show more taxonomic diversity than the silicoflagellates or palynomorphs, but there is little consistent stratigraphic variation in their occurrence which usually marks the Late Cretaceous assemblages. The composition of the Alpha Ridge assemblages most closely resembles that documented for Late Campanian sediments from the northern Ural Mountains and it differs markedly from known Maastrichtian assemblages at lower latitudes and the circum-Antarctic region. The limited high latitude data available on non-paralic Cretaceous diatom assemblages constrain precise correlation, but the simplest interpretation indicates a Late Campanian age. The abundance of diatom resting spores and lack of shallow water species in Alpha Ridge sediments suggests that deposition occurred near a shelf or bank edge which was distant from the shoreline. The lack of evolutionary change in the Alpha Ridge assemblages could indicate that the laminated sediment represents a relatively short time interval which would be consistent with an upwelling environment and presence of annual varves. However, the absence of differences in diatom

effondré ou glissé par gravité. *Vallacerta siderea* est l'espèce dominante de silicoflagellé (étude 9) tandis que *Lynamula deflandrei* et *Lynamula burchardae* sont des espèces sous-dominantes. *Lynamula deflandrei* est l'espèce dominante à la base de l'unité 4 et plusieurs autres espèces de *Lynamula* disparaissent immédiatement au-dessus de cette zone basale. L'une d'elles, *Lynamula furcula*, disparaît également dans la partie supérieure du sédiment siliceux dans la carotte FL437 prélevée dans la crête sud de la dorsale Alpha. *Lynamula furcula* est un silicoflagellé abondant et très répandu qui est connu du Santonien-Campanien au Maastrichtien récent dans les zones circumocéaniques arctique, pacifique et indienne. Ainsi, surtout en raison de l'absence de cette espèce dans la carotte CESAR 6, on estime que l'unité 4 date du Maastrichtien moyen ou récent. Toutefois, le caractère unique des assemblages de silicoflagellés de la dorsale Alpha nuit à la mise en corrélation et à l'interprétation paléoenvironnementale exactes. La faible diversité des espèces et l'absence de radiolaires semblent indiquer que la nature locale des assemblages de la dorsale Alpha résulte de facteurs écologiques comme un faible ensoleillement et peut-être le degré de salinité. Des conditions nutritives inhabituelles pourraient s'avérer un autre facteur écologique limitatif. On a trouvé aucune trace de variation dans la composition des lamines claires et des lamines sombres qui pourrait appuyer l'hypothèse selon laquelle il s'agirait de varves annuelles.

La carotte CESAR 6 fournit trop peu de données palynologiques (étude 11) pour permettre de reconstituer le paléoenvironnement, mais la présence d'assemblages de dinoflagellés dans l'échantillon arraché au trépan souligne davantage la nature locale des assemblages fauniques. Ces dinoflagellés comportent des variantes auparavant inconnues d'espèces similaires à *Spongodinium delitiense* et *Paleoperidinium pyrophorum*, espèces caractéristiques des assemblages de dinoflagellés du Campanien récent-Danien des îles arctiques canadiennes et du littoral atlantique. La rareté des dinoflagellés dans les sédiments laminaires suggère également que des conditions de salinité ou des conditions nutritives inhabituelles sévissaient; en outre, on a observé aucune différence de pollens ou de microplancton dans les lamines claires et les lamines sombres qui pourrait confirmer l'hypothèse selon laquelle il s'agirait de varves annuelles. Des pollens ont été trouvés dans la plupart des échantillons de l'unité 4 ainsi que dans des échantillons des unités 3 et 2 sus-jacentes de centres volcaniques. Les assemblages à la base de l'unité 4 sont similaires à ceux des sédiments campaniens-daniens de l'Arctique canadien mais les taxons au sommet de l'unité 4 et dans les unités 3 et 2 s'apparentent plus aux assemblages trouvés dans la boue siliceuse d'âge éocène provenant de la carotte FL422 de la dorsale Alpha et peuvent être mis en corrélation avec des assemblages de l'Arctique canadien dont l'âge varie du Paléocène récent à l'Éocène.

Les diatomées de l'unité 4 de la carotte CESAR 6 ont une diversité taxonomique plus marquée que les silicoflagellés ou les microfossiles organiques mais leur répartition montre très peu de variation stratigraphique comme le font normalement les assemblages du Crétacé récent. La composition des assemblages de la dorsale Alpha ressemble le plus à celle des sédiments du Campanien récent de la partie nord des monts Oural et diffère grandement des assemblages maestrichtiens connus trouvés à de plus basses latitudes et dans la région circumantarctique. La quantité limitée de données disponibles sur des assemblages de diatomées crétacées non paraliques provenant de hautes latitudes nuit à l'établissement de corrélations exactes, mais l'interprétation la plus simple indique



assemblages from light and dark laminae does not support this interpretation.

In conclusion, the biostratigraphic studies of three different microfossil groups in CESAR core 6 are unanimous in assigning a maximum Late Campanian age to the core catcher sample and base of unit 4, and there is agreement that an offshore marine deposit with little terrigenous influence is indicated. There is also a consensus that the dark and light laminae do not show marked variations in microfossil content such as those typically found in varved sediments. However, the precise age of upper unit 4 and the overlying volcanic units remains uncertain because of the lack of analogues from high latitude Cretaceous-Tertiary offshore marine sections. Similarly, the possibility of provincialism in the early Arctic Ocean and the present lack of definite data regarding deep water connections with the global oceans strongly constrain the accuracy of paleoceanographic or paleoclimatic interpretations.

un âge campanien récent. L'abondance des spores en sommeil de diatomées et l'absence d'espèces d'eau peu profonde dans les sédiments de la dorsale Alpha semblent indiquer que la sédimentation a eu lieu en bordure d'une plate-forme ou d'un banc situés à quelque distance du littoral. L'absence de modifications évolutives dans les assemblages de la dorsale Alpha pourrait indiquer que les sédiments laminaires représentent un intervalle de temps relativement court, conclusion concordant d'ailleurs avec la présence de varves annuelles et un milieu marin ascendant. Toutefois, le manque de différences entre les assemblages de diatomées dans les lamines claires et les lamines sombres réfute cette interprétation.

En conclusion, les études biostratigraphiques de trois groupes différents de microfossiles dans la carotte CESAR 6 indiquent, à la satisfaction de tous, que l'échantillon arraché au trépan et la base de l'unité 4 date au maximum du Campanien récent et que la sédimentation aurait eu lieu dans un milieu marin littoral peu touché par l'influence terrigène. En outre, les lamines sombres et claires ne présentent aucune variation marquée du contenu en microfossiles comme le font normalement les sédiments varvés. On n'a pas encore toutefois déterminé l'âge exact de la partie supérieure de l'unité 4 et des unités volcaniques sus-jacentes puisqu'aucune unité équivalente n'a été trouvée dans les sections marines littorales d'âge crétacé-tertiaire gisant à haute latitude. De même, le caractère local possible de l'ancien océan Arctique et l'absence de données certaines relatives aux passages reliant les eaux profondes et les océans du globe nuit fortement à l'établissement précis des interprétations paléocéanographiques ou paléoclimatiques.

## KNOWLEDGE OF THE ALPHA RIDGE PRIOR TO CESAR

H.R. Jackson<sup>1</sup>  
Geological Survey of Canada

*Jackson, H.R., Knowledge of the Alpha Ridge prior to CESAR; in Initial Geological Report on CESAR — the Canadian Expedition to Study the Alpha Ridge, Arctic Ocean, ed. H.R. Jackson, P.J. Mudie and S.M. Blasco; Geological Survey of Canada, Paper 84-22, p. 11-14, 1985.*

### Abstract

*Bathymetric data, geological samples and geophysical information collected prior to CESAR are reviewed. This material provides a framework in which the CESAR data set can be interpreted.*

### Résumé

*Les données bathymétriques, les échantillons géologiques et les renseignements géophysiques qui ont été obtenus avant l'expédition CESAR sont examinés. Ces informations fournissent le cadre nécessaire à l'interprétation des renseignements recueillis au cours de l'expédition CESAR.*

The Alpha Ridge is a major bathymetric feature that crosses the Arctic Ocean and abuts the continental shelf of Arctic Canada northwest of Ellesmere Island (Fig. 1.1). The ridge is 250 to 800 km across between the 2000 m contour. It is unclear whether the Alpha Ridge and Mendeleev Ridge are a continuous feature. The 2500 m contour encloses both bathymetric highs (Johnson et al., 1978). The topography of the Alpha Ridge is rugged and exhibits thermal decay. The sediment corrected relief is  $2900 \pm 500$  m (DeLaurier, 1978).

Sediment thickness on the Alpha Ridge is reported to be 0.5 km on the crest increasing to 2 km on the flanks (Hall, 1970). These measurements were obtained with a 9000 joule sparker and are, therefore, likely to be minimum thicknesses. Control of sediment type and age was established by coring.

A summary of the previously collected cores follows (excluding data held by the U.S.S.R., which are difficult to access at present). Most cores recovered from the Arctic Ocean were collected by the United States Geological Survey from the Amerasian Basin (Canada Basin and Makarov Basin; Fig. 1.1) and the sampling was done from ice stations. The first 16 cores retrieved in 1957 from ice station Alpha had a maximum length of 2.3 m (Hunkins, 1965). Ice station Charlie, originally called Alpha II, was the platform from which 22 piston cores with a length of up to 2.5 m (Crombie, 1960) were recovered. On Arlis II cores were also collected during 1963-1965 (Herman, 1974). Most of the coring in the Arctic Ocean was done from T-3, Fletcher's Ice Island (also called IGY Drifting Station Bravo). From this ice island 580 piston cores up to 5.5 m long were recovered during the period 1963-1973 (Clark et al., 1980). Following this, on ice station AIDJAX, in 1975 10 short cores up to 0.6 m long were

retrieved (Bornhold et al., 1975). On ice station LOREX 42 cores, 0.2 to 1.7 m long, were collected from the Lomonosov Ridge area in 1979 (Blasco et al., 1979; Morris, 1983). A few cores have been collected from the Eurasian Basin (Nansen Basin and Fram Basin; Fig. 1.1); from Fram I eight cores from 0.07 to 0.9 m long were retrieved; from Fram II and III, 14 gravity cores from 0.2 to 0.8 m long were obtained, and in 1980 about 25 cores up to 8.9 m long were retrieved from the ship *Ymer*, north of  $80^\circ$  (Bostrom, 1981). From this entire suite of cores only 3 penetrated pre-Neogene sediments and these were collected from the Alpha Ridge in the vicinity of CESAR. One core was a siliceous ooze that indicated a minimum age for the Alpha Ridge of Late Cretaceous.

A review of the available geophysical data is assembled here to provide a tectonic background for interpreting the geological samples. The magnetic field over the Alpha Ridge has several characteristics that may be useful in understanding its crustal structure and origin. The aeromagnetic data reveal magnetic anomalies of up to 1500 nt that are sublinear to irregular. There is some evidence that these magnetic anomalies correlate with the topography of the Alpha Ridge (Hall, 1970). The patterns of anomalies are too irregular to correspond to normal oceanic linear anomalies (King et al., 1966). Estimated mean source depths (EMSD) calculated from the magnetic anomalies (Kovacs and Vogt, 1982) are consistent with the water depths. The EMSD contours, however, are not similar to those associated with spreading ridges. Depths to basement of 7.5 to 10 km are calculated for areas north of the ridge compared to an average of 3 km for the ridge. This suggests a more rapid change than can be attributed to typical oceanic crustal subsidence. Kovacs and Vogt (1982) postulated that the abrupt change in basement

<sup>1</sup>Atlantic Geoscience Centre, Bedford Institute of Oceanography, Box 1006, Dartmouth, Nova Scotia B2Y 4A2

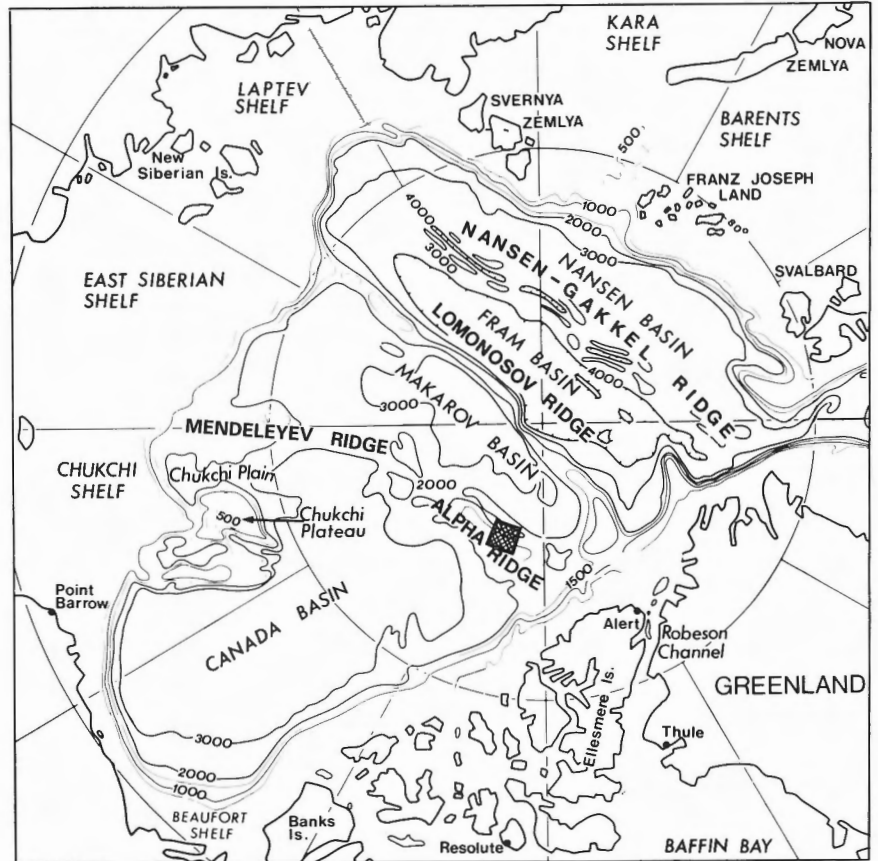


Figure 1.1 Map of the Arctic Ocean showing the location of the CESAR ice camp.

depths could be due to a relict oceanic subduction zone, with the ridge a back-arc plateau, or it may be indicative of continental crust. Satellite data show an overall magnetic high that is a major magnetic feature on the global scale (Langel and Thorning, 1982).

Heat flow values on the Alpha Ridge average  $50 \pm 7 \text{ mWm}^{-2}$ . These measurements are similar to those on aseismic ridges in other oceans and do not suggest presently elevated temperatures (Judge and Jessop, 1978; Lachenbruch and Marshall, 1966).

The Alpha Ridge has a free air gravity anomaly with values in excess of  $100 \text{ mGal}$  (Bowin et al., 1981). However, the major valleys in the ridge are associated with negative values of up to  $30 \text{ mGal}$  (Hall, 1970). Furthermore, at the junction of the Alpha Ridge and the Ellesmere Island continental shelf, there is a  $100$  to  $150 \text{ km}$  wide zone with low gravity values of  $10 \text{ mGal}$  (Vogt et al., 1982). The magnetic anomalies also show changes in character across this region, which is nearly perpendicular to the strike of the ridge, with depth to magnetic basement increasing to  $5$  or  $6 \text{ km}$ . Bathymetry from ice stations shows this area to be a closed depression. The gravity, magnetics and bathymetry indicate that the ridge is not connected to the shelf and therefore is unlikely to be founded continental crust. The contact between crustal types is sharp and could be due to faulting.

The trough might also delineate a trench where the crust of the ridge was thrust under the shelf (Vogt et al., 1982).

Seismic reflection data collected from Fletcher's Ice Island, T-3 indicate  $100$  to  $1200 \text{ m}$  of sediment that thickens towards the continental shelf. Basement topography is mountainous. Traces of normal faults extend to the surface, and are cited by Hall (1970) as evidence that the ridge is now under tension. Pre-CESAR seismic refraction results (Hunkins, 1961) from three short lines indicate a  $2.0 \text{ km.s}^{-1}$  sedimentary layer of  $0.3$  to  $0.5 \text{ km}$  thickness overlying a  $4.7 \text{ km.s}^{-1}$  layer that is  $2.8 \text{ km}$  thick and a  $6.4 \text{ km}$  layer of undetermined thickness.

As yet the available geophysical data have not uniquely determined the origin of the Alpha Ridge. Postulated tectonic origins include: an active or inactive spreading centre, a fossil subduction zone, a continental fragment or the trace of a hot spot.

In the framework of few geological samples and an unknown tectonic history and crustal structure for the Alpha Ridge the CESAR experiment was undertaken. The following papers describe and interpret the data collected from the ice island.

It is important to note that cores were collected from three base camps. The main camp and at two temporary and remote stations (Fig. 1.2).

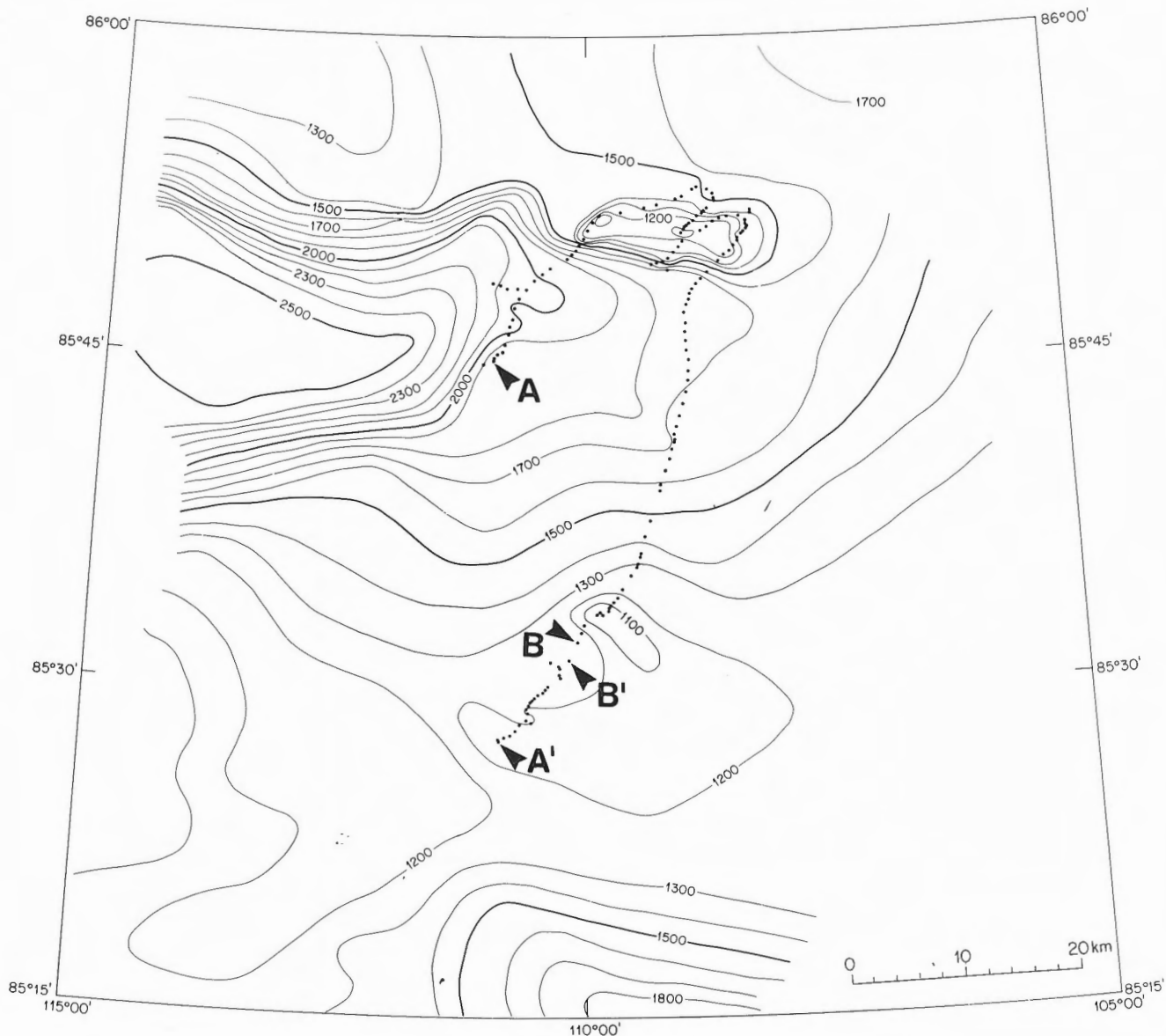


Figure 1.2 A simplified track plot for the various CESAR camps. The start and end positions (A) that the main camp sailed across are indicated by large arrows, while the drift of the second remote camp (A'-B') is marked with small arrows. Fortunately the two tracks nearly meet. The position of remote camp I is shown by an asterisk.

## REFERENCES

- Bornhold, B.D., Blasco, S.M., and Lewis, C.F.M.  
1979: Preliminary results of surficial geology and geomorphology studies of the Lomonosov Ridge, central Arctic Basin; in *Current Research, Part C, Geological Survey of Canada, Paper 79-1C*, p. 73-83.
- Bornhold, B.D., Lewis, C.F.M., and Fenerty, N.E.  
1975: Arctic marine surficial geology: AIDJAX 1975; in *Report of Activities, Part C, Geological Survey of Canada, Paper 75-1C*, p. 79-84.
- Bostrom, A.K.  
1981: Expedition YMER-80; Svenska sällskapet för antropologi och geografi, p. 90-109.
- Bowin, C., Warsi, W., and Milligan, J.  
1981: *Free Air Gravity Anomaly Map of the World*; The Geological Society of America Inc.
- Clark, D.L., Whitman, R.R., Morgan, K.A., and Mackey, S.D.  
1980: Stratigraphy and glacial marine sediments of the Amerasian Basin, central Arctic Ocean; *Geological Society of America, Special Paper 181*, 58 p.
- Crombie, W.J.  
1960: Preliminary results of investigations on Arctic Drift Station Charlie; *Geology of the Arctic*, p. 690-707.
- DeLaurier, J.M.  
1978: The Alpha Ridge is not a spreading centre, in *Arctic Geophysical Review*, ed. J.F. Sweeney; *Earth Physics Branch Publication*, v.45, p.87-90.

- Hall, J.K.  
1970: Arctic Ocean geophysical studies; The Alpha Cordillera and Wendelejev Ridge; Lamont Doherty Geological Observatory, Technical Report no. 2, 125 p.
- Herman, Y.  
1974: Arctic Ocean sediments, microfauna, and the climatic record in Late Cenozoic time; *in* Marine Geology and Oceanography of the Arctic Seas, ed. Y. Herman, p. 283-348.
- Hope, E.R.  
1959: Geotectonics of the Arctic Ocean and the great Arctic magnetic anomaly: *Journal of Geophysical Research*, v. 64, p. 407-427.
- Hunkins, K.L.  
1961: Seismic studies of the Arctic Ocean floor; *in* Geology of the Arctic, v. 1, ed. G.O. Roash; University of Toronto Press, p. 645-655.  
  
1965: Some features of Arctic deep-sea sedimentation; *in* U.S. - I.G.Y. Drifting Station Alpha Arctic Ocean 1957-1958, G.H. Cabaniss, K.L. Hunkins and N. Untersteiner (eds.), 322 p.
- Johnson, G.L., Taylor, P.T., Vogt, P.R., and Sweeney, J.F.  
1978: Arctic Basin Morphology; *Polarforschung*, v. 48, p. 20-30.
- Judge, A.S. and Jessop, A.M.  
1978: Heat flow north of 60°N; *in* Arctic Geophysical Review, ed. J.F. Sweeney; Earth Physics Branch Publication, v. 45, p. 25-33.
- King, E.R., Dietz, I., and Alldredge, L.R.  
1966: Magnetic data on the structure of the central Arctic region; *Geological Society of America, Bulletin*, v. 77, p. 619-646.
- Kovacs, L.C. and Vogt, P.R.  
1982: Depth to magnetic source analysis of the Arctic Ocean region; *Tectono-physics*, v. 89, p. 255-294.
- Lachenbruch, A.H. and Marshall, B.V.  
1966: Heat flow through the Arctic Ocean floor; the Canadian Basin-Alpha Ridge-Rise boundary; *Journal of Geophysical Research*, v. 71, p. 1223-1248.
- Langel, R.A. and Thorning, L.  
1982: Satellite magnetic field over the Nares Strait region; *in* Nares Strait and the Drift of Greenland; a Conflict in Plate Tectonics, ed. P.R. Dawes and J.W. Kerr; Meddelelser om Grønland, Geoscience, v. 8, p. 291-293.
- Morris, T.H.  
1983: The stratigraphy and Late Pleistocene sedimentological history of the Lomonosov Ridge - Makarov Basin, central Arctic Ocean; unpublished M.Sc. thesis, University of Wisconsin, Madison, 100 p.
- Vogt, P.R., Taylor, P.T., Kovacs, L.C., and Johnson, G.L.  
1982: The Canada Basin; aeromagnetic constraints on structure and evolution; *Tectonophysics*, v. 89, p. 295-336.

## CESAR BATHYMETRY

J.R. Weber<sup>1</sup> and H.R. Jackson<sup>2</sup>

Weber, J.R. and Jackson, H.R., *CESAR bathymetry*, in *Initial Geological Report on CESAR — the Canadian Expedition to Study the Alpha Ridge, Arctic Ocean*, ed. H.R. Jackson, P.J. Mudie and S.M. Blasco; Geological Survey of Canada, Paper 84-22, p. 15-17, 1985.

### Abstract

*The bathymetric data collected during CESAR are reported along with the navigation control for main and remote camps and the spot soundings. The major topographic low between the north and south ridge crests is called a graben.*

### Résumé

*Le présent rapport décrit les données bathymétriques recueillies au cours de l'expédition CESAR ainsi que le canevas de navigation utilisé pour les camps principal et éloignés et les sondages intermittents. L'importante dépression topographique située entre les crêtes des dorsales nord et sud est un graben.*

### METHOD

The CESAR bathymetry survey, a co-operative venture between the Earth Physics Branch (EPB) and the Canadian Hydrographic Service (CHS), consists of some 440 helicopter spot soundings. Starting at the 1000m isobath at the edge of the continental shelf, the survey covers a strip 250km wide and 360km long extending over the Alpha Ridge. Only part of this survey is described in this paper, namely that part surrounding the CESAR main and remote camps outlined on Figure 2.1. Spot soundings in this area were carried out at an approximate 10km grid interval. Water depth was determined partly by echo sounding through the ice (CHS) and partly by the seismic method using explosives (EPB). Station positions were determined from the Global Navigational System with an estimated accuracy of about  $\pm 2$ km. In addition to the spot soundings, the Atlantic Geoscience Centre operated two echo sounders continuously, one at the main camp (12kHz), from day 91 to 141 and the other at the remote camp (3.5kHz) from day 107 to 131. The navigation at mainland remote camp II was with a Marconi 761 Satnav and was accurate to  $\pm 20$ m (J. Popelar, personal communication, 1984). Two-way travel times of the soundings were converted to water depths using Matthews' Tables (1939). The depths thus determined agreed to within 20m with the water depths determined independently from wireline measurements. Results are shown in Figure 2.2 which shows the locations where soundings were taken and the bathymetry in 100m contour intervals.

### RESULTS

This map represents only a small part of the Alpha Ridge, which in this region, is about 300km wide. The bottom topography is complex, ranging in depth from 2536 to 1087m; it appears roughest where the sounding density is greatest. There are many short wavelength topographic features visible on the continuous echo sounder and on shallow seismic records along the drift track, which remain unresolved in the 10km grid of spot soundings, the smallest grid interval that could be surveyed during the time period available.

An examination of the bathymetry from Figure 2.2 shows that the CESAR camp (consecutive black dots) drifted over a valley and two ridge crests. The majority of the piston cores were taken on what will be referred to as the northern Alpha Ridge crest at approximately 85°50'N while the longer gravity cores were retrieved close to what will be called the southern Alpha Ridge crest at about 85°31'N. The intervening large valley will be referred to here as the Alpha Ridge graben (as designated by Hall, 1970).

### REFERENCES

- Hall, J.K.  
1970: Arctic Ocean geophysical studies: The Alpha Cordillera and Mendeleyev Ridge; Lamont-Doherty Geological Observatory of Columbia University, Technical Report CU-2-70, 125p.
- Matthews, D.J.  
1939: Tables of the velocity of sound in pure and sea water; British Admiralty, Hydrographic Department Report 282.

<sup>1</sup>Gravity, Geothermics and Geodynamics Division, Earth Physics Branch, Ottawa, Ontario, K1A 0Y3

<sup>2</sup>Atlantic Geoscience Centre, Geological Survey of Canada, Bedford Institute of Oceanography, Box 1006, Dartmouth, Nova Scotia, B2Y 4A2



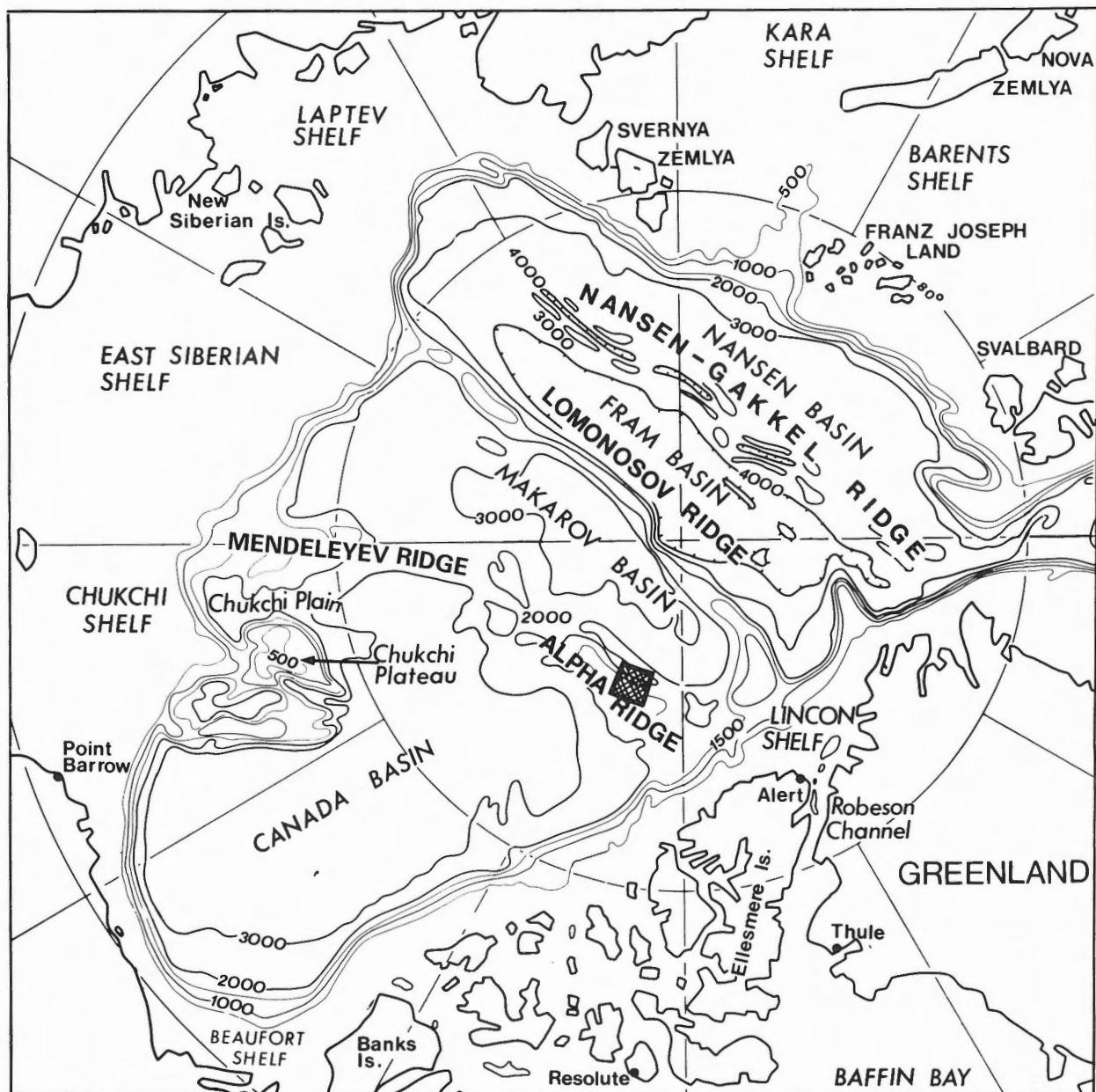


Figure 2.1 Map of the Arctic Ocean with cross-hatched area showing the location of the CESAR bathymetry survey.



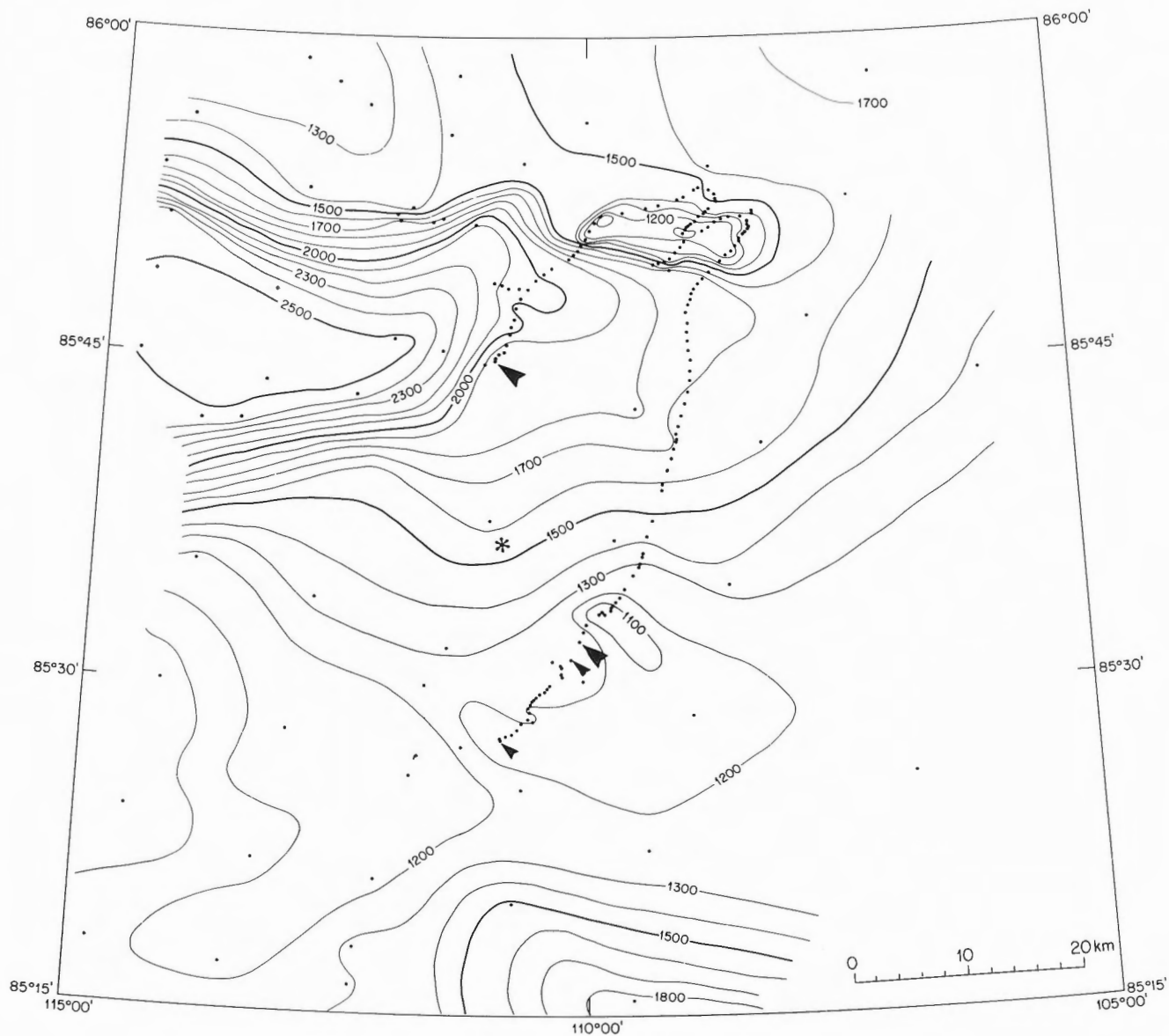


Figure 2.2 A bathymetry chart in the vicinity of the CESAR camp. The heavy arrows on the dotted line indicate the drift of the main camp while the smaller arrows indicate the drift of the second remote camp. The position of the first remote camp is shown with an asterisk because no satellite positions are available for it and it was occupied for a short period. The individual dots are the positions of spot soundings.



## SEISMIC REFLECTION RESULTS FROM CESAR

H.R. Jackson<sup>1</sup>

Geological Survey of Canada

Jackson, H.R., *Seismic reflection results from CESAR; in Initial Geological Report on CESAR — the Canadian Expedition to Study the Alpha Ridge, Arctic Ocean*, ed. H.R. Jackson, P.J. Mudie and S.M. Blasco; Geological Survey of Canada, Paper 84-22, p. 19-23, 1985.

### Abstract

*The seismic reflection information collected on CESAR is presented to provide a continuous record of sedimentary horizons and basement relief. The sedimentary reflectors on the highs are flat lying and layered while those in the topographic lows are less regular and probably slumped. Faults predate and postdate the sediment. The age of the Alpha Ridge is estimated from its magnetic character and fossil information. The ridge's topography, sedimentary and basement structures and bedrock samples resemble those of an oceanic plateau.*

### Résumé

*Le rapport présente les données prélevées par sismique réflexion au cours de l'expédition CESAR en vue de fournir un enregistrement continu des horizons sédimentaires et du relief du socle. Les réflecteurs sédimentaires sont stratifiés et reposent à plat sur les hauteurs; dans les dépressions topographiques par contre, ils présentent un aspect moins régulier, vraisemblablement en raison de glissements. Des failles se sont produites avant et après l'accumulation des sédiments. La nature magnétique de la dorsale Alpha ainsi que les fossiles qu'elle contient permettent d'évaluer l'âge de la structure. La topographie, les structures sédimentaires, le relief du socle et les échantillons rocheux sont similaires à ceux d'un plateau sous-marin.*

### METHOD

A seismic reflection record was collected at main camp (Fig. 3.1). The record is presented here to provide control and insight for interpreting the cores and understanding the tectonic development of the Alpha Ridge. The sound source for the seismic reflection survey was a 40cu.in. airgun that was received by a single hydrophone. Analogue recording was used. The lack of ship's noise and towing turbulence enabled this simple system to record good sedimentary and basement reflections.

Some problems were encountered making the reflection system operational; no record is available to accompany piston cores 1 and 2, as the airgun was not sealing properly. This problem was eventually solved by heating the airgun untouchably hot before immersing it in the cold Arctic water. The airgun was fired once every five minutes; therefore, apparent distances on the record depend on the drift rate. The seismic reflection record must be carefully interpreted in conjunction with the navigation. The detailed track of the main ice station plotted with true distance is shown in Figure 3.2.

### RESULTS

The seismic reflection record (Fig. 3.3, in pocket) shows from 0.2 to 0.5s of layered, generally flat-lying and internally conformable sediment overlying acoustic basement. In cases where basement is irregular the sedimentary horizons follow its trend (1200z-(GMT)/134). From 1200z/123 to 1200z/134 a bottom simulating reflector (BSR) is mapped 0.15s later than the seafloor arrival. A characteristic transparent interval occurs before the onset of the B.S.R. The temperature-depth range is compatible with a gas hydrate producing the B.S.R. In some locations the bottom is offset in a step-like fashion (1200z/111 and 0000z-/125) that is probably fault controlled. Faults with greater offsets are also observed at 0000z-/120 to 0000z-/122. At these locations sedimentary reflectors terminate against basement and suggest the faults postdate the deposition of the sedimentary reflectors. The sediments on top of the uplifted block conform to basement and are gently dipping. CESAR core 6, retrieved from the sediments on the edge of this faulted portion of the ridge, contains Cretaceous fossils (Barron, 1985; Bukry, 1985).

The major valley crossed (1200z-/135 to 1200z-/140) exhibits 750m relief and is 30km across. This valley is ori-

<sup>1</sup>Atlantic Geoscience Centre, Bedford Institute of Oceanography, Box 1006, Dartmouth, Nova Scotia, B2Y 4A2

ented roughly parallel to the northern side of the Alpha Ridge as indicated on the bathymetric map of the Arctic Ocean (Johnson et al., 1979). Uplifted basement rims on the valley (0000z-/105 and 1200z-/134) occur on the northern wall which is a steep sediment-free scarp. The sediments in the valley are thicker and more chaotic than those on the plateau. The apparent flat-lying sequence in the valley between 0000z-/138 and 1200z-/138 does not exist and is an artifact of varying drift rates; that is, no motion occurred during this interval. The sediments on the southern wall and in the valley appear to be slumped. The sedimentary reflectors adjacent to the northern scarp have an onlap relationship to it (1200z-/135); truncation of sediment is more typical of a fault-produced feature which suggests the faulting here occurred prior to the deposition of the sediments. Thus, this valley may be a primary feature formed by the processes that produced the Alpha Ridge.

The seismic reflection record illustrates that basement topography is rough and irregular. One probable outcrop of

basement is a dome-shaped feature indentified on day 123. A photograph of the outcrop is shown in Figure 3.4A. It has an irregular surface texture due to thick manganese coating indicative of its long term presence on the ocean floor. It is contrasted to an ice-rafted dropstone with smooth surface and angular outline (Fig. 3.4B).

Using the available information: magnetics, refraction, dredge material and cores, it is possible to interpret the age and type of basement. Sublinear magnetic anomalies of amplitude up to 1500nT with many irregular peaks are associated with the Alpha Ridge. Basement topography and the magnetic anomalies have been shown to be correlatable (Hall, 1970), and this is also evident on the aeromagnetic map of the Arctic (Kovacs et al., in press). Thus the topographic expression of the valley is reflected in the magnetic characteristics of the ridge. If the magnetic anomalies are due to oceanic basalts the ridge must have formed during a long period of non-reversals such as the Cretaceous positive polarity chron from 80 to 120 Ma (Harland et al., 1982).

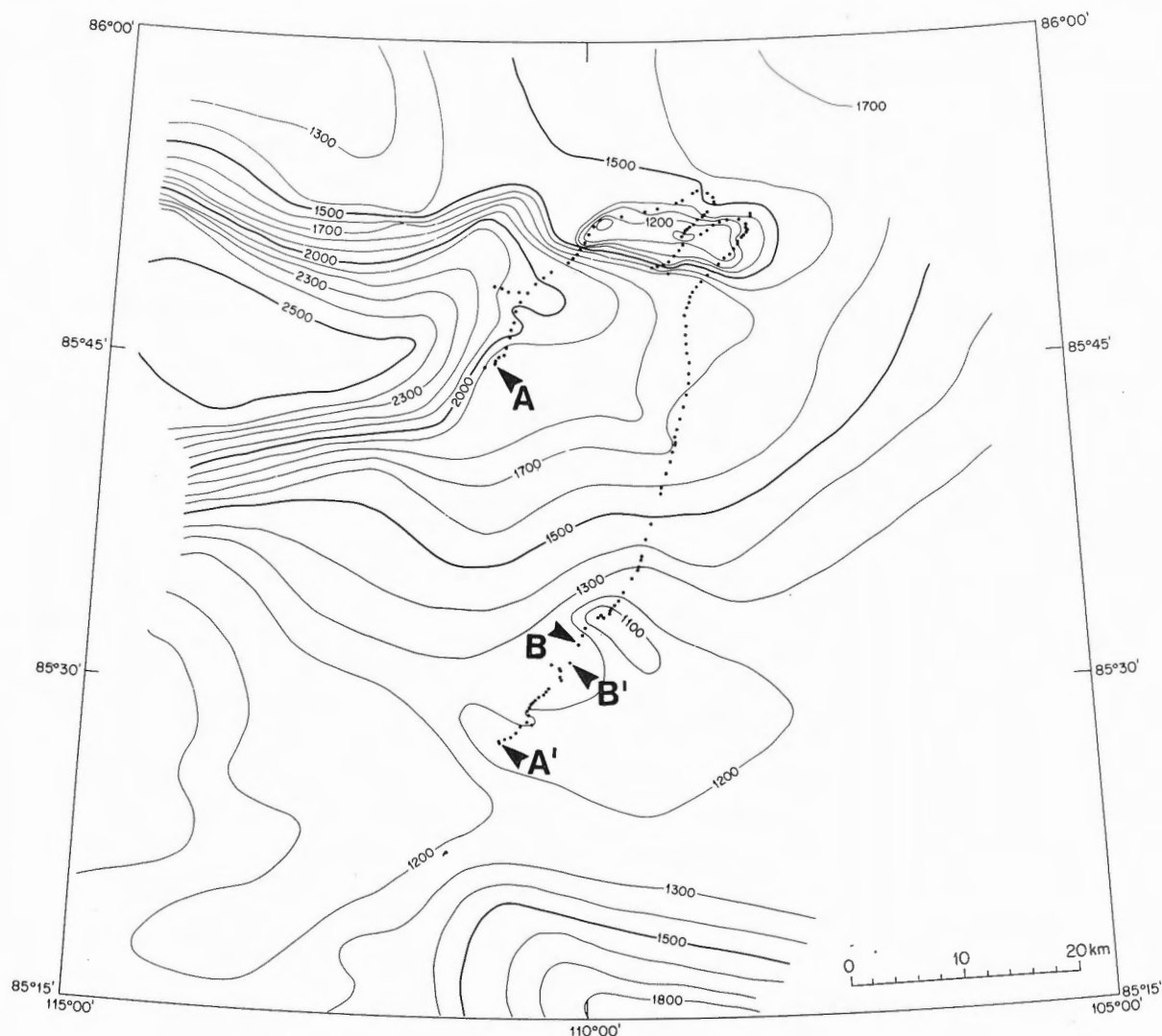


Fig. 3.1 The drift of the ice station from A to B is the region where the seismic reflection record was recorded.



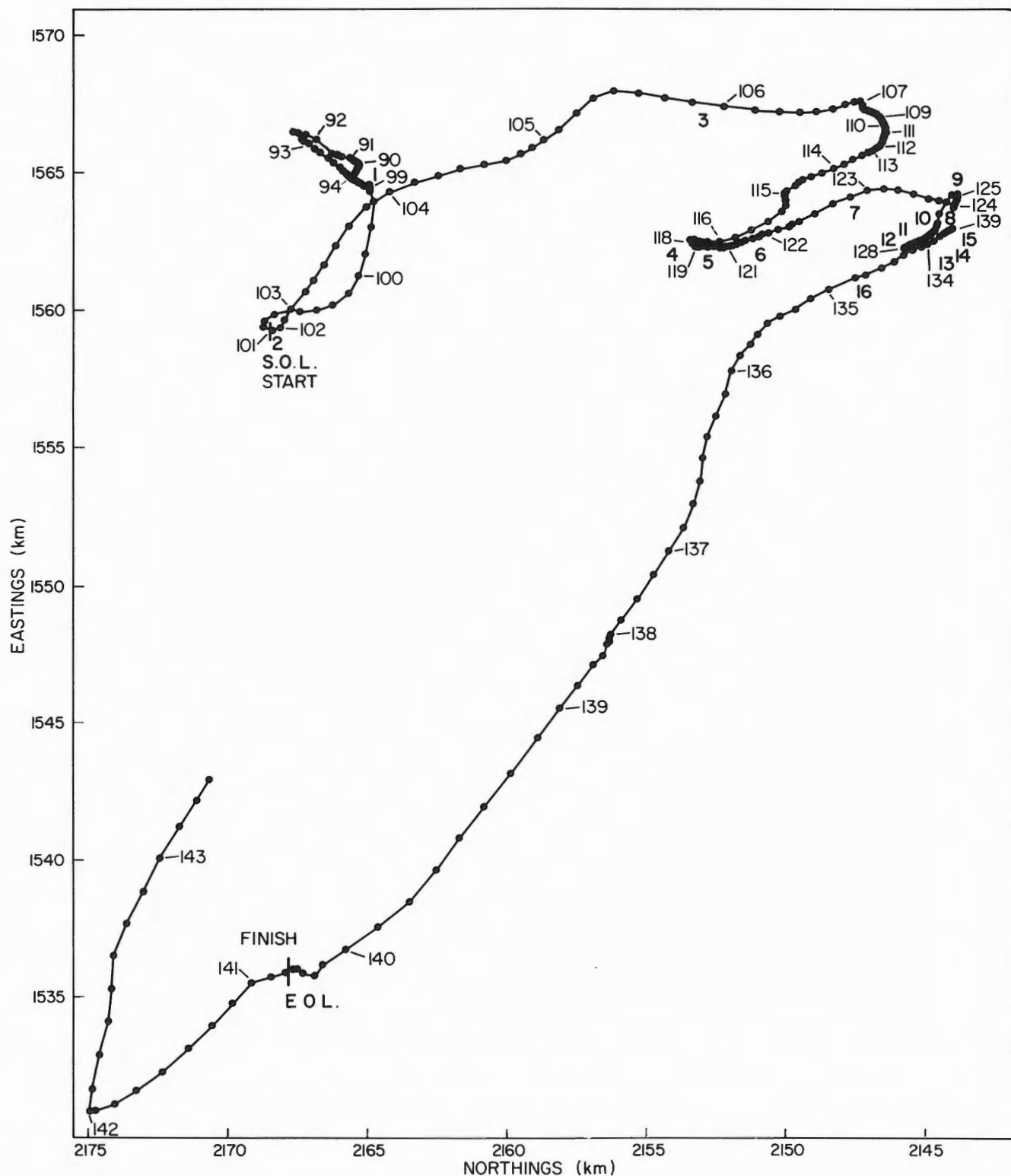


Figure 3.2 A detailed track plot with distance in kilometres is shown. The heavy type numbers are the core locations. The lighter type number are the ice camp position at 0000z- of each day. The dots are the position of the camps as a three hour mean. The start (S.O.L.) and finish (E.O.L.) refer to the seismic reflection line.



Figure 3.4A Bottom photograph, 1m by 2m, showing basement outcrop.

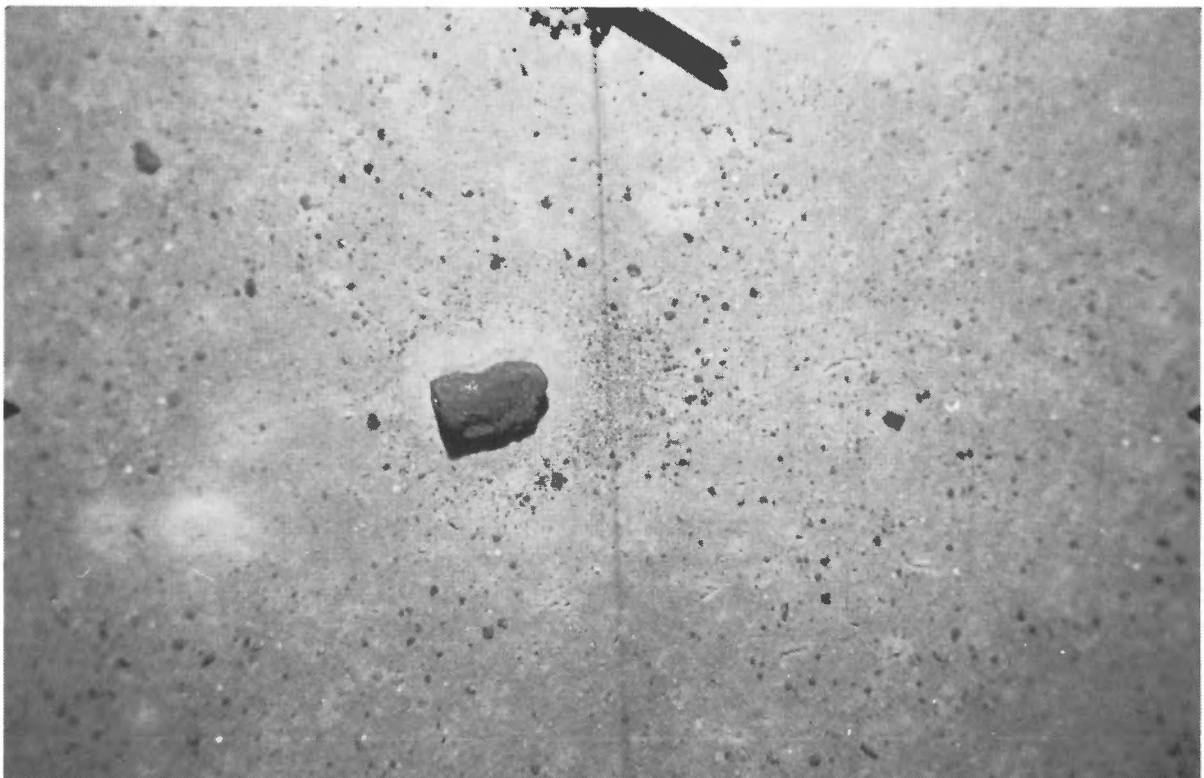


Figure 3.4B Bottom photograph, 1m by 2m, showing ice-rafted dropstone.

Preliminary refraction results show P-wave velocities for basement in the range of 4.7 to 5.2 km/s (Forsyth, personal communication), which is typical of oceanic basalts (Christensen and Salisbury, 1975). The in situ rocks from the ridge are highly altered but the texture and relict minerals suggest that they were originally an alkaline basalt (Van Wagoner and Robinson, 1985). The available information is consistent with a basaltic basement.

Information from the cores as well as magnetic data can be used to place limits on the age of the basement. Sedimentation rates of about 1 mm/1000 yr are reported (Aksu, 1985) for the upper 5 m of the section. If this rate is extrapolated through the sequence with an assumed  $2.0 \text{ km} \cdot \text{s}^{-1}$  velocity for the thin 0.2 s of sediment observed in the vicinity of core 8, then the age of the oldest sediment is 200 Ma. However, if the average sedimentation rate is adjusted upward to 1.5 mm/1000 yr for the 0.1 s of sediment observed on the reflection record above and adjacent to CESAR core 6, then this first 100 m can be estimated to be 65 Ma. This is consistent with the age of the fossils in the core. Extrapolating for the age of the lower portion of the sedimentary sequence near core 8 would produce an estimate of 130 Ma. This estimate is consistent with the magnetic anomalies which suggest Cretaceous during the positive polarity chron between 80 and 120 Ma (Harland et al., 1982).

The topography and sedimentary and basement structure of the Alpha Ridge are similar to that observed on the Manihiki Plateau. The Manihiki Plateau is a large area ( $0.5 \times 10^6 \text{ km}^2$ ) of shallow water depth in the Pacific. The plateau has a system of deep internal troughs that are oriented roughly parallel to one of the boundaries of the plateau. In cross-section the troughs are similar to those observed on the Alpha Ridge; that is, they are steep-sided basins with basement rims. The troughs on the Manihiki Plateau are thought due to dip-slip motion or to be grabens formed along transform faults. On this plateau faulting is frequent and it is difficult to assess the amount of it that is due to the process that formed the feature and the degree of tectonism that occurred subsequently.

The rocks dredged from the Manihiki Plateau have all been highly altered basalts and volcanic breccias; in situ samples of the Alpha Ridge are weathered fragmental volcanic rocks. Segments of the Manihiki Plateau are associated with magnetic amplitudes of 1000 nT. The anomalies follow the trends in basement relief. Magnetic anomalies caused by topography suggest the plateau formed during a time interval with no magnetic reversals. Seismic refraction measurements revealed an oceanic layer two velocity 10 km thick overlying layer three of undetermined thickness (Winterer et al., 1974).

The sediments on the highs of the Manihiki Plateau are about 0.5 km thick and are layered and continuous. In contrast, in the troughs the sediments are 1 km thick and have clastic reflectors thought to be deposited by slumping. The deeper reflectors and basement are offset by faulting. The top of the sedimentary section is not always disturbed by the faults (Winterer et al., 1974).

The resemblance of many features from the reflection profile of the Alpha Ridge to those observed on records from

the Manihiki Plateau provides an analogue for comparison and insight into the structure of the Alpha Ridge. Although even the better studied Manihiki Plateau is not well understood it is considered to be oceanic crust of Cretaceous age (Winterer et al., 1974).

## REFERENCES

- Aksu, A.E.  
1985: Paleomagnetic stratigraphy of the CESAR cores; in Initial Geological Report on CESAR — The Canadian Expedition to Study the Alpha Ridge, Arctic Ocean, ed. H.R. Johnson, P.J. Mudie and S.M. Blasco; Geological Survey of Canada, Paper 84-22, report 7.
- Barron, J.A.  
1985: Diatom biostratigraphy of the CESAR 6 core; in Initial Geological Report on CESAR — The Canadian Expedition to Study the Alpha Ridge, Arctic Ocean, ed. H.R. Johnson, P.J. Mudie and S.M. Blasco; Geological Survey of Canada, Paper 84-22, report 10.
- Bukry, D.  
1985: Correlation of Late Cretaceous Arctic silicoflagellates from Alpha Ridge; in Initial Geological Report on CESAR — The Canadian Expedition to Study the Alpha Ridge, Arctic Ocean, ed. H.R. Johnson, P.J. Mudie and S.M. Blasco; Geological Survey of Canada, Paper 84-22, report 9.
- Christensen, N.I. and Salisbury, M.H.  
1975: Structure and constitution of the lower oceanic crust; Reviews of Geophysics and Space Physics, v.13, p. 57-86.
- Hall, J.K.  
1970: Arctic Ocean Geophysical Studies: The Alpha Cordillera and Mendeleev Ridge; Lamont Doherty Geological Observatory, Technical Report No. 2, 125 p.
- Harland, W.B., Cox, A.V., Llewellyn, P.G., Pickton, C.A.G., Smith, A.G., and Walters, R.  
1982: A Geologic Time Scale; Cambridge University Press, 131p.
- Johnson, G.L., Monahan, D., Gronlie, G., and Sobczak, L.  
1979: General Bathymetric chart of the Oceans (GEBCO); Polar Sterographic Projection published by the Canadian Hydrographic Service, Ottawa, Canada.
- Kovacs, L.C., Bernero, C., Johnson, G.L., Pilger, R.H. Jr., Taylor, P.T., and Vogt, P.R.  
— Residual Magnetic Anomaly Chart of the Atlantic Ocean: Geological Society of America (in press).
- Van Wagoner, N.A. and Robinson, P.T.  
1985: Petrology and geochemistry of a CESAR bedrock sample: implication for the origin of the Alpha Ridge; in Initial Geological Report on CESAR — The Canadian Expedition to Study the Alpha Ridge, Arctic Ocean, ed. H.R. Johnson, P.J. Mudie and S.M. Blasco; Geological Survey of Canada, Paper 84-22, report 5.
- Winterer, E.L., Lonsdale, P.F., Matthews, J.L., and Rosendahl, B.R.  
1974: Structure and acoustic stratigraphy of the Manihiki Plateau; Deep-Sea Research, v. 21, p. 793-814.





## BOTTOM PHOTOGRAPHY AND SEDIMENT ANALYSES ON CESAR

C.L. Amos<sup>1</sup>

Geological Survey of Canada

Amos, C.L., *Bottom photography and sediment analyses on CESAR*; in *Initial Geological Report on CESAR — the Canadian Expedition to Study the Alpha Ridge, Arctic Ocean*, ed. H.R. Jackson, P.J. Mudie and S.M. Blasco; Geological Survey of Canada, Paper 84-22, p. 25-45, 1985.

### Abstract

An evaluation is made of the sediment transport pathways which lead to the accumulation of the bottom material in the vicinity of the Alpha Ridge. An estimate is also given of the sources of the material, the factors controlling deposition and, where appropriate, on the accumulation rates. Biogenic material, ice-rafted debris and weathered bedrock by-products make up the majority of the seabed sediment. The relative abundance of each component varies from the Alpha Ridge crest to the trough. Minor amounts of eolian-derived debris were detected in the pack ice and yet lower amounts of inorganic debris were measured in the water column.

Ice-rafted pebbles and cobbles were generally rounded and calcareous. Which suggests a source from a coastal region on the adjacent Canadian landmass.

The recovery of bedrock in the dredging program verifies the occurrence of outcrops on the south flank of the northern Alpha Ridge crest. The samples recovered are (1) well weathered basalts which have an elemental composition similar to floes sampled in the ice pack and water column, and (2) from fine grained sediment samples recovered from adjacent basins. A local bedrock source of bottom sediments had not hitherto been considered significant.

### Résumé

Le rapport présente une évaluation des trajectoires suivies par les sédiments qui se sont accumulés sur le fond océanique aux alentours de la dorsale Alpha. Il évalue également les sources des matériaux, les facteurs contrôlant l'accumulation et, le cas échéant, les vitesses d'accumulation. La plupart des sédiments du fond océanique se composent de matériaux organogènes, de débris glaciels et de sous-produits de l'érosion du socle rocheux. L'abondance relative de chacune des composantes varie de la crête à la dépression de la dorsale Alpha. De petites quantités de débris éoliens ont été identifiées dans la banquise et des quantités encore plus réduites de débris inorganiques ont été décelées dans la colonne d'eau.

Les galets et les gros cailloux glaciels sont généralement arrondis et calcaires, ce qui porte à croire qu'ils proviennent d'une région côtière sur la masse continentale contiguë du Canada.

Les échantillons de socle rocheux prélevés par dragage confirment l'existence d'affleurements sur le flanc sud de la crête nord de la dorsale Alpha. Ces échantillons comportent (1) des basaltes fortement altérés dont la composition élémentaire est similaire à celle des flocons échantillonnés dans la banquise et dans la colonne d'eau et (2) des sédiments à grains fins provenant des bassins contigus. Une source locale de sédiments du fond dérivés du socle rocheux n'avait pas jusqu'ici été jugée importante.

<sup>1</sup>Atlantic Geoscience Centre, Bedford Institute of Oceanography, Box 1006, Dartmouth, Nova Scotia, B2Y 4A2

## INTRODUCTION

The sources of sediment comprising the unconsolidated Cenozoic sequence in the region of the Alpha Ridge have been speculated over, but no systematic analysis of the various sediment transport pathways had been made. Thus uncertainty remained over the depositional history of the region and the processes which control the lithology and rate of accumulation of the sequence.

The purpose of this study was to sample the particulate matter, both at the seabed and along the transport paths in order to determine sediment source, and to quantify, where possible, the contributions of each source to the sedimentary cover. This was achieved by adopting a number of accepted techniques such as filtration of the ice cover melt water and water column for particulate matter and subsequent elemental analysis using electron microscopy, by seabed sampling and photography, and by the application of sedimentation laws to the observations.

Due to the limitations imposed by drift rate, sampling strategy and breakdown, the data recovered were not necessarily representative of the region as a whole and therefore results should be considered only as a guide to the nature and origin of sediments at the Alpha Ridge. The results reported are tentative and may be subject to change as further analyses and interpretation are made.

## ACKNOWLEDGMENTS

I thank Ruth Jackson, K.W. Asprey and H. Wiele for their support at the CESAR Camp, F. Cole for analysis of the microfauna and production of Plate 4.4, and P. Stoffyn for

assistance with SEM work and EDAX analysis. Ruth Jackson, Peta Mudie, D.J.W. Piper and S. Bell reviewed this manuscript; their comments were of great value.

## BOTTOM CAMERA STATIONS

Camera stations were occupied at regular intervals between 17 April 1983 (day 117) and 3 May 1983 (day 133). The UMEL camera was used on the frame designed by N. Fenerty (Bedford Institute of Oceanography, Photographic Laboratory) for use on ice station AIDJAX. The camera frame used in this program was originally designed to be lowered through 40cm diameter hydroholes. The frame, which is about 2m in length, was deemed not appropriate to the hydroholes cut at CESAR (a more conventional frame, such as those used at sea, may be easier to handle and should be considered for future ice camps). A trip weight, which fired the camera, was suspended 2m below the frame. The resulting field of view of photographs was approximately 1 × 2m (lens focal length: 35mm). Table 4.1 shows the camera stations occupied in association with the latitude, longitude, water depth, and general bottom conditions. Both black-and-white and colour slides were used in the program. A total of 605 useable seabed photographs were taken during 14 lowerings. No results were obtained from stations 1, 6 and 7.

The positions of the camera lowerings relative to regional bathymetry are shown in Figure 4.1. The lowerings cover a range in depths from 1160 to 1690m. The shoalest point is situated on the crest of an eastward-plunging sub-ridge in the northern Alpha Ridge chain. The deepest lowering was situated in the trough (Alpha Ridge graben) south of the northern Alpha Ridge crest.

Table 4.1. CESAR bottom camera stations

Station no.	Film type	No. of exposures	Day/ time (GMT)	Latitude (°N)	Longitude (°E)	Water depth (m)	Description
1	B & W	—	117, 2200	85° 53' 0.5"	251° 15' 39.1"	—	Flash did not work.
2	B & W	63	118, 2230	85° 52' 58.4"	251° 18' 40.6"	1500	Flocculated silts with rounded dropstones.
3	B & W	50	119, 2330	85° 52' 49.4"	251° 20' 53.0"	1530	Flocculated silts with rounded dropstones.
4	B & W	80	120, 1830	85° 52' 45.4"	251° 22' 11.8"	1520	Flocculated silts with rounded dropstones.
5	Colour	40	121, 2130	85° 52' 24.9"	251° 21' 41.0"	1490	Gravelly, silts with dropstones.
6	—	—	—	—	—	—	—
7	—	—	—	—	—	—	—
8	B & W	90	125, 2200	85° 49' 49.4"	250° 52' 37.0"	1630	Gravelly, silts with dropstones.
9	B & W	83	127, 1700	85° 49' 32.2"	250° 45' 12.8"	1680	Gravelly, silts with dropstones.
10	Colour	30	129, 1530	85° 49' 29.4"	250° 45' 35.3"	1690	Scouring around dropstones.
11	B & W	50	130, 1530	85° 49' 34.2"	250° 50' 30.9"	1630	Gravelly silt with dropstones (scour around dropstone).
12	B & W	10	131, 2400	85° 50' 8.3"	251° 0' 29.4"	1282	Gravelly silt with dropstones (scour around dropstone).
13	B & W	13	132, 1900	85° 51' 4.3"	251° 14' 9.6"	1195	Gravelly silt with dropstones (scour around dropstone).
14	B & W	96	133, 0130	85° 51' 31.5"	251° 21' 55.9"	1222–1160	V. gravelly silt with dropstones (scouring visible abundant bioturbation and starved ripples).
		605					

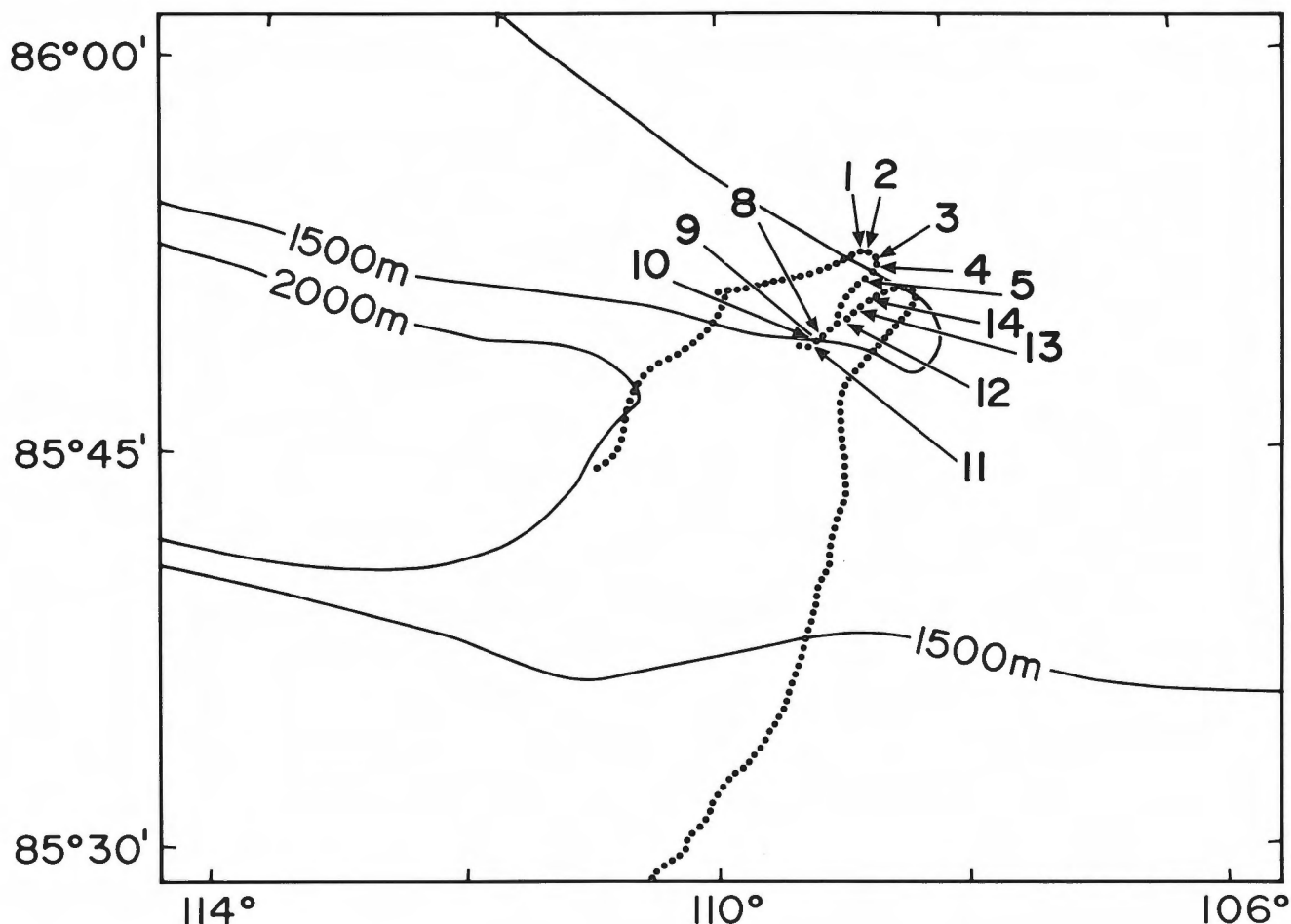


Figure 4.1 Position of CESAR bottom camera stations.

Lowerings 2 to 9 (Plate 4.1) all show similar seabed character. The sediment is bimodal in constituent grain sizes and reflects two modes of origin. The fine matrix of clayey material, which is easily suspended, is thought to be derived principally from the erosion of bedrock which outcrops locally.

The second mode is a coarser fraction, which shows a gradation in size from fine sand to boulders. The gravel size material occurs with random distribution and, where observed, was restricted almost exclusively to the surface (drag marks of the trip weight show an exposed, well sorted fine sediment beneath the surface veneer). These coarser sediments are considered to be ice-rafted and subsequently released from melting multiyear ice. No postdepositional transport of either the finer or coarser fraction was evident. The gravelly "dropstones" show a variety of shapes and sizes consistent with the findings of Schwarzacher and Hunkins (1965). However, many are subrounded to rounded suggesting previous reworking in a fluvial or beach environment. Schwarzacher and Hunkins (1965) and Crombie (1960), by contrast, suggested the source of the dropstones is glacial till.

The gravel fraction shows no evidence of burial, as the clasts always occurred with an Fe/Mn coating. It is thus inferred that the deposition rate of fine grained sediment is

extremely slow. This is consistent with the previous studies of Clark et al. (1980).

The impact marks of the 5kg trip weight was never greater than approximately 1cm (depth inferred from shadow length). The inference thus made is that the sediment is well compacted, suggesting an extremely low deposition rate.

Bottom currents have been interpreted from the bottom photographs. They are based on sediment drift rates of the trip weight impact plume observed from frame to frame. The drift rates are 1-2cm s<sup>-1</sup> to the west at stations #2, 5, and 8, and 1-2cm s<sup>-1</sup> to the south at station #4. Hunkins et al. (1960) observed flows of less than 1cm s<sup>-1</sup> from the Alpha station, while Hall (1979) working in the same region, reported a near bed flow of 1cm s<sup>-1</sup>. Hunkins et al. (1969), in a similar fashion, measured bottom currents of 4-6cm s<sup>-1</sup>.

Successive trip weight impact prints were seen from image to image of the bottom photographs. The distance between impacts shows an ice drift rate of approximately 20cm min<sup>-1</sup> or less. On the short term it appears that the ice moves in bursts of motion, separated by short intervals of no motion. Furthermore, the direction of ice drift appears to fluctuate  $\pm 30^\circ$  about the net drift direction. It should be noted, however, that some of the above observations may be

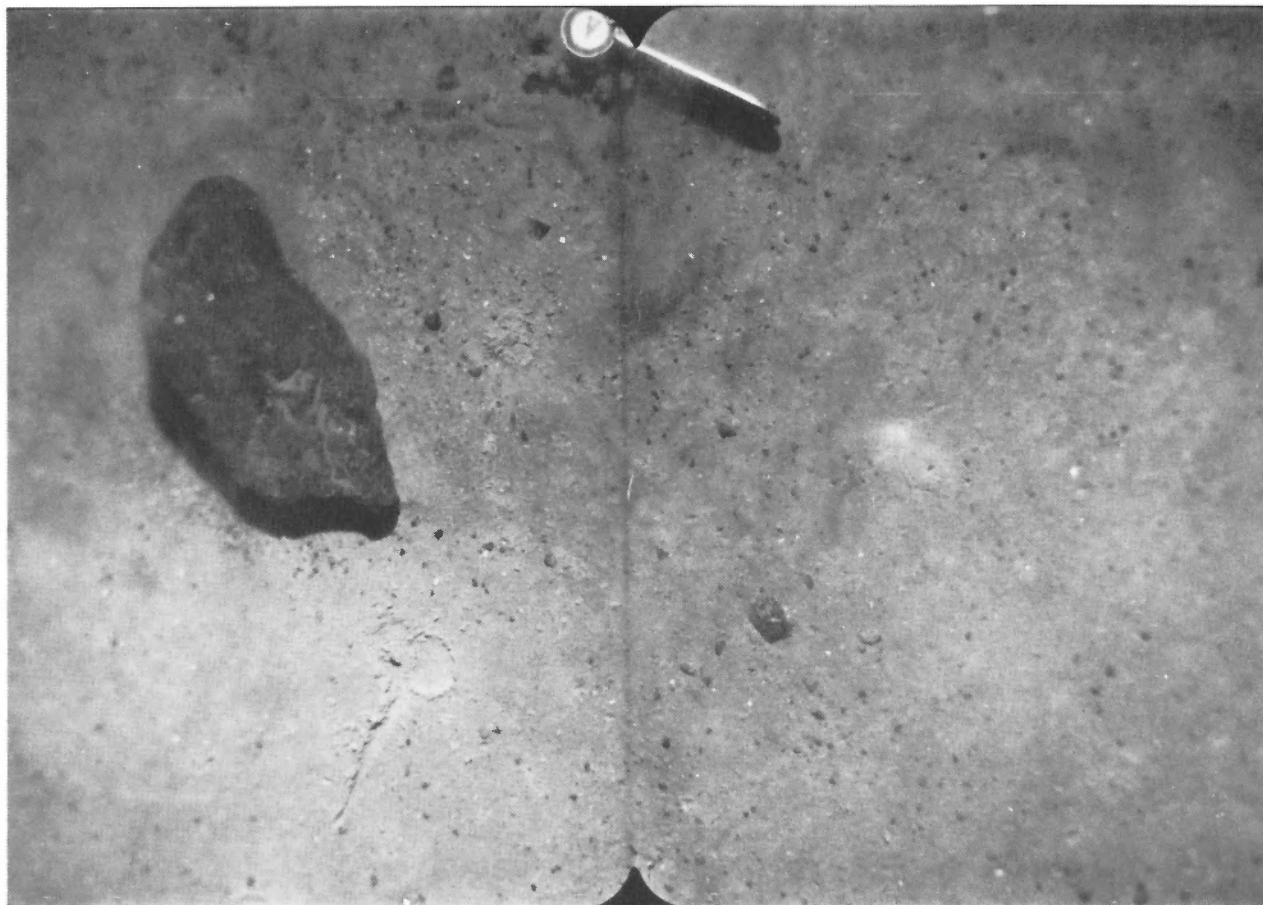


**Plate 4.1**

Seabed at site 9, 1680m water depth, showing poorly sorted, randomly distributed coarse material on a well compacted surface of well sorted fine sediment. Field of view  $1 \times 2\text{m}$ .

the result of variations in the wire angle on which the camera is suspended.

All photographs from stations #2 to 10 show some evidence of bioturbation. The surface is covered with a film of what appears to be organic debris. Bioturbation is greatest in the deepest stations #8, 9, and 10. Star-shaped imprints are common. These imprints are approximately 15cm in diameter and usually have 6 radial arms. Gravel fragments, considered to have been derived from ice rafting, litter the seabed in a random fashion (Plate 4.1).

The results from stations #9 to 14 show a gradual increase in the gravel fraction and decrease in the finer mode as the bathymetry shoals from 1680 to 1160m. Station #11 shows a gravel cover of 30% (by area) and an irregular distribution of material. Haloes around the larger fragments are seen, but are considered biogenic in view of the abundant trail marks. Station #12, in 1282m of water, shows a gravel cover of 50%. No evidence of any currents were observed. Station #13, in 1195m of water, shows a 70% gravel cover. The increase in gravel is paralleled by a decrease in evidence of bioturbation. Crombie (1960) observed a coarsening of bottom sediments over the Alpha cordillera, but offered no explanation of the processes responsible for the trend.

Station #14, the shoalest station (1160m water depth), shows 70 to 100% gravel cover (Plate 4.2). Only a small sediment plume was given off by the impact of the trip weight at the seabed, indicating a prior winnowing of the ubiquitously deposited fine grained material. The trip weight imprint is scarcely visible, showing that the seabed is relatively hard. The gravel is weakly aligned parallel to the current observed from adjacent stations and shows a motion to the southwest. Scour marks around cobbles show typical current scour patterns with asymmetric tails which are oriented east and west. Such marks are considered not to be associated with a biogenic origin.

Starved ripples were observed at station #14 (Plate 4.3). The ripple crests are interpreted to be oriented  $90^\circ$  to the flow direction. These ripples appear to be composed of sand-size Fe/Mg rich micromodules. The crests of the ripples are rounded and undulate in plan view. Such features are usually formed by near bed unidirectional flows of about  $20\text{cm s}^{-1}$  (Middleton and Southard, 1978). No ripple marks are present in the bottom photographs described by Cromie (1960) and Schwarzacher and Hunkins (1965). Therefore their occurrence is unusual and the distribution of these features is considered to be limited. This is probably due to the paucity



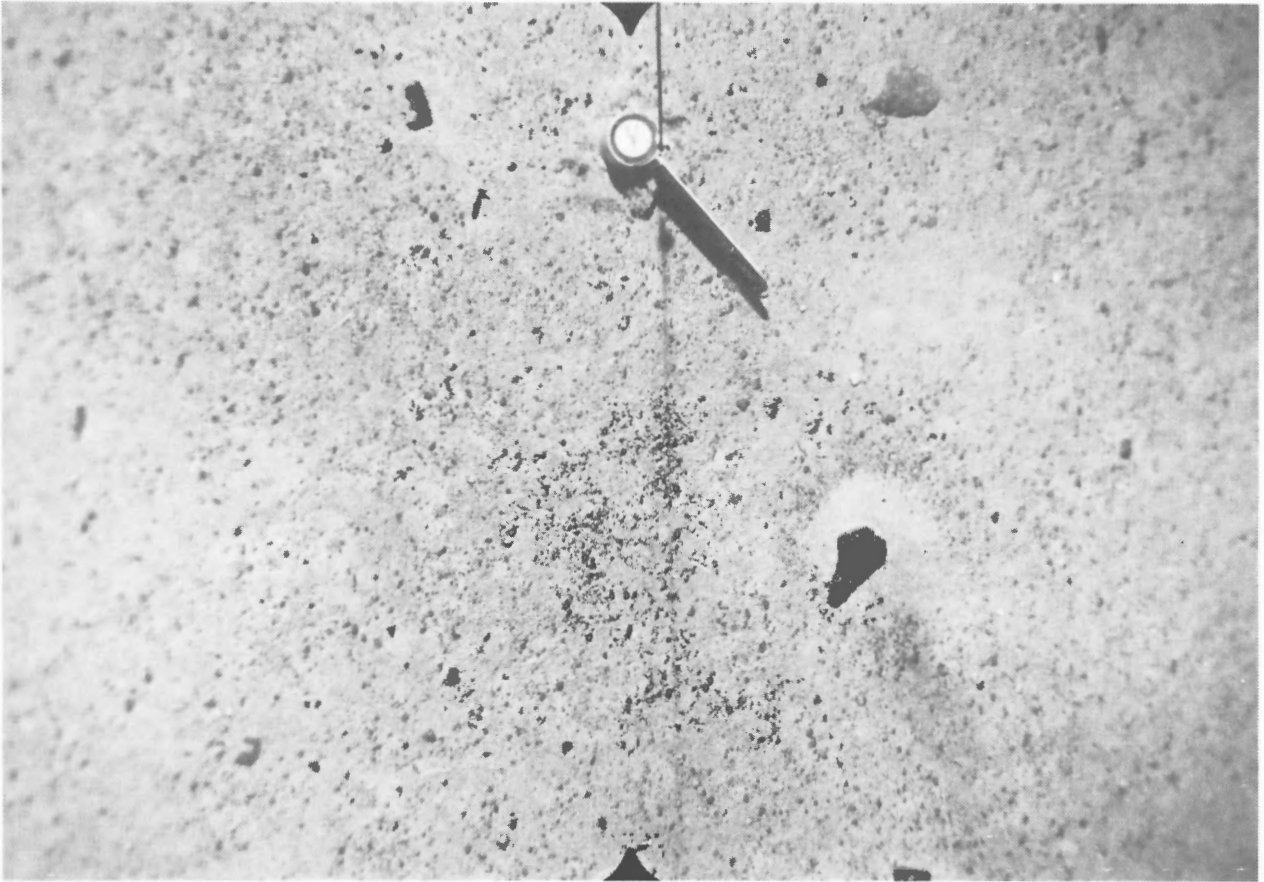


**Plate 4.2**

The seabed at site 14 (1160m water depth) showing a dense gravel cover comprising a relatively hard seabed. Scour current patterns around cobbles show east-west orientation. Field of view  $1 \times 2$ m.

Bedrock is thought to outcrop at the surface at station #10 (see Fig. 4.2). Analysis of this material recovered in dredges show it to be well weathered basalt (Van Waggoner and Robinson, 1985). The outcrop shows evidence of in situ fracturing and mechanical breakdown. The breakdown of the exposed bedrock surface appears to be providing clay material to the adjacent deeper troughs. Herman (1974), who classified bottom sediment into six types on the basis of source and mode of transport, does not consider seabed weathering of bedrock. Yet in the region pertaining to this study it appears to be a dominating supplier of fine grained material.

## DISCUSSION

The change in bed texture from pelagic deposition in 1600m of water, to a winnowed, hard gravelly bed in 1100m of water is difficult to explain. It is not associated with surface wave activity (due to depth of water and ice cover). Moreover, there was no obvious water column stratification or vertical variation in water mass. Thus sedimentation is likely related

to the winnowing of the sub-ridge crest by the infrequent passage of near-bottom storm driven currents. The troughs between the sub-ridges appear to be regions of accumulation of ponded sediment. Such sedimentation patterns are not always expected in the deep sea, where conformable bedding, as defined by Piper et al. (1983) is often more appropriate. The relative sheltering of the troughs suggests storm currents moving transverse to the ridge system, i.e. possibly in the north-south quadrants.

Clark et al. (1980) plotted the distribution of coarse sediment (greater than 64 microns) in the bottom sediments over the Alpha cordillera. They show the highest proportions (approximately 25%) to occur on the south flank of the ridge. This is the site of bedrock outcrop and perhaps argues for a significant supply of seabed material by weathering and dispersal of local material.

## BOTTOM DREDGING

Dredging was attempted at 18 sites from 10-20 April 1983 (day 110-120) and in water depths ranging from 1040-2050m. A list synthesizing the dredging activities is given in Table 4.2. The positions of the dredge sites in relation to the camp drift is shown in Figure 4.2.

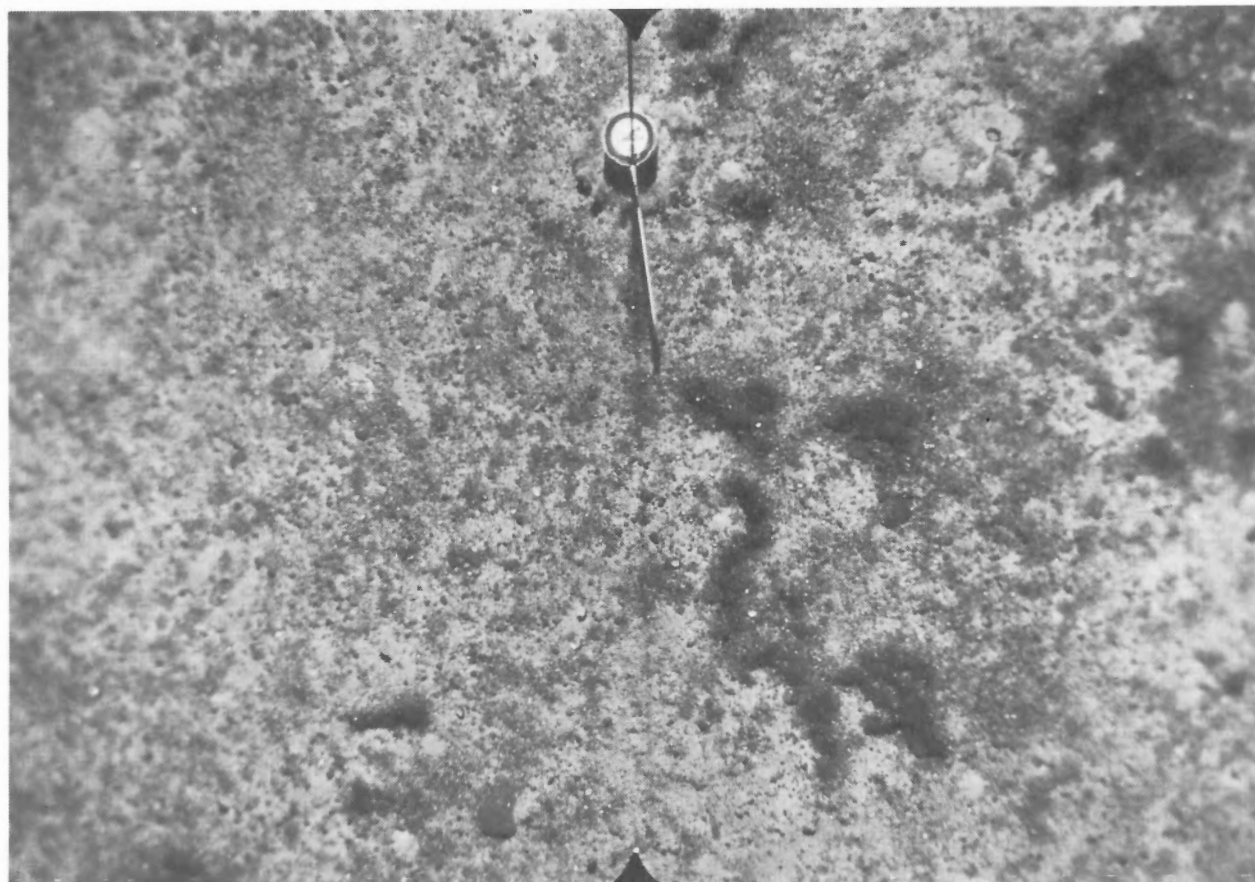


**Plate 4.3**

Seabed at site 14, 1160m water depth, showing undulating ripples with rounded crests, formed in sand. Field of view 1 × 2m.

**Table 4.2. CESAR bottom dredge stations**

Station no.	Day – Time (Down)	Latitude (°N)	Longitude (°E)	Water depth (m)	Time up (GMT)	Description
D1	110, 1200	85° 45' 38.9"	249° 10' 46.5"	1850		No recovery – one dropstone.
D2	110, 2400	85° 45' 5.9"	249° 3' 13.6"	1890	0800	No recovery.
D3	112, 2100	85° 45' 22.6"	249° 7' 37.6"	1850	0110	No recovery.
D4	113, 0140	85° 45' 36.8"	249° 8' 23.6"	1852	0700	Rock samples + mud.
D5	113, 1540	85° 47' 5.4"	249° 13' 27.4"	2050	2130	Rock samples + mud.
D6	113, 2230	85° 48' 1.1"	249° 17' 27.5"	2000	0530	No recovery.
D7	114, 0550	85° 49' 4.0"	249° 32' 23.3"	1984	1630	Trace of fine material.
D8	114, 1730	85° 50' 0.7"	249° 51' 6.0"	1850	0016	Dropstones.
D9	115, 0030	85° 50' 24.7"	249° 55' 45.1"	1650	0520	No recovery – high tension on cable.
D10	115, 0540	85° 51' 7.4"	250° 1' 30.5"	1100	1620	Bedrock & dropstones.
D11	115, 1630	85° 51' 52.9"	250° 15' 20.3"	1040	2300	No recovery.
D12	115, 2330	85° 52' 11.3"	250° 38' 10.2"	1200	0400	One dropstone.
D13	116, 0430	85° 52' 18.8"	250° 46' 21.8"	1380	1540	Muddy sediment with one dropstone.
D14	116, 1600	85° 52' 49.6"	251° 6' 8.5"	1450	2330	No drift of ice.
D15	117, 0440	85° 53' 8.1"	251° 12' 39.7"	1500	1650	No drift of ice-mud on bucket.
D16	118, 0120	85° 53' 0.6"	251° 15' 36.9"	1550	2109	No recovery.
D17	119, 0600	85° 52' 58.9"	251° 18' 54.4"	1550	2012	No recovery.
D18	120, 0630	85° 52' 44.7"	251° 21' 49.8"	1500	1639	No recovery.

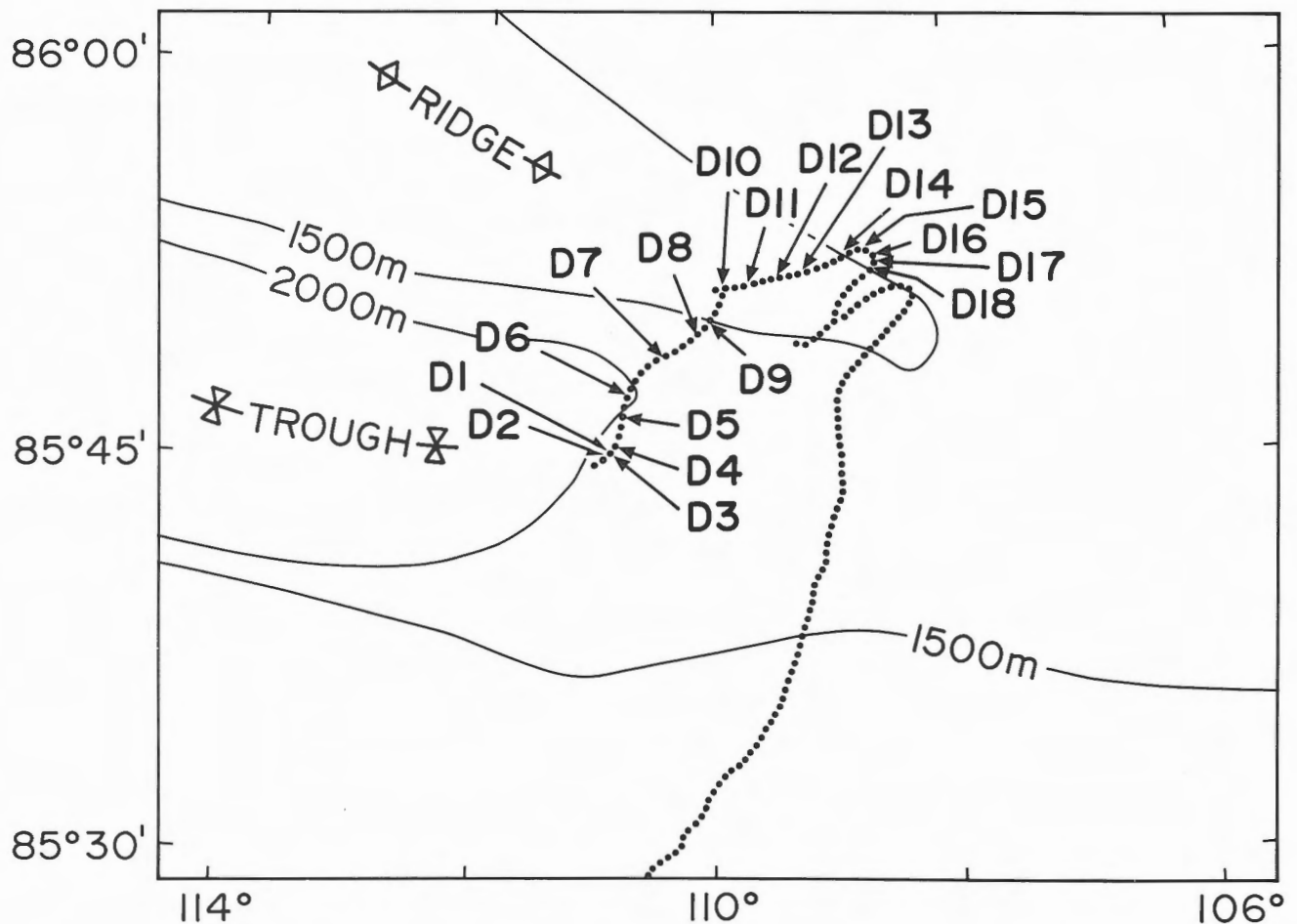


Figure 4.2 Position of CESAR bottom dredge samples.

The recovery of bottom material was variable due to the low drift rate of the ice and due to variations in bottom roughness. Material dredged from the deeper trough (D1-D7) was composed of a fine grained plastic ooze which was recovered interspersed with granule- and cobble-sized fragments. In general the size frequency histogram of bottom sediments follows closely type IV sediments recovered by Clark et al. (1980) over the Alpha cordillera (see Fig. 4.4 A to I).

The sand-sized sediment (greater than  $63\mu\text{m}$ ) is typically bimodal. The finer mode is composed of angular grains of clear and yellow stained quartz ( $d_{50}$ :  $100\text{--}200\mu\text{m}$ ) which comprise approximately 40% of the mode, and biogenic material which comprises the remainder. The biogenic material is composed predominantly of globigerinids ( $d_{50}$ :  $200\mu\text{m}$ ), benthic foraminifera ( $d_{50}$ :  $800\mu\text{m}$ ) and sponge spicules (Plate 4.4, Table 4.3). The allogenic material of the finer mode is well sorted, reflecting hydraulic transport. The quartz is associated with a subpopulation of semiprecious metals and mafics which have a modal size of  $100\mu\text{m}$ . These fragments are considered to be hydraulically equivalent to the angular siliceous material. The population, by virtue of its composition, is considered to be derived by ice rafting. A

discussion of the original sources of this ice-rafted material will be given later.

The coarser mode is poorly sorted and shows a gradation in size from  $800\mu\text{m}$  to  $0.3\text{m}$ . This mode is composed predominantly of well rounded quartz and lithic fragments which are partially Fe/Mn stained. It comprises very little biogenic debris. This mode is considered to be derived by the process of ice rafting. The material entrapped in the pack-ice is released during summer melting and is dropped in situ. The distribution of this material is therefore not controlled by bathymetry. The Fe/Mn coating (usually restricted to one side) shows no postdepositional transport and indicates extremely slow sedimentation rates.

Four dropstones were recovered in dredge D4 and five in dredge D5. Macroscopic analysis and acid testing suggest that they are predominantly composed of dolomite, with minor amounts of calcite. One of the fragments was composed of yellow stained gypsum (Table 4.4). The majority of these hand specimens are very well rounded and lack fracturing or pitting typical of a glacial origin. It is thought that they were incorporated into the ice after either a period of fluvial transport to the coast, or by reworking in a beach zone.

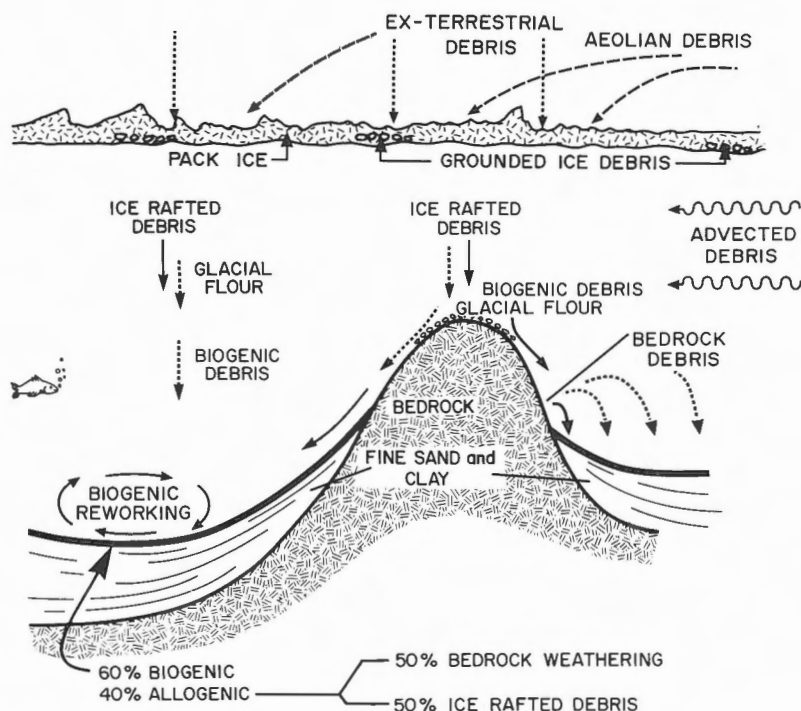


Figure 4.3 Sketch depicting the main sources of sediment supplied to the seabed of the northern Alpha Ridge crest and graben.

Dropstones recovered by Crombie (1960) from the same general region were reported to be principally composed of limestone. Schwarzacher and Hunkins (1965) described both angular and well-rounded dropstones from 8 dredges carried out to the west of the Alpha Ridge. These samples were predominantly sandstone and shale with 20 to 50% of fragments composed of dolomite. We recovered, by contrast, only one sample composed of sandstone/shale.

Dolomite and limestone is abundant on eastern Bathurst Island (Disappointment Bay Formation) and on the north coast of Ellesmere Island (Wilderness Carbonates of Ordovician age). These formations are considered to be the sources of the dropstones. The similarity in clast compositions is remarkable, and suggests a longstanding constant drift pattern of the polar ice pack.

Six dropstones recovered in dredge D8 are similar in composition (dolomite) to those recovered from the deeper trough to the south (D5). Two of the samples were composed of carbonaceous dolomite perhaps associated with the Ellesmere Island Wilderness Carbonates.

The most significant recovery was made during dredge D10, which recovered what we consider to be fragments of bedrock interspersed with 7 ice-rafted dropstones. The bedrock material showed "fresh" surfaces of well weathered basalt and an upper surface of manganese encrusted serpulid tubes (G. Gross, personal communication, 1985). The bedrock samples were recovered from the steeply dipping south flank of the northern Alpha Ridge crest (see Table 4.2) and were associated with extremely high wire tension, chattering of the dredge bucket and an acoustically "hard" seabed. Mineralogical and chemical analysis of the bedrock sample is given by Van Wagoner and Robinson (1985). A cursory binocular microscope examination of the sample suggests it is

well weathered pyroclastic basalt. The dominant constituent is well weathered feldspar which has become broken down to friable pseudomorphs. The weathering of the feldspar and its subsequent dispersal is considered to produce the finer (silt/clay and fine sand) material of the local surficial sediments.

The northern Alpha Ridge crest was sampled during dredges D11, D12, and D13. Sand or fines (silt/clay) were recovered only in dredge D13. Similar sediment characteristics to those in dredge samples D4 and D5 were observed, except that much less clayey material and a higher percentage of iron-stained quartz was present.

One dropstone was recovered in each of dredges D12 and D13. These samples were composed of siltstone and dolomite respectively. Both specimens were well rounded.

The interpretation of the regional pattern of sedimentation is depicted in Figure 4.3 and the grain size statistics are given in Table 4.5. Ice-rafted debris is deposited over the entire seabed irrespective of topography. This material is principally derived from the Ellesmere Island coast (or Axel Heiburg and North Greenland as suggested by Schwarzacher and Hunkins, 1965) and is composed of an entire spectrum of sizes (up to 0.3m in diameter).

Biogenic debris in the form of globigerinids, foraminifera, radiolaria, sponge spicules and ostracods are deposited pelagically and appear to collect preferentially in the deeper areas. This source comprises approximately 40% of the sand size fraction on the ridge crest and 60% in the trough centre.

The inorganic silt and clay fractions are interpreted to be derived from three major sources: (1) breakdown of bedrock outcropping on the flanks of the northern Alpha Ridge; (2) ice rafting; and to a lesser extent (3) advection in the water column.



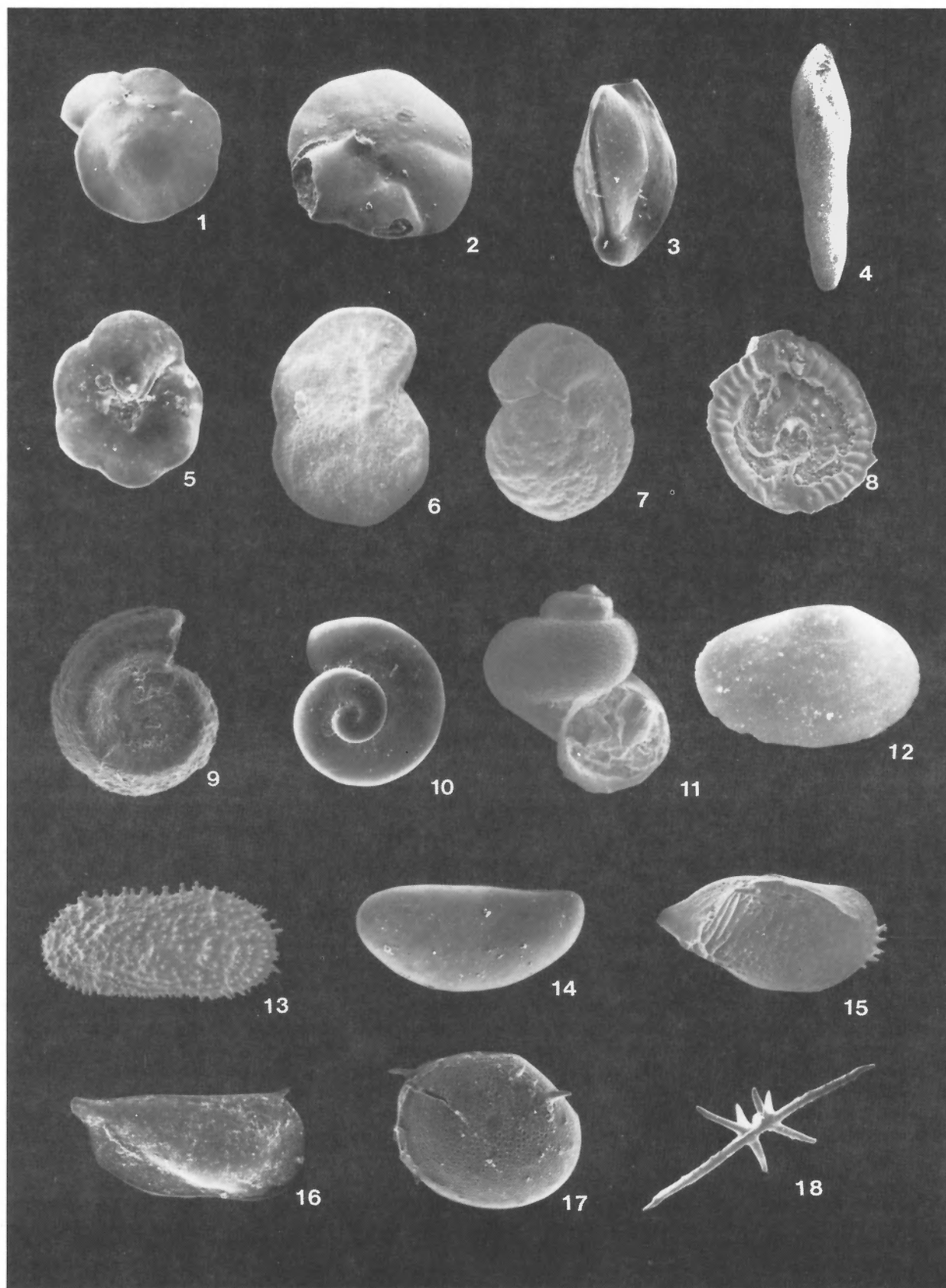


**Plate 4.4**

SEM photographs of benthic foraminifera, molluscs, ostracods and sponge fragments from CESAR dredge samples.



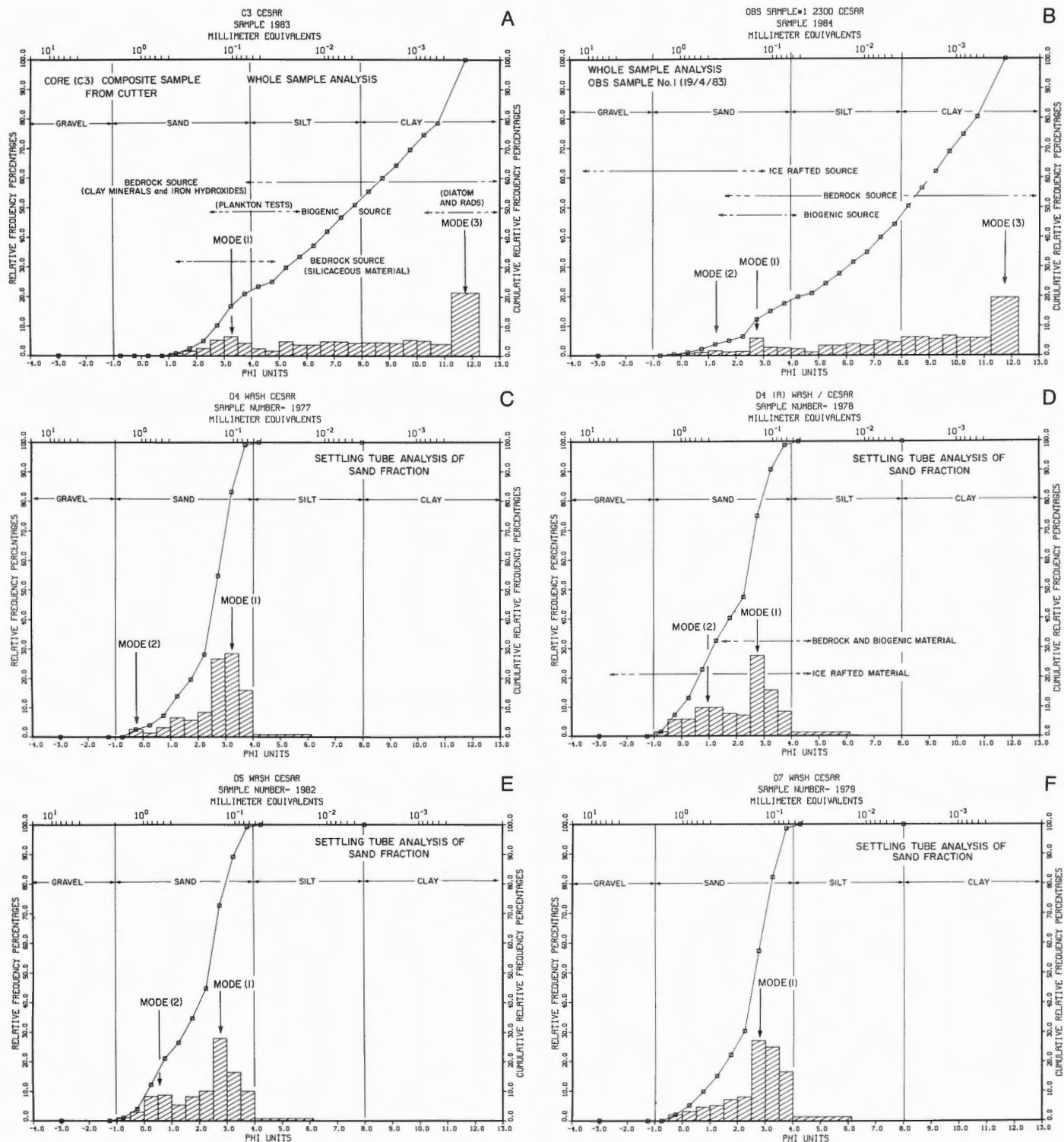


Figure 4.4 Seabed sediment size analysis of eight samples collected during the dredging coring program. An interpretation of the size class histogram modes is also presented.

A Core cutter sample from core C3.

B Surface sample from OBS station (19/4/84).

C Settling tube analysis of coarse fraction ( $>63\mu\text{m}$ ) from dredge D4.

D Duplicate analysis of coarse fraction ( $>63\mu\text{m}$ ) from dredge D4.

E Settling tube analysis of coarse fraction ( $>63\mu\text{m}$ ) from dredge D5.

F Settling tube analysis of coarse fraction ( $>63\mu\text{m}$ ) from dredge D7.

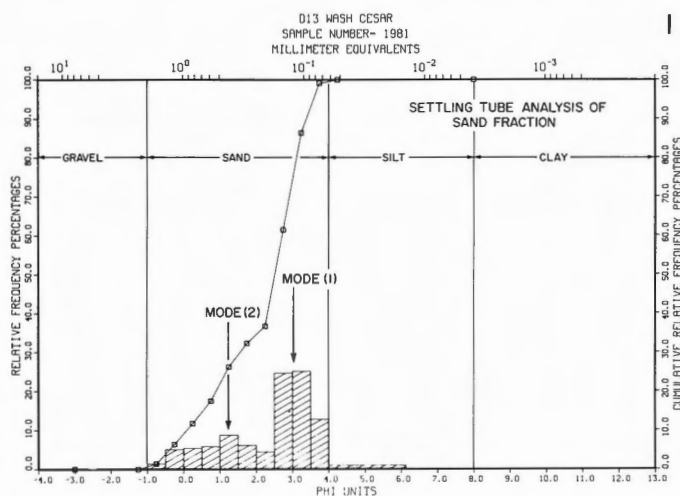
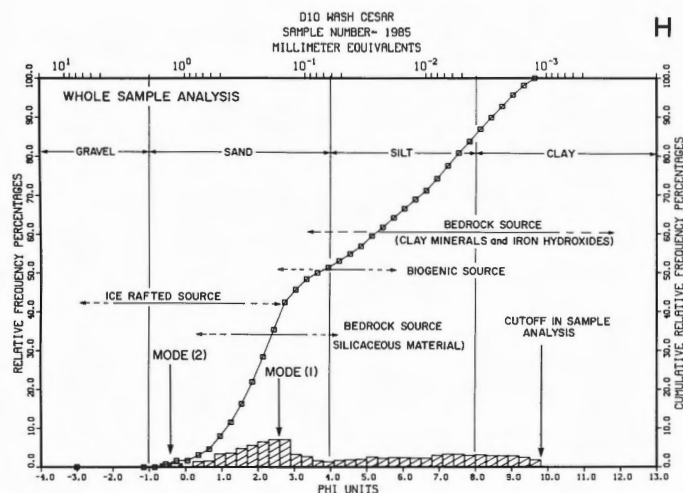
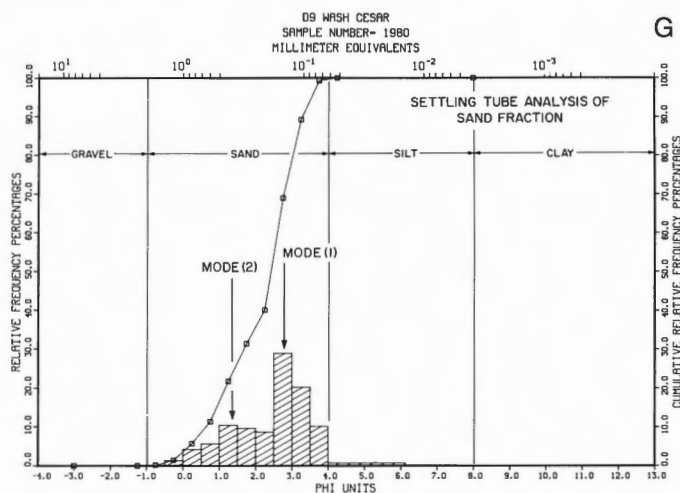


Figure 4.4 (cont'd)

- G Settling tube analysis of coarse fraction (>63 $\mu$ m) from dredge D9.
- H Whole samples analysis of material from dredge D10.
- I Settling tube analysis of coarse fraction (>63 $\mu$ m) from dredge D13.

Once deposited, the seabed appears to consolidate to form a semi-indurated sediment presumably by the process of gravity settling with time. The resulting cohesive material (assuming a vane shear strength of 4 KPa which is considered representative) would erode at a near bed current of approximately 1.5m. s<sup>-1</sup> (Kamphuis and Hall, 1983). Therefore, postdepositional erosion is unlikely to have taken place. Well preserved sponge spicules also attest to a lack of erosion.

## SUSPENDED PARTICULATE MATTER (SPM)

The concentrations of suspended particulate matter were determined at regular intervals throughout the water column during the period, 4-6 April 1983. Up to 12 L of seawater, collected using Niskin sample bottles, was filtered through 0.45 $\mu$ m NuclePore<sup>R</sup> filters. Due to the extremely low concentrations of SPM and the uncertainty associated with the results, the program was repeated by filtering 100 L of seawater collected using Niskin samplers. The results are given in Table 4.6.

The depth averaged suspended sediment concentration (SSC) of the water column was 0.08mg. L<sup>-1</sup> ( $\pm$  0.07). The maximum recorded value was 0.24mg. L<sup>-1</sup>, though much of

this (20 to 50%) can be ascribed to residual salts precipitated on the filter pad during filtering. Concentrations were generally higher than anticipated and showed a general decrease from the surface to the seabed. The concentration of particulate matter in the ice samples (taken from 3 different sites away from main camp) were remarkably consistent at 0.11mg. L<sup>-1</sup> ( $\pm$  0.05) and were significantly higher than concentrations in the underlying water mass.

A detailed analysis of the particulate matter has been made on samples from the ice, the water column and seabed. This involved grain size analysis of the disaggregated material, a visual analysis of particles using a Cambridge<sup>®</sup> Stereo Scan 180 scanning electron microscope, and an elemental analysis of particles using the EG & G EEDS II EDAX elemental analyzer fitted to the SEM. Results of the microscopic analysis are given in Table 4.7. The synthesis includes an analysis of an ice sample and the breakdown products from the dredged bedrock sample.

The ice sample exhibited particles ranging from 3 to 100 $\mu$ m in diameter. A variety of these particles are illustrated in Plates 4.5 and 4.6. In general terms, two major sources of material were detected. The major source is considered to be terrestrial, derived by eolian transport. Angular unweathered

Table 4.3. Taxonomic composition of biogenic material in coarse fraction (> 63 µm) of CESAR dredge samples D4, D5, D7, D9, D13 and core sample C13

Group	Species Fauna	Abundance
Foraminifera – Planktonic	<i>Neogloboquadrina pachyderma</i>	Abundant
– Benthic:		
Calcareous –	<i>Dentalina frobisherensis</i>	Occasional
	<i>Eponides tumidulus</i>	Occasional
	<i>Oridorsalis tener</i>	Occasional
	<i>Patellina corrugata</i>	Occasional
	<i>Planulina wuellerstorfi</i>	Common
	<i>Pyrgo</i> Sp.	Occasional
	<i>Quinqueloculina elongata</i>	Occasional
	<i>Quinqueloculina vulgaris</i>	Common
	<i>Robertinoides charlottensis</i>	Occasional
	<i>Stetsonia</i> Sp.	Occasional
	<i>Triloculina carinata</i>	Occasional
	<i>Virgulina</i> Sp.	Occasional
– Benthic arenaceous –	<i>Trochammina nitida</i>	Very rare
Molluscs	Gastropod	Occasional
	Pelecypod	Occasional
	Serpulid worm	Occasional
	<i>Spiratella helicina</i>	Common
Ostracods	<i>Echinocythere</i> Sp.	Frequent
Otoliths	Ca. 12 unknown Sp.	Frequent
	Unknown	Very rare
Radiolaria	None	Absent
Sponge	Few Spp.	
Occasional		
	<i>Flora</i>	
Diatoms	<i>Coscinodiscus</i> Sp.	Rare
Dino/layellate calcispheres	None	Absent

Table 4.4. Identification based on reflected light microscopic examination, acid testing (HCl) and hardness.

Dredge No. – Sample No.	Composition	Shape
D4-1	Dolomite	Well rounded
-2	Dolomite	Subangular
-3	Limestone/dolomite	Subrounded
-4	Dolomite	Subrounded
D5-1	Dolomite	Angular
-2	Dolomite	Rounded
-3	Dolomite	Rounded
-4	Red-stained dolomite	Rounded
-5	Carbonaceous dolomite	Rounded
-6	Carbonaceous dolomite	Rounded
D8-1	Dolomite	Subrounded
-2	Dolomite	Rounded
-3	Dolomite	Subangular
-4	Dolomite	Rounded
-5	Carbonaceous dolomite	Rounded
-6	Carbonaceous dolomite	Rounded
D10-1	Dolomite/limestone	Angular
-2	Dolomite/limestone	Rounded
-3	Limestone	Rounded
-4	Limestone	Subrounded
-5	Limestone	Angular
-6	Greywacke	Subrounded
-7	Vuggy volcanic	Rounded
D12-1	Siltstone	Well rounded
D13-1	Dolomite	Well rounded

Table 4.5. Grain size analysis of bottom sediment samples.

Sample #	Gravel	Sand	Percentage Silt	Clay	Mean (Phi)	Sorting (Phi)	Skew
OBS # 1 (19/4/83)	0	17.5	26.8	55.7	7.8	3.2	-0.6
Core # 3 (Barrel)	0	21.0	30.0	49.0	7.6	3/2	-0.2
D4(A) ( $>53\mu\text{m}$ )	0	98.8	1.2	0	2.1	1.2	-0.5
D4 ( $>53\mu\text{m}$ )	0	99.1	0.9	0	2.7	1.0	-1.2
D5 ( $>53\mu\text{m}$ )	0	99.2	0.8	0	2.2	1.2	-0.6
D7 ( $>53\mu\text{m}$ )	0	98.6	1.4	0	2.6	1.0	-1.0
D9 ( $>53\mu\text{m}$ )	0	99.3	0.7	0	2.4	1.0	-0.7
D10	0	50.9	32.9	16.2	4.5	2.8	0.3
D13 ( $>53\mu\text{m}$ )	0	99.1	0.9	0	2.3	1.2	-0.8

fragments of mica (Plate 4.5E), orthoclase (Plate 4.5B) and quartz (Plate 4.5A) are dominant components of this source. Many of these fragments show sharp "feather" edges (Plate 4.5B), and conchoidal fracturing (Plate 4.6A) indicating a lack of abrasion. Similar fragments have been documented by Clark et al. (1980) from various horizons within cores collected throughout the Arctic Ocean. Wood fragments (Plate 4.5C) and pollen grains (Plate 4.6F) were also present. The composition and crystalline nature of the eolian material suggests ablation of granitic rocks. The Paleozoic gneisses, schists and granites from north and east Ellesmere Island may well be the source.

The marine component of the ice trapped sediment includes diatom tests (Plate 4.5D), iron rich rosettes and clay floccules (Plate 4.6D). The floccules are bound by undifferentiated organic matter and comprise material finer than  $30\mu\text{m}$ . Fine silt and clay size particles appear to be entirely marine. By contrast to previous studies, no ice-rafted silt or clay particles were unequivocally identified. One pure iron spherule, interpreted to be a micro-meteorite, was observed in the ice sample. The specimen is shown in Plate 4.6B and 4.6C.

The marine particulate material was analyzed from depths of 25m (Plate 4.7), 350m (Plate 4.8A, 4.8B), 1000m (Plate 4.8C), and 1330m (Plate 4.8D to 4.8F). Particles ranged in size up to  $150\mu\text{m}$ . Material was in general bimodal with particles of approximately  $30\text{--}50\mu\text{m}$  and  $1\text{--}5\mu\text{m}$  dominating the size spectrum.

The majority of particles fall within either of two classes; iron-rich to pure iron agglomerates or silica- and aluminum-rich clay mineral floccules. The iron-rich floccules occur at all depths and at all sizes. They are interpreted to be derived from the iron-rich pyroclastic basalt which outcrops on the south flank of the Alpha Ridge subcrest.

The clay floccules shows variations in preservation of plate structure, composition and size. The floccules are principally composed of smectite (see Table 4.7) and often include diatom fragments. They also show traces of titanium, chromium, lead, zinc, manganese and magnesium. The dominance of silica, aluminium and potassium suggests that the material is a well weathered feldspar (possibly microcline). The most probable source of this material is the local bedrock as previously discussed.

A predominance of mica flakes was observed in the sample taken from a depth of 1000m. Although the significance of this "mica peak" is not known, the advection of material from the North Atlantic may well be the source. There appears to be no other segregation of particles either on the basis of size or composition. No evidence was found to support the hypothesis of Clark et al. (1980), that mid-depth flow is an important mechanism for the sorting of sediment deposited at the seabed.

An analysis was made of the weathered bedrock material from dredge D10 (Plates 4.9) to compare results to those derived from the suspended particulate matter (SPM) of the

Table 4.6. The results of the analysis of the concentrations in suspended particulate matter from ice and seawater samples. The analysis error, based on sample variability, is approximately  $\pm 0.07 \text{ mg L}^{-1}$  at the 68% confidence level. A sample volume of 100 L was filtered in all cases.

Sample #	Depth (m)	SSC (mg L <sup>-1</sup> )	SEM. #
5412	ice	0.10	84-09
5351	ice	—	
5379	ice	0.11	—
5302	2.7m	0.11	
5353	75m	—	
5283	100m	—	
5408	150m	0.08	
5411	150m	0.16	
5285	200m	0.04	
5419	250m	0.21	
5418	250m	0.01	
5402	300m	0.24	
5404	400m	0.05	
5406	350m	0.04	84-10
5369	500m	0.01	
5416	600m	0.01	
5360	750m	—	
5414	875m	0.16	
5323	1000m	0.08	
5321	1100m	—	
5306	1200m	0.03	
5337	1300m	0.19	
5304	1300m	0.02	
5332	1310m	0.01	
5358	1330m	—	
5358	1330m	—	
5435	1500m	0.08	
5427	1700m	0.03	
5433	1740m	0.12	
		SSC = 0.07	

Table 4.7 S.E.M. analysis of particulate matter from the ice pack, the water column and seabed from the CESAR site.

Sample #	Grain diam. $\mu\text{m}$	Elements Si Al Fe K Mg Mn Ti Na Ca Cu Cr											Micrograph No. (Mag.)	Interpretation
F.229 (Ice)	100	M	M	T	M								09-5	Ortho-felspar (unweathered angular)
84-09	100	I		M									09-1-4 (1020)	Ferro-silicate (conc. fract.)
	100												09-6 (410)	Wood fibre
	30	M											09-7 (2150)	(1) Diatom test
	6	M											09-7 (2150)	(2) Angular qtz. fragment
	6		M										09-7 (2150)	(3) Fe rich particle
	15	M											09-7 (2150)	(4) Angular qtz. fragment
	60												09-7 (2150)	(5) Organic fibre
	50	M	M	I	M								09-8 (1810)	Mica flake – unweathered
	20													Pollen grain
	30	M	M	I	T	T		I	T	T			09-9 (2610)	Clay particle showing cleavage
	20	M	I	I	T	T		I	T	T	T		09-10 (1022)	(1) Silicate fragment
	10	M	I	I	T	T		I	T				09-10 (1022)	(2) Clay mineral
	5	M	I	I	T	T		I					09-10 (1022)	(3) Fe-rich smectite particle
	3	M											09-10 (1022)	(4) Diatom fragment
	15	M	M			I				I			09-10 (1022)	(5) Marine flocc.
	100	M											09-11 (4900)	Qtz. fragment – faceted
	100	M											09-12 (1300)	(1) organic fragment
	30	M	M	M	T			T					09-12 (1300)	(2) rounded clay pellet
	20			M									09-13 (3000)	(3) Fe spherule (tektite)
	10	T		M									09-14 (5500)	Fe rich rosettes on clay mineral
	50													Pollen grain
	20												09-16 (5300)	Pollen Grain



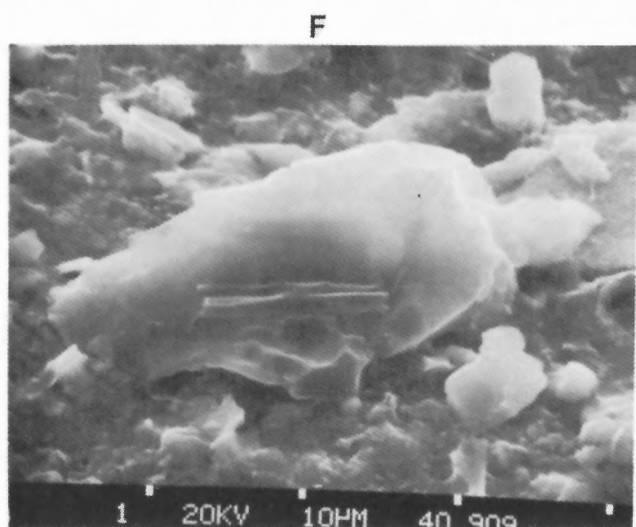
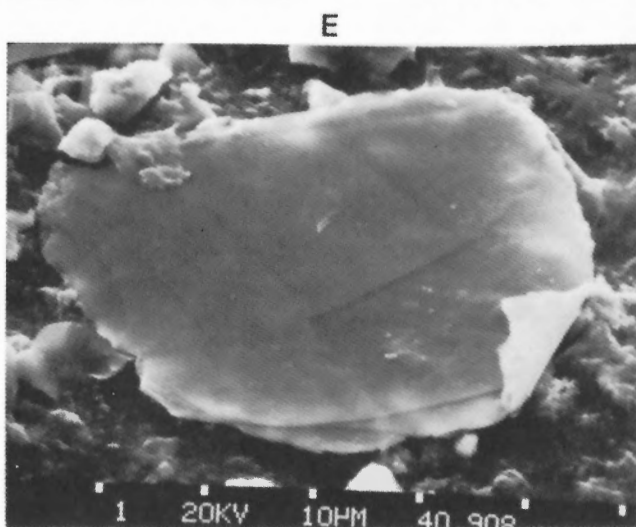
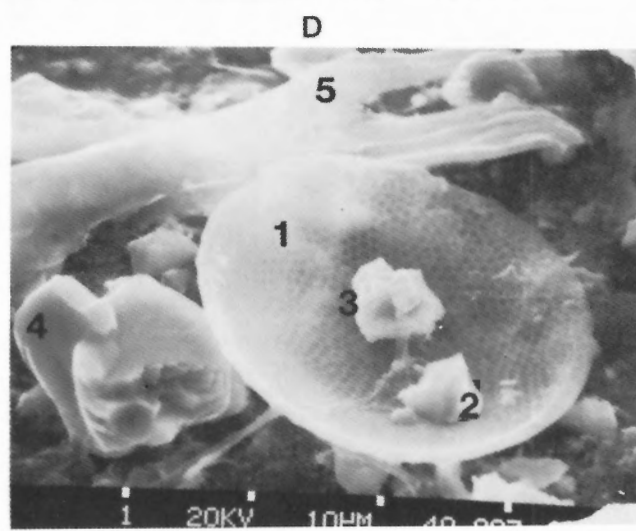
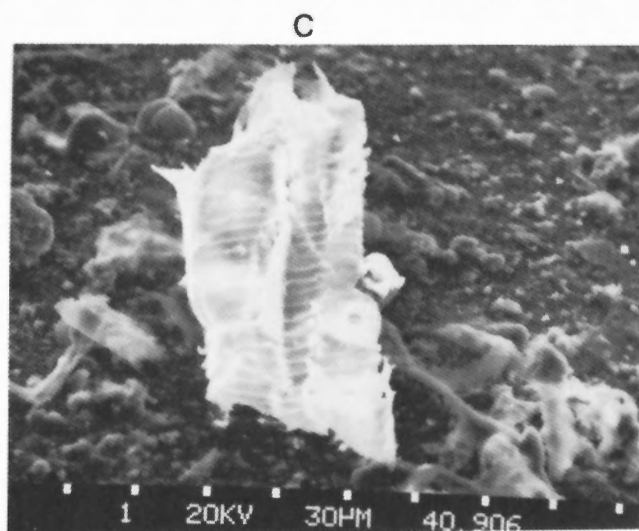
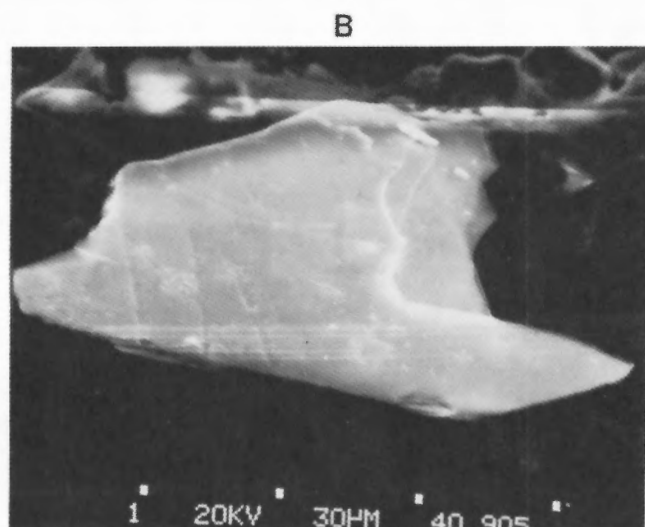
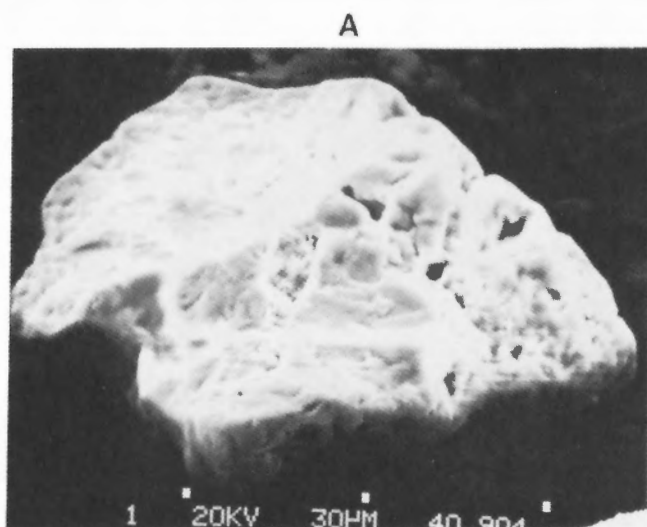


**Plate 4.5**

Micrographs of particulate matter from the ice pack. A, ferrosilicate clast; B, orthoclase; C, wood fibre; D, 1, diatom test, 2, quartz fragment, 3, iron-rich particle, 4, quartz fragment, 5, organic fibre; E, mica plate; F, clay particle.

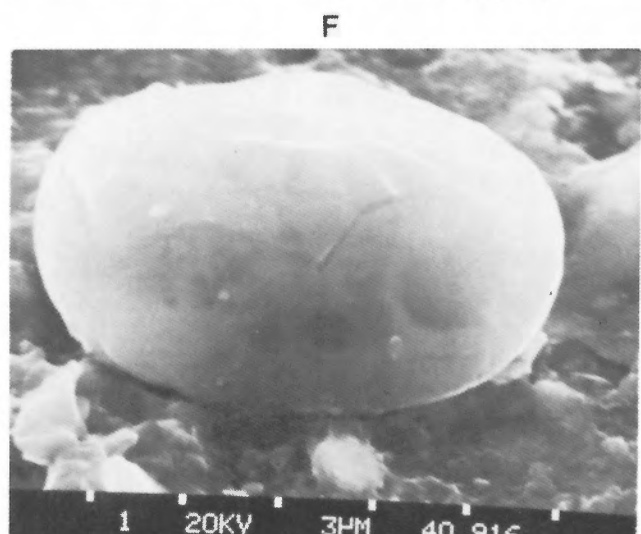
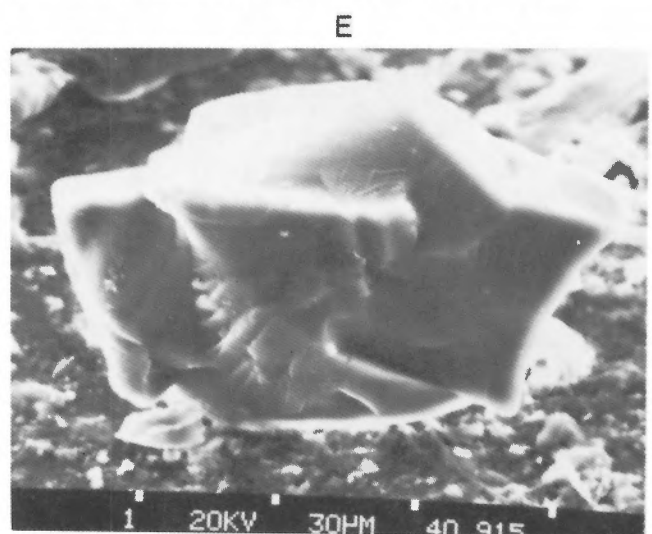
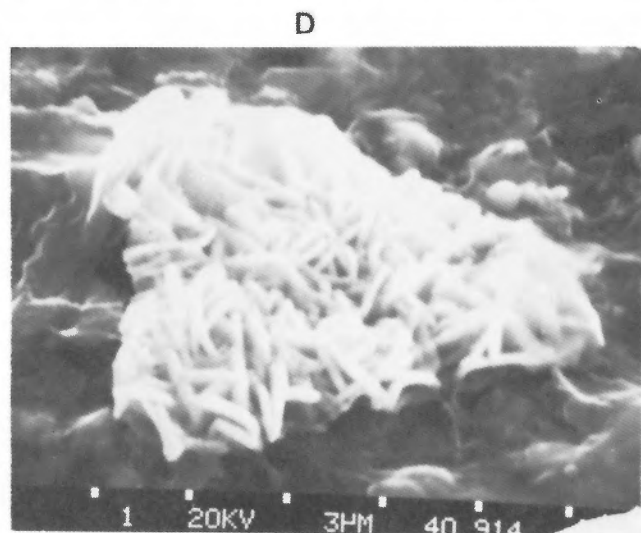
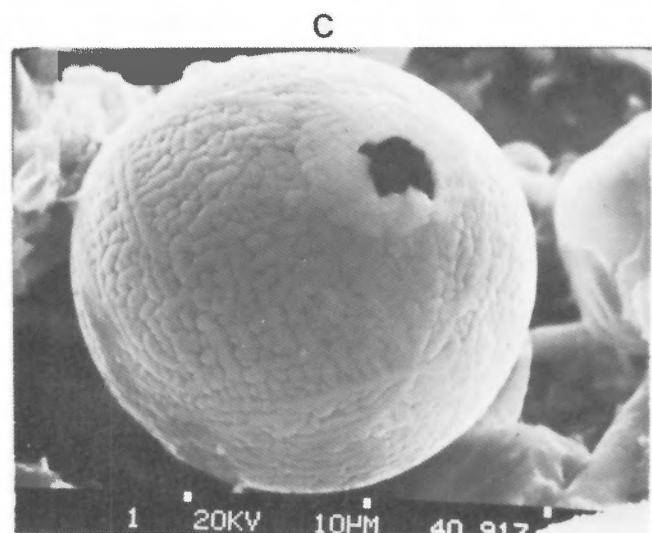
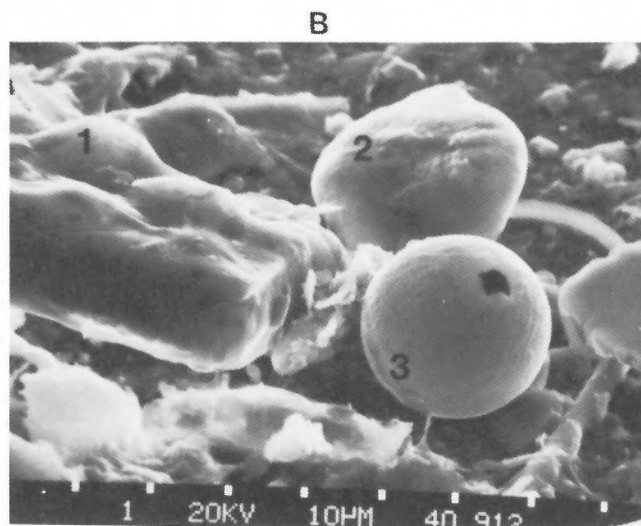
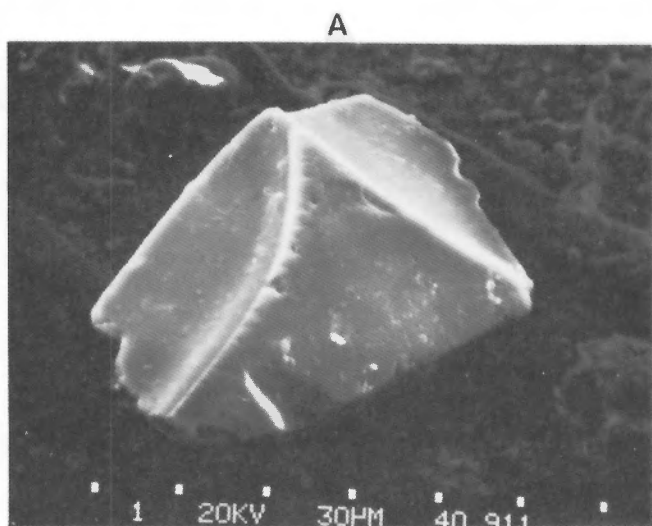


**Plate 4.6**

Micrographs of particulate matter from the ice pack. A, faceted quartz fragment; B.1, organic matter, 2, rounded clay pellet, 3, iron-rich spherule (micro-meteorite); C, iron-rich spherule (micro-meteorite); D, iron-rich rosettes; E, phosphorus-rich soap (contamination resulting from use of deflocculant); F, pollen grain.

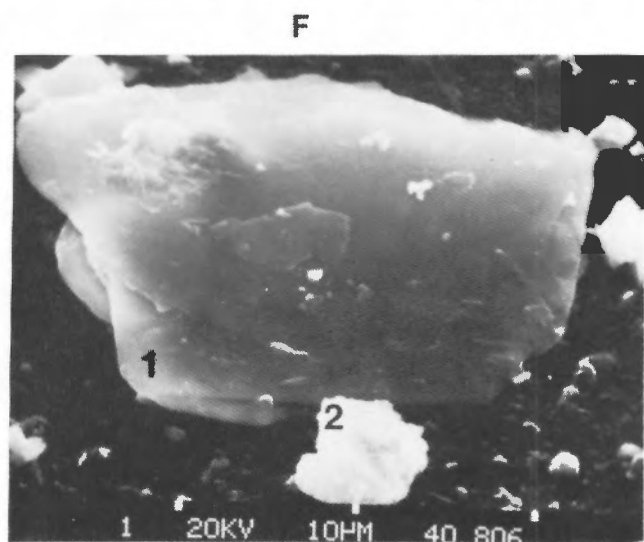
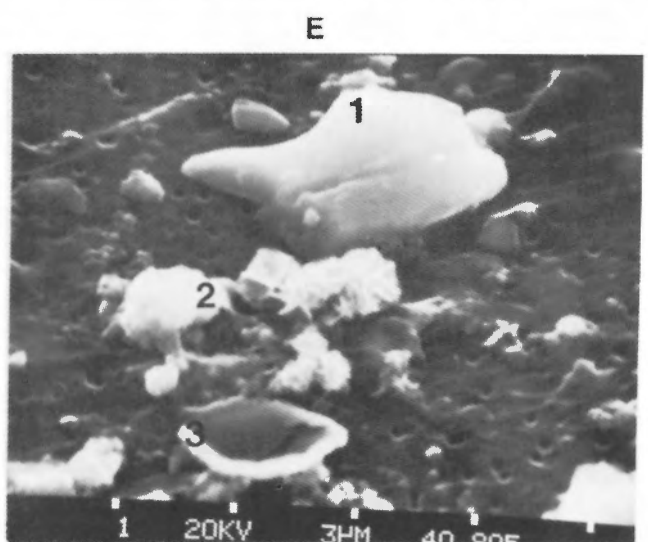
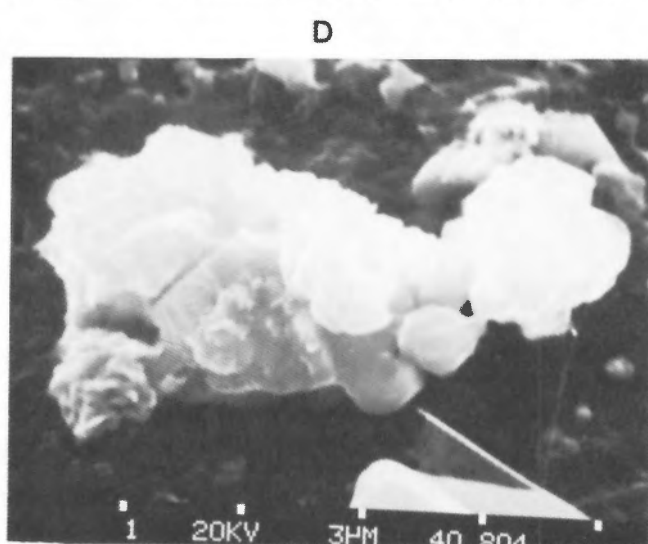
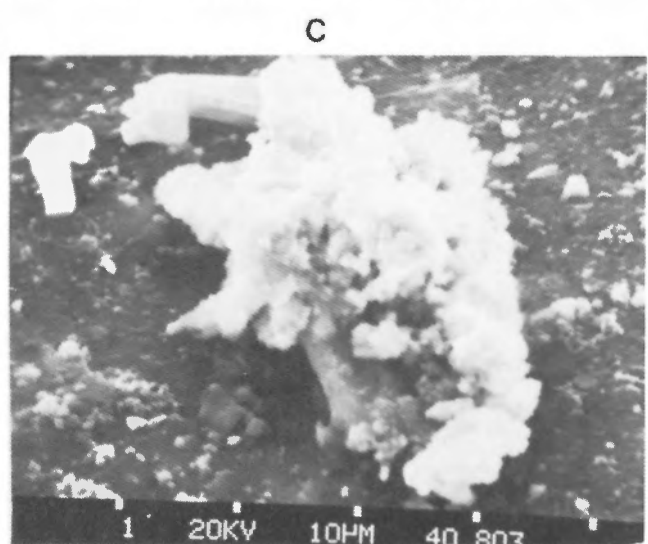
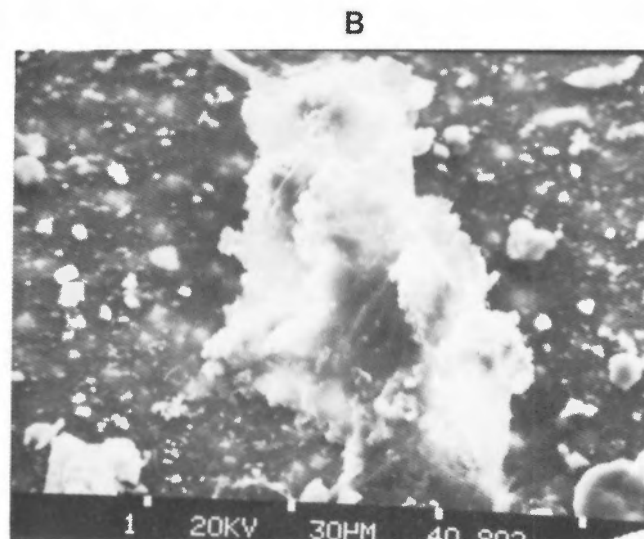
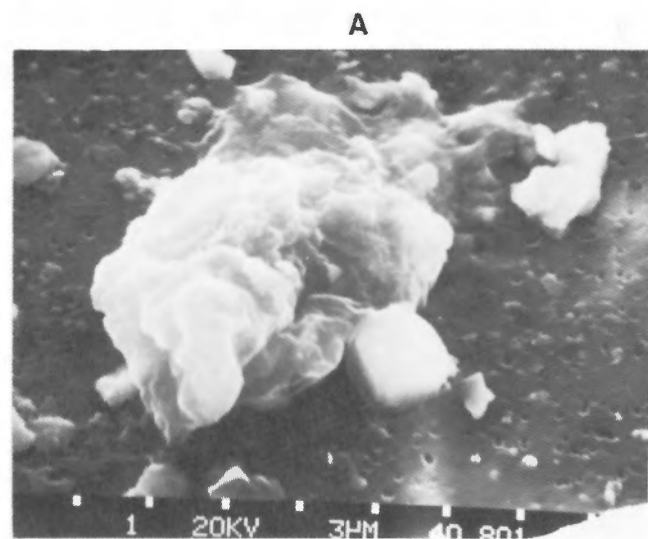


**Plate 4.7**

Micrographs of particulate matter from 25m water depth. A, clay (smectite) floccule; B, organic-rich clay floccule; C, organic-rich floccule; D, iron-rich smectite floccule; E.1, clay plate, 2, iron-rich particle, 3, diatom fragment; F.1, mica plate, 2, iron-rich particle.

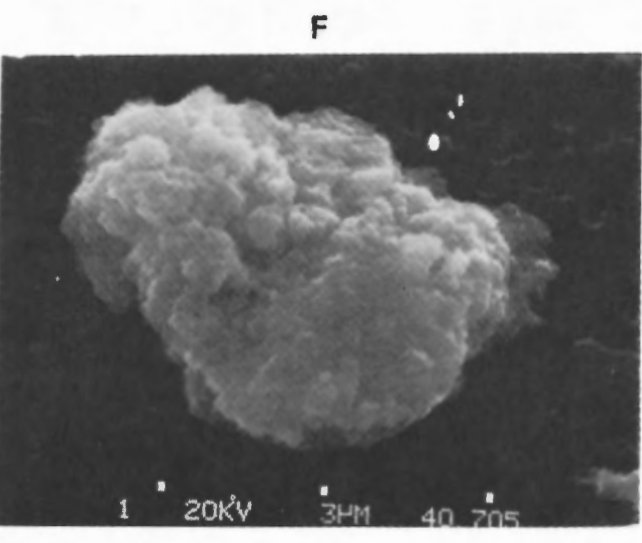
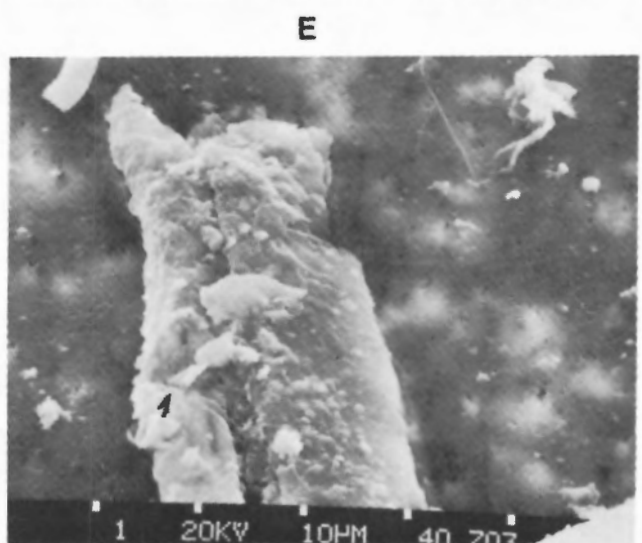
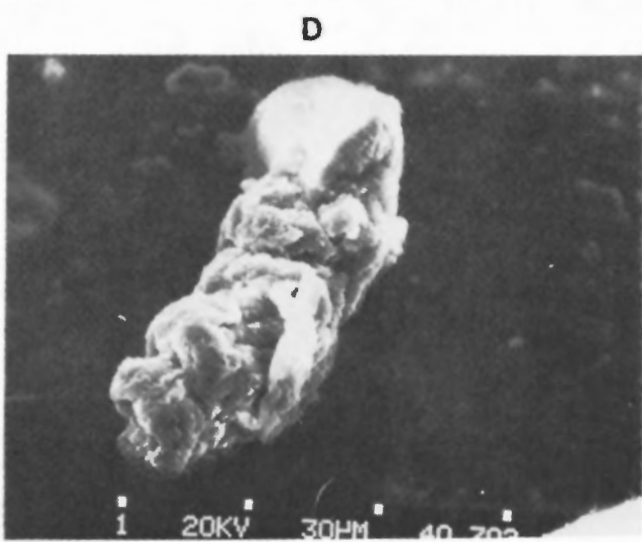
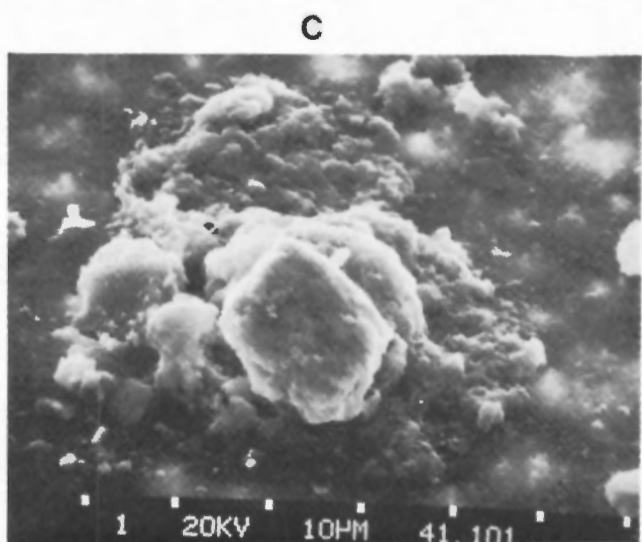
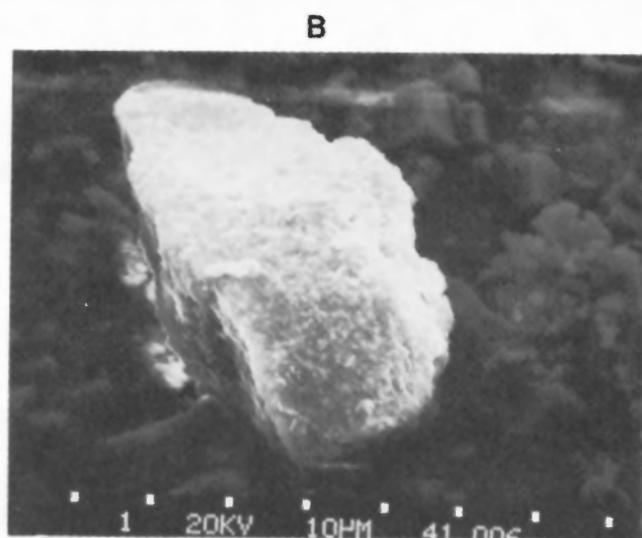
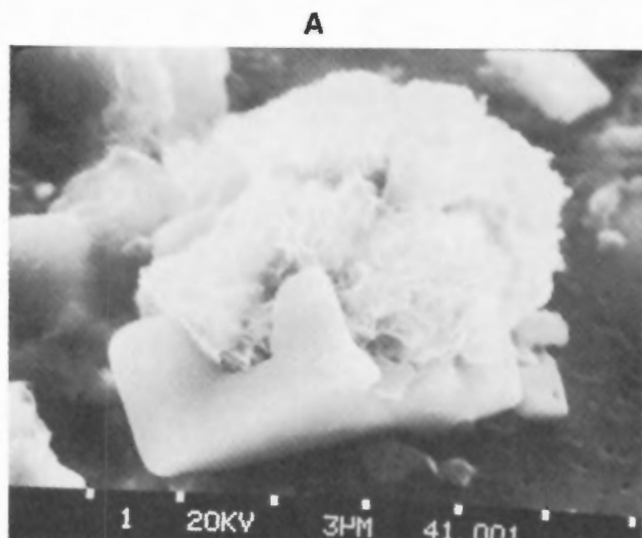


**Plate 4.8**

Micrographs of particulate matter from 350m (A and B), 1000m (C) and 1330m (D, E and F). A, iron-rich rosettes on salt; B, lead-rich particle (possibly crocoite); C, iron-rich floccule; D, quartz fragment; E, weathered feldspar; F, iron-rich floccule.



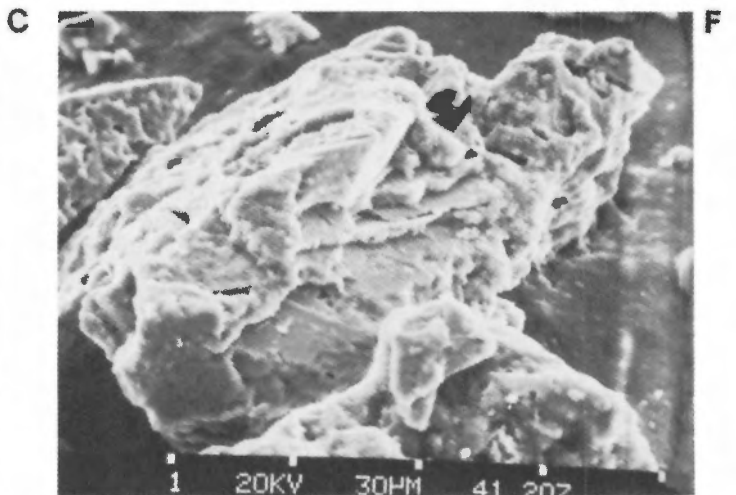
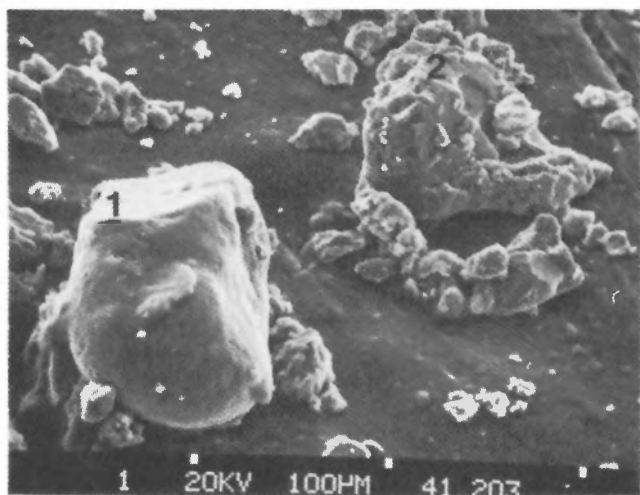
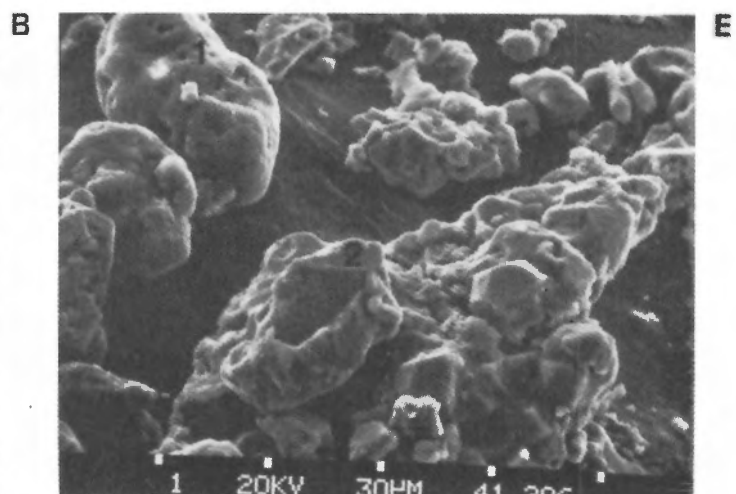
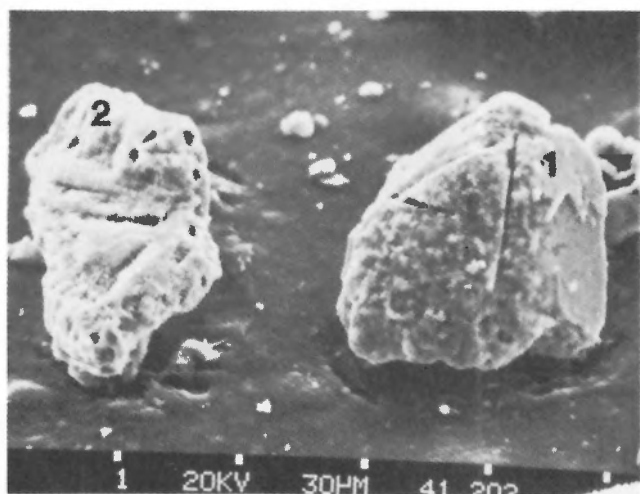
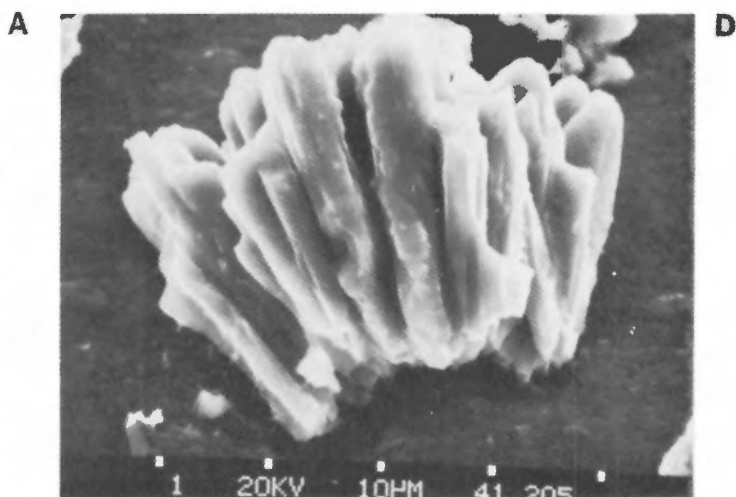
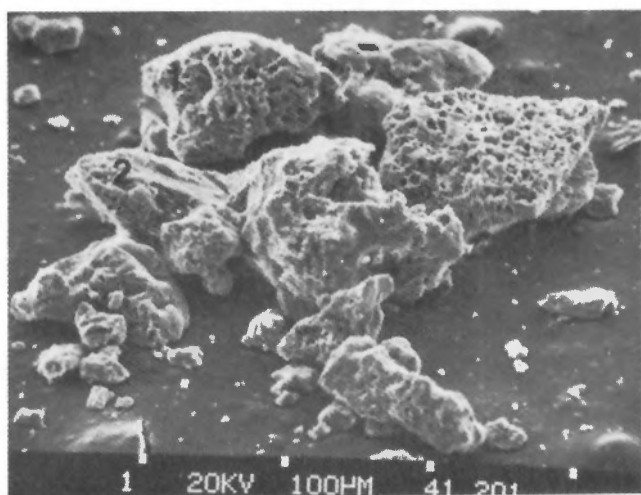


#### Plate 4.9

Micrographs of weathered products of bedrock sample recovered in dredge D10. A.1, iron-rich coating on clay particle; 2, feldspar crystal; B.1, cleavage planes on pseudomorph of feldspar, 2, weathered feldspar; C.1, well rounded Fe/Mn/Mg precipitate, 2, weathered feldspar; D, clean feldspar; E, rounded Fe/Mn/Mg precipitate; F, well weathered feldspar.



water column. The analysis reflected the SPM modes. That is, there is a predominance of iron-rich amorphous material (Plate 4.9A) and silica-aluminum-potassium-rich well weathered pseudomorphs (Plate 4.9B). The pseudomorphs show perfect basal and B- plane cleavage patterns and cross-sections similar to microcline phenocrysts. Such crystals vary in size from 30 to 100 $\mu$ m and, if interpreted correctly, are typically associated with hydrothermal veins or pegmatites. The weathering of the pseudomorphs shows a continuum from partially leached crystals to fully altered smectite flocules. Well rounded spherules of Fe/Mg rich material were also present. The trace metals measured in these spherules were titanium and potassium with intermediate amounts of aluminum, silica and calcium. The spherules are similar in composition to the pyroxene group, although no crystal faces were observed. An alternate hypothesis is that they are amorphous concretions associated with hydrothermal activity which created the Fe/Mg rich crust covering the bedrock surface.

The following is an approximate element composition table of the bedrock crust derived from the EDAX system:

Element	%
Na	trace
Mg	13
Al	16
Si	8
K	trace
Ca	4
Ti	trace
Mn	37
Fe	19

(traces of Ni also present)

## DISCUSSION

The sedimentation rate to the basins of the Alpha Ridge can be computed from a knowledge of the depth average suspended sediment concentration (SSC), from information on floccule bulk density and settling rate and by assuming no significant current flow. Accretion rate is derived from sedimentation rate assuming a bulk density for the bottom sediment of 1800kg (m<sup>3</sup>)<sup>-1</sup>. Specifically, a sediment concentration of 0.01 x 10<sup>-3</sup>kg (m<sup>3</sup>)<sup>-1</sup> and a floccule settling rate (V<sub>0</sub>) of 630 m.a.<sup>-1</sup> were used. The value of V<sub>0</sub> is based on experimental evidence.

$$\begin{aligned}
 \text{Accumulation rate} &= (\text{SSC}) \cdot (V_0) \cdot \left( \frac{1}{1800} \right) \text{ m.a}^{-1} \\
 &= (1 \times 10^{-5}) \cdot \left( \frac{1}{1800} \right) \text{ m.a}^{-1} \\
 &= 3.5 \times 10^{-3} \text{ mm.a}^{-1}
 \end{aligned}$$

The results show an extremely slow sedimentation rate of 1mm in approximately 300 years. Thus it would take 0.3 Ma to accumulate 1m of bottom sediment assuming normal pelagic sedimentation. Due to the pulse-like nature of eolian sediment input to the water column (which occurs during

summer ice melting) and the inferred resuspension of ridge-top sediments during seabed storms, the above calculation is considered to be conservative. Notwithstanding this, previously published data on sedimentation rates fall generally within the range specified. Herman (1974) quoted rates of 1 to 3mm (1000 a)<sup>-1</sup> as a general value for the Alpha Ridge and suggested higher rates for the adjacent plains. Clark et al. (1980), based on core data, suggested a rate of 1.14mm (1000 a)<sup>-1</sup>, while Aksu (1985) derived a value of 1mm (1000 a)<sup>-1</sup>.

## CONCLUSIONS

Notwithstanding the incomplete data set, the following are the significant conclusions of this study.

1. The UMEL camera and frame, used originally in the AIDJAX project, is not appropriate for operations such as CESAR. A more compact system, that could be lowered directly through the hydrohole without tilting, would reduce the risks of injury or instrument damage.
2. A sum of 605 useable bottom photographs were obtained from 14 sites. The photographs showed the northern Alpha Ridge crest is current winnowed, while the troughs show evidence of tranquil sedimentation. Ripples and scouring around cobbles, observed at the ridge crest, are suggestive of periodic currents in excess of 20cm.s<sup>-1</sup>.
3. The nearbed currents, interpreted from the drift rates of trigger weight impact plumes seen in bottom photographs, were approximately 1cm.s<sup>-1</sup>.
4. The principal type of bottom sediment found at the ridge crest was allogenic and inorganic. By contrast, 60% of the material in the adjacent troughs was biogenic. Of the remaining inorganic sediment, the silt/clay component was principally derived from local bedrock weathering, whereas the sand/gravel population was principally derived from ice rafting of debris from adjacent land masses.
5. The majority of the particulate matter in the ice pack comprised eolian debris although marine flocs were also found. The concentration of particulate matter in the ice was an order of magnitude higher than in the water column suggesting that the sediment supply from eolian processes is greater than advection to the region within the water column.
6. Gravel clasts, recovered from the seabed and interpreted to be ice rafted to the region, are predominantly rounded to well rounded and are calcareous. This suggests a source from a beach or river delta on the adjacent Canadian land mass.
7. Bedrock material, dredged from the south flank of the northern Alpha Ridge crest, verifies the occurrence of outcrops in the region. This material is an extremely well weathered, buff basaltic rock with a surface crust of Fe/Mn rich precipitate.
8. The mean sediment concentration in the water column was 80mg.L<sup>-1</sup> ( $\pm$  70mg.L<sup>-1</sup>). A layer of micaceous rich

material was detected at a depth of 1000m, although no obvious stratification in the sediment concentration was observed.

9. A first-order calculation of sedimentation rate, using the measured sediment concentration in the water column, was 1m in 0.3 Ma. This correlates well with estimates derived by other methods.

## REFERENCES

- Aksu, A.E.  
1985: Paleomagnetic stratigraphy of the CESAR cores; *in* Initial Geological Report on CESAR — the Canadian Expedition to Study the Alpha Ridge, Arctic Ocean, ed. H.R. Jackson, P.J. Mudie and S.M. Blasco; Geological Survey of Canada, Paper 84-22, report 7.
- Clark, D.L., Whitman, R.R., Morgan, K.A. and MacKey, S.D.  
1980: Stratigraphy and glacial-marine sediments of the American basin, central Arctic Ocean; Geological Society of America, Special Paper, 131, 57p.
- Crombie, W.J.  
1960: Preliminary results of investigations on Arctic Drift Station Charlie; *in* Geology of the Arctic, ed. G.O. Raasch; University of Toronto Press, p.670-703.
- Hall, J.K.  
1979: Sediment waves and other evidence of paleo-bottom current at two locations in the deep Arctic Ocean; *Sedimentary Geology*, v.23, p.269-299.
- Herman, Y.  
1974: Arctic Ocean sediments, microfauna and the climatic record in late Cenozoic time; *in* Marine Geology and Oceanography of the Arctic Seas, ed. Y. Herman; Springer-Verlag, New York, p.223-348.
- Hunkins, K.L., Ewing, M., Heezen, B.C. and Menzies, R.J.  
1960: Biological and geological observations on the first photographs of the Arctic Ocean deep-sea floor; *Limnology Oceanography*, v.5, p.154-160.
- Hunkins, K.L., Thorndike, E.M. and Mathieu, G.  
1969: Nepheloid layers and bottom currents in the Arctic Ocean; *Journal of Geophysical Research*, v.74, p.6995-7008.
- Kamphuis, J.W. and Hall, R.  
1983: Cohesive material erosion by unidirectional current; *Journal of Hydraulic Engineering, ASCE*, v.109, p.49-61.
- Middleton, G.V. and Southard, J.B.  
1978: Mechanics of sediment movement; *SEPM Short Course No.3*, 10.2p.
- Piper, D.J.W., Letson, J.R.J., De Iure, A.M. and Barrie, C.Q.  
1983: Sediment accumulation in low-sedimentation, wave dominated, glaciated inlets; *Sedimentary Geology*, v.36, p.195-215.
- Schwarzacher, W. and Hunkins, K.L.  
1965: Dredged gravels from the central Arctic Ocean U.S.; *in* I.G.Y. drifting station Alpha Arctic Ocean 1957-1958, ed. G.H. Cabaniss, K.L. Hunkins and N. Untersteiner; Office of Aerospace Research, p.173-174.
- Van Wagoner, N.A. and Robinson, P.T.  
1985: Petrology and geochemistry of a CESAR bedrock sample: implications for the origin of the Alpha Ridge; *in* Initial Geological Report on CESAR — the Canadian Expedition to Study the Alpha Ridge, Arctic Ocean, ed. H.R. Jackson, P.J. Mudie and S.M. Blasco; Geological Survey of Canada, Paper 84-22, report 5.



## PETROLOGY AND GEOCHEMISTRY OF A CESAR BEDROCK SAMPLE: IMPLICATIONS FOR THE ORIGIN OF THE ALPHA RIDGE

Nancy A. Van Wagoner<sup>1</sup> and Paul T. Robinson<sup>2</sup>

Van Wagoner, N.A. and Robinson, P.T., *Petrology and geochemistry of a CESAR bedrock sample: implications for the origin of the Alpha Ridge*; in *Initial Geological Report on CESAR — the Canadian Expedition to study the Alpha Ridge, Arctic Ocean*, ed. H.R. Jackson, P.J. Mudie and S.M. Blasco; Geological Survey of Canada, Paper 84-22, p. 47-57, 1985.

### Abstract

During CESAR expedition, 20 similar bedrock samples were dredged from the walls of a major graben of the Alpha Ridge. These rocks are the only bedrock samples ever recovered from the ridge, providing the only direct evidence for its nature, composition and possible origin.

The sample analyzed is a highly altered fragmental volcanic rock which was rimmed with a crust of manganese oxide. Clasts form about 90% of the rock, are up to 1 cm, and are subround to angular. The rock is heterolithic comprising 92% aphyric, 5% clinopyroxene-phyric, and 3% plagioclase-microphyric clasts. Plagioclase microlites display skeletal form. Clasts commonly contain 50 to 60% vesicles up to 4mm in size and spherical to irregular in shape. Some vesicles may be relict spherulites. The skeletal form of plagioclase microlites, lack of abundant relict crystals, and possible relict spherulites suggests volcanic fragments were glassy to very fine grained. The combined textural evidence (quench textures, high vesicularity, fragmental nature and small clast size) suggests that the volcanic fragments were erupted in shallow water during a phreatomagmatic or Plinian-type eruption.

Rare clinopyroxene phenocrysts comprise the only unaltered portion of the rock. The range of compositions of these phenocrysts is  $Wo_{51-53}$ ,  $En_{32-37}$ ,  $Fs_{12-16}$ , with significant amounts of Ca, Al, and Ti. These compositions are similar to clinopyroxenes of alkali basalts of Hawaii, Fanning Island and the Hess Rise. Geochemical discriminators also suggest a within plate tectonic environment.

### Résumé

Au cours de l'expédition CESAR, 20 échantillons de socle rocheux ont été arrachés des parois d'un grand graben de la dorsale Alpha. Il s'agit des seuls échantillons du socle récupérés de la dorsale et donc de la seule source d'indications directes sur la nature, la composition et l'origine probable de cette dernière.

On a procédé à l'analyse d'un échantillon de roche volcanique détritique fortement altérée et entourée d'une croûte d'oxyde de manganèse. Presque 90% de la roche se compose de fragments dont la dimension peut atteindre 1cm et dont la forme varie de subarrondie à angulaire. Il s'agit d'un échantillon de roche hétérolithique composée à 92% de fragments aphyriques, à 5% de clinopyroxène porphyrique et à 3% de fragments de plagioclase microporphyrique. Les microlites plagioclases présentent des formes squelettiques. Les vacuoles constituant souvent 50 à 60% des fragments, mesurent 4mm de diamètre.

<sup>1</sup>Acadia University, Department of Geology, Wolfville, Nova Scotia, B0P 1X0.

<sup>2</sup>Dalhousie University, Centre for Marine Geology, Halifax, Nova Scotia, B3H 3J5.

*et leur forme varie de sphérique à irrégulière. Dans certains cas, il peut s'agir de sphérulites résiduelles. La forme squelettique des microlites plagioclases, l'absence de cristaux résiduels et la présence présumée de sphérulites résiduelles semblent indiquer que la texture des fragments volcaniques variait de vitreuse à très fine. Toutes les indications recueillies (texture de refroidissement, l'abondance des vacuoles, la nature fragmentaire et la petite taille des fragments) semblent indiquer que les fragments volcaniques proviennent d'une éruption de type phréatomagmatique ou phinien au cours de laquelle ils auraient été projetés dans un milieu marin peu profond.*

*Seule la partie de la roche composée de rares phénocristaux de clinopyroxène ne présente pas de traces d'altération. Les phénocristaux présentent une gamme de compositions, soit  $Wo_{51-53}$ ,  $En_{32-37}$  et  $Fs_{12-16}$ , et renferment des quantités importantes de Ca, Al et Ti. Ces compositions s'apparentent à celles des clinopyroxènes provenant des basaltes alcalins d'Hawaï, de l'île Fanning et de la crête Hess. Les données géochimiques semblent également indiquer que le développement du milieu tectonique s'est produit à l'intérieur des plaques.*

## INTRODUCTION

The geology and tectonics of the Arctic has been the subject of much discussion, most recently summarized by Sweeney (1981), Trettin and Balkwill (1979) and Irving and Sweeney (1982). Plate tectonic models for the evolution of mobile belts of Arctic Canada are highly speculative, partly because the history of the Arctic Ocean is not well understood, and plate tectonic theory postulates that the history of mobile belts is determined by the tectonic events of the adjacent ocean basin (Trettin and Balkwill, 1979). An understanding of the tectonics of the Canadian Arctic therefore requires an understanding of the geology of the Arctic Ocean.

The Arctic Ocean is divided into two major basins, the Amerasian Basin and Eurasian Basin, both of which are floored by oceanic crust overlain by as much as 5km of sediment (Mair and Lyons, 1981). The Lomonosov Ridge forms the boundary between these basins. The Nansen-Gakkel Ridge bisects the Eurasian Basin and the Alpha Ridge bisects the Amerasian Basin (Fig. 5.1). The Nansen Ridge is the northern continuation of the Mid-Atlantic Ridge. The Lomonosov Ridge is believed to be a fragment of continental crust of the Barents shelf that was left behind when spreading began on the Nansen Ridge about 63 Ma.

In the Amerasian Basin, however, neither continental outlines nor magnetic anomalies give a clear picture of plate motion. In addition, the nature of the Alpha Ridge is uncertain. It has been interpreted as a Mesozoic and Cenozoic spreading axis (Vogt and Ostenso, 1970; Hall, 1973), a volcanic arc (Herron et al., 1974), a fossil transform fault (Yorath and Norris, 1975) or a continental fragment (King et al., 1966).

This paper gives a preliminary report on the petrography and geochemistry of one of the first bedrock\* samples ever

recovered from the Alpha Ridge. This sample provides us with our first direct observation of this elusive feature.

## ACKNOWLEDGEMENTS

We are grateful to H.R. Jackson, and C.L. Amos who provided us with the sample and information on dredging location procedure. H.R. Jackson also provided helpful discussions concerning the origin of the Alpha Ridge and its relationship to other volcanic areas. This paper was improved by comments from D.J.W. Piper and G. Pe-Piper, who reviewed the manuscript.

## SAMPLING

The dredge which recovered the bedrock sample was lowered on 15 April 1983 at 0540 hours. At this time the ice station began to drift over the southern graben of the northern ridge at 85°51'7.4"N latitude, 110°1'30.5"W longitude. The dredge was retrieved on the same day at 1640 hours at ice station location 85°51'52.9"N, 110°15'20.3"W.

During the time the dredge was on the bottom, the ice station drifted about 4km to the north, travelling across the ridge and dragging the dredge up the face of the southern scarp. Seismic reflection profiles across the scarp show that it is composed of acoustic basement (Fig. 5.2). During dredging there were times when the wire was under tension suggesting that pieces of rock were being broken from outcrops.

The two types of rock fragments recovered during this dredging operation were 1) well rounded dropstones, presumably transported by ice from the continent, and 2) about 20 fragments of deeply weathered mafic volcanoclastic rocks. The latter are partly covered with a black layer of manganese oxide. This layer is not continuous around the surface of the samples further suggesting that they were broken from outcrops (Fig. 5.3).

\*Bedrock refers to the rocks that comprise the irregular topography of the ridge, as opposed to the overlying, subhorizontal sediments.



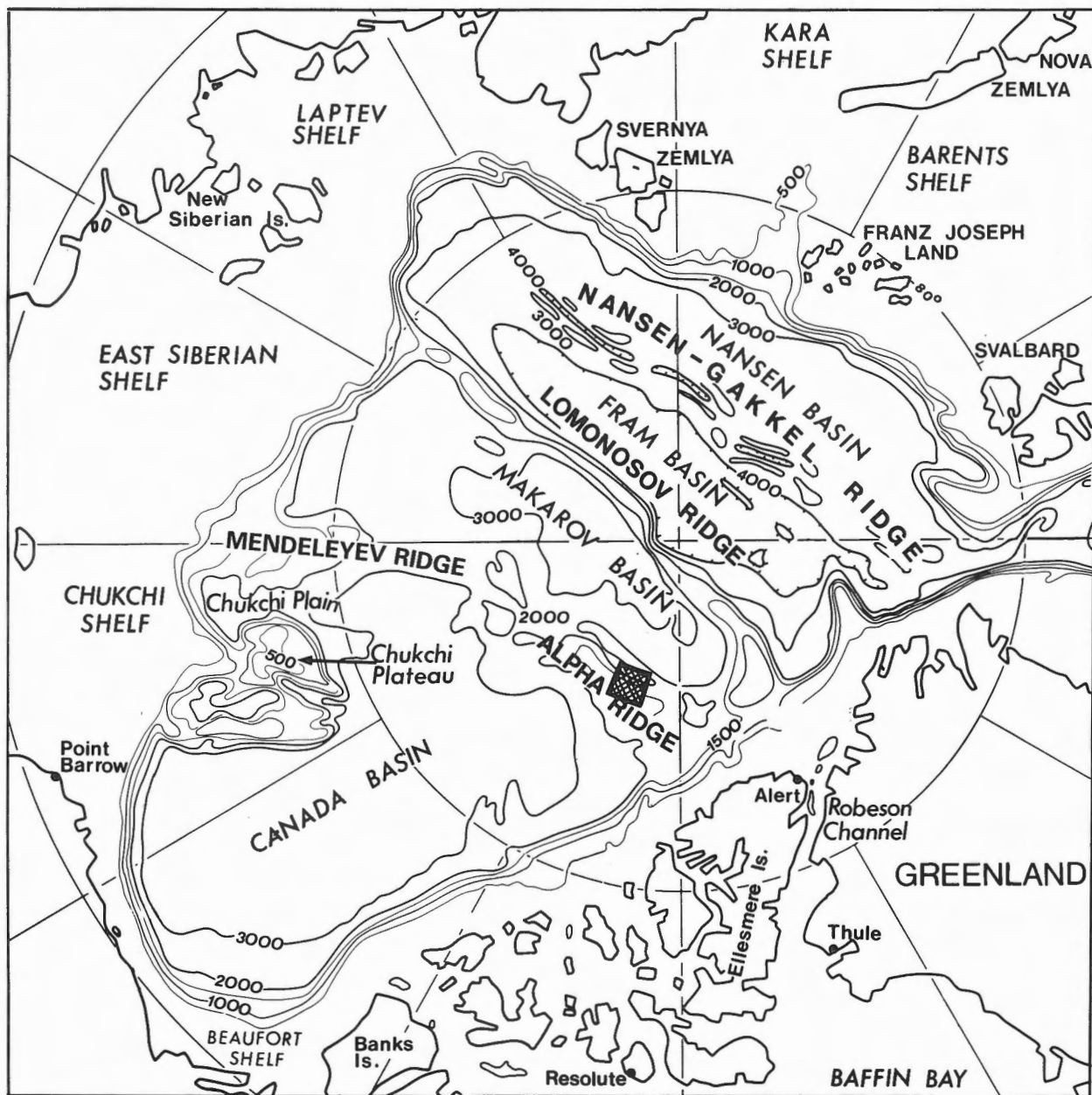


Figure 5.1 Major bathymetric features of the Arctic Ocean, showing the location of the CESAR ice station.

## SAMPLE DESCRIPTION

Most of the bedrock samples are archived at the Atlantic Geoscience Centre, Bedford Institute of Oceanography, but pieces of these samples were sent for analysis by the authors and by G.M. LeCheminant at the Geological Survey of Canada in Ottawa. The sample we received is almost completely altered to clays (possibly halloysite and montmorillonite) in a matrix of amorphous material and disordered goethite. It was rimmed by a discontinuous 0.5 to 1cm thick crust of manganese oxides which occur as botryoidal clumps. This outermost crust contains worm tubes which are coated, inside and out, with manganese oxide (LeCheminant, 1983). Although the sample is highly altered,

many primary textures and rare primary minerals are preserved and are discussed in this report. For a discussion of secondary minerals see LeCheminant (1983).

The sample is a fragmental volcanic rock (Fig. 5.4). It comprises 85 to 90% clasts which are 0.5 to 1cm in size and angular to subround, although some rounding may be due to alteration. Rare clasts contain curvilinear and vesicle controlled boundaries.

The rock is heterolithic and the three clast types observed are 1) 93% brown to orange-yellow, apparently aphyric clasts; 2) 5% yellow-brown clasts containing up to 30% euhedral to subhedral pyroxene phenocrysts which are 1 to 2mm in size (Fig. 5.5); and 3) 2% dark brown clasts

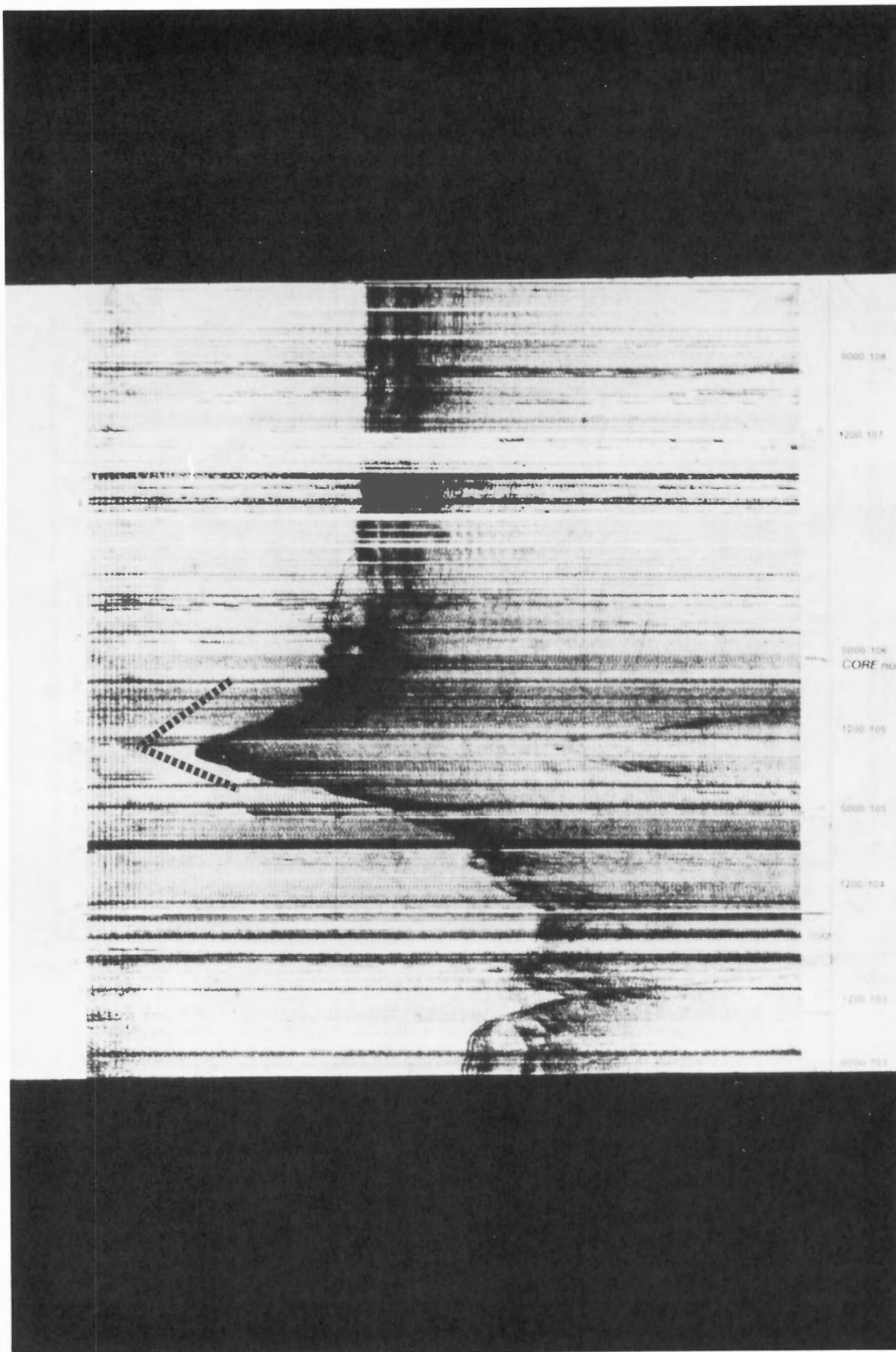


Figure 5.2 Seismic reflection profile showing the location of the dredge which recovered bedrock samples.

containing 3 to 5% pseudomorphs of plagioclase microlites up to 0.2mm in length (Fig. 5.6), which occasionally display skeletal form. Some of these clasts contain rare possible pseudomorphs of olivine. The matrix is now mostly secondary clay minerals.

Most clasts are moderately to highly vesicular or scoriaceous, containing up to 50 or 60% vesicles, but the third clast type tends to be moderately or sparsely vesicular. Vesicles generally are either 0.5 to 1mm in diameter and apparently spherical, or 2 to 4mm in size and irregular in shape. Most fragments contain both types of vesicles (Fig. 5.7). Vesicles are rarely elongate perpendicular to grain boundaries. All vesicles are filled with white to yellow secondary clay minerals which commonly are spherulitic. These may be pseudomorphs of clay minerals and goethite after spherulites but these would be difficult to distinguish from filled vesicles.

The presence of skeletal plagioclase microlites and absence of abundant relict crystals and spherulites(?) suggests the volcanic rock fragments were glassy, hypocrystalline, or cryptocrystalline.

### *Clinopyroxene phenocrysts*

Rare clinopyroxene phenocrysts comprise the only unaltered portion of the rock. Pyroxene compositions from a glomerophytic grain were determined by microprobe at Dalhousie University. Spots of several different grains were analyzed, without regard for the position of the spot with respect to the rim or core of the grains. These spot analyses are shown on Table 5.1, along with a clinopyroxene microprobe analysis done by the Geological Survey of Canada on a different sample from the CESAR bedrock collection. The GSC analysis is significantly higher in Na<sub>2</sub>O than the Dalhousie analyses. We do not know the reason for this discrepancy, but it may be a function of the standards used at the different microprobe facilities, chemical zonation of the grains (the GSC analysis apparently represents only one spot), or reflect slightly different chemistry of the different samples. The range of compositions is Wo<sub>51-53</sub>, En<sub>32-37</sub>, Fs<sub>12-16</sub>. These compositions plot above the salite field on the pyroxene quadrilateral (Fig. 5.8) and also contain significant amounts of Ca, Al, and Ti.

Table 5.1 CESAR clinopyroxene chemistry. Samples 1A-1H were analyzed at Dalhousie University. Data for sample GSC is from LeCheminant (1983).

CESAR pyroxene chemistry									
Sample CESAR 10									
Number	1A	1B	1C	1D	1E	1F	1G	1H	GSC
SiO <sub>2</sub>	49.19	49.49	48.18	49.48	45.27	45.77	44.61	48.47	44.19
TiO <sub>2</sub>	1.78	1.96	2.16	1.64	2.96	2.81	2.15	2.19	3.16
Al <sub>2</sub> O <sub>3</sub>	4.68	5.08	6.01	5.54	8.63	8.93	6.05	5.70	8.64
Cr <sub>2</sub> O <sub>3</sub>	—	0.16	—	0.21	0.09	—	0.07	—	0.26
FeO*	5.96	6.17	5.95	6.24	5.84	7.79	7.14	6.84	7.99
MnO	—	—	—	0.07	—	0.06	—	—	0.08
MgO	14.12	14.20	13.29	14.26	12.21	11.92	13.59	13.68	12.04
CaO	23.22	23.42	23.19	23.69	23.41	23.55	22.55	23.22	23.47
Na <sub>2</sub> O	—	0.12	—	0.16	—	0.43	0.31	—	1.07
K <sub>2</sub> O	—	—	—	—	—	—	—	—	0.01
V <sub>2</sub> O <sub>5</sub>	—	0.16	—	0.07	0.08	0.16	0.14	—	—
Total	98.94	100.77	99.79	101.36	99.47	101.41	97.63	100.11	100.91
Si	1.842	1.828	1.799	1.818	1.706	1.700	1.728	1.803	1.644
AlIV	0.158	0.172	0.201	0.182	0.294	0.300	0.272	0.197	0.336
AlVI	0.049	0.049	0.063	0.058	0.089	0.091	0.005	0.053	0.048
Fe**	0.187	0.191	0.217	0.192	0.216	0.242	0.231	0.213	0.252
Mg	0.788	0.782	0.740	0.780	0.682	0.660	0.784	0.758	0.676
Ca	0.932	0.927	0.928	0.933	0.945	0.937	0.977	0.925	0.947
Na	—	0.009	—	0.011	—	0.031	0.023	—	0.078
Ti	0.050	0.054	0.061	0.045	0.084	0.078	0.063	0.061	0.090
Mn	—	—	—	0.002	—	0.002	—	—	0.003
En	37.33	37.15	35.24	36.97	33.25	32.00	35.36	35.97	32.15
Fs	11.61	11.90	13.61	11.93	13.73	15.41	13.69	13.26	15.73
Wo	51.06	50.95	51.15	51.09	53.02	52.58	50.95	50.78	52.12
*Total Fe analyses as FeO									
**Fe <sup>2+</sup> +Fe <sup>3+</sup>									

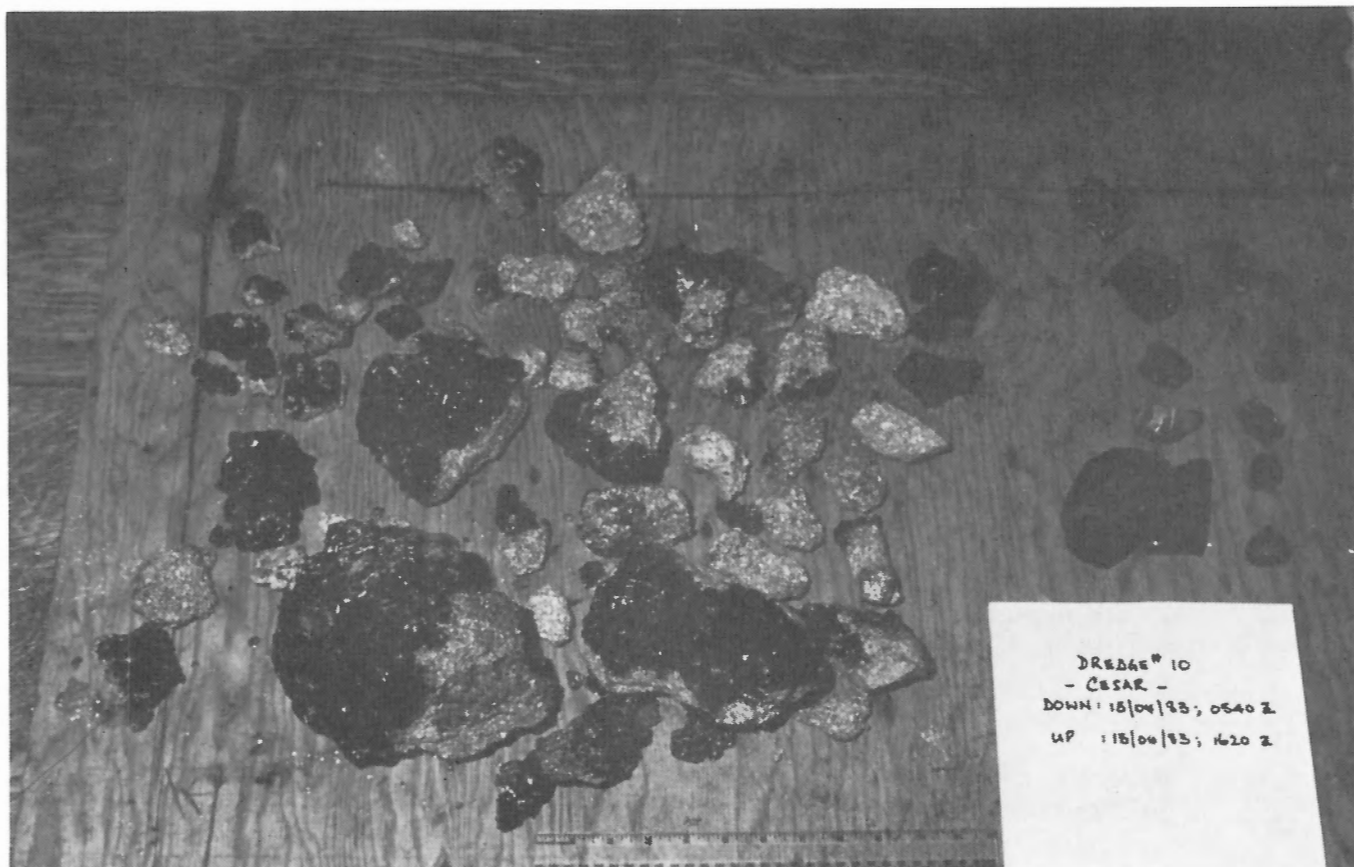


Figure 5.3 Rocks recovered by dredge. Those on the right are ice rafted dropstones, which are surrounded on all sides by manganese oxides. The rocks on the left are highly altered basaltic volcanoclastic rocks. The dark material is manganese oxides highly riddled with worm tubes. It only covers one side of the rocks suggesting that these rock fragments were broken from outcrops.

## INTERPRETATION OF TECTONIC ENVIRONMENT

It is not possible to determine the origin of the Alpha Ridge based on only one sample. Such interpretation requires a suite of strategically positioned samples. Even so, textural and geochemical information gained from this sample may place important constraints on the origin of the ridge.

Textural analyses indicate that the volcanic rock fragments were rapidly cooled. The fragments apparently were glassy or very fine grained and rare plagioclase microlites have a skeletal form which is typical of rapidly quenched submarine basalts (Bryan, 1972).

Most rock fragments are highly vesicular suggesting a shallow water extrusive depth, at least less than 400m depth (Moore and Schilling, 1973; Jackson et al., 1976). However, highly vesicular basalts may be erupted at depth greater than 200m if the magma has a high volatile content (Dudas, 1983; Moore et al., 1982).

The fragmental nature of the rock, small clast size and high vesicularity of the clasts suggests phreatomagmatic or Plinian eruption (Self, 1982a, 1982b). The fragments may have been transported after initial deposition but little reworking is suggested because 1) although the rock is heterolithic, a

single clast type predominates; 2) many grains are angular or subangular; and 3) any amount of reworking would be expected to result in destruction of the delicate, scoriaceous clasts.

Because the rock is highly altered, the original composition can only be interpreted on the basis of primary and relict mineralogy. The salitic composition of the CESAR clinopyroxenes and their high  $\text{TiO}_2$  and  $\text{Al}_2\text{O}_3$ , but low  $\text{SiO}_2$  content is typical of alkali basalts (Deer et al., 1966; Nisbet and Pearce, 1977; Leterrier et al., 1982), and the CESAR clinopyroxenes are chemically similar to alkali basalts of Hawaii, Fanning Island, and the Hess Ridge (Fig. 5.8). This chemical similarity of clinopyroxenes suggests that the clasts of the CESAR sample were alkali basalt. The occurrence of pseudomorphs of plagioclase microlites and possibly olivine is consistent with this interpretation.

Geochemical characteristics of volcanic rocks may be related to their tectonic setting. For such highly altered samples whole-rock geochemistry is of questionable significance, although these analyses are in progress. However, because there is a relationship between clinopyroxene composition and the composition of the host magma, unaltered clinopyroxene mineral grains can give an indication of the



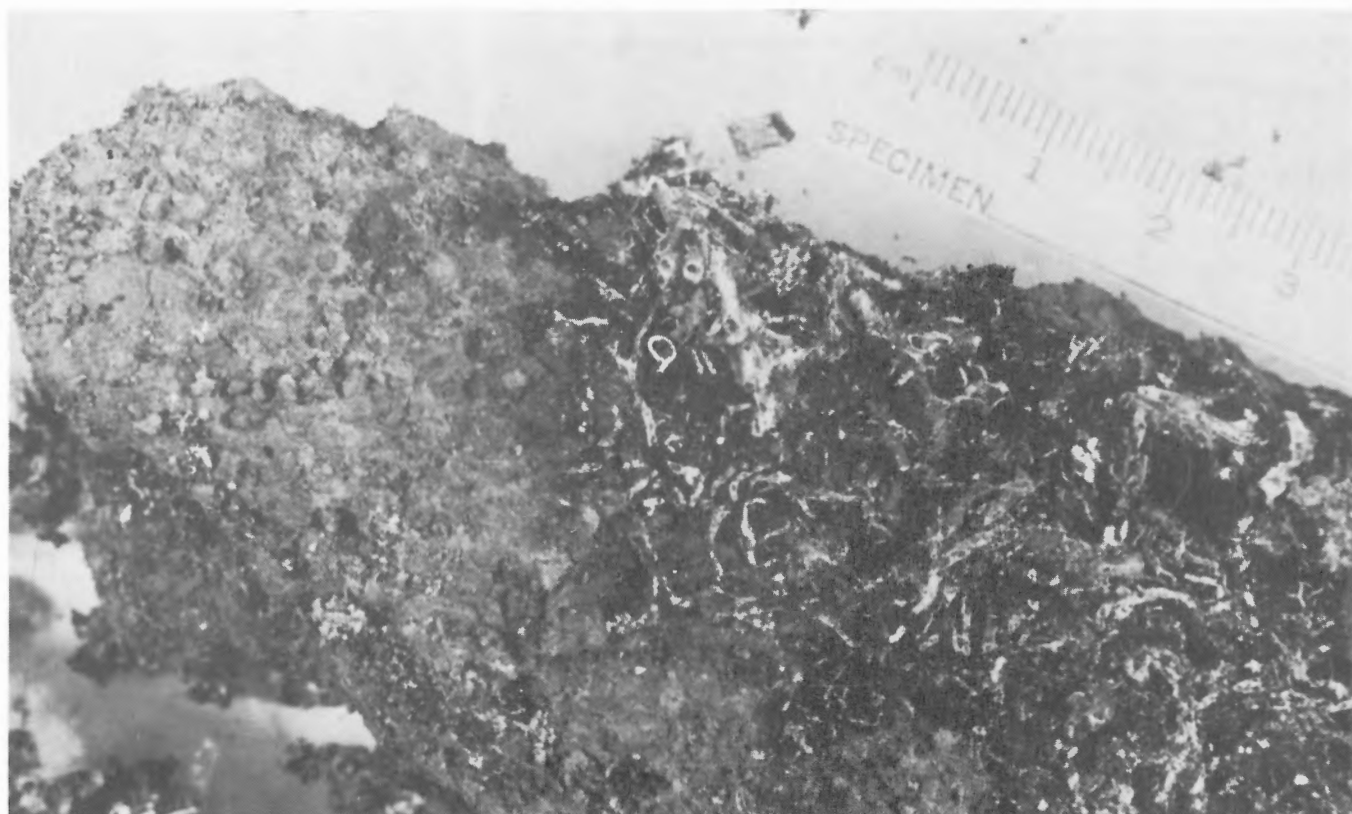


Figure 5.4 Close-up of volcanic rock sample showing the fragmental nature of the rock and the black manganese oxides with worm tubes.

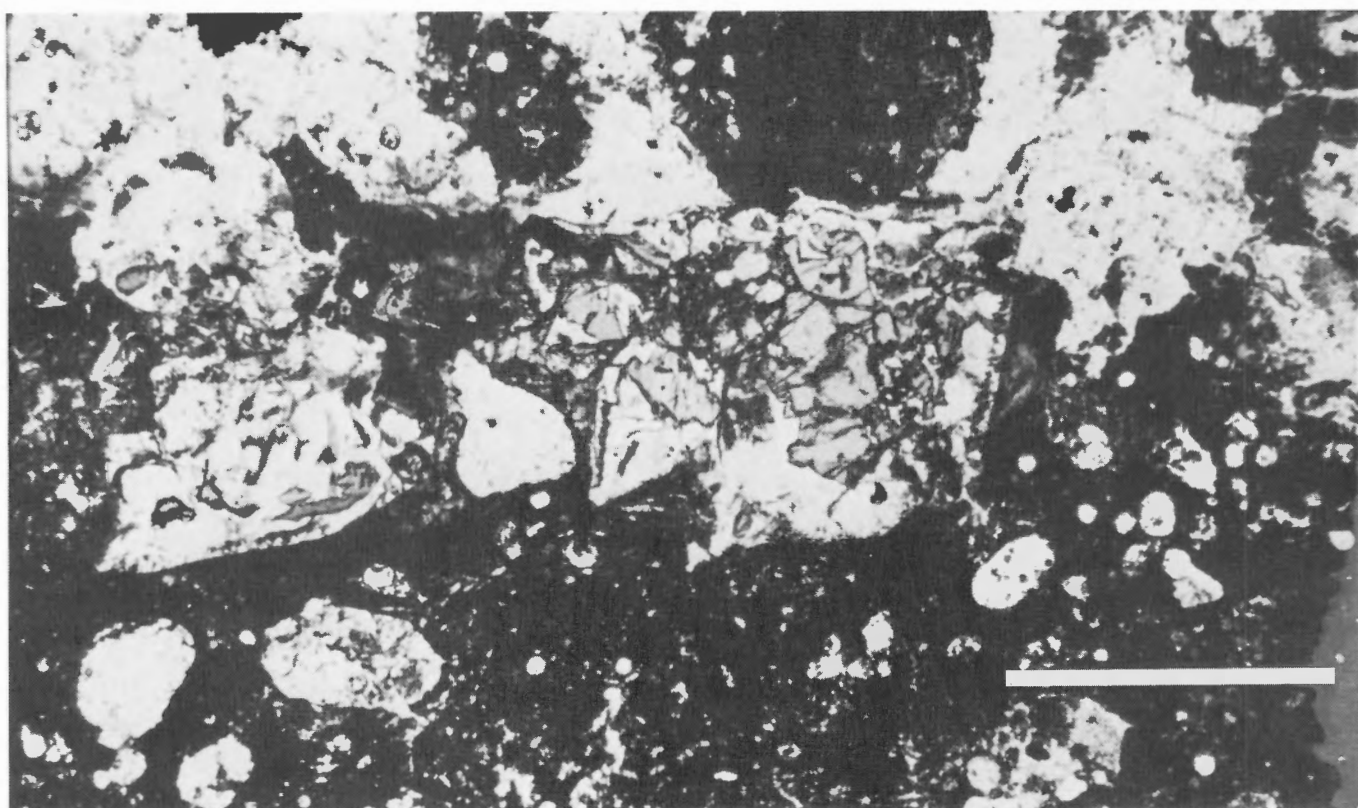


Figure 5.5 Highly altered volcanic clast which contains fresh clinopyroxene phenocrysts. Bar scale is 1mm, plane polarized light.



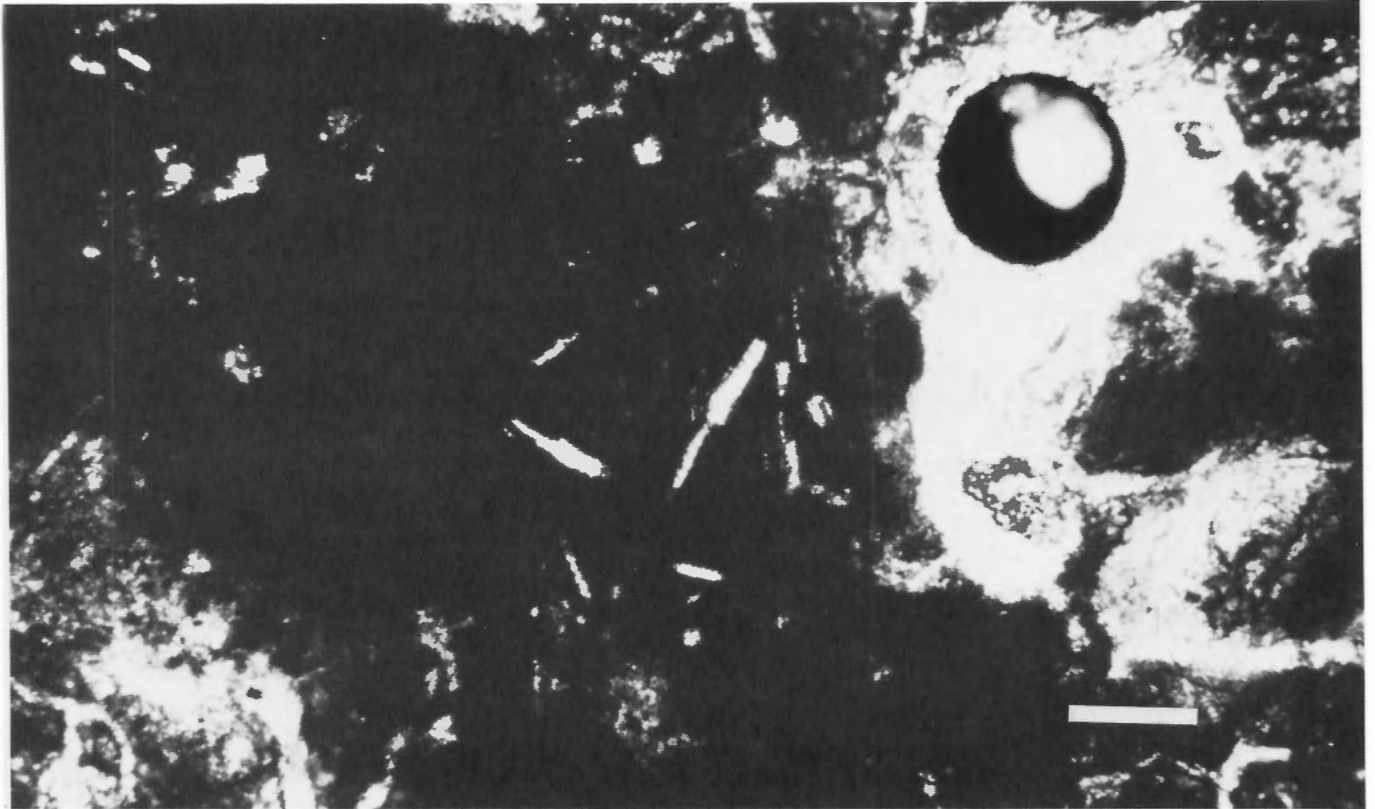


Figure 5.6 Plagioclase microlites in one of the volcanic rock fragments. Bar scale is 0.1mm, crossed nicols.

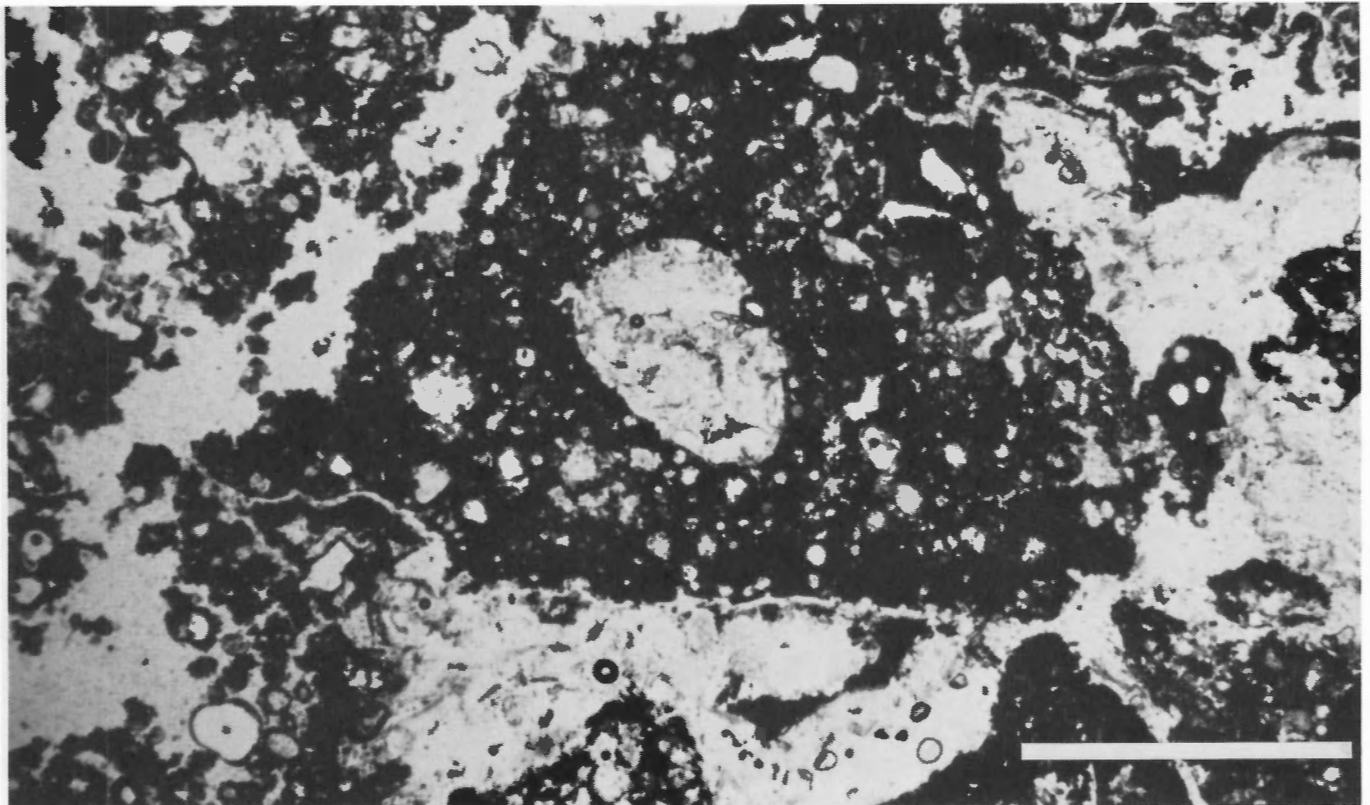


Figure 5.7 Highly vesicular and angular volcanic rock fragment. Bar scale is 1mm, plane polarized light.

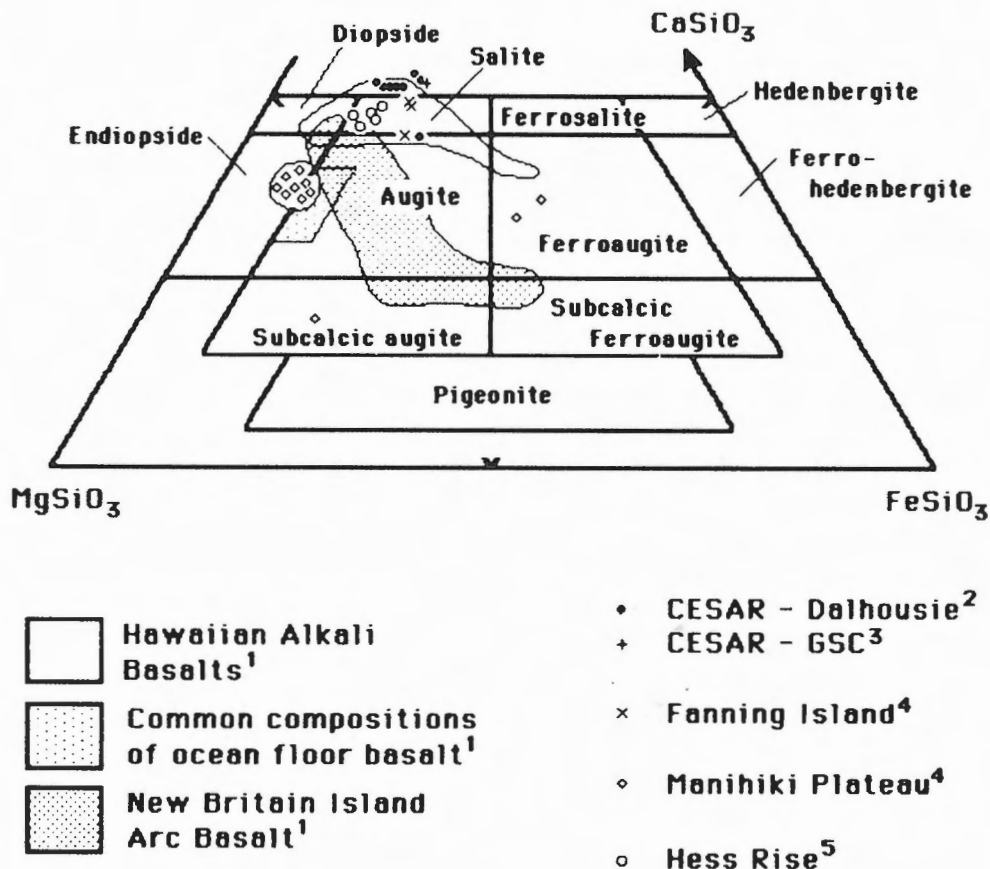


Figure 5.8 Pyroxene quadrilateral showing the composition of the CESAR clinopyroxenes in comparison with the compositions of clinopyroxenes from other areas. Data are from 1) Basaltic Volcanism Study Project, (1981), 2) this study, 3) LeCheminant, (1983), 4) Jackson et al., (1976), and Clague, (1976), and 5) Vallier et al., (1981).

original rock type and extrusive environment (Leterrier et al., 1982; Nisbet and Pearce, 1977). Discrimination diagrams from Leterrier et al. (1982) distinguish between ocean island and intracontinental alkali basalts and related rocks (basanites, etc.), and orogenic and nonorogenic tholeiitic and calc-alkali basalts with about 87% confidence based on the cationic values of Ca, Na and Ti for the structural formulae of the clinopyroxenes. The CESAR samples clearly plot in the alkali basalt field (Fig. 5.9). CESAR clinopyroxene compositions also plot in the within plate alkali basalt field (WPA) on the  $\text{TiO}_2$ , MnO,  $\text{Na}_2\text{O}$  discriminator from Nisbet and Pearce (1977; Fig. 5.10). These diagrams do not discriminate between continental and oceanic within plate alkali basalts.

The similarity of the CESAR clinopyroxenes to those of ocean islands, along with results of the discrimination diagrams suggests a within plate tectonic environment of extrusion for the CESAR bedrock sample. Alkali basalts are most common in intraplate areas but are found elsewhere (Best, 1982).

## CONCLUSIONS

The CESAR bedrock sample is composed of highly altered fragments of hypocrystalline or cryptocrystalline,

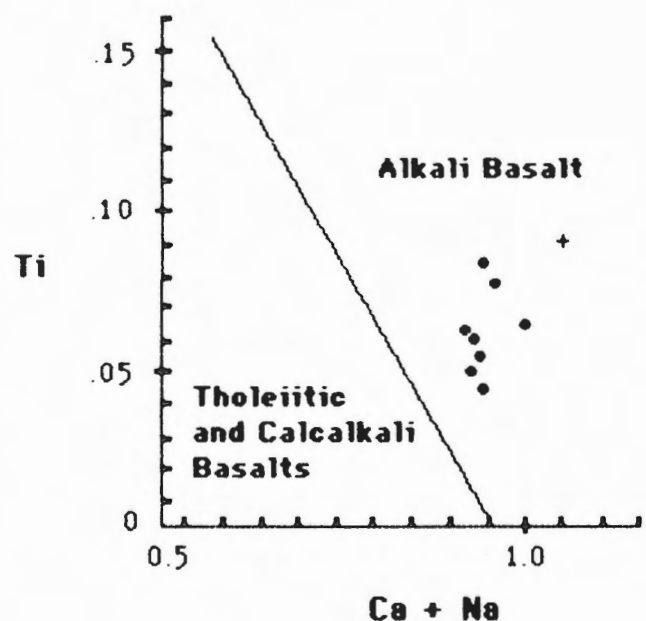
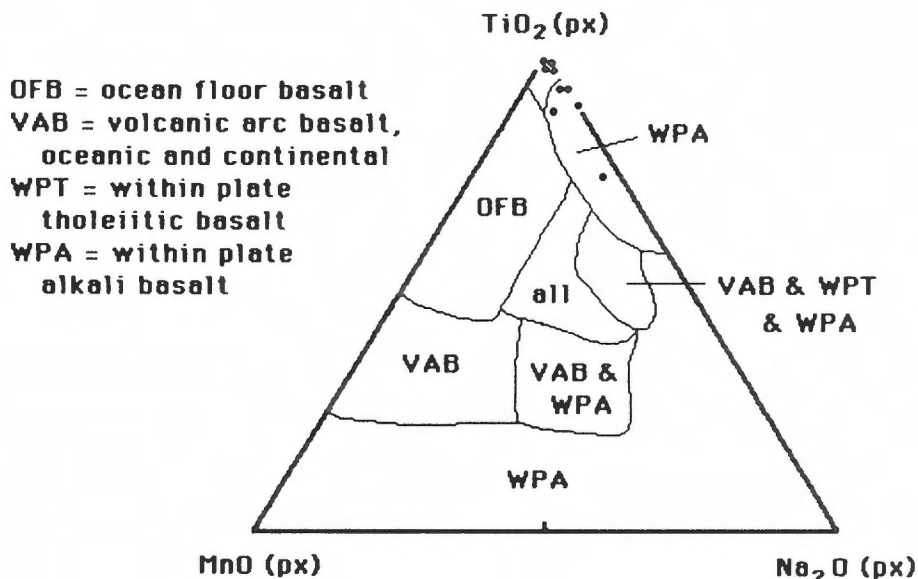


Figure 5.9 CESAR clinopyroxene compositions plotted on discrimination diagram from Leterrier et al. (1982). These compositions clearly plot in the alkali basalt field.

Figure 5.10 Triangular diagram from discriminating between basalts of different tectonic settings based upon the relative amounts of  $\text{TiO}_2$ , MnO and NaO in pyroxenes, from Nisbet and Pearce (1977). The CESAR compositions clearly plot in the within plate alkali basalt field.



sparsely to highly vesicular, and sparsely clinopyroxene and olivine(?)-phyric alkaline basalt. The fragments probably were erupted subaqueously, but in shallow water. Geochemical discriminators suggest a within plate tectonic environment, although alkali basalts are found elsewhere.

Further geochemical studies of this rock are underway and include major, trace, and rare earth element analyses. However, if the Alpha Ridge was at a shallow depth, as we suggest, then it may have been the source rock for much of the sediment recovered in the CESAR sediment cores. These cores then probably will provide the best available suite of rock and mineral samples for determining the volcanic evolution and paleogeography of the Alpha Ridge.

## REFERENCES

- Basaltic Volcanism Study Project  
1981: Basaltic volcanism on the terrestrial planets: Pergamon Press Inc., New York, Chapters 1.2.5, 1.2.6 and 1.2.7.
- Best, M.G.  
1982: Igneous and metamorphic petrology; W.H. Freeman and Company, San Francisco, 630 p.
- Bryan, W.B.  
1972: Morphology of quench crystals in submarine basalts; *Journal of Geophysical Research*, v. 77, p. 5812-5819.
- Clague, D.A.  
1976: Petrology of basaltic and gabbroic rocks dredged from the Danger Island Troughs, Manihiki Plateau; *in* Initial Reports of the Deep Sea Drilling Project, v. 33, ed. S.O. Schlanger, E.D. Jackson et al. U.S. Government Printing Office, p. 891-900.
- Deer, W.A., Howie, R.A. and Zussman, J.  
1966: An Introduction to the Rock Forming Minerals; Longman Group Ltd., London, England, 528 p.
- Dudas, F.O.  
1983: The effect of volatile content on the vesiculation of submarine basalts: *Economic Geology, Monograph 5*, p. 134-141.
- Hall, J.K.  
1973: Geophysical evidence for ancient sea floor spreading from Alpha Cordillera and Mendeleev Ridge; *in* Arctic Geology, ed. M.G. Pitcher, American Association of Petroleum Geologists, Memoir 19, p. 542-561.
- Herron, E.M., Dewey, J.F., and Pitman, W.C. III  
1974: Plate tectonics model for the evolution of the Arctic; *Geology*, v. 2, p. 377-380.
- Irving, E. and Sweeney, J.F.  
1982: Origin of the Arctic Basin; *Royal Society of Canada, Transactions, Series 4*, v. 20, p. 409-416.
- Jackson, E.D., Bargar, K.E., Fabbri, B.P. and Heropoulos, C.  
1976: Petrology of the basaltic rocks drilled on Leg 33 on the Deep Sea Drilling Project; *in* Initial Reports of the Deep Sea Drilling Project, v. 33 ed. S.O. Schlanger, E.D. Jackson et al. ; Washington, U.S. Government Printing Office, p. 571-605.
- King, E.R. Zeitz, I., and Alldredge, L.R.  
1966: Magnetic data on the structure of the central Arctic region; *Geological Society of America, Bulletin*, v. 77, p. 619-646.
- LeCheminant, G.M.  
1983: Project CESAR, Alpha Ridge: Mineralogy Report M83-66, Geological Survey of Canada, 4 p.

- Leterrier, J., Maury, R.C., Thonon, P., Girard, D. and Marchal, M.  
1982: Clinopyroxene compositions as a method of identification of magmatic affinities of paleo-volcanic series; *Earth and Planetary Science Letters*, v. 59, p. 139-154.
- Mair, J.A. and Lyons, J.  
1981: Crustal structure and velocity anisotropy beneath the Beaufort Sea; *Canadian Journal of Earth Sciences*, v. 18, p. 724-741.
- Moore, J.G., Clague, D.A. and Normark, W.R.  
1982: Diverse basalt types from Loihi seamount, Hawaii; *Geology*, v. 10, p. 88-92.
- Moore, J.G. and Schilling, J.G.  
1973: Vesicles, water and sulfur in Reykjanes ridge basalts; contributions to *Mineralogy and Petrology* v. 41, p. 105-118.
- Nisbet, E.G. and Pearce, J.A.  
1977: Clinopyroxene composition of mafic lavas from different tectonic settings: *Contributions to Mineralogy and Petrology*, v. 63, p. 149-160.
- Self, S.  
1982a: Terminology and classifications for pyroclastic deposits, in *Pyroclastic Volcanism and Deposits of Cenozoic Intermediate, to Felsic Volcanic Islands with Implications for Precambrian Greenstone-Belt Volcanoes*, ed. L.D. Ayres; Geological Association of Canada, Short Course Notes, Winnipeg, Manitoba, May 13-15, v. 2 p. 18-37.  
1982b: Deposits of the vent area and air-fall deposits; in *Pyroclastic Volcanism and Deposits of Cenozoic Intermediate, to Felsic Volcanic Islands with Implications for Precambrian Greenstone-Belt Volcanoes* ed. L.D. Ayres; Geological Association of Canada, Short Course Notes, Winnipeg, Manitoba, May 13-15, v. 2, p. 64-70.
- Sweeney, J.F.  
1981: Arctic research for the 1980s, an expose of problems; *Geoscience Canada*, v. 8, p. 162-166.
- Trettin, J.P. and Balkwill, H.R.  
1979: Contributions to the tectonic history of the Innuitian Province, Arctic Canada; *Canadian Journal of Earth Sciences*, v. 16, p. 748-769.
- Vallier, T.L., Windom, K.E., Seifer, K.E., and Lee-Wong, F.  
1981: Petrological and tectonic significance of volcanic clasts in Upper Cretaceous nanofossil ooze, Deep Sea Drilling Project site 466, Southern Hess Rise; in, Thied, J., T.L. Vallier, et al., *Initial Reports of the Deep Sea Drilling Project*, v. 62, (U.S. Government Printing Office), p. 961-966.
- Vogt, P.R. and Ostenso, N.A.  
1970: Magnetic and gravity across the Alpha Cordillera and their relation to Arctic sea floor spreading; *Journal of Geophysical Research*, v. 75, p. 4925-4937.
- Yorath, C.J. and Norris, D.K.  
1975: The tectonic development of the southern Beaufort Sea and its relationship to the Origin of the Arctic Ocean Basin; in *Canada's Continental Margins* ed. C.J. Yorath, E.R. Parker and D.J. Glass : Canadian Society of Petroleum Geologists, Memoir 4, p. 589-611.





# LITHOSTRATIGRAPHY OF THE CESAR CORES

P.J. Mudie<sup>1</sup> and S.M. Blasco<sup>1</sup>  
Geological Survey of Canada

Mudie, P.J. and Blasco, S.M., *Lithostratigraphy of the CESAR core; in Initial Geological Report on CESAR — the Canadian Expedition to Study the Alpha Ridge, Arctic Ocean*, ed. H.R. Jackson, P.J. Mudie and S.M. Blasco; Geological Survey of Canada, Paper 84-22, p. 59-99, 1985.

## Abstract

Sixteen piston cores and twelve gravity cores were successfully recovered from northern and southern crests of the eastern Alpha Ridge and from the Alpha Ridge graben. All but one core contain late Cenozoic muds with variable amounts of sand- to pebble-sized clastic material that probably reflects transport by ice during the past 4-5 Ma. Sixteen Cenozoic-Holocene lithostratigraphic units have been delimited on the basis of sediment texture, structure, colour, detrital carbonate and authigenic ferromanganese content. The composition of the upper 13 units in the CESAR cores is similar to the Fletcher's Ice Island cores; hence most units can be broadly correlated over most of the Central Arctic Ocean. Three new lithostratigraphic units (A1-A3) occur at the base of CESAR cores from the northern Alpha Ridge crest. Paleomagnetic and palynological data indicate a Late Miocene-Early Pliocene age for unit A3, which confirms previous reports of a slow sedimentation rate during the Cenozoic.

CESAR core 6 was obtained from an erosional surface on top of a fault block at the north edge of the Alpha Ridge graben. This core contains ca. 2m of laminated diatom ooze of Campanian-Maastrichtian age and two ?Paleogene volcanic ash units below a brown mud unit which probably corresponds to units A2 and A3. The biosiliceous ooze contains no foraminifera or silicoflagellates and only few dinoflagellates. There is little difference in biogenic or clastic sediment content between light and dark laminae and the rhythmites do not appear to be annual varves produced in an upwelling environment. The microstructure and fluctuating mineral composition of the laminae most closely resemble those of laminated chert beds in the Triassic forearc basins of Japan.

## Résumé

Seize carottes ont été prélevées au moyen d'une carotteuse à piston et douze au moyen d'une carotteuse à chute libre dans les crêtes nord et sud de la partie est de la dorsale Alpha et du graben de la dorsale Alpha. Toutes les carottes sauf une contiennent des boues du Cénozoïque récent ainsi que diverses quantités de matériau clastique dont les dimensions varient de celles du sable à celles du galet et dont la présence reflète vraisemblablement un transport par la glace au cours des quatre ou cinq derniers millions d'années. Seize unités lithostratigraphiques d'âge cénozoïque-holocène sont délimitées en fonction de la texture sédimentaire, la structure, la couleur et le contenu en matériau carbonaté détritique et en ferromanganèse authigène. La composition des treize unités supérieures dans les carottes CESAR s'apparente à celle des carottes qui proviennent de l'île de glace Fletcher et ces unités peuvent être corrélées plus ou moins sur la plus grande partie de l'océan Arctique central. On a décelé la présence de trois nouvelles unités lithostratigraphiques (A1 à A3) à la base des carottes CESAR prélevées dans la crête nord de la dorsale Alpha. Les données paléomagnétiques et palynologiques indiquent que l'unité A3 date du Miocène récent-Pliocène ancien, ce qui confirme que la sédimentation s'est faite lentement au cours du Cénozoïque, conclusion à laquelle avaient abouti d'autres travaux.

<sup>1</sup>Atlantic Geoscience Centre, Bedford Institute of Oceanography, Box 1006, Dartmouth, Nova Scotia, B2Y 4A2

*La carotte CESAR 6 provient d'une surface d'érosion située au-dessus d'un bloc faillé sur la marge nord du graben de la dorsale Alpha. Elle contient environ 2 m de boue de diatomées laminaire qui date du Campanien-Maestrichtien et deux unités de cendres volcaniques du ?Paléogène sous-jacentes à une unité de boue brune correspondant vraisemblablement aux unités A2 et A3. La boue siliceuse de nature organogène ne contient pas de foraminifères ni de silicoflagellés et seulement quelques dinoflagellés. Le contenu en sédiments organogènes ou clastiques varie très peu dans les lames claires et sombres et les lames rythmiques ne semblent pas être des varves annuelles produites dans un milieu caractérisé par la remontée des eaux marines. La microstructure et la composition minérale variée des lames s'apparente étroitement à celles des couches de chert laminaires dans les bassins d'avant-arc triasiques du Japon.*

## INTRODUCTION

During the Canadian Expedition to Study the Alpha Ridge (CESAR), 28 sediment cores were successfully recovered from the central Arctic Ocean. These cores include the first piston cores taken specifically for sedimentological study of the bathyal Arctic Ocean region. Previous sedimentological studies of this region (Herman, 1974; Clark, 1977; Clark et al., 1980) had to rely on cores taken primarily for geophysical studies; hence, many of these cores were disturbed by sampling or desiccation prior to the commencement of the sediment studies (Clark, 1982). The purposes of this report are to provide the following data on the fresh Arctic Ocean sediment cores: 1) a detailed account of the field and laboratory methods used to obtain, curate and sample the CESAR cores; 2) a description of the lithofacies and their regional correlation; and 3) initial paleoecological interpretation of the lithofacies.

## ACKNOWLEDGMENTS

We are grateful to several persons who contributed considerable time to logging the CESAR cores (especially Oliver Maass, Department of Geology, University of Toronto and F.E. Cole, Atlantic Geoscience Centre) and who provided initial biostratigraphic/SEM data (F.E. Cole and B. Deonarine, Atlantic Geoscience Centre). Dr. Patricia Stoffyn (Atlantic Geoscience Centre) has been especially helpful in providing initial geochemical data; W. LeBlanc (Atlantic Geoscience Centre) provided the data for Table 6.3. Several persons provided valuable ideas regarding analysis of the CESAR 6 laminated sediments, particularly Carolyn Isaacs (United States Geological Survey, Menlo Park), Wolfgang Berger and Andy Soutar (Scripps Institute of Oceanography), and David J.W. Piper (Atlantic Geoscience Centre) who also reviewed this paper.

## METHODS

### *Field operations*

During CESAR, both piston and gravity coring were possible because the necessary equipment could be transported to the ice camps by C-130 Hercules aircraft. All CESAR piston cores were obtained from the main ice camp; CESAR gravity cores were obtained from both the main camp and the remote camp.

In order to obtain piston cores from the ice platform, in  $-40^{\circ}\text{C}$  weather, several modifications of the normal ship-board coring procedures had to be adopted. The required equipment modifications and operational procedures are described in detail by Jodrey and Heffler (1985). Aspects of the coring operations that affected the quality and length of core recovery are outlined below.

The piston corer was constructed from two or three 10ft (3.1m) Benthos core barrels connected by an adapter to a 1200lb (545kg) Alpine core head in order to meet the 550kg weight handling restrictions of the camp and transport facilities. Coring was performed using a standard Benthos split-piston system. Because of the limited size of the hole ( $1.8 \times 1.2 \times 2\text{m}$ ) that could be kept open for access through the ice, initially a shortened (0.5m) trip arm was used for the trigger weight. CESAR cores 1-3 were obtained with this system; however, the trigger weight frequently became tangled around the main cable and a core head was lost on the fourth attempt. Thereafter, a standard trip-arm length of 1.0m was used for all piston coring. This usually resulted in full corer penetration but the piston always advanced about 60cm above the core sediment and usually less than 3/4ths of the core barrel was filled. A damaged piston valve also reduced the quality of core recovery at sites 2-7; a new valve could not be installed until after recovery of CESAR core 10.

Gravity coring at the main camp was carried out using a light weight corer constructed from a Benthos core head and a 1.5m length of plastic core liner, with an attached corecutter and catcher. CESAR cores 201-211 were obtained by this method which was used successfully for coring on the Lomonosov Ridge (Blasco et al., 1979). At water depths of more than 1475m on the flanks of the northern crest of Alpha Ridge, sediment penetration and core recovery mostly ranged from 44-76cm. At shallower depths, however, less than 10cm of sediment was penetrated and recovered, apparently due to a shallow layer of carbonate-rich "hardgrounds" (see CENOZOIC SEDIMENTS). Gravity coring from the mobile camp was performed using a Benthos gravity corer and a 10ft (3.3m) core barrel. This coring system was used to obtain CESAR cores 101-112 from the north side of the southern crest of Alpha Ridge. Penetration ranged from 63-145cm in sediments below the 1475m isobath, and recovery ranged from 9cm at 1490m to 133cm at the deepest site, 1882m. Above the 1475m isobath, penetration ranged from 0-90cm and recovery was 50-100% complete.

Handling and storage of piston cores on CESAR also presented problems due to the confined lab space and very low outdoor temperatures ( $-40^{\circ}$  to  $-10^{\circ}\text{C}$ ). A few sections of CESAR cores 1-6 were lost during derigging operations because of problems during initial attempts to keep the core barrels in a vertical position. The core liners were cut into 1.5m sections and stored vertically in a heated area to prevent freezing and subsequent loss of detailed sediment structure. This procedure was generally successful and freezing only

affected small sections of 2 cores: CESAR core 102, at 10cm depth and CESAR core 3, at depths of 110, 130, and 570cm. During transport from the ice camp, the cores were stored vertically in narrow wooden crates and loaded upright into an aircraft cargo-hold which was heated to above freezing.

Table 6.1 lists the locations of the core sites, water depths, and lengths of the sediment recovered. Location of the core sites was controlled by two main logistical con-

Table 6.1 Core numbers, locations, water depths, total length recovered, and time at sediment penetration.

Field number	Latitude °N	Longitude °W	Depth (m)	Length (m)	Day	Time (hr)
CESAR 83-001	85 48.5	110 44.0	2150	5.40	098	1530
" 83-002	85 45.1	110 54.7	1900	6.70	101	0900
" 83-003	85 52.0	109 49.1	1300	7.52	105	2145
" 83-004	85 49.3	109 18.2	1725	4.57	118	1746
" 83-005	85 49.5	109 15.2	1680	3.96	119	2030
" 83-006	85 49.8	109 09.2	1365	3.65	121	1950
" 83-007	85 51.1	108 42.8	1250	3.13	122	2045
" 83-008	85 51.7	108 16.0	1460	4.73	123	2045
" 83-009	85 52.0	108 15.5	1500	5.79	125	0130
" 83-010	85 51.3	108 18.0	1425	4.97	125	2205
" 83-011	85 50.9	108 21.2	1380	5.44	126	2340
" 83-012	85 50.7	108 24.5	1345	5.03	127	2220
" 83-013	85 50.7	108 23.1	1360	5.10	129	0252
" 83-014	85 50.8	108 21.6	1370	4.40	130	0130
" 83-015	85 50.9	108 19.5	1405	4.95	131	1515
" 83-016	85 49.5	108 36.3	1500	3.89	134	2322
Remote camp gravity cores						
CESAR 83-101	85 38.1	111 07.01	1490	0.09	103	1732
" 83-102	85 38.1	111 07.1	1495	1.18	103	1945
" 83-103	85 38.1	110 07.0	1882	1.33	104	0206
" 83-104	85 31.2	110 20.5	1253	0.15	107	2048
" 83-105	85 31.2	110 20.5	1175	0.20	107	2325
" 83-106	85 31.3	110 18.5	1188	0.11	108	1624
" 83-107	85 31.2	110 17.9	1227	0.00	109	ND
" 83-108	85 31.3	110 17.3	1226	0.16	109	1611
" 83-109	85 29.2	110 36.5	1190	0.08	115	0239
" 83-110	85 28.8	110 37.5	1184	0.00	115	1410
" 83-111	85 28.3	110 43.2	1170	0.11	115	2145
" 83-112	85 27.9	110 51.8	1180	0.45	116	1325
Main camp gravity cores						
CESAR 83-201	85 52.4	108 38.8	1533	0.76	110	1655
" 83-202	85 52.2	108 39.2	1585	0.10	111	2103
" 83-203	85 52.3	108 39.7	1480	0.44	112	1620
" 83-204	85 52.2	108 40.2	1475	0.01	113	0330
" 83-205	85 52.2	108 43.2	1400	0.09	113	1557
" 83-206	85 51.9	108 46.1	1400	0.00	113	1900
" 83-207	85 51.9	108 47.0	1375	0.00	113	2040
" 83-208	85 51.3	108 54.5	1188	0.00	114	0550
" 83-209	85 49.5	109 16.2	1690	0.00	116	1640
" 83-210	85 49.5	109 15.2	1680	0.52	117	1420
" 83-211	85 43.9	108 51.9	1730	0.46	118	ND

straints: a) the random direction and speed of the ice camp drift, and b) the time required for setting up the coring operation and re-rigging the corer. The loss of the core head delayed sampling between sites 3 and 4, and coring time was also limited by other demands on winch operation and personnel. Rigging and lowering of the corer took 12 hours and the maximum repetition rate for piston coring was one per 24 hours. The locations of the 16 piston core sites and 14 gravity core sites are shown in Figures 6.1 and 6.2. It should be noted that the water depths for the core sites were measured using echo sounder records corrected for an estimated water sound velocity of  $1.47\text{km.s}^{-1}$ ; the depths have maximum errors of ca.  $\pm 100\text{m}$ . Navigational positioning was determined from four Marconi-761 receivers and is accurate to  $\pm 20\text{m}$ .

### Laboratory procedures

The crates of CESAR cores were transported to the Atlantic Geoscience Centre (AGC) core facilities where they have been curated and stored in a  $4^\circ\text{C}$  refrigerated room. From late June through July 1983, all the cores were split, photographed in colour, X-radiographed, and visually described. At all times during these procedures, great care was taken to avoid contamination of the cores by contact with metal tools or by dust, and to prevent drying or cracking of the sediments. The unsplit core liners were first engraved with the core number and length on 2 sides at the top end. The core liners were then placed in a steel tray to which a precision adjustable router blade was attached, and shallow grooves were cut along the two opposite sides of the core length. The

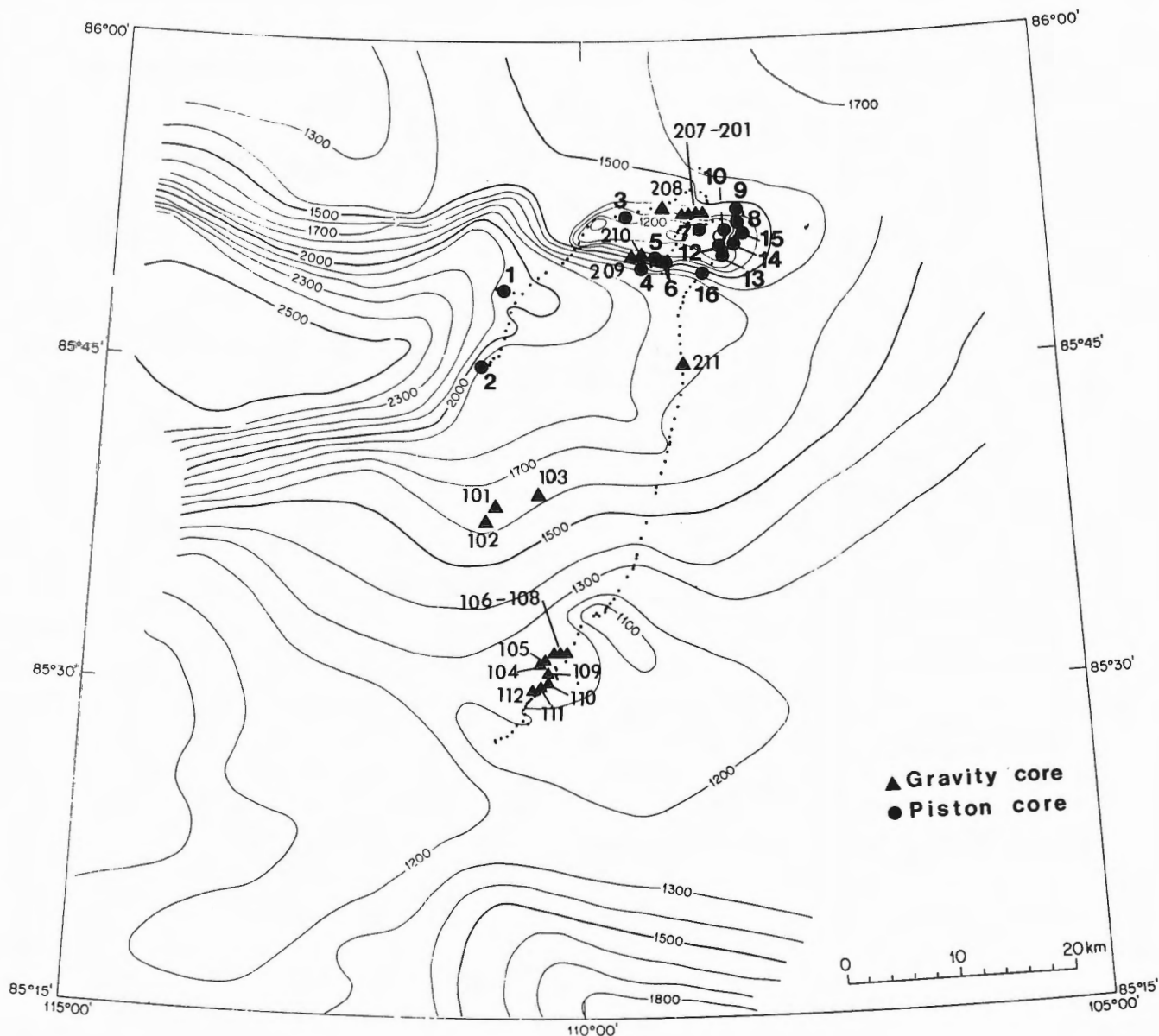


Figure 6.1 Bathymetric map of the eastern Alpha Ridge and locations of the core sites; fine dotted line is the drift track of the CESAR main camp.

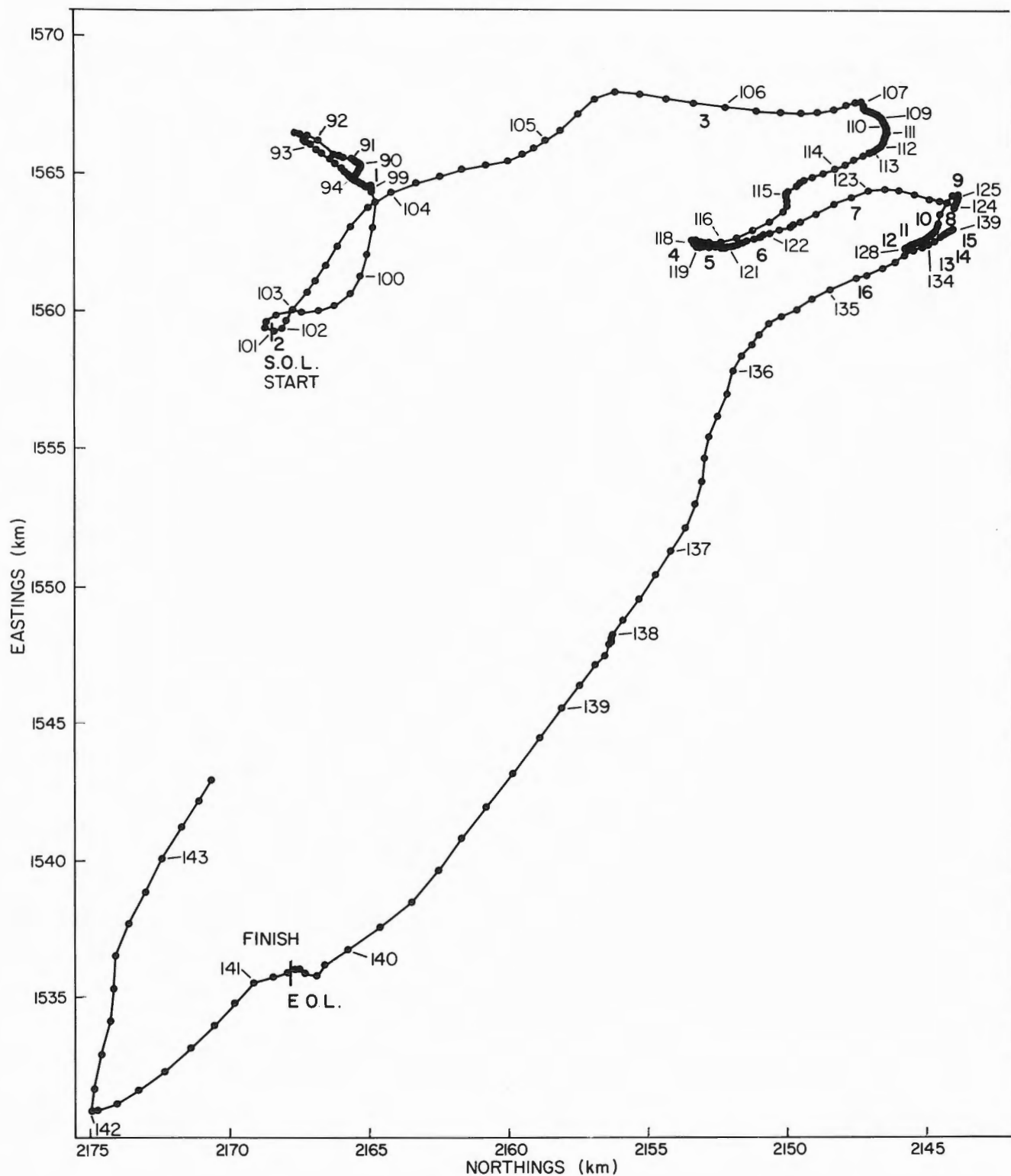


Figure 6.2 Drift track of CESAR main camp, showing time in Julian days and piston core locations (circled numbers). Vertical lines mark the start of the survey line (S.O.L.) and end of the survey line (E.O.L.).



grooves were carefully cut through with a metal blade, then the sediment was split in half by drawing nylon line down the grooves. Immediately after separation of the two core halves, sediment surfaces were covered by thin transparent plastic wrap. One core half was designated as the archive core and this was immediately enclosed in heavy plastic tubing, labelled, and stored in sealed, labelled D-tubes on horizontal racks in the refrigerated room. Wherever possible during the examination and subsequent sampling of the working core halves, care was taken to leave the thin plastic wrapping over the core surface. When not in use, the working halves were stored in the refrigerator in plastic tubing and D-tubes, as described above for the archive cores.

Figure 6.3 shows the total length of the CESAR piston cores and their composite section lengths as recovered in the field. By the time of core splitting and description, however, many of the sediment sections were slightly shorter (ca. 1-4cm) due to dewatering and settling. According to AGC core description procedures (Mudie et al., 1984), the core lengths were measured and logged in the laboratory by setting the top of the sediment in section 1 as 0cm and by assuming continuity between the sediment at the base of each section and the sediment surface at the top of the adjoining section (i.e. disregarding the presence of small empty sections at the tops of some core liners). This procedure should be carefully noted by all persons who wish to re-examine or sample the CESAR cores. It should also be noted that the field numbering system, which logged the cores as CESAR 83-001 to CESAR 83-211 was systematically changed in the laboratory to the shorter format of CESAR 1 to CESAR 211.

Because of the irreplaceable value of the CESAR cores and the need to carry out detailed multidisciplinary chronostratigraphic, sedimentological, biostratigraphic and geochemical studies on sediments with very slow deposition rates (average ca. 1mm per 1000 years according to studies of USGS ice island cores by Clark et al., 1980), a systematic sampling routine had to be carefully determined. This system (Fig. 6.4) was designed to ensure that the sediments were not disturbed or contaminated by sampling tools prior to high resolution paleomagnetism studies (*see* Aksu, 1985), or for CESAR 6, prior to geochemical studies of the laminated sediments.

## CENOZOIC SEDIMENTS

### Introduction

All except one of the CESAR cores, viz. CESAR 6, contained soft brown muds similar to those described by Clark et al. (1980) and by Herman (1974). Although the precise maximum age and paleoenvironmental interpretation of these sediments is presently uncertain (compare Herman, 1983, and Clark, 1982), there is unanimous agreement that these sediments are of late Cenozoic age. Clark et al. (1980) have also demonstrated that there is a strongly correlatable down-core sequence of 13 sediment units present in about 500 USGS cores collected over a 400,000km<sup>2</sup> area of the Canada Basin, including the southern crest of Alpha Ridge. For the sake of inter-regional comparison between CESAR

cores and those from other parts of the Canada Basin, we adopted the following procedures for describing the CESAR cores:

1. David L. Clark (U. Wisconsin) visually examined all the CESAR cores when they were split and he delimited those lithofacies which probably correspond to the thirteen units, A-M, in the USGS cores described by Clark et al. (1980).
2. In this report, we have tried to use Clark's sedimentological criteria and nomenclature for the lithostratigraphic summaries, although our preliminary studies suggest that some of Clark's units should be redefined to better reflect mesoscale sedimentary structures and to clarify the definition of boundaries between lithofacies.

Since Clark's visit in June 1983, a more detailed description of 48 USGS cores from the eastern Alpha Ridge has been published (Minicucci and Clark, 1983), which defines several new lithostratigraphic units in order to facilitate correlation between these cores and those obtained earlier from the Chukchi Rise and western Alpha Ridge. Lithological units in four CESAR cores which have been sampled at 1-2cm intervals for magnetostratigraphic, lithostratigraphic, and biostratigraphic studies, appear to correspond more closely to Minicucci and Clark's (1983) redefined lithofacies. The details of the lithofacies in these 4 CESAR cores are described in the following section, but much more study is required before the lithofacies in all the CESAR cores can be defined and correlated precisely. Therefore, the summary diagram and descriptions in this report will mainly continue to use the generalized lithostratigraphic system of Clark et al. (1980).

### Piston cores CESAR 14 and 15

These two piston cores were selected for detailed study because they appeared to contain the least disturbed and most complete lithological sequences. Both cores were obtained from a relatively small (ca. 5km wide), gently sloping basin or terrace extending from 1345-1425m on the northeastern margin of Alpha Ridge. Seismic profiles at these sites (*see* Jackson, 1985) show that subsurface reflectors are flat-lying.

Figures 6.5 and Plate 6.1 show the detailed structures and salient lithological features of CESAR 14 and 15 as determined from visual inspection, X-radiographs and initial sedimentological studies. Eleven lithological units (M to A-B) can be discerned, which correspond fairly closely to those described by Minicucci and Clark (1983); however, two or three additional units (A1-A3) are present at the base of the CESAR cores; paleomagnetic data (*see* Aksu, 1985) indicate that these units are up to 0.5 Ma older than the AB unit (ca. 3.7 Ma) at the base of the USGS cores from eastern Alpha Ridge (Minicucci and Clark, 1983).

Unit M in CESAR 14 (Fig. 6.5) is a foraminifera-rich sandy mud with a distinctive coarse yellowish (10 YR 5/4) carbonate bed at the base. This carbonate layer corresponds to the pink-white layer, PW2, of unit M and M' (in USGS cores), but the overlying soupy mud in CESAR 14 was highly disturbed during coring, and the typical uppermost pink-

# CESAR 83

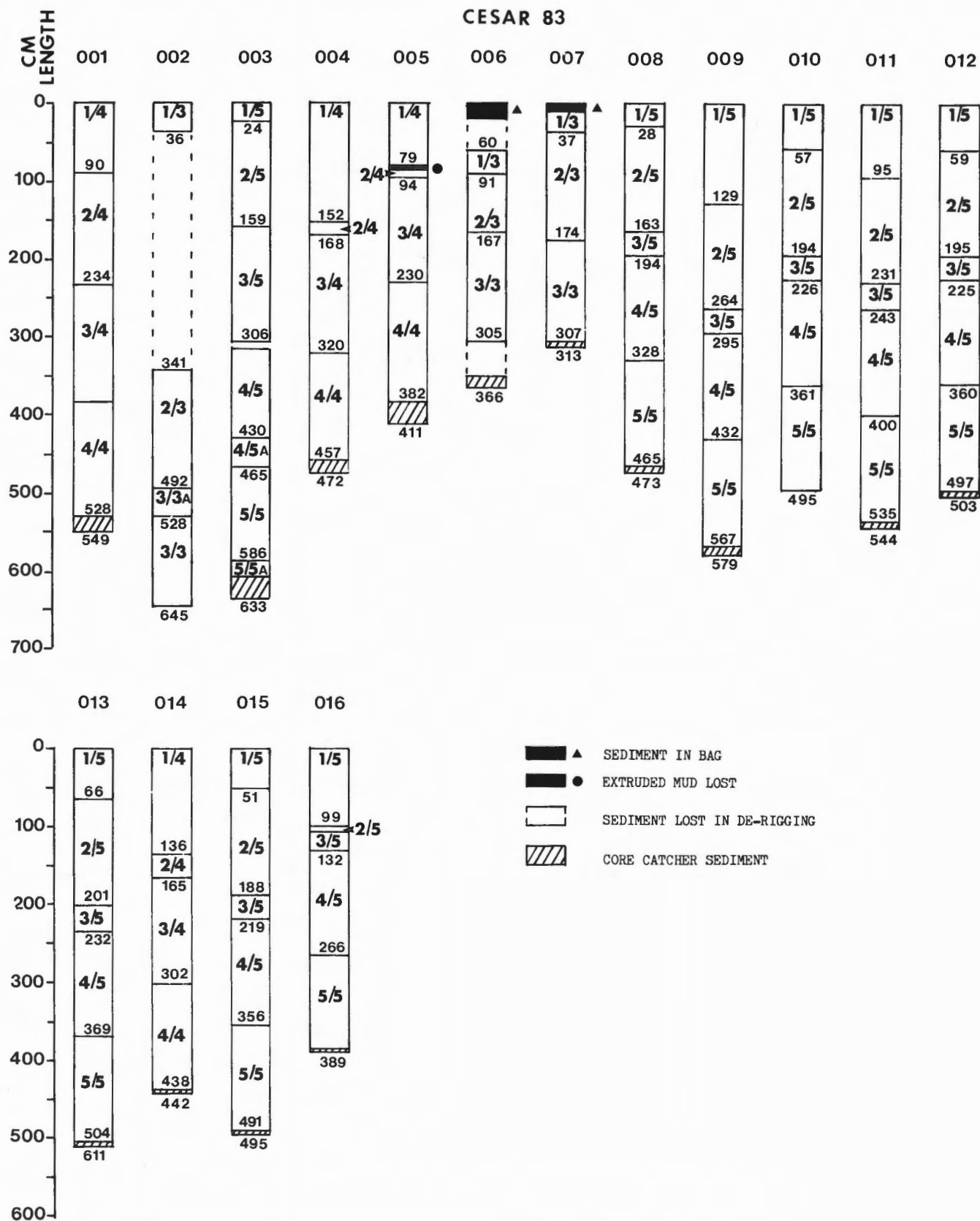


Figure 6.3 CESAR piston cores: liner section numbers (shown as fractions) and sediment lengths recovered (in cm) as recorded in the field.

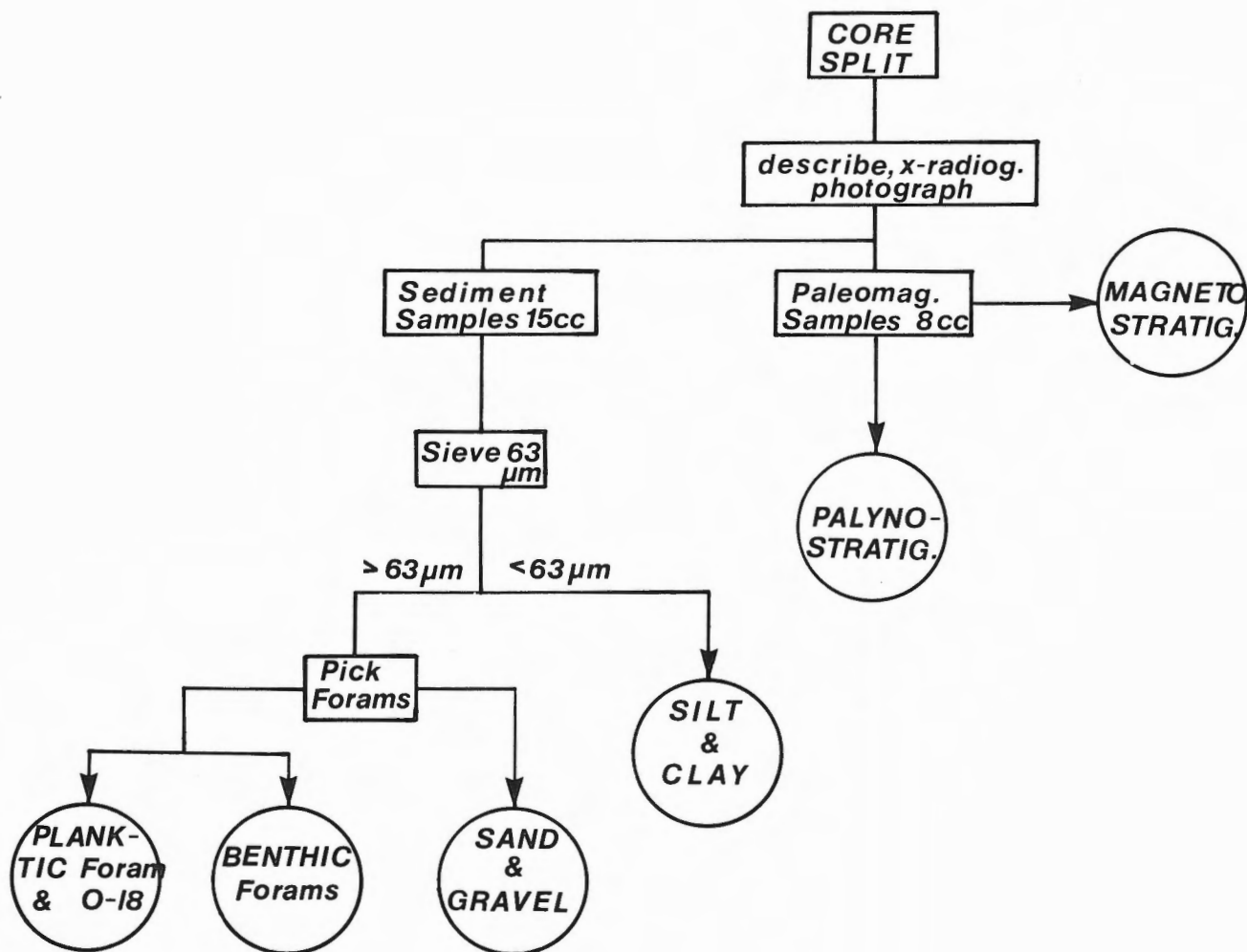


Figure 6.4 Flow chart for sampling and study of CESAR cores.

white layers, W2 and W3, appear only as scattered pebble- to gravel-sized pinkish-brown (10 YR 7/4) clasts. These upper carbonate layers and intervening sandy or silty mud beds may be more clearly seen, however, in CESAR 15 (Plate 6.1) and in several CESAR gravity cores, e.g. CESAR 103 (Fig. 6.6).

Unit L is a distinctive light olive-brown (2.5 YR 5/4), fine sandy mud, which has a darker, slightly mottled silty mud at the top. These features are typical of all the USGS cores. CESAR 14 and other CESAR cores with a well developed unit L, however, show a coarser, greyish sandy base grading upwards to finer sandy silt with 2-4 distinctive thin (2-4mm) grey sand laminae at 5-10cm intervals. Scattered grey or pinkish carbonate clasts may be present in the upper mottled layer.

Unit K is a dark brown (10 YR 3/3) silty to sandy mud which is heavily mottled at the base and top, and grades in the centre to a sandy bed mottled with grey or pale brown carbonate-rich clasts. This carbonate layer appears to correspond to W1 of Minicucci and Clark (1983) but their other subunits K'1 and K'2 cannot be discerned in the CESAR cores.

Unit J is a pale pinkish brown (10 YR 6/3) carbonate-rich sandy to silty mud with gradational contacts at the top and base. The coarse pinkish sediment generally corresponds to the PW1 layer in the USGS cores (Clark et al., 1980; Minicucci and Clark, 1983) but no overlying white zone appears in the CESAR cores. Instead, there is a wispy, thin (4mm) basal pinkish lamina in CESAR 14, which is overlain by a mottled brown mud layer, then a less mottled greyish mud with a distinctive thin (0.5cm) grey sand lamina, above which is a firm pinkish carbonate layer ca. 4cm thick. A similar sequence is found in CESAR 15, but in other cores, e.g. CESAR 103, the upper carbonate layer is mixed with dark brown mud.

Unit I is a faintly banded brown silty to sandy mud which is gravelly at the base and becomes finer grained towards the top. The banding consists of layers (ca. 5-10cm thick) of heavily mottled dark brown mud that alternate with lighter brown, sparsely mottled sandy mud containing thin (3-5cm) grey sandy laminae. Unit I in CESAR 14 and 15 differs from unit I of Clark et al. (1980) in having a mottled base and gradational contact with unit H, but the charac-

# CESAR CORE 14

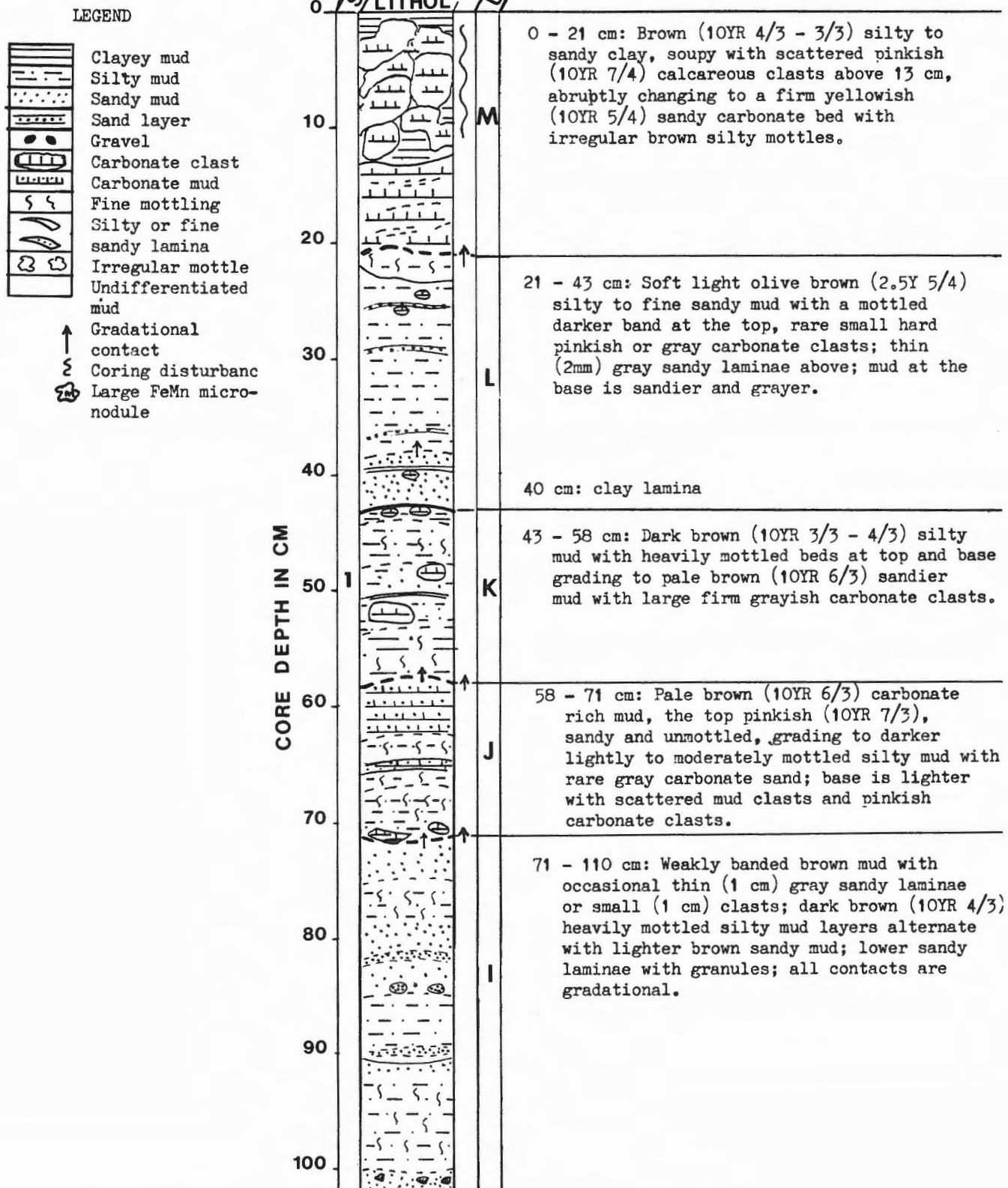


Figure 6.5 Lithological log of sediment types and structures in CESAR 14 and summary descriptions of the lithological units.

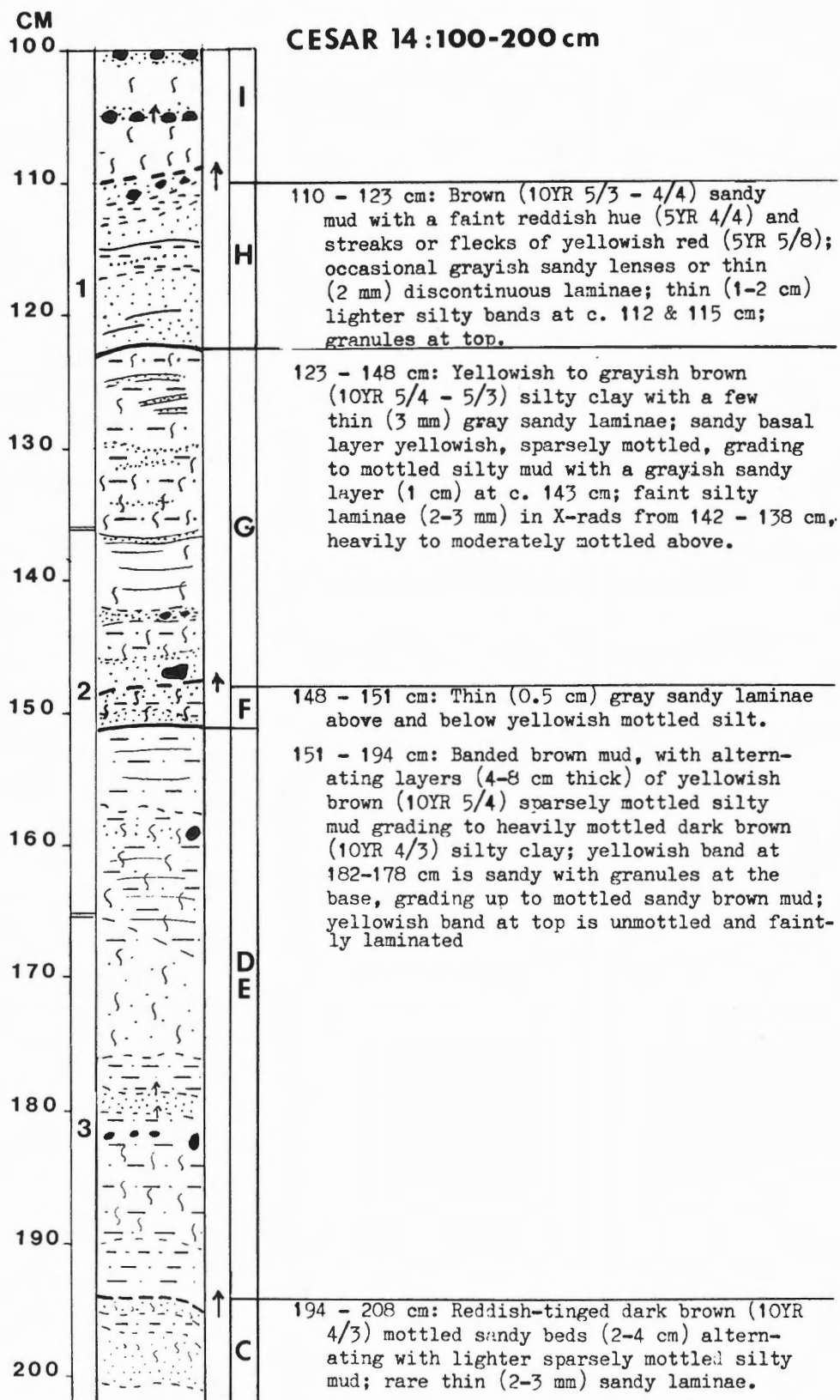


Figure 6.5 (cont'd)



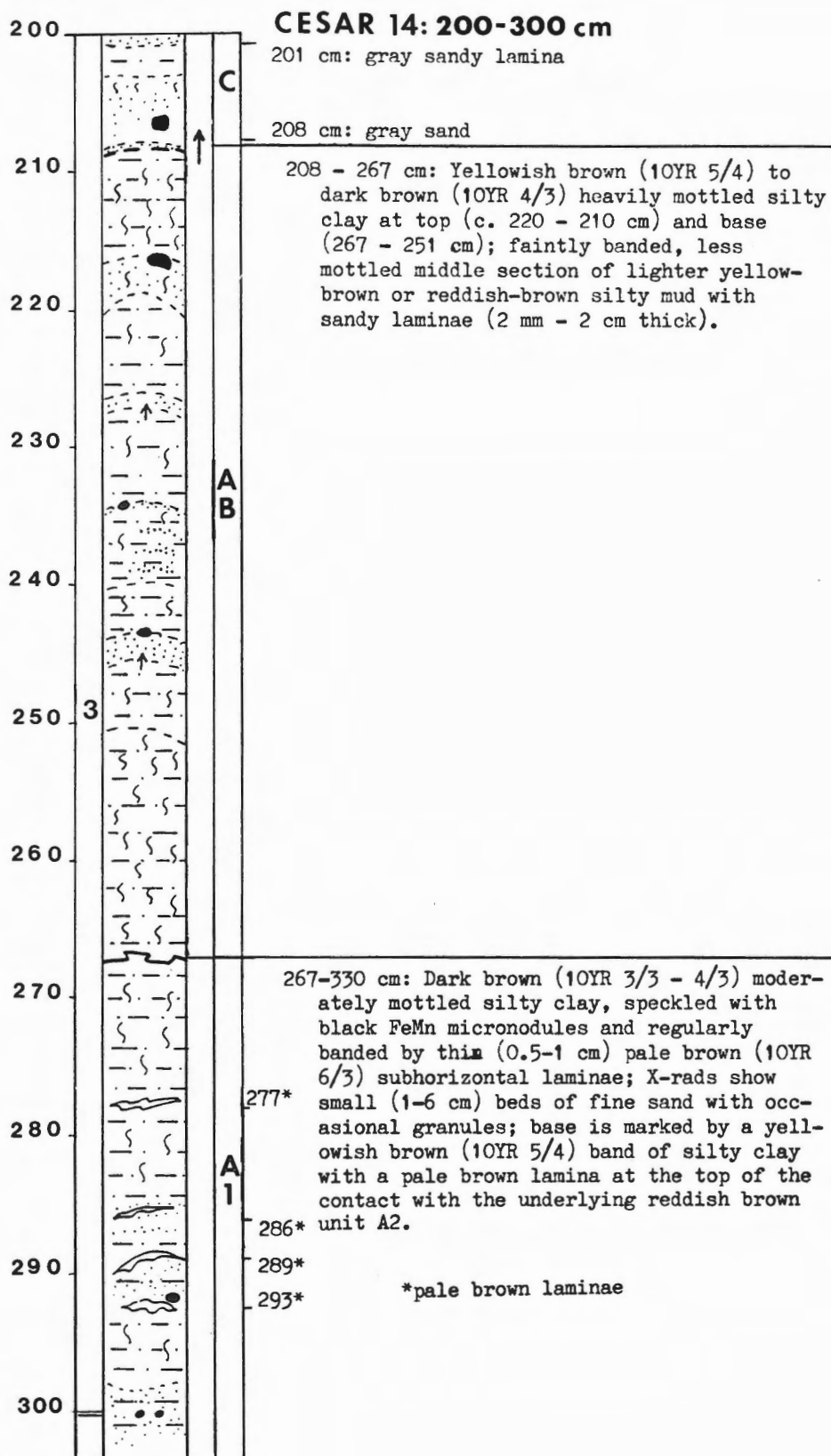
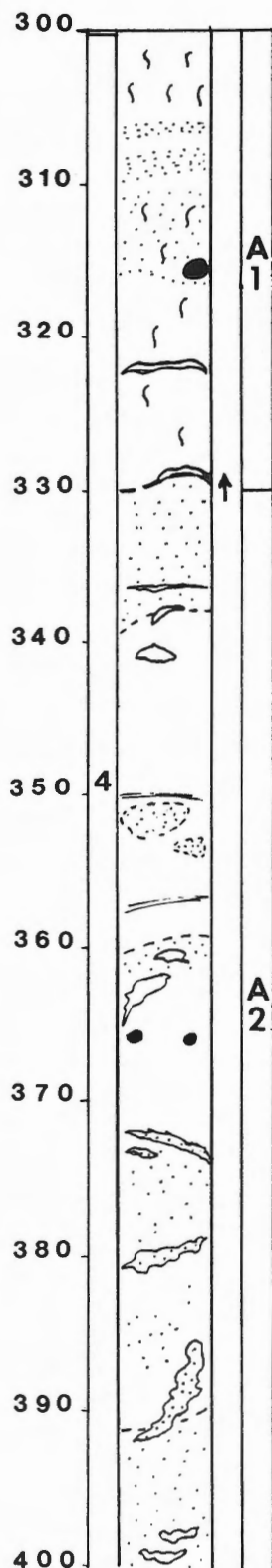
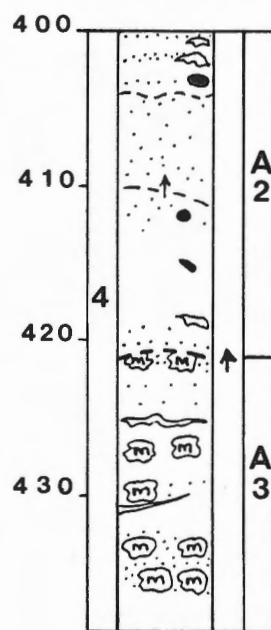


Figure 6.5 (cont'd)

# CESAR 14:300-439 cm



330 - 421 cm: Dark reddish brown (5YR 3/4) to brown (10YR 4/3 - 3/3) silty mud in thick bands (10-30 cm) with sparse to massive mottling and irregular light yellowish brown laminae; bands at top (338-330 cm) and base (420-404 cm) are strongly red-tinged, sandy & sparsely mottled with small (2 mm) FeMn micronodules; from 404-392 cm, mud is browner, sandier and densely speckled with FeMn; reddish mud from 392-360 cm has conspicuous, irregular yellowish laminae and rare FeMn; from 360-338 cm, brown mud has larger, unspeckled grayish patches and rare thin clayey laminae.



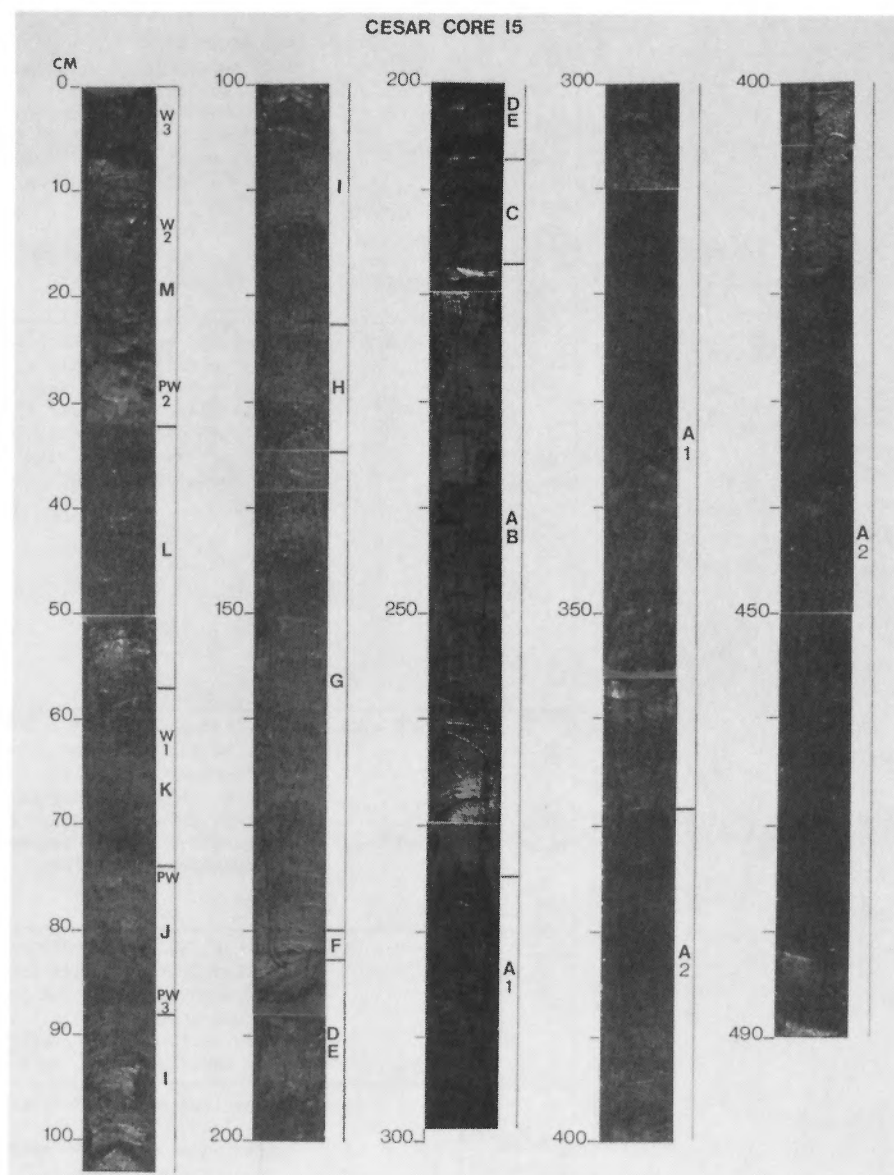
421 - 439 cm: Dark brown (10YR 3/3) sandy mud heavily mottled with large (0.5 cm) & small FeMn micronodules; rare thin (2 mm) light brown laminae below; mottled brown (10YR 5/3) band (3 cm) at top.

End of core at 439 cm

Figure 6.5 (cont'd)

**Plate 6.1**

Photographic log of sediments in CESAR 15, showing the distribution of lithological units M to A2, and the position of the PW and W marker beds.



teristic central lighter brown, less mottled, sandy zone with thin grey sand laminae is present. Subunits I'1 and I'2 of Minicucci and Clark (1983) cannot be discerned in the CESAR cores.

Unit H in CESAR 14 and 15 is a reddish-tinged brown sandy mud, with a central layer (ca. 2-3cm) of lighter, less mottled silty mud. It is also characterized by the presence of three thin (4mm) grey sand laminae spaced 2-4cm apart. The basal contact is fairly sharp but the top is heavily mottled and grades into unit I. Subunits Ha through He of Clark et al., (1980) cannot be distinguished in CESAR 14 and 15.

Unit G is a moderately to lightly mottled yellowish to greyish brown silty mud with several thin (3mm) grey sandy laminae. The basal half is generally lighter coloured than the top and the basal contact is gradational, making it difficult to distinguish from unit F in all the CESAR cores. Unit F is characterized by two thin (1cm) mottled dark brown layers

containing grey sand laminae and separated by lighter brown, sparsely mottled silty mud. A sandy grey lamina at the base of unit F forms a sharp contact overlying the light brown mud at the top of unit D-E; the top of the unit is gradational. In general, unit F in the CESAR cores does not closely match either unit F of Clark et al. (1980) or F' of Minicucci and Clark (1983).

Unit D-E is a banded brown mud with a yellowish, sparsely mottled silty layer (5-10cm) at the top and base, and a yellowish central band of sandy to gravelly mud. Other darker brown, mottled layers with gradational contacts are also present. Unit E of Clark et al. (1980) cannot be distinguished in the CESAR cores; however, unit D-E in CESAR 14 and 15 seems similar to unit DE in the USGS cores from eastern Alpha Ridge (Minicucci and Clark, 1983).

Unit C consists of two or three reddish-tinged dark brown (10 YR 4/3) mottled sandy layers (ca. 2-4cm) which

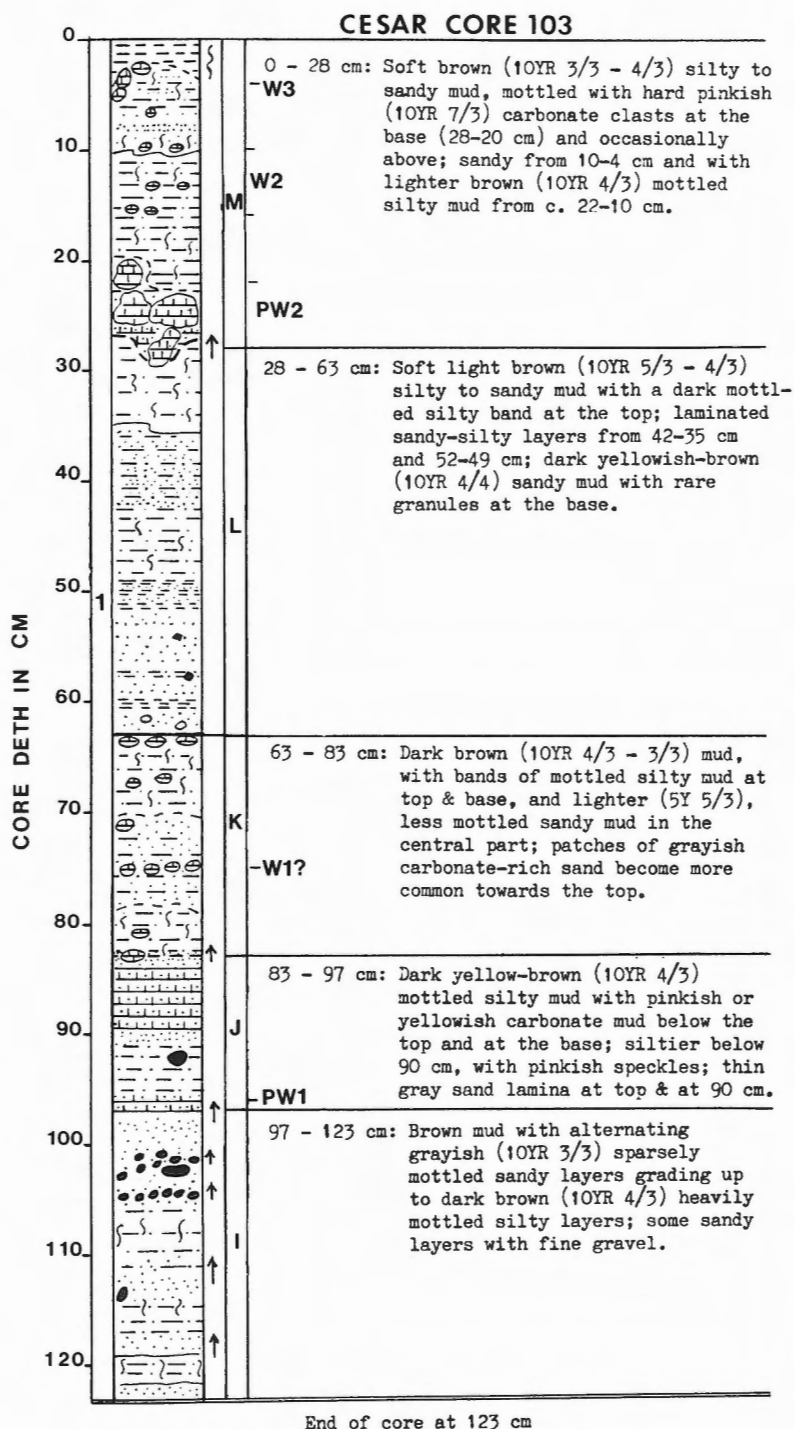


Figure 6.6 Lithological log of sediment types and structures in CESAR 103 and summary descriptions of the lithological units. See Figure 6.5 for legend to symbols used to illustrate sedimentological features.

are separated by lighter brown sparsely mottled silty mud. A thin grey sand lamina marks the base of the unit, but other contacts are gradational. This unit is only 10-20cm thick in CESAR 14 and 15, and it is not clearly distinguishable from sandy sections of unit D-E in some CESAR cores.

Unit A-B is an irregularly banded brown mud, speckled throughout with small black FeMn micronodules. From the base up, the bands consist of alternating yellowish (10 YR 5/4) mottled silty clay which grades upwards to a moderately mottled dark brown (10 YR 4/3) mud, often with sand and rare gravel at the top of the dark bands. The middle section of the unit is a lighter coloured, less mottled silty mud with thin sandy laminae. In CESAR 14 and 15, this unit appears to be similar to unit AB of the USGS eastern Alpha Ridge cores (Minicucci and Clark, 1983). In some CESAR cores, however, unit A-B is not clearly distinguishable from unit D-E.

Unit A1 is a dark brown (10 YR 3/3-4/3), moderately mottled, silty clay which is prominently marked by wispy, pale brown (10 YR 6/3), subhorizontal laminae, about 3mm to 1cm thick. The dark brown mud is regularly speckled by abundant small black FeMn micronodules. The unit contains occasional gravel, greyish mud clasts, and sandy layers or thin sand laminae. The top of the unit is marked by a sharp transition from the yellowish-brown silty mud at the base of A-B to the top of a massive dark brown mud unit with thin yellowish laminae at intervals of ca. 5-20cm. The basal contact is marked by a yellowish-brown subhorizontal lamina at the top of ca. 20cm of dark brown mud with coarse yellow mottling.

Unit A2 is a massive dark reddish-brown (5 YR 3/4) silty to sandy mud which is less speckled by FeMn micronodules than unit A1 and is conspicuously marked by blotchy or oblique-angled light yellowish-brown (10 YR 6/3) structures which resemble burrows ca. 1cm thick. The lower half of the unit and the top 10cm are sandy; the middle section is more silty, less speckled by FeMn, and includes greyish sandy layers 2-10cm thick in CESAR 14. The base of the unit is marked by a conspicuous increase in relatively large (ca. 0.5cm) FeMn micronodules at the top of unit A3.

Unit A3 is a very dark brown (10 YR 3/3), slightly sandy mud which is conspicuously mottled by relatively large (0.5cm) black FeMn micronodules in addition to abundant small black FeMn speckles. Irregular bands (2cm) or small blotches of speckled light brown mud are occasionally present. The top of unit A3 is marked by a subhorizontal band of greyish dark brown mud with large black FeMn micronodules at the base of the massive dark reddish-brown mud of unit A2.

### **Gravity cores CESAR 102 and 103**

These two cores were selected for detailed study because they contain the longest sequences of sediment recovered by the gravity corer. Both cores were obtained from gently sloping areas on the southeast side of the Alpha Ridge graben, at depths of ca. 1500m or more. Only shallow seismic data (3.5 kHz) are available for these sites, but a similar stratigraphy was obtained in CESAR 201 from the edge of a

basin on the north side of the northern Alpha Ridge crest (Fig. 6.1). The seismic profile for this area (*see* Jackson, 1985) shows smooth, flat-lying surface reflectors at this site, compared to neighbouring sites of CESAR cores 202 and 203 where surface reflectors appear truncated, and shorter gravity cores were obtained.

Figure 6.6 shows the detailed structures and salient lithological features of CESAR 103, the longest gravity core; Figure 6.7 depicts the lithofacies and marker beds in CESAR 102, 103 and all other gravity cores containing more than 5cm of sediment. The magnetostratigraphy, foraminiferal biostratigraphy, and palynostratigraphy of CESAR cores 102 and 103 are described by Aksu (1985a,b) and Mudie (1985) respectively. The main lithostratigraphic characteristics of the gravity cores are outlined as follows.

Unit M in core 103 consists of ca. 28cm of dark brown (10 YR 3/3) soft mud which is variably mottled or banded by pinkish (2.5 YR 6/4) to yellowish-brown (10 YR 7/3) carbonate-rich "hardground" layers. At the surface (0.2cm) there is a soupy, foram-rich, dark brown mud layer which coarsens downwards to mud with scattered carbonate hardgrounds and much lower foram concentrations. This carbonate layer probably corresponds to the W3 subunit of the USGS cores (Minicucci and Clark, 1983). From ca. 4-9cm, there is a greyish (5 YR 5/3) sandy mud layer with dark mottles and low foram concentrations. From 9-ca. 22cm, there is a layer of heavily mottled, foram-rich, dark brown (10 YR 3/3) silty mud with scattered small (<1cm) pinkish hardgrounds. These pinkish clasts are most conspicuous in the middle of this dark layer and may correspond to the W2 subunit of the USGS cores; in general, however, there is no distinctive whitish W2 carbonate layer in the CESAR cores. At ca. 22cm in CESAR 103, the dark brown mud is interlayered with large pinkish (10 YR 7/3) semiconsolidated carbonate-rich clasts which increase in size towards the base at ca. 28cm. This layer clearly corresponds to the PW2 subunit of the USGS cores. It also corresponds to an interval over which foram concentrations decrease greatly.

Similar lithological sequences are easily recognised in unit M of CESAR 102, 201, and 210, all of which are from water depths of ca. 1500m or more. In these cores, unit M varies in thickness from 41cm in CESAR 210 to 37cm in CESAR 102. The main differences among the cores appear to be in the thickness (10-20cm) of the mottled brown mud containing the ?W2 layer; however, the sandy mud is also thicker (10cm) in CESAR 210, and the PW2 layer ranges from ca. 8cm in CESAR 103 to 12cm in CESAR 102 and 210.

Unit L in CESAR 103 consists of about 35cm of light brown (10 YR 5/3-4/3) to olive (2.5 YR 5/4) silty or sandy mud which has a distinctive mottled brown band at the top and a dark brown layer with thin (ca. 2cm) greyish sandy laminae and scattered gravel below 50cm; the contact with unit M is gradual. The top of the upper mottled band contains relatively low foraminiferal concentrations which increase downwards in the mottled layers to ca. 35cm; from here to the base of the unit, however, foraminifera are rare or absent. The base of unit L in CESAR cores 103 and 102 is sharply defined by a greyish, coarse sandy layer overlying the dark brown,



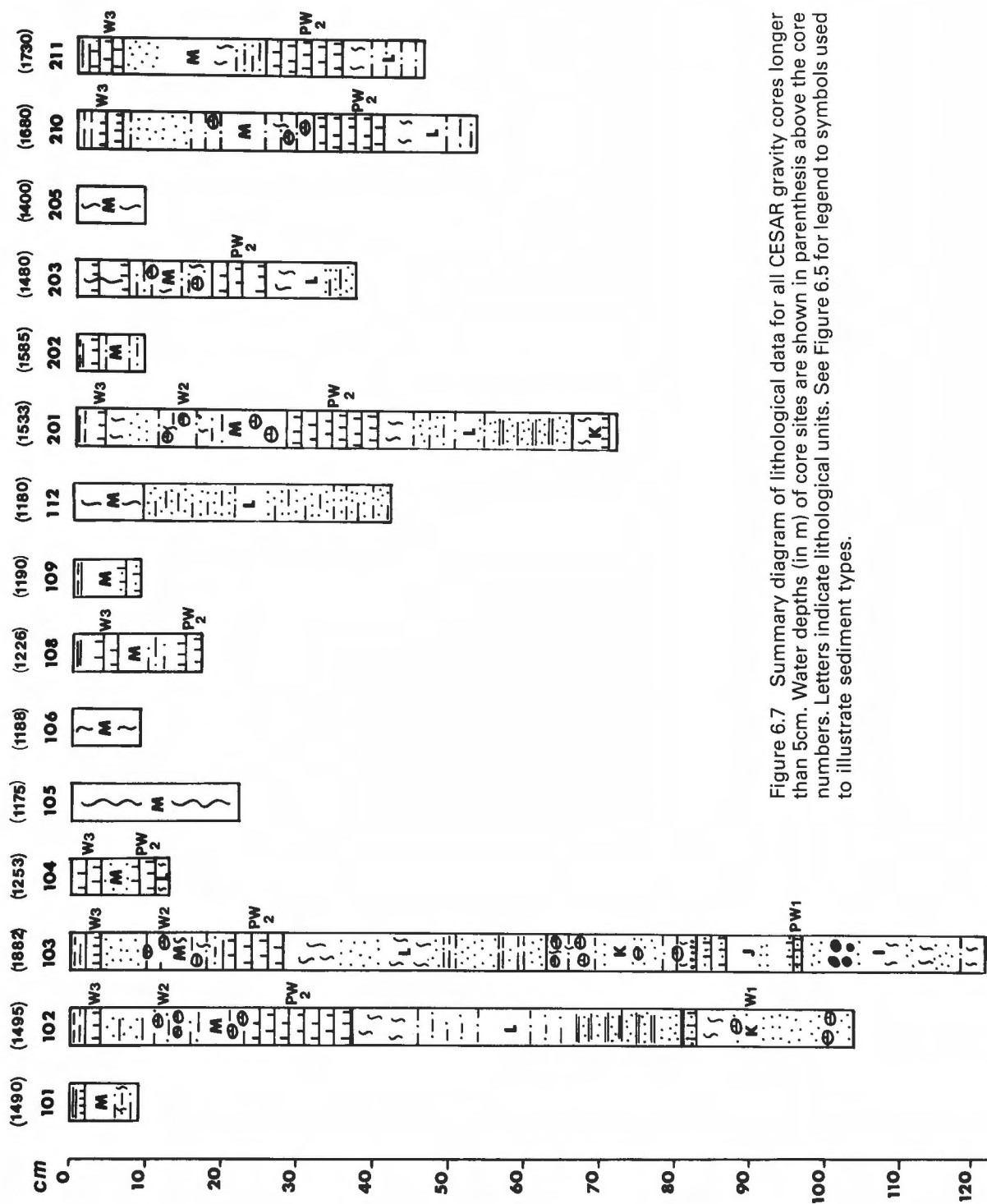


Figure 6.7 Summary diagram of lithological data for all CESAR gravity cores longer than 5cm. Water depths (in m) of core sites are shown in parenthesis above the core numbers. Letters indicate lithological units. See Figure 6.5 for legend to symbols used to illustrate sediment types.

mottled carbonate-rich mud layer at the top of unit K. From the base of unit L up to core depths of 35cm in CESAR 103 and ca. 46cm in CESAR 102, there is a fining-upward sequence of dark yellow (10 YR 4/4) sandy layers (2-6cm thick) alternating with thinner (ca. 1cm) silty layers, followed by a lighter brown slightly mottled silt layer ca. 6cm thick, then unmottled olive-brown fine sandy silt.

In the 4 gravity cores containing a complete unit L, the thickness of this unit ranges from 26-44cm; in the piston cores, the thickness of unit L ranges from 15-31cm. This difference is probably partly due to greater compaction in the piston cores, but in both piston and gravity cores, the unit appears to be thinner and less well differentiated at shallower (<1500m) sites. This feature requires further study in order to understand the depositional origin of unit L.

Unit K in CESAR 103 consists of ca. 20cm of dark brown mud with 5-7cm of heavily mottled silt at the top and base, and a lighter brown, sandy middle section containing greyish patches and rare carbonate-rich clasts. Foraminifera are abundant in the top layer but they decrease substantially towards the base. The base of unit K is marked by a greyish sandy layer, but it is not sharply distinguished from the top of unit J. The grey carbonate-rich clasts in the centre of the unit may correspond to the W1 layer of the USGS cores, but none of the CESAR cores show the distinct whitish band described by Minicucci and Clark (1983).

Unit J in CESAR 103 consists of ca. 14cm of mottled yellow-brown sandy to silty mud with pinkish carbonate-rich mottles at the top and a distinctive thin (1cm) pinkish-yellow layer at the base. As in unit K, the top mottled layer is rich in foraminifera, but they become very sparse below the 90cm level which is marked by a thin (1cm) grey sand layer. The pinkish carbonate layer at the base corresponds to the PW1 marker in the USGS cores.

Unit I in CESAR 103 consists of 26cm of brown mud with greyish (10 YR 3/3) sandy layers 2-8cm thick which fine upwards to dark brown (10 YR 4/3) heavily mottled silty layers. Foraminifera are rare in this unit which appears to be very similar to the top of the much longer (36-80cm) unit I found in CESAR piston cores.

### ***Correlation and paleoenvironmental interpretation***

Figures 6.7 and 6.8 show that the lithological units in most of the CESAR gravity and piston cores can be correlated over the 3600km<sup>2</sup> area covered by CESAR, despite the wide range in water depth (2150-1180m) and the differences in bottom topography at the core sites. Magnetostratigraphic data for CESAR cores 14, 102 and 103 (Aksu, 1985a) indicate that the boundary between the Brunhes and Matuyama magnetochrons lies in unit K. The generally accepted age of this boundary is 0.73 Ma (Harland et al., 1982). If a constant sedimentation rate is assumed for those cores containing units M-K, it can be estimated that sedimentation rates during the past 0.73 Ma are between 0.77 and 1.2mm per Ka. These values agree well with the mean sedimentation rate of 1.17mm.<sup>-1</sup>Ka obtained for non-turbidite Late Pleistocene

deposits in the USGS cores from Alpha Ridge and Chukchi Rise (Minicucci and Clark, 1983).

In general, the top sections (units M-I) of the CESAR cores and the USGS cores from Alpha Ridge show a similar succession of bioturbated, foram-rich carbonate muds alternating with less bioturbated silty-sandy intervals containing relatively few foraminifera. Clark et al. (1980) interpret the silty muds as representing intervals of sea ice sedimentation corresponding to glacial maxima; the sandy muds, including carbonate-rich layers, are considered to represent intervals of sediment deposited by sea ice and icebergs during warmer climatic stages. Glacial-marine sediment transport is the most reasonable explanation for the very widespread occurrence of these correlatable lithologies in the Canada Basin and for the presence of coarse material of non-local origin on the Alpha Ridge during the past 1 Ma. However, further sedimentological study is required in order to provide a more definite interpretation of the factors responsible for the foram-poor carbonate hardground layers and the unproductive sandy mud facies of units L and I. Palynomorphs in unit L (Mudie, 1985) suggest increased fluvial input during this interval.

Chronostratigraphic correlation and paleoenvironmental interpretation of units H to A3 in the CESAR piston cores is presently much less certain than for the upper Pleistocene units, M-I. This is due to several factors: i) difficulty in defining the boundaries and distinguishing between the lithologies of the sandy units H, F and C which are the primary means of delineating the tops of silty mud units G, D-E and A-B; ii) in CESAR cores 2, 4-7 and 11, there are either large hiatuses due to coring disturbance or due to intervals of nondeposition in sediments above unit A-B; iii) flow-in and other coring artifacts, such as re-entry of the corer at the seabed, have disturbed the primary structures in the lowest parts of several cores. For example, pinkish carbonate clasts with abundant planktonic forams are present up to 75cm above the bases of CESAR 8, 10 and 11, in sharp contrast to typical siliciclastic mud of units A1-A3 which usually contain only thin layers of arenaceous forams.

The summary data (Table 6.2) for unit thickness in the CESAR piston cores, however, can be used in conjunction with seismic reflection data (Jackson, 1985) to draw some tentative conclusions about older Late Cenozoic sediments on Alpha Ridge.

1. The sandy-gravelly muds of units H, F and C are relatively uniform in thickness and contain coarse sediment that could only have been transported to the Alpha Ridge by ice during intervals of extensive continental glaciation. Paleomagnetic data (Aksu, 1985a) indicate that unit C approximately corresponds to the Pliocene-Pleistocene boundary (ca. 1.8 Ma).

2. The mottled brown silty mud units (G, D-E, A-B, A1 and A2) generally increase in thickness down-core and the number of clasts decreases, especially below unit D-E. This suggests that intervals of iceberg-transported glacial debris were much less frequent during the late Tertiary interval. In CESAR 14, the boundary between the Gauss and Gilbert magnetochrons (ca. 3.4 Ma) lies near the base of unit A1, and

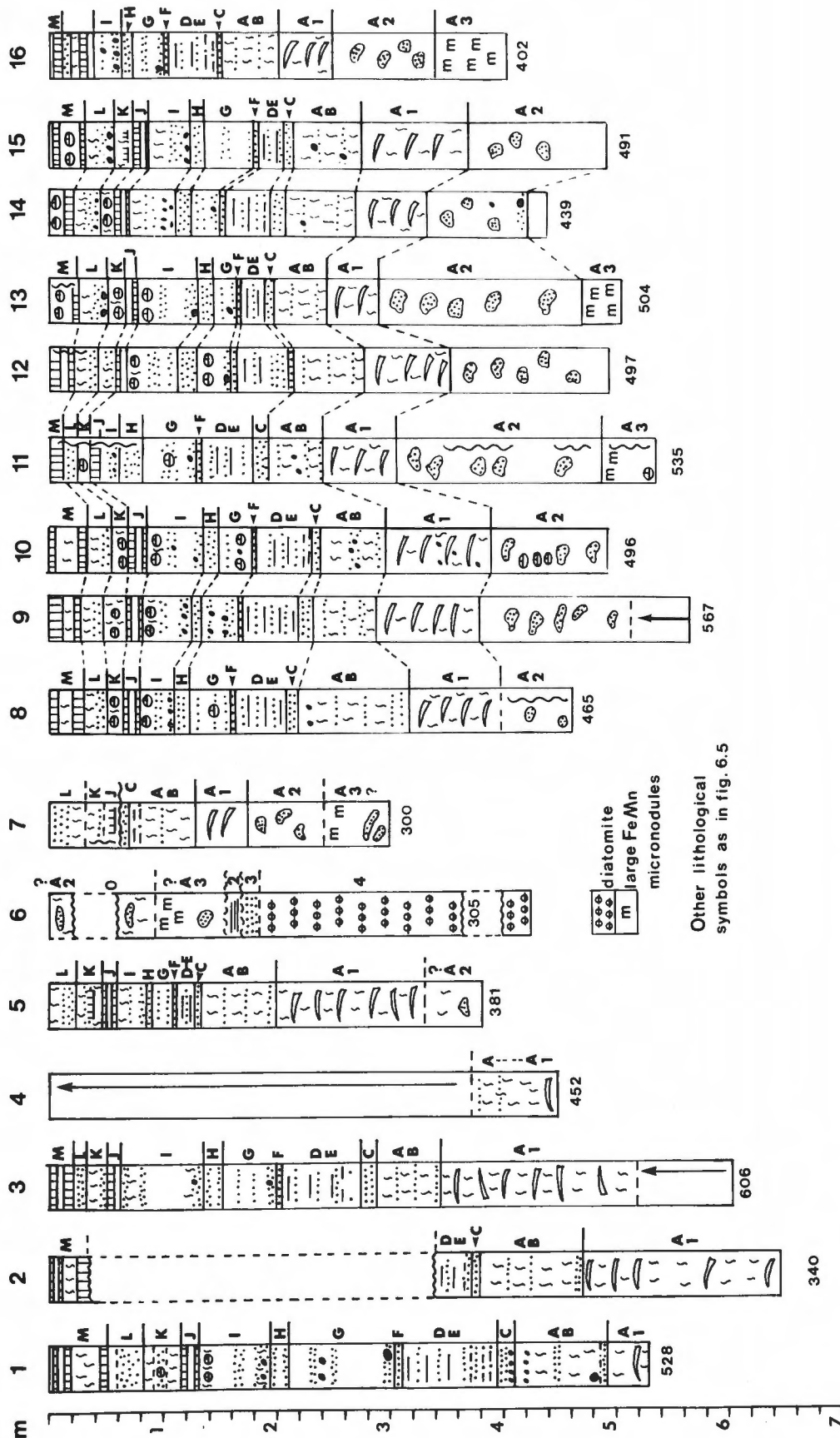


Figure 6.8 Summary diagram of lithological data for CESAR piston cores. Upper case letters indicate lithological units for late Cenozoic sediments; core lengths (in cm) as logged in the laboratory are shown for each core.

Table 6.2 Thickness of sediment units (in cm) in CESAR piston cores.

Core No.	1	2	3	4	5	6	7	8	9	10	11	12	13	14	15	16	
Water Depth (m)	2150	1900	1300	1725	1680	1365	1250	1460	1500	1425	1380	1345	1360	1370	1405	1500	Mean & (Range)
Unit M	51	30	22	ND	0	0	0	30	29	32	8	20	24	21	32	9	26 (8-51)
Unit L	31	0	15*	ND	23	0	29	21	21	21	15	21	26	22	25	10	22 (10-31)
Unit K	32	0	17	ND	24	0	23	13	17	17	10	13	16	15	17	7	17 (7-32)
Unit J	20	0	12	ND	13	0	5	9	15	18	9	11	12	13	14	14	13 (9-20)
Unit I	62	0	69	ND	23	0	0	38	44	47	18	47	56	39	35	24	42 (18-69)
Unit H	14	0	19	ND	5	0	0	14	9	14	21	17	11	13	12	11	13 (5-19)
Unit G	97	0	46	ND	21	0	0	37	32	30	47	30	19	25	45	26	38 (19-51)
Unit F	6	0	4	ND	3	0	0	2	5	3	4	6	3	3	4	3	4 (2-6)
Unit D-E	89	24	71	ND	18	0	8	48	47	50	47	37	23	43	23	43	45 (23-89)
Unit C	6	5	14	ND	5	0	3	8	14	8	13	12	8	14	10	3	9 (3-14)
Unit A-B	86	85	58	ND	65	0	61	100	57	59	48	62	47	59	59	51	64 (47-86)
Unit A1	34	180	429	ND	130	0	43	80	91	92	64	78	43	63	92	48	75 (43-130)
Unit A2	ND	ND	ND	ND	51	90	66	52	186	104	206	142	182	91	122	91	137 (91-182)
Unit A3	ND	ND	ND	ND	ND	70	58	ND	ND	ND	25	0	34	18	0	62	45

\*part missing

the base of this core has an estimated age of ca. 4.5 Ma. Palynological data from unit A3 in CESAR 14 (Mudie, 1985) also indicate a Late Miocene to Early Pliocene age for the base of this core.

3. Several of the lithofacies below unit F contain beds of graded sediment ca. 10-20cm thick. The relatively uniform thickness of the units in cores from different topographic settings, however, combined with the ubiquitous presence of bioturbation and apparently authigenic ferromanganese micronodules, indicates that the thick pre-Pleistocene brown mud units are not gravity flow deposits but were laid down slowly in an oxidizing sedimentary environment.

4. Units A2 and A3 contain thin beds of well preserved deep-water arenaceous foraminifera which alternate with layers of corroded planktonic forams and poorly preserved arenaceous foraminifera. This suggests that the southeastern Alpha Ridge was not continuously covered by ice during the Pliocene but that cyclical paleoceanographic changes regulated the productivity and/or preservation of biogenic material. Palynological data (Mudie, 1985) suggest some aeolian transport of fine sediment from regions of subarctic vegetation, but there is little evidence for increased fluvial sediment transport to the Alpha Ridge during the early Pliocene.

5. Despite the relatively shallow water depth (1500m) of most of the CESAR piston cores, there is a remarkable

change from intervals of carbonate-rich sediments in the Pleistocene-Recent sediments to Late Tertiary siliciclastic sediments in which both calcareous and siliceous microfossils are rare and poorly preserved. Herman (1983) considers that these unfossiliferous sediments reflect productive subarctic waters with a very shallow lysocline which inhibited preservation of calcareous microfossils, as presently found in Baffin Bay (Aksu, 1983). Holocene sediments in Baffin Bay, however, are very rich in diatoms and dinoflagellates (Mudie and Aksu, 1984), whereas the Alpha Ridge sediments are relatively unproductive. This difference can probably be explained by: i) a much slower sediment accumulation rate in the Arctic Ocean (2mm.Ka<sup>-1</sup> compared to 20mm.Ka<sup>-1</sup> in Baffin Bay); and ii) lower influx of humic organic material to the Alpha Ridge area. Slow sedimentation would mean long exposure to oxidizing silica-depleted bottom water, hence the dissolution of thin-walled planktonic siliceous microfossils and the oxidation of organic matter, including palynomorphs. Low influx of humic acids due to infrequent transport of terrigenous debris by ice or meltwater would also suppress dinoflagellate productivity. Future studies of sand grain surfaces, clay mineralogy and the provenance of clasts in the Tertiary lithofacies are required, however, before the existence of an extensive ice-cover (Clark, 1982) can be dismissed as a possible cause of the unproductive Early Pliocene muds in the Arctic Ocean.

## CRETACEOUS LAMINATED SEDIMENT

### Introduction

CESAR 6 (Plate 2) was recovered from a water depth of 1365m on the south side of the northern crest of Alpha Ridge, at latitude 85°49.8'N, longitude 109°09.2'W. Shallow seismic reflection profiles near this site (Fig. 6.9) show that the core site is located on a fault block where a prominent subsurface reflector lies very close to the seabed. West of the core site, a fault line appears to mark the edge of the Alpha Ridge graben, and chaotic reflectors suggest the accumulation of massive slump-block and debris-flow sediments on the side of the trough below the site of CESAR 6.

Figure 6.10 illustrates the salient lithological characteristics and sediment structures in CESAR 6. The core catcher recovered about 12cm of very soft, olive-grey to yellow-brown siliceous mud, containing common unweathered quartz sand and thin, bubble-wall, glassy volcanic shards. Traces of laminated structure are indicated by crumbly blocks of firm, light olive siliceous ooze containing thin (2-5mm) continuous layers of light brown mud. Silicoflagellates (Bukry, 1985), diatoms and palynomorphs (Mudie, 1985) indicate a Late Campanian to Danian age for the

siliceous ooze. Bulk samples, however, contain rare specimens of very well preserved *Neogloboquadrina pachyderma* (identified by W.H. Berger and G. Keller) which has an age range of Miocene-Recent, thereby indicating that the corer probably bounced on the seabed and dragged in some surface mud prior to penetration and triggering of the piston. Some yellowish sediment also washed out from the core base on removal of the catcher (see Fig. 6.3 for reconstruction of sediments cored at Site 6).

The core liner of CESAR 6 retained 305cm of sediments, including 4 visually distinctive lithological units. Unit 1 (0-99cm) is a soft brown (10 YR 4/3) silty to clayey mud, irregularly mottled with yellowish-brown (10 YR 5/4) streaks. Occasional silt to fine sand laminae or scattered coarse sand and rare gravel are present. Small to large (0.5cm) black FeMn micronodules occur below 30cm. Microfossils are very rare and are mostly poorly preserved, including biogenic silica fragments, rare highly oxidized pollen and rare foraminifera. At present this unit cannot be dated with certainty but its appearance, mineralogy and microfossil content is very similar to units A2 and A3 of CESAR core 14, which are of Late Miocene-Early Pliocene age. Rare palynomorphs from the base of unit 1 (Mudie,

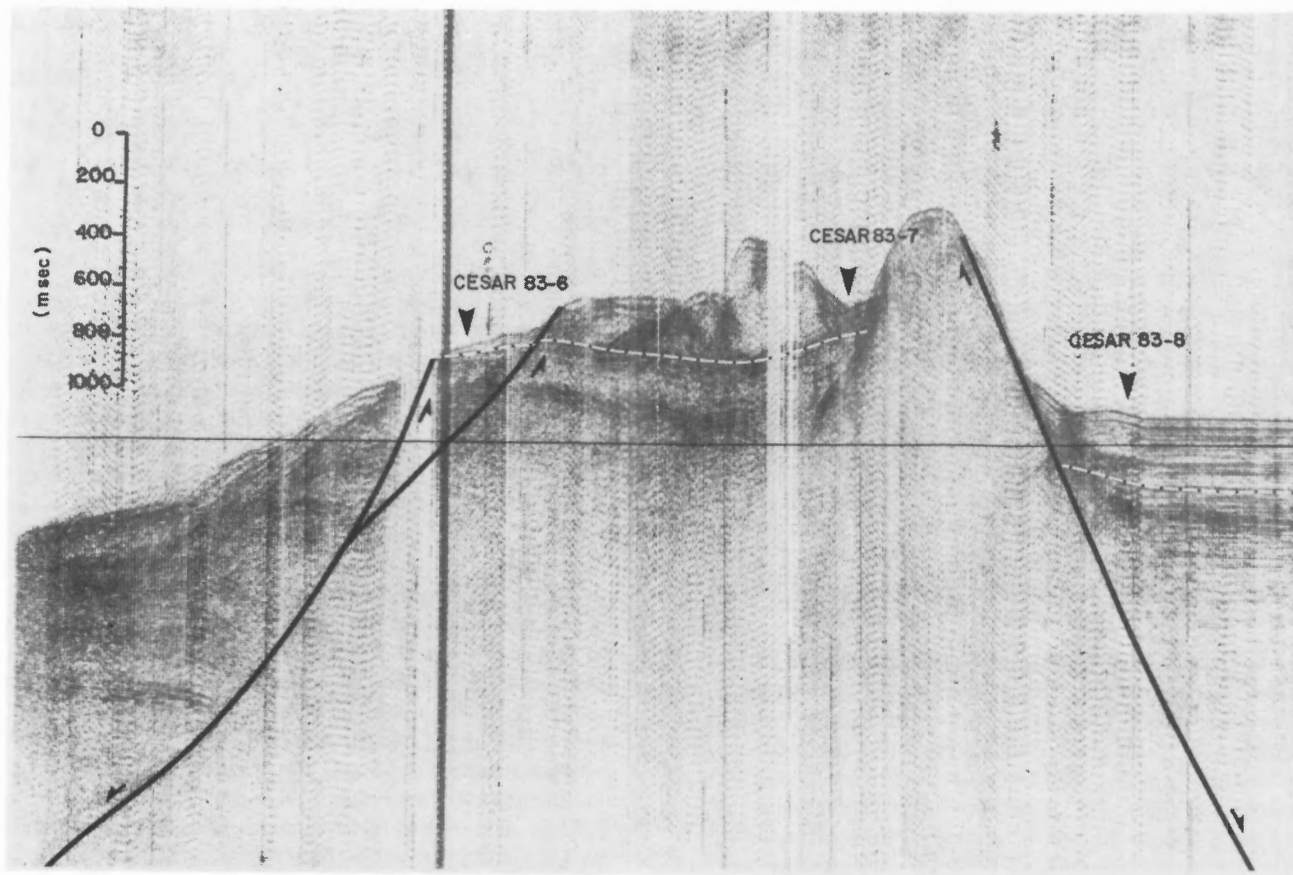
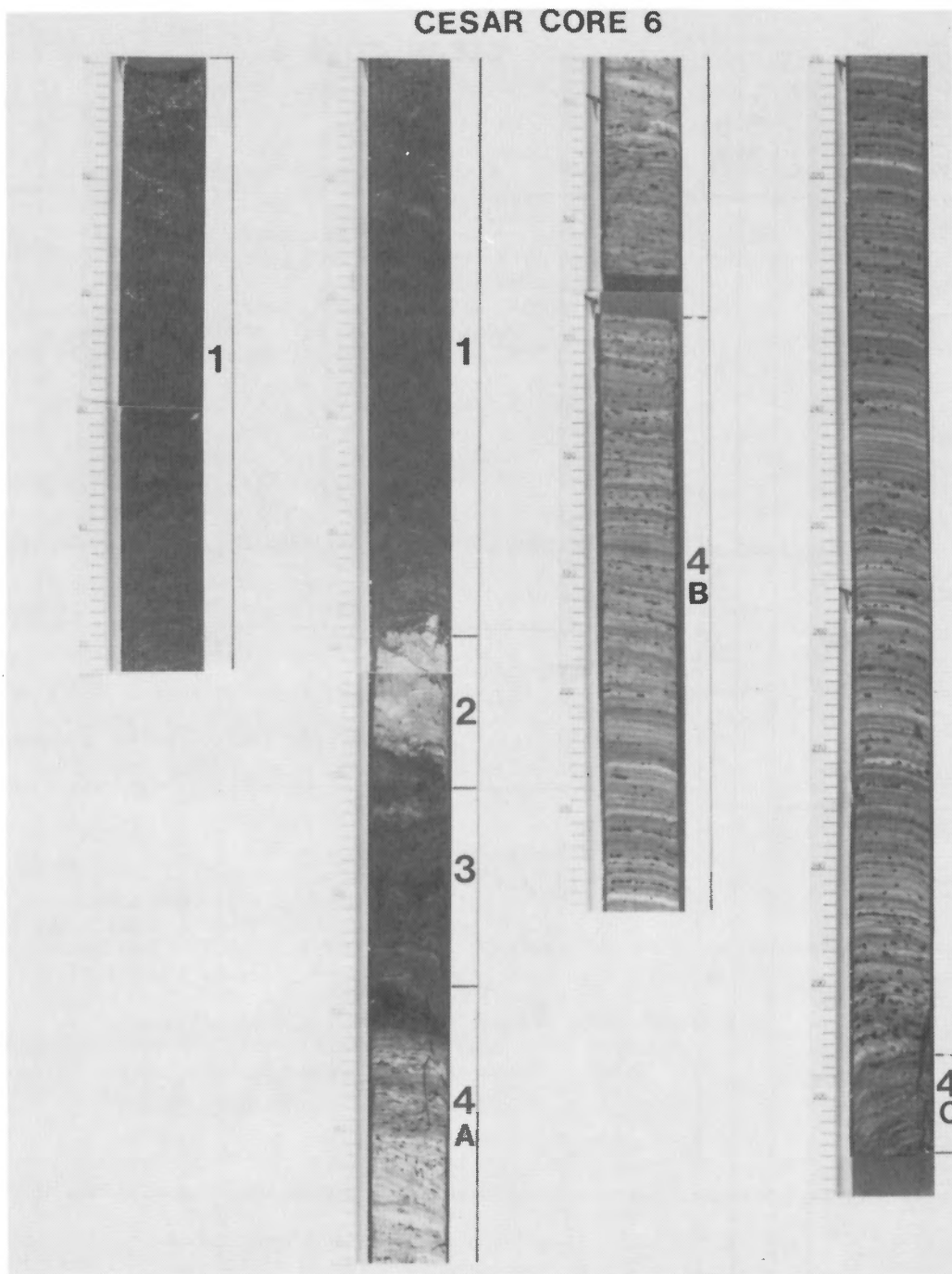


Figure 6.9 Seismic reflection profile of the northern Alpha Ridge crest, showing sediment thickness and the tectonic setting of the CESAR 6 core site (CESAR 83-6). Horizontal distance from CESAR 83-6 to CESAR 83-8 is about 8km.





**Plate 6.2**

Photographic log of sediments in CESAR 6, showing the distribution of lithological units 1 to 4. Vertical scale divisions are in centimetres; note that the numbers at the base of core section 2 (top of column 3) are offset by 3cm – the base of section 2 is at 167.5cm core depth and there is no sediment missing between sections 2 and 3.

# CESAR CORE 6

(Symbols & abbreviations as for DSDP)

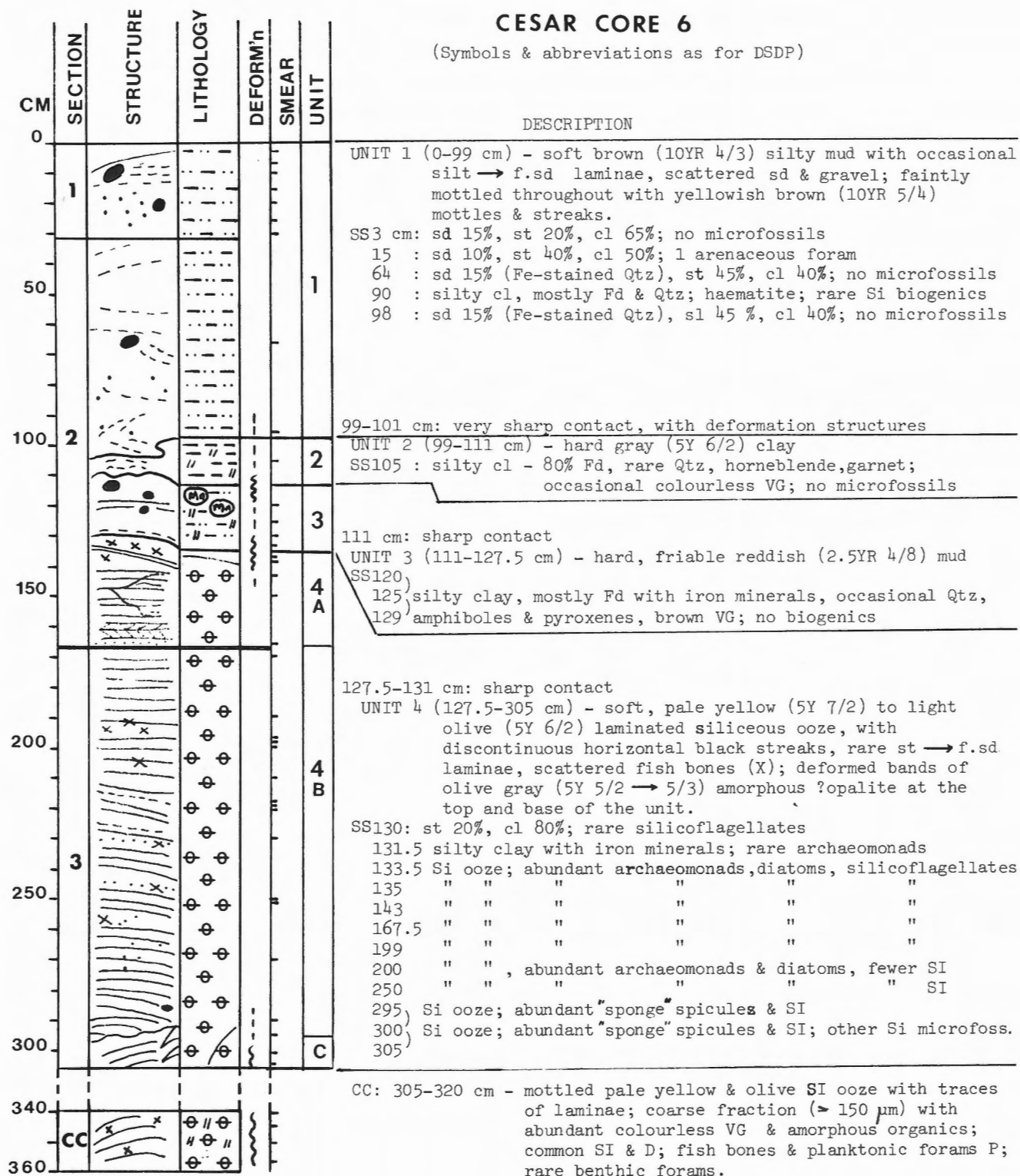


Figure 6.10 Lithological summary of CESAR core 6. Abbreviations used for descriptions: f sd = fine sand; st = silt; cl = clay; Fd = feldspar; Qtz = quartz; VG = volcanic glass shards; SI = silicoflagellates; D = diatoms.

1985) have a Late Cretaceous to Paleogene age but their dark colour suggests they are reworked. Palynomorphs from a bulk sample of surface sediment at site 6 (see Fig. 6.3) indicate a Late Miocene-Pliocene age. The presence of mica and vermiculite in the fine sand and silt-to clay-size fractions of unit 1, and common silt-sized pyroxene suggest an origin from highly weathered volcanic rock, probably including the exposed flanks of the northern Alpha Ridge Crest.

Unit 2 (99-111cm) is a hard grey (5 YR 6/2) silty clay, with sharp but irregular contacts with units 1 and 3. Thin (2-4mm) fractures cut these contacts (probably due to coring disturbances) and are infilled with brown mud. No microfossils or palynomorphs have been found in this unit, and its age is presently unknown. Most of the sediment consists of fine silt-to clay-sized feldspar which is aggregated into sand-sized soft pellets. The mineral composition, in situ colour and texture of this unit suggest that it is a volcanic ash deposited in an oxygen-poor environment. Some colourless volcanic glass is also present (see Fig. 6.10), and rare grains of garnet.

Unit 3 (111-127.5cm) is a hard reddish (2.5 YR 4/8) silty mud with traces of irregular, alternating lighter (10 YR 7/6) and darker (10 YR 5/6) laminae (0.5-2cm thick) from 111-118cm and at the base. The rest of the unit is highly mottled, ranging from small (0.5-1cm) dark brown streaks or black speckles to large (5 × 4cm) dark brown patches with black inclusions. A sharp but irregular contact separates units 3 and 2, and a reddish brown lamina at the base visually suggests a sharp contact at the top of unit 4. However, it is possible that this lamina and the contorted grey and light brown bands of soft sediment from 127.5-133.5cm in unit 4 are part of a gradation from units 3 to 4. Most of the sediment in unit 3 consists of iron-stained, silt-sized feldspar which is loosely aggregated into coarse sand- to granule-sized pellets, the largest of which show faint laminations. Opaque minerals are common, and brown volcanic glass is present. No microfossils or well-preserved palynomorphs are present, therefore the age of this unit is uncertain. The deformed laminae at the top of unit 4, however, show a gradient from occasional well-preserved Late Cretaceous silicoflagellates at 134-130cm to rare fragments at 127-129cm. Some pollen and spores from 127-129cm and 134-136cm have a Paleogene age range (Mudie, 1985) suggesting that the base of unit 3 is not much younger than Late Cretaceous. The mineral composition, colour and structure of unit 3 suggest a volcanic ash deposit similar to that of unit 2 but with oxygen-rich bottom water and a higher influx of ferric hydroxides accounting for the redder colour and higher ferromanganese content (P. Stoffyn, personal communication, 1984).

Unit 4 (127.5-305cm) is a soft, laminated, siliceous ooze which contains complex and variable sequences of laminations and microstructures. Most of the unit consists of uncompacted diatomite with a siliceous microfossil content of 80-95%. The lithology, mineralogy and microstructures of unit 4 are described in detail in the next section of this report and the paleomagnetic record of the entire core is described by Aksu (1985a). Bukry (1985) and Barron (1985) document the taxonomy and biostratigraphy of silicoflagellates and diatoms, respectively. Palynomorphs, which are rare in all but the core catcher sediment of CESAR core 6, are

described by Mudie (1985). The combined data establish the following facts for CESAR core 6, unit 4.

1. The siliceous ooze is a biogenic marine deposit of Late Cretaceous age, no older than Late Campanian (ca. 73-78 Ma on the time scale of Harland et al., 1982).

2. The paleomagnetic inclination predominantly records a reversed polarity interval, which means that the section was probably not deposited during the Cretaceous "Quiet Interval" (Anomaly 33, from ca. 79-72.5 Ma); therefore, the unit is most likely younger than 73 Ma.

3. The very low concentration of terrigenous clastics in the laminated sediment establishes that the core site must have been isolated from continental sediment sources.

4. The absence of diagenetic alteration of siliceous microfossils from Opal-A to Opal-CT in most of unit 4 establishes that the Cretaceous sediment in CESAR core 6 was never subjected to prolonged heating (>35°C; Siever 1983) or deep burial (>400m; Isaacs 1981).

5. The absence of large-scale sorting and rare breakage of delicately spined siliceous microfossils makes it highly unlikely that unit 4 is a turbidite, gravity flow or slump deposit, although microscale crossbedding and grading features suggest intermittent intervals of current sorting and influx of fine grained turbidites. The complete absence of calcareous microfossils or calcite in unit 4 is unique among all reported laminated siliceous sediments, especially compared to regions of nutrient upwelling where high primary productivity accounts for high rates of biogenic siliceous sediment accumulation.

The apparently unique nature of the Alpha Ridge laminated biosiliceous sediment makes it very difficult to determine what kind of paleoenvironment the Arctic Cretaceous sediments represent. Other short cores of siliceous sediment from the flanks of the southern crest of Alpha Ridge have been interpreted as slide blocks (Clark, 1977) or in situ deposits (Kitchell and Clark, 1982) of pelagic biosiliceous sediment that indicate seasonal very high productivity in a warm Cretaceous-Paleogene Arctic Ocean. Laminae in these cores were not well preserved, however, and this hypothesis must be re-examined in light of the new data on sediment structure, microfossils, palynology, geochemistry, and the paleomagnetic record of the laminated sediments in CESAR 6.

#### *Fine structures and composition of the laminated sediment*

The laminated sediments in unit 4 of CESAR 6 can be grouped into 3 subunits based on differences in gross structure and orientation of the laminae. From the base up, the following subunits are distinguished.

*Subunit C (305-296cm)* This consists of a group of greyish-hued (5 YR 5/2-5 YR 6/3) discontinuous laminae which dip at a 30° angle, mostly have indistinct contacts and a mottled appearance, and rarely contain FeMn "micro-nodules" (small clusters of black particles with a high Fe and Mn content).

Table 6.3 CESAR core 6: organic matter analysis\*

Unit	Sample depth (cm)	H%	C%	N%	C/N	H/C
1	5.5 – 8.0 (brown)	0.43	0.07	0.13	0.54	6.14
	89 – 91.5 (brown)	0.53	0.08	0.06	1.33	6.63
2	103 – 105.5 (grey)	0.65	0.55	0.04	13.75	1.18
		0.61	0.20	0.01	20.00	3.05
	105 – 107.5 (grey)	–	0.34	0.54	0.63	–
		0.43	0.45	0.02	22.50	0.96
3	114 – 116.5 A (brown)	0.96	0.05	0.10	0.50	19.2
	B (white)	0.65	0.10	0.17	0.59	6.5
	123 – 125.5 (olive)	0.77	0.11	0.15	0.85	7.0
4	129.5 – 132 A (grey)	1.04	0.21	0.17	1.23	4.95
	B (yellow)	1.26	0.11	0.37	0.30	11.45
	131 – 133.5 (brown)	1.37	0.24	0.05	4.80	5.7
	139 – 141.5 A (olive)	1.03	0.27	0.04	6.75	3.8
	B (white)	1.11	0.69	0.11	6.27	1.6
	146.5 – 149 (pale y)	0.92	0.29	0.52	0.56	3.17
	186 – 188.5 A (grey)	0.90	0.55	–	–	1.64
		0.44	0.68	–	–	0.65
	B (pale y)	1.19	0.43	2.37	0.18	2.77
	214.5 – 217 A (yellow)	1.05	0.34	0.85	0.40	3.08
	B (pale y)	1.09	0.47	0.17	2.76	2.32
		1.01	0.20	0.16	1.25	5.05
	C (bn-y)	0.99	0.19	0.44	0.43	5.21
		1.05	0.27	3.19	8.46	3.89
	217 – 219.5 A (white)	1.05	0.23	0.92	0.25	4.57
		1.05	0.25	0.75	0.33	3.20
	B (white)	1.04	0.16	0.41	0.39	6.50
		1.04	0.24	0.05	4.80	4.33
	C (yellow)	1.09	0.40	0.77	0.52	2.73
		1.09	0.39	0.49	0.80	2.79

\*C, H and N were measured using a Perkin-Elmer model 240B elemental analyzer.

**Subunit B (296-167cm)** This consists of very regular, thin (2cm) pale yellow (5 YR 7/4) to olive (5 YR 5/4) or brown (10 YR 5/6) laminae which dip 10-20° in the opposite direction to subunit C, often have sharp contacts, and are frequently speckled by small (2-4mm) FeMn “micro-nodules” which often occur as short bead-like chains.

**Subunit A (167-127.5cm).** From the base upwards, this unit consists of the following sequence: i) 8cm of olive (5 YR 5/4) to brownish-yellow (10 YR 6/6) irregular laminae with mostly graded contacts and a faintly crossbedded structure; ii) ca. 12cm of lighter (5 YR 6/2-6/4) laminae with sharpish bases, variable thickness (from 0.5-3cm) and irregular orientation due to areas of slip-strike displacement (ca. 2 cm) along microfaults; and iii) a 20cm section of thickish (2-3cm), light olive (5 YR 6/2) to dark yellowish-brown (10 YR 3/4) mottled laminae which are primarily flat-lying but become strongly deformed in the top 7cm. FeMn mottles or streaks are common throughout this subunit.

Very detailed, lamina-by-lamina textural, mineralogical and geochemical studies are required to understand the nature and probable causes of these meso- and micro-scale changes

in unit 4. Preliminary studies have been carried out for selected samples, using smear slides, organic matter (CHN) analysis (Table 6.3), scanning electron microscopy (SEM), Energy Dispersive System (EDS) element analysis and visual inspection of the coarse (125µm) sediment fractions. The main results are described below.

**Subunit C (305-296cm).** Studies of light and dark lamina couplets from 305cm and 301.5-304cm show that:

1) Light and dark laminae differ mainly in the larger amount of iron oxyhydroxides and bone fragments present in the dark laminae (see Plate 6.3, fig. 1 and 2; Plate 6.4, fig. 1).

2) There is no conspicuous difference in silicoflagellate or diatom composition between light and dark laminae within the subunit.

3) There are no conspicuous differences in preservation state of siliceous microfossils between light and dark laminae, although there are more brown-stained *Coscinodiscus* with thin coatings of Fe in the dark laminae (see Plate 6.4, fig. 3, 5 and 6).



In general, thin rod-shaped biosiliceous fragments are much more abundant in subunit C than elsewhere in unit 4. The siliceous rods appear to reflect the frequent occurrence of *Rhizosolenia cretacea*, presence of several *Lyrarula* species in addition to ubiquitous *Lyrarula deflandrei*, and perhaps (not yet confirmed), the presence of sponge spicules. The top of the subunit corresponds to the last occurrences of *Lyrarula minor*, *Lyrarula porta* and *Lyrarula* spp. (see Bukry, 1985), the last occurrence of *Coscinodiscus symbolophorus*, and a change from common or frequent *Rhizosolenia cretacea* and *Hemiaulus polymorphus* v. *frigida* to very rare occurrences (see Barron, 1985). Ferromanganese "micronodules" are very rare and small (<20µm) throughout the subunit, whereas larger, dark brown grains of iron-stained apatite (CaPO<sub>4</sub>) are relatively common, some irregular shaped CaSO<sub>4</sub> particles are present, and some siliceous microfossils show patchy overgrowths of CaSO<sub>4</sub> (Plate 6.4, fig. 5).

It is not clear if the changes at the top of subunit C represent an unconformity or disturbance during coring. The laminae at the bottom of subunit B are strongly bowed upwards, suggesting partial flow-in which might account for the rare occurrence of *Lyrarula furcula* at 290-292cm, but most of the diatom species are the same in subunits C and B. In general, it appears more likely that the subunits represent a change in frequency of clay and iron-rich mineral influx, and a change in sediment bottom water chemistry as indicated by the more common occurrence of FeMn deposits in subunit B.

**Subunit B (296-167cm).** Despite the ostensibly regular appearance of laminae in this subunit, detailed study reveals complex and variable microstructures which make it difficult to characterize either dark-light laminae couplets or lamina sets. This difficulty is due to 3 main factors: a) colour changes cover a spectrum from sharply defined couplets of very dark and very light laminae to graded sets in which the colour changes gradually from darker to lighter and back to darker (see Plate 6.2); b) X-radiograph microstructures (Plates 6.5 to 6.8) mostly do not correspond directly to conspicuous differences in lamina colour; and c) there are no obvious differences in microfossil concentrations, size, shape or species composition between light and dark laminae.

In order to try and discern repetitive patterns in the rhythmites of subunit 4B, laminae were mapped on a millimetre by millimetre scale from colour photographs, using different colours to characterize brown (10 YR 5/6), olive (5 YR 5/4) and pale yellow (5 YR 4/4) laminae. This procedure revealed 5 categories of lamina sets which correspond to 5 of 10 lamina types described in the literature on laminated siliceous sediments (Fig. 6.11). Four of these categories correspond to units in chert beds studied by Iijima and Utada (1983); for convenience these are referred to here as 'single layered', 'triple layered', 'laminar' and 'striped'. The fifth category corresponds to turbidite-derived rhythmites described by Nisbet and Price (1974) which are referred to here as 'cross-stratified'. Using the symbols shown in Figure 6.11, the distribution of the rhythmite units from 288-160cm in subunit 4B is mapped in Figure 6.12 and 6.13. The major features revealed by the maps are outlined as follows.

1. There is a gradual change from a prevalence of striped (δ-type) and single (α-type) beds in the lower one-third of subunit 4B (289-250cm, Plate 6.5), to a prevalence of triple-layered (β-type) and laminar (λ-type) beds in the middle section (250-ca. 181cm, Plate 6.6), and a prevalence of crossbedded sets at the top of subunit B (181-167cm, Plate 6.7). The change in prevalent lamina type at 250cm roughly corresponds to the boundary between silicoflagellate zones A3 and A2 described by Bukry (1985), with *Vallacerta siderea* dominating alone in A3 and *Lyrarula burchardae* becoming co-dominant with *Vallacerta siderea* in the upper (A2) biostratigraphic unit.

2. The striped beds (δ-type) range in thickness from 5-7cm at the base of the subunit (e.g. Plate 6.5, 289-275cm) to 2cm above 250cm-depth. Below 250cm, each bed is characterized by a brown lamina at the base which grades to, or is abruptly followed by a series of 5-7 alternating pale yellow and olive laminae, with either sharp or wispy contacts. X-radiographs show that the brown laminae correspond to relatively fine grained muddy layers, which often show very faint lighter and darker silt-clay couplets (ca. 2mm thick) and sometimes have a sharply defined dark-light couplet at the base. The yellow and olive laminae are either structureless, or they contain wispy light-dark microlamina couplets (ca. 1-2mm thick) with graded, or rarely, sharp contacts. Smear slides indicate that the brown laminae contain more clay-size particles than the pale laminae; the latter contain abundant large flocs of biosiliceous material and many cylindrical diatoms.

3. The single beds (α-type) range in thickness from ca. 4-10mm; X-radiographs (Plate 6.5, 263-260cm) show that they are mostly weakly graded, with a sharp, thin (1mm) light-dark microlamina couplet at the base or top.

4. The triple-layered beds (β-type) range in thickness from ca. 1-2cm and are characterized by a brown lamina at the base and top, both of which grade to pale yellow or olive in the centre. X-radiographs (e.g. Plate 6.6, 241-239cm, 234-231cm) show that the brown laminae are muddier, with wispy dark-light microlamina couplets ca. 1mm thick; the light coloured laminae contain denser sediment and wispy microlaminae 2-3mm thick. Smear slides, EDS analysis, and SEM studies (Plate 6.9) show that the brown and olive-brown layers contain common sand-size particles of CaPO<sub>4</sub> (probably bone) and clay-size particles containing Fe and Al in addition to abundant biosiliceous material. The white layers contain bone fragments but clay and metallic minerals are rarely detectable in the biosiliceous sediment (P. Stoffyn, personal communication, 1984). Large flocs of biosiliceous material are common in the white laminae (Plate 6.9, fig. 1). In both light and dark laminae, fine grained particulate FeMn occurs in patches resembling small burrows. Overgrowths of Mn were found on some diatoms (Plate 6.9, fig. 8).

5. The laminar beds (λ-type) in subunit 4B range in thickness from 2-10cm, and consist of sets of 3-10 alternating dark and light layers with sharp contacts. The dark-light pairs are variable in thickness, ranging from a thin (1mm) dark lamina and thicker (4mm) white lamina to dark-light layers



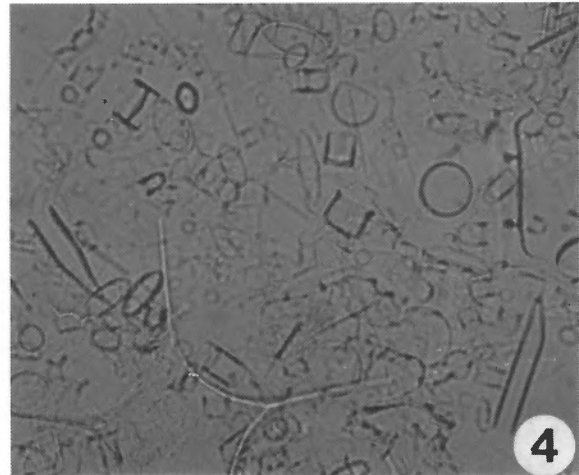
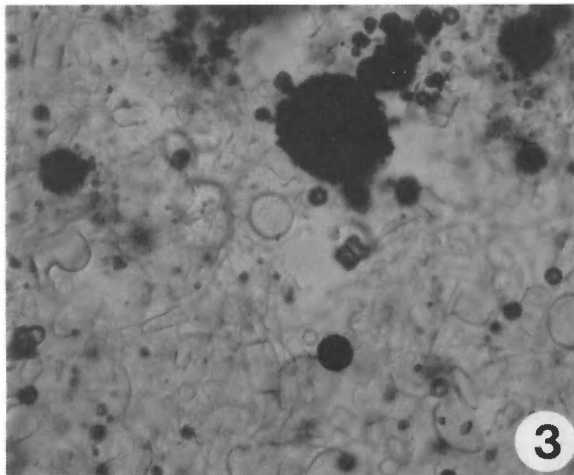


### Plate 6.3

Smear slide samples of sediment from CESAR 6; light photomicrographs  $\times 400$ ;  
# = photo negative; bar scale = 50  $\mu\text{m}$ .

- Figure 1 Brown lamina at 305cm, showing *Vallacerta siderea* and *Rhizosolenia* sp. (thick form) in loose aggregates of silt – clay sized particulates with common small diatoms and resting spores (# 830613-3).
- Figure 2 White lamina at 305cm, showing *Rhizosolenia cretacea*, *Anaulus sibericus*, *Hemiaulus* valves and many small diatoms. Note the absence of clay and mineral aggregates (# 830613-2).
- Figure 3 Black micronodule at 226cm, showing FeMn particles in a dense matrix of small diatoms and resting spores (# 840126-3).
- Figure 4 White lamina at 226cm, showing *Vallacerta siderea*, *Rhizosolenia* sp. (thin form) and abundant diatoms, resting spores and thin biosiliceous rods (# 840126-7).

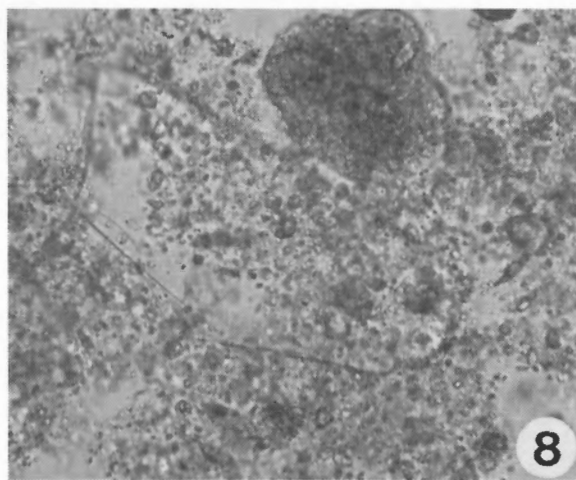
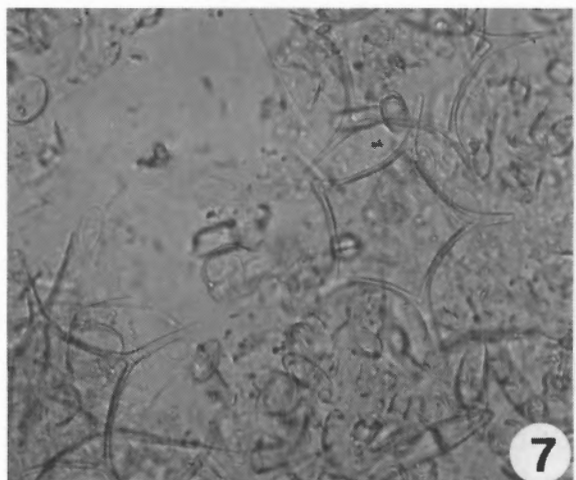
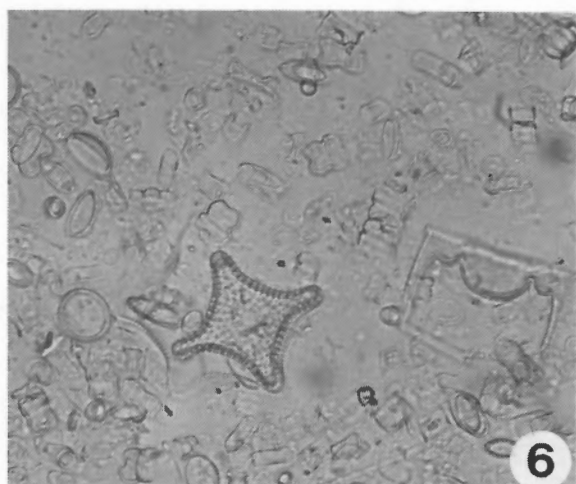
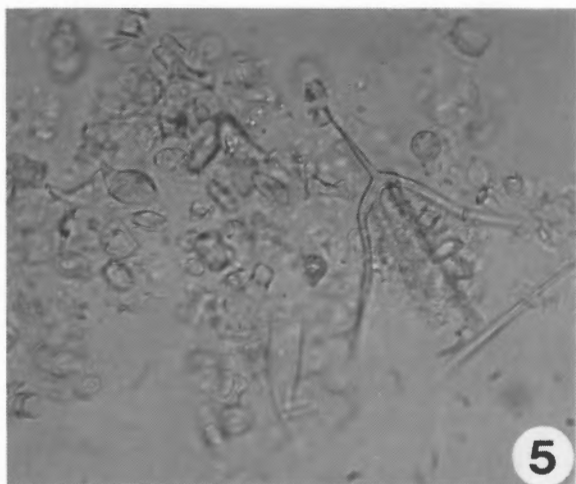
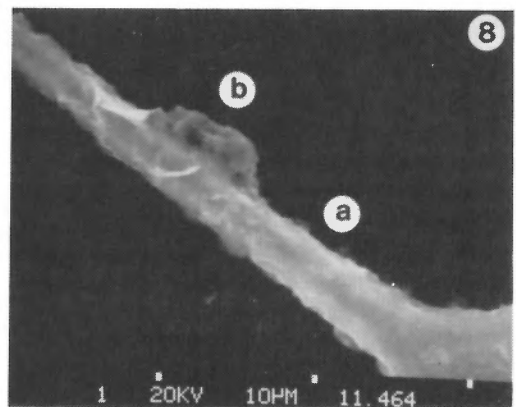
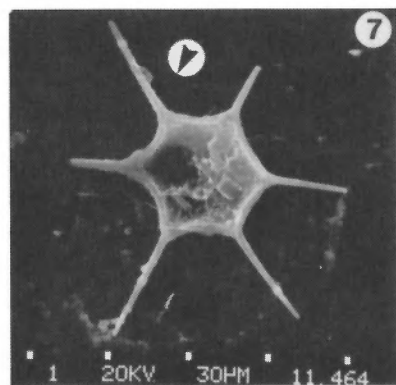
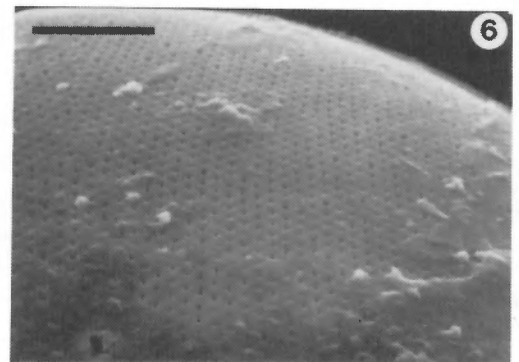
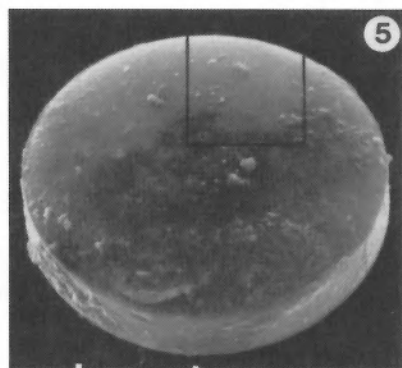
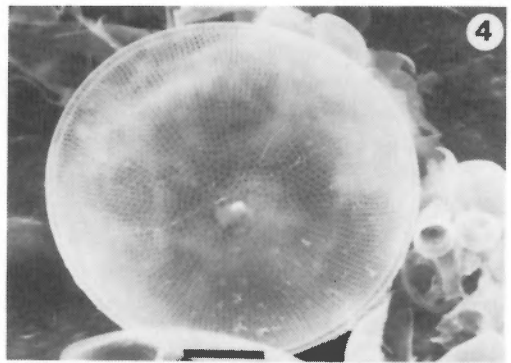
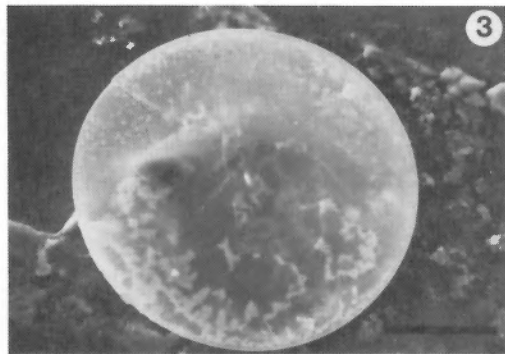
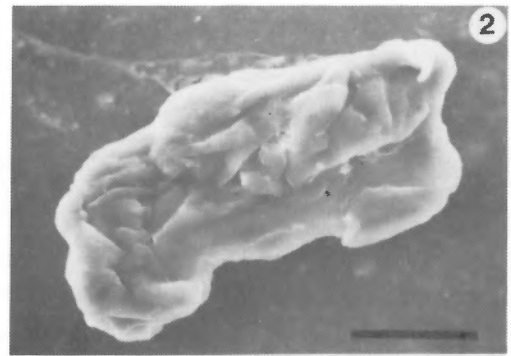
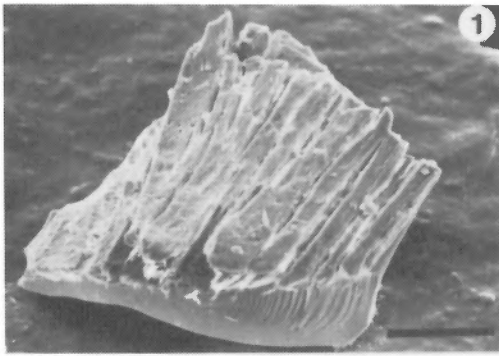


**Plate 6.3 (cont'd)**

- Figure 5 Brown lamina at 167.5cm, showing *Lyramula burchardae*, *Rhizosolenia* sp. and abundant small diatoms in a loose matrix of silt – clay sized particulates (# 830613-6).
- Figure 6 White lamina at 167.5cm, showing *Triceratium tessela*, *Hemiaulus* and *Skeltonema* valves and traces of diatom plus particulate Fe agglomerates (# 830613-4).
- Figure 7 Pale brown lamina streaked with FeMn particulates at 137.5cm, showing *Vallacerta siderea* and abundant small diatoms in a dense matrix of silt – clay sized particulates (# 830613-8).
- Figure 8 Grey, semiconsolidated, sandy mud at 106cm, showing volcanic glass shard, sand pellet, and silt to clay-sized feldspar grains (# 830613-7).



each of which is ca. 1cm thick. X-radiographs (e.g. Plate 6.7, 206-198cm) indicate that the brown laminae contain more clay than the light laminae, and they show wispy dark-light microlamina couplets, ca. 2mm thick. The denser, light-coloured laminae are unstructured and faintly mottled or show very wispy microlaminae. Smear slides (Plate 6.10) show that there is very little difference in the microfossil content of the dark and light laminae.

6. The cross-stratified sets ( $\chi$ -type) resemble those characterizing turbidite-derived laminated beds in the Neraida chert member of the Agrilia Formation in Greece (Nisbet and Price, 1974), but they do not always show a distinct structureless sandy silt layer at the base. In unit 4, each set usually consists of a basal muddy brown lamina 1-2cm thick which is faintly parallel laminated in X-radiographs (e.g. Plate 6.7, 178-167cm), followed by 1-2 cm of 20-30° dipping cross laminae. These beds are cut by a parallel laminated muddy brown layer at the top, followed by a structureless light-coloured lamina of biogenic silica.

*Subunit A (167-127.5cm).* Cross-stratified laminae similar to those described above are found from 167-159cm. From 159 to 153cm, the laminae are generally sharp-based and have graded contacts between light and dark couplets. From 153-134cm, distinct laminae cannot be delimited although wispy, thin light-dark couplets can be seen in X-radiographs (Plate 6.8). Subparallel, elongated mottles rich in FeMn also become conspicuous in this interval which corresponds to the top silicoflagellate zone (A1) of Bukry (1985). The top of subunit A (Plate 6.8) is marked by relatively thick (2-3cm), heavily mottled laminae with scattered, well-preserved, small fish bones. Traces of microlamina couplets can be seen in places. No identifiable microfossils are

present above 132cm core depth; however, palynomorphs are fairly common, and clay minerals and iron flocs increase in frequency.

### *Paleoenvironmental interpretation*

Kitchell and Clark (1982) and Clark (1977) have postulated that the Alpha Ridge biosiliceous deposits reflect seasonally high productivity in a warm ocean with wind-driven cyclonic circulation and polar upwelling. According to Barron (1985), this hypothesis now is further supported by lack of evidence for major diatom evolutionary changes in the CESAR laminated sediments, which may indicate that a relatively short time interval and high rate of deposition is represented. However, the low diversity of siliceous microfossil species and present sparse knowledge of Cretaceous high latitude marine floras makes this judgment difficult to evaluate (see Bukry, 1985). The problem is further confounded by evidence for strong provincialism in the Late Cretaceous-Paleogene marine flora and fauna (Marincovich, et al., 1983). Furthermore, the upwelling hypothesis suffers greatly from the remarkable absence of calcareous microfossils and dinoflagellates, both of which are normally associated with high organic productivity and seasonal upwelling. The presence of penecontemporaneous foraminiferal and dinoflagellate deposits in the Kanguk Formation of the Canadian Arctic Islands (Miall, 1979; Plauchut and Jutard, 1976) seems to eliminate the likelihood that the absence of these microfossils in Alpha Ridge sediments was due to their lack of occurrence in the Cretaceous Arctic Ocean. A more likely explanation seems to be that the Alpha Ridge depositional environment was unfavourable for the preservation of calcareous and organic-walled microfossils.

### **Plate 6.4 (opposite)**

Scanning electron microscope (SEM) photographs of minerals and siliceous microfossils in a brown lamina in subunit C (302.5cm) or a white lamina in subunit B (211cm) of CESAR 6. SEM photos by B. Deonaraine, AGC.

Figure 1 Dark brown mineral from 302.5cm, composed of  $\text{CaPO}_4$  with surface flakes containing Na, Cl and S; laminated structure suggests a fish otolith. AGC # 1146.9; bar = 100 $\mu\text{m}$ .

Figure 2 Glassy white mineral composed of  $\text{CaSO}_4$ , from 302.5cm. AGC # 1146.6; bar = 30 $\mu\text{m}$ .

Figure 3 Surface view of semitranslucent white valve of *Coscinodiscus circumspectus* from 302.5cm, showing thin patchy coating containing Si, Na, Cl and Ca. AGC # 1146.1; bar = 30 $\mu\text{m}$ .

Figure 4 Surface view of translucent white valve of *Coscinodiscus circumspectus* from 211cm, showing lack of surface mineral coating. AGC # 1139.2; bar = 10 $\mu\text{m}$ .

Figure 5 Oblique surface view of a dark brown specimen of *Coscinodiscus circumspectus* from 302.5cm, showing the heavy coating of material containing Si, Ca, S, K and Cl; black lines delimit area enlarged in figure 6. AGC # 1146.2; scale marks = 30 $\mu\text{m}$ .

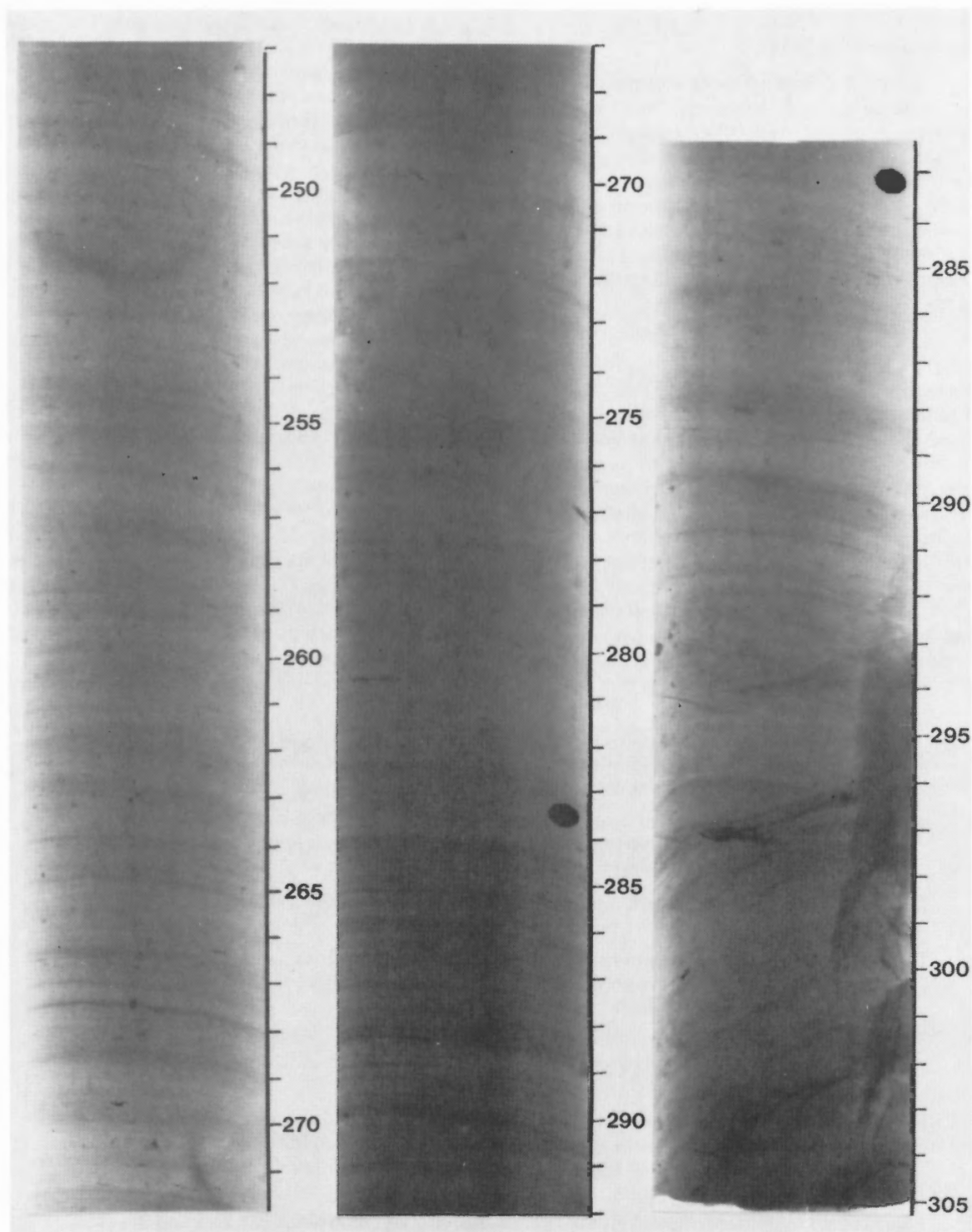
Figure 6 Enlargement of area outlined in figure 5, showing fine detail of pores and the edge of the mineral coating. AGC # 1146.3; bar = 10 $\mu\text{m}$ .

Figure 7 *Vallacerta siderea* (6-spined form) from 302.5cm, showing a patchy coating of minerals containing Si, Ca, P and S. AGC # 1146.4; white squares along bottom delineate 30 $\mu\text{m}$  scale intervals.

Figure 8 Enlargement of spine base indicated by arrow in figure 7, showing "clean" area containing only Si mineral, and warty area containing Ca, S and Si. AGC # 1146.4; white squares along bottom delineate 10 $\mu\text{m}$  intervals.

**Plate 6.5, 6.6, 6.7 and 6.8**

Photoprints of X-radiographs of CESAR 6, split core halves. Darker and lighter horizontal lines indicate denser and less dense sediment, respectively. Small black speckles are FeMn "micronodules" and burrow linings or fish bones. Very bright white lines are air-filled cracks.



**Plate 6.5**

247-305cm core depth; vertical wedges from 290-305cm are probably flow-in features.



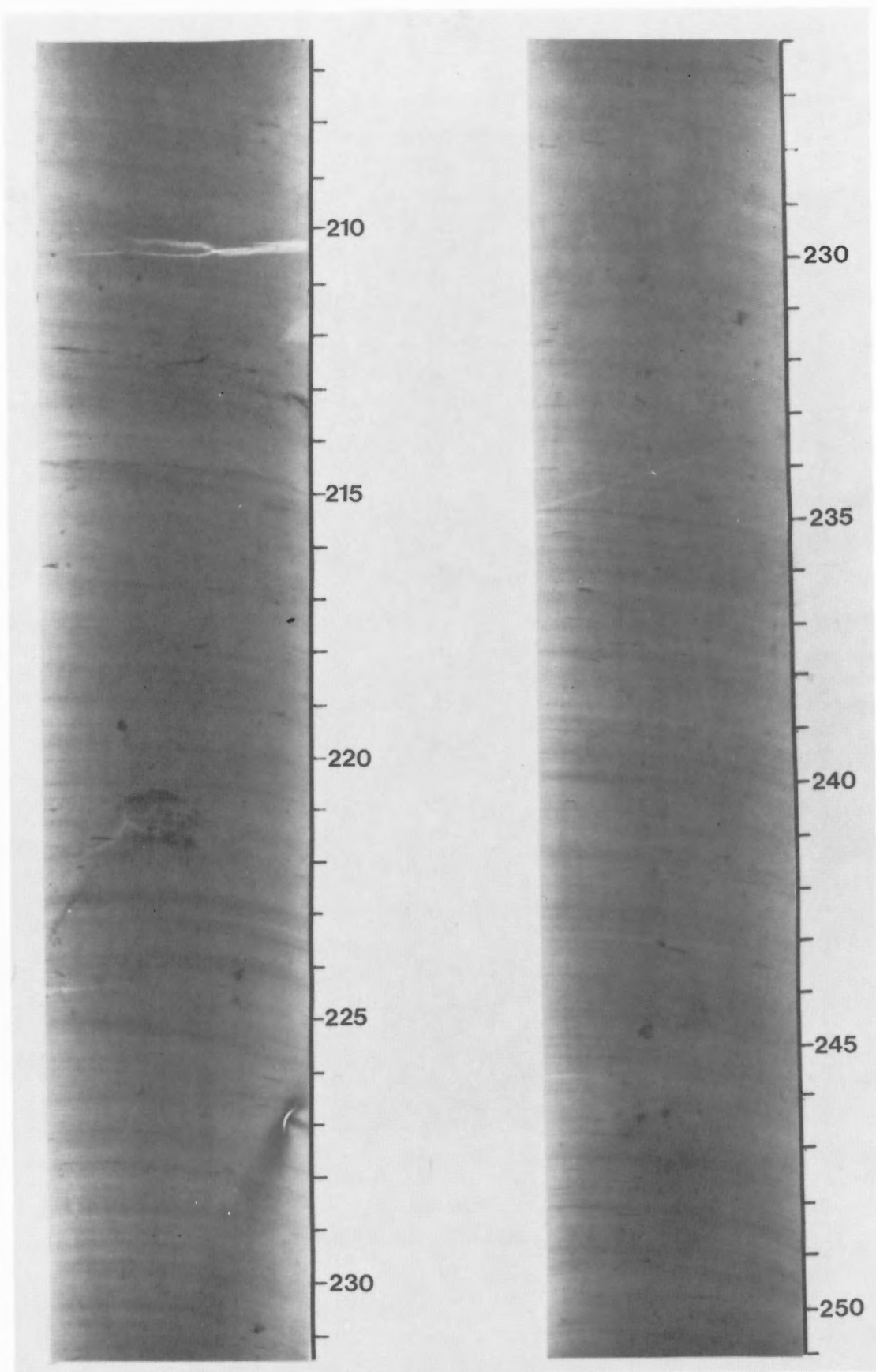


**Plate 6.6**  
251-207cm core interval.

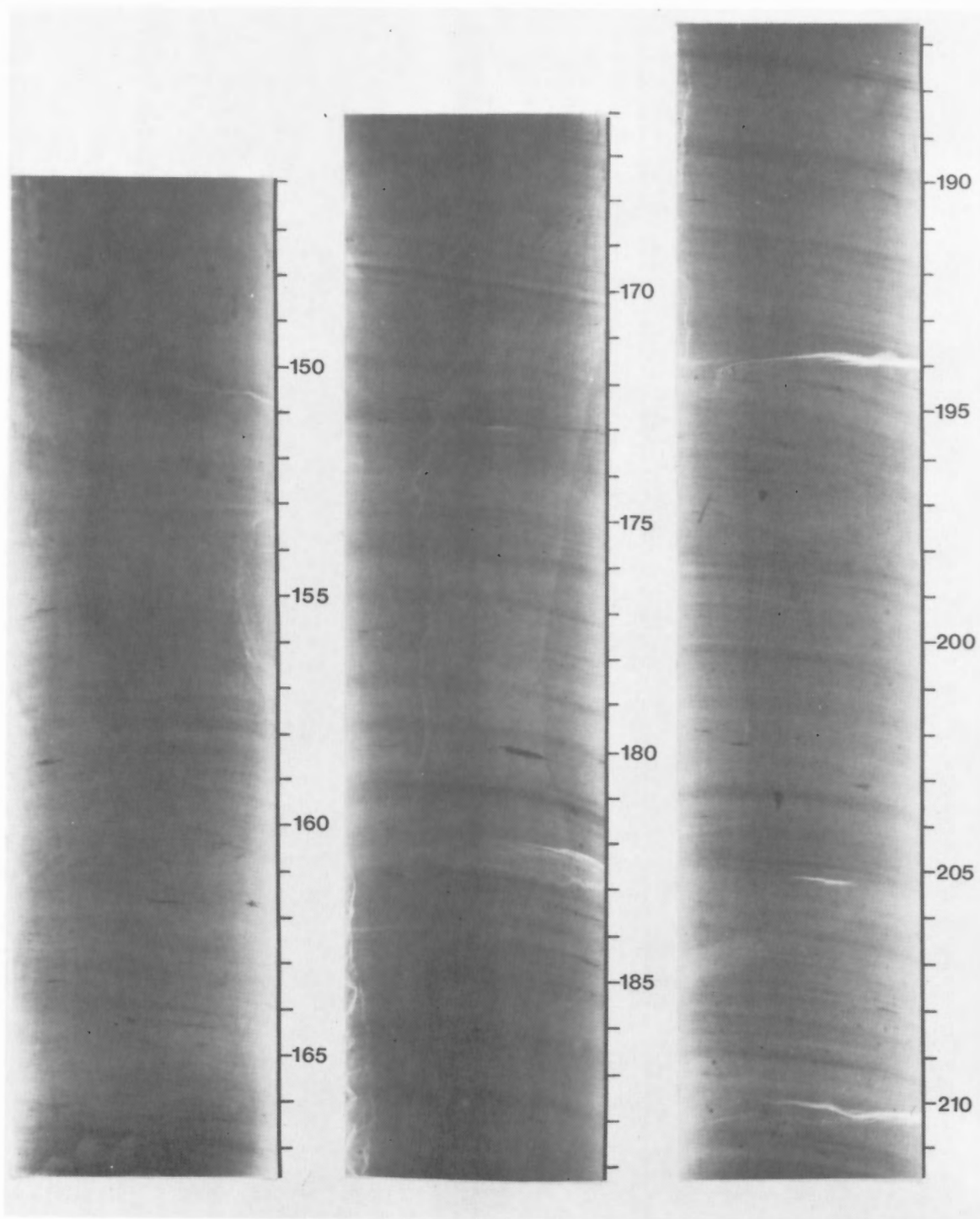


**Plate 6.7**

211-146cm; long vertical smears mark surface indentations caused during core splitting.

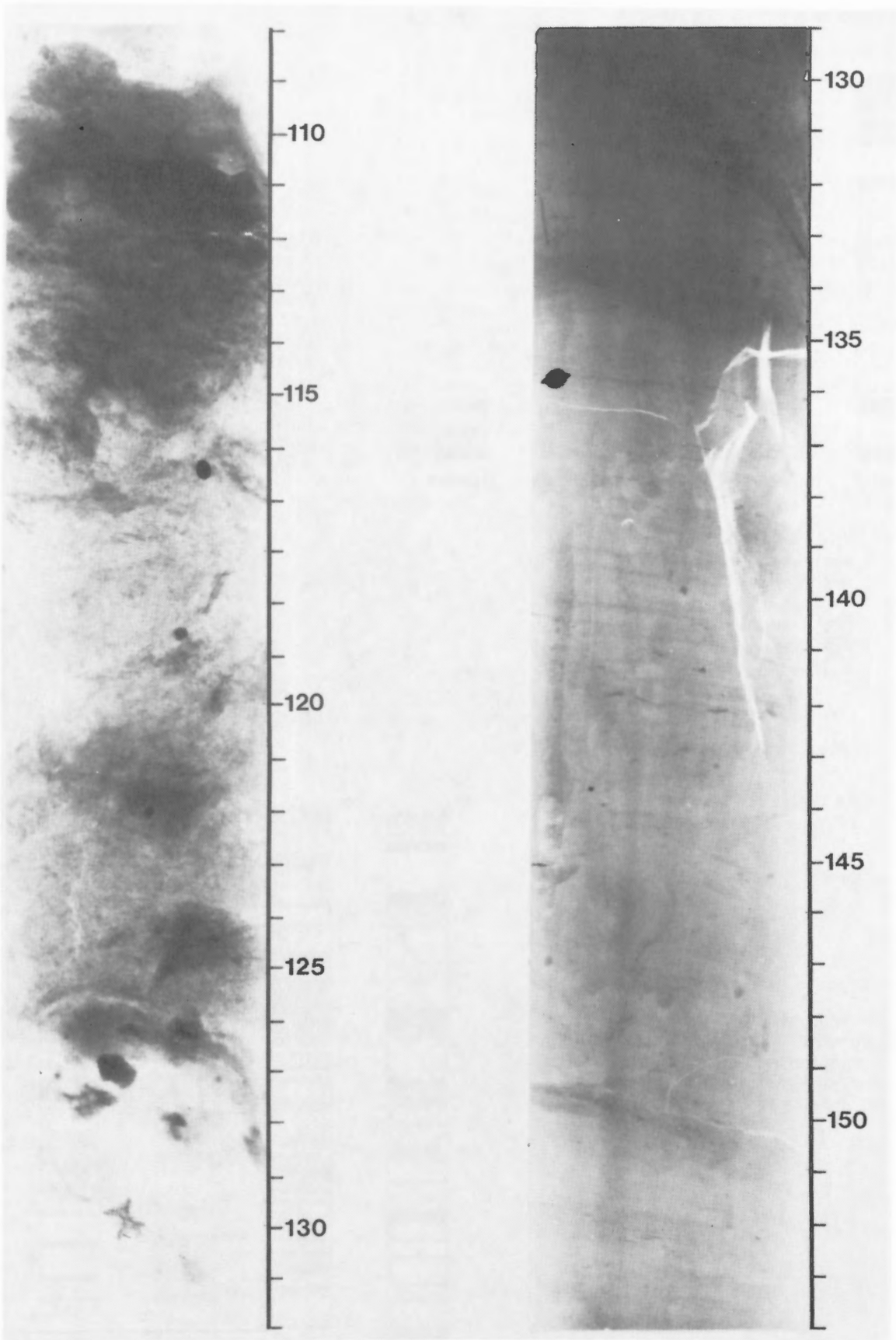


**Plate 6.8**

154-108cm core depth; photo on right was taken with a short exposure time to emphasize fine laminae below 135cm; photo on left was exposed longer to emphasize medium density sediment components, e.g. the fish vertebra at 130cm.

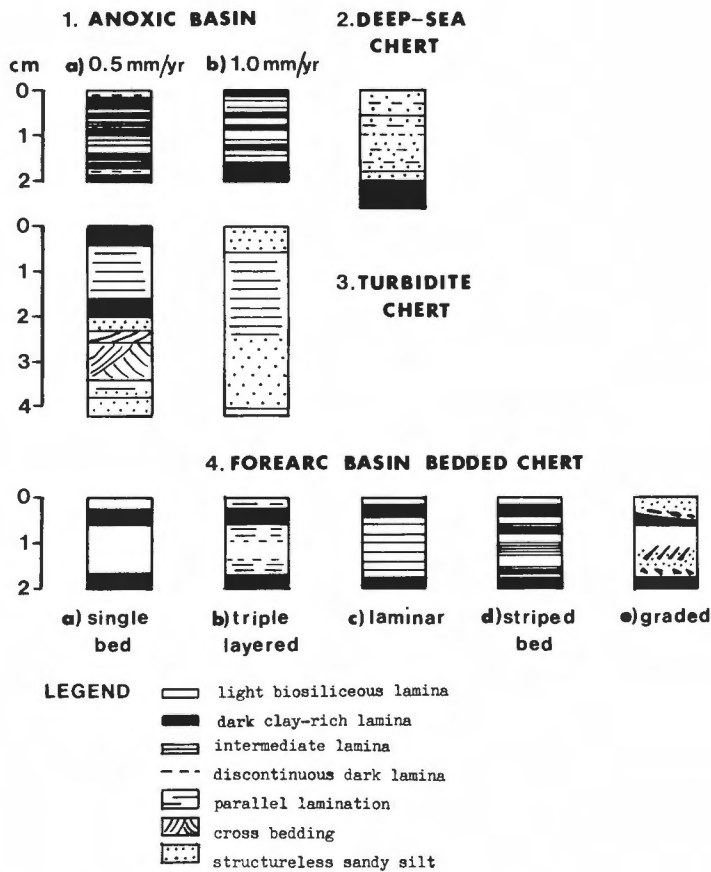


Figure 6.11 Lamina sequences characterizing biosiliceous marine sediments of various depositional environments. 1a – Cariaco Trench, 900m (Heezen and Hollister, 1971, p.224); 1b – Guaymas Basin, 675m, DSDP site 480 (Soutar et al., 1982); 2 – N. Pacific deep-sea bedded chert and shale (Hein and Karl, 1983) and Cretaceous black shale (Thiede et al., 1982); 3a and 3b – Agrilia Formation biosiliceous turbidites (Nisbet and Price, 1974); 4a-4e – Japanese Island forearc basin bedded cherts (Iijima and Utada, 1983).

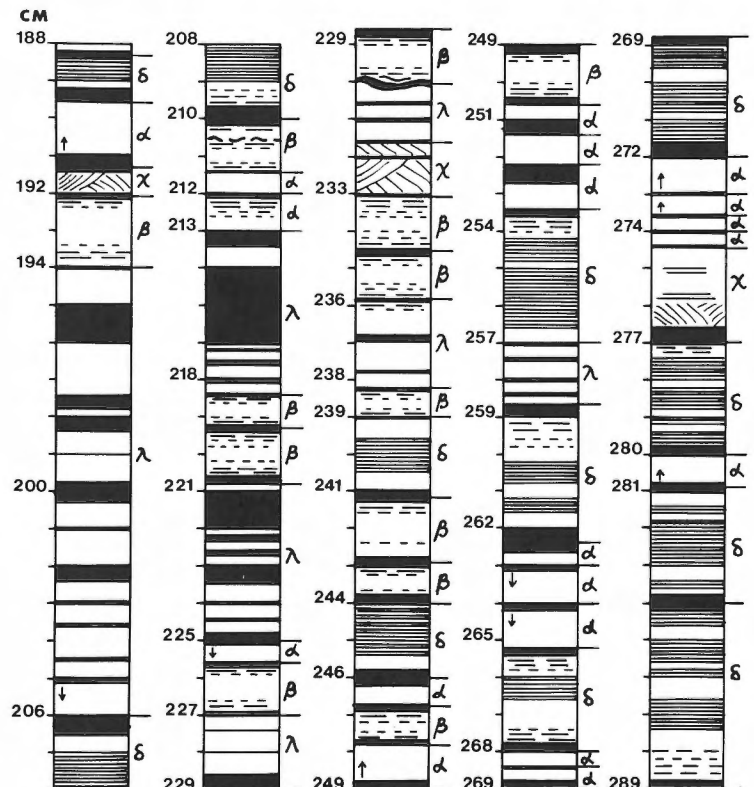


Figure 6.12 Map of lamina sets in subunit B, CESAR 6, from 289-188cm core depth (see Fig. 6.11 for lithological description). Greek letters refer to types of lamina beds described in the text; arrows indicate grading.

Berger and Winterer (1974) have presented strong arguments to the effect that absence of calcareous microfossils in deep sea sediments almost invariably indicates one or more of the following conditions: a) deposition below the CCD (calcite compensation depth) which ranges from ca. 1-4km in the present global oceans; b) lack of calcium supply; c) postdepositional dissolution. With regard to CESAR 6, the high proportion of diatom resting spores in unit 4 implies a

relatively shallow water, upper continental slope or offshore bank environment (Barron, 1985), and this interpretation is further supported by the similarity of diatom taxa (Vincent et al., 1983) and silicoflagellates (Bukry, 1981) in the Kanguk Formation of the Canadian Arctic. If primary productivity was extraordinarily high and calcium supply was also limited, it is possible that the Cretaceous CCD was shallower than 1365m (present water depth of CESAR 6) in the Arctic Basin. However, the common presence of calcium phosphate deposits in the CESAR 6 rhythmites argues against an inadequate supply of calcium, especially if seasonal upwelling were to take place. The absence of arenaceous foraminifera is also inconsistent with a productive boreal marine environment. This leaves postdepositional dissolution as the most likely explanation for the lack of calcareous microfossils.

The possibility of postdepositional calcite solution is given further weight by a) presence of  $\text{CaSO}_4$  crystals in some laminae, b) the common occurrence of FeMn particulates which indicate an intermittently oxidizing environment, and c) the presence of Fe-infilled foraminiferal linings in some samples (see Mudie, 1985). Slow oxidation of FeS in the presence of oxygen is known to cause dissolution of both calcareous and agglutinated foraminifera (Schnitker et al., 1980). Prolonged oxidation would also account for the destruction of dinoflagellates and other palynomorphs, hence accounting for their rare occurrence in the laminated sediment of CESAR 6, whereas a shallow CCD would not explain this feature.

In conclusion, the combined evidence from sediment structure, texture, microfossils, palynomorphs and limited geochemical data point towards the likelihood that the Cretaceous depositional environment of CESAR 6 was a shallow water offshore basinal environment in a marginal sea, analogous to the Upper Triassic bedded chert deposits in the forearc basins of the Japanese Islands (Iijima and Utada, 1983). Sedimentation rates in these Triassic basins (after decompaction of the cherts) was high: ca. 10mm/1000 yrs. A similar sedimentation rate for Alpha Ridge would mean that unit 4 represents an interval of about 150,000 years. This small amount of time, however, is not in accord with the palynostratigraphy (see Mudie, 1985) or with the paleomagnetic record for CESAR 6 (see Aksu, 1985a), both of which suggest a time-framework of several million years. Hence, it seems more likely that primary productivity and biogenic sediment accumulation in the high latitude (ca. 75°N) Late Cretaceous Arctic Ocean was much lower than in the Pacific island-arc region. Furthermore, according to Berger and Roth (1975), biosiliceous deposits intercalated with phosphatic fossils and apatite indicate low fertility oceanic conditions. Slow deposition in a nutrient-poor, offshore basinal environment, with intermittent influxes of metallic minerals from the Alpha Ridge crest, presently best accounts for the absence of foraminifera, radiolarians and dinoflagellates in the laminated sediments of CESAR 6.

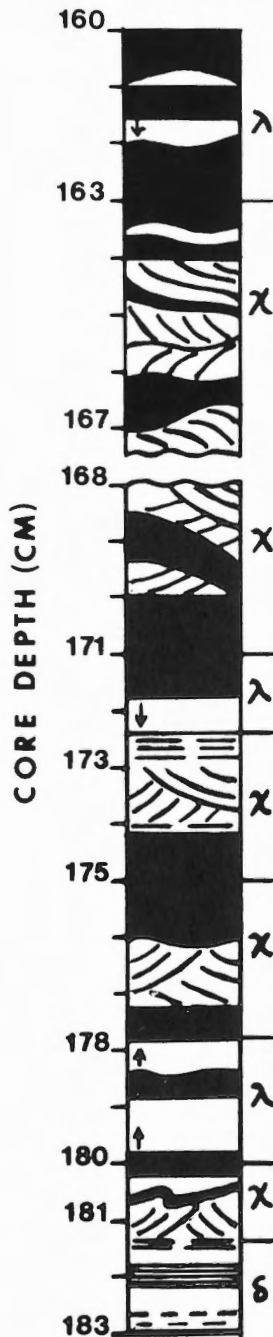
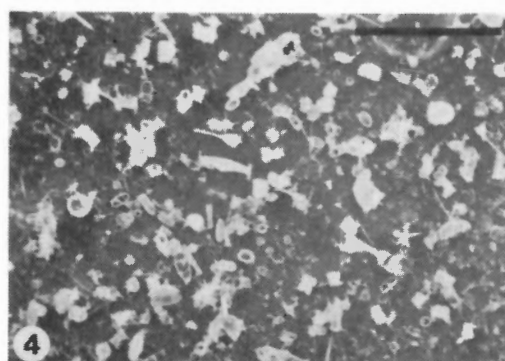
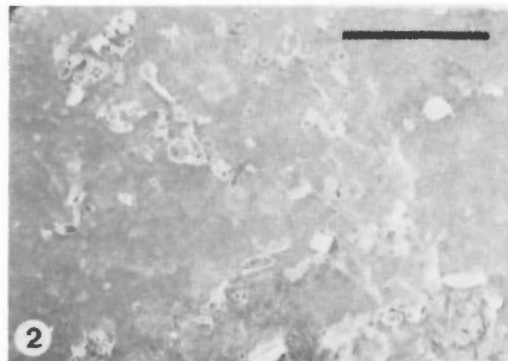
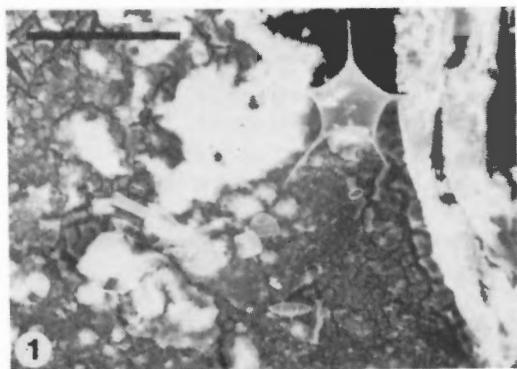


Figure 6.13 Map of lamina sets at the top of subunit B (183-188cm) and the base of subunit C (167-160cm), CESAR 6 (see Fig. 6.10 for lithological description). Greek letters refer to types of lamina sets described in the text; arrows indicate grading.





#### Plate 6.9

Scanning electron microscope (SEM) photographs of minerals and siliceous microfossils from laminae between 205 and 211cm depth in CESAR 6. SEM photos by B. Deonarine, AGC.

Figure 1 Suspended particulate material (SPM) from a white lamina at 207cm, showing a bone fragment, large fluffy white flocs of biogenic silica, and the wide size range of siliceous microfossils. AGC # 1138.6; bar = 100 $\mu$ m.

Figure 2 and 3 SPM from a brown lamina at 206.5cm. Figure 2: fine fraction, showing numerous medium to small-sized diatoms or resting spores in a filmy layer of Fe-rich flocs with traces of Al. Figure 3: coarse fraction, showing large and small particles of CaPO<sub>4</sub> and numerous medium to small diatoms or silica particles. AGC # 1137.11; bar = 300 $\mu$ m.

Figure 4 SPM fine fraction from a very light brown lamina at 205cm, showing abundant diatom frustules of various shapes and sizes, and common rod-shaped silica particles. AGC # 1136.15; bar = 100 $\mu$ m.

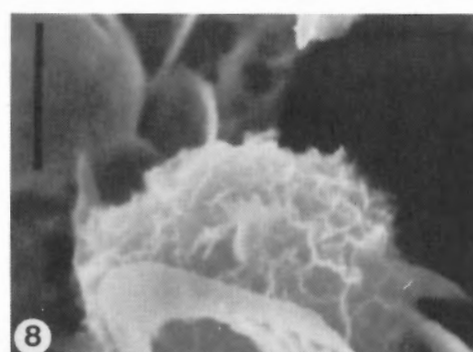
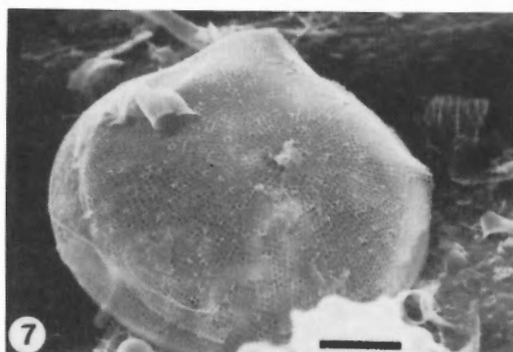
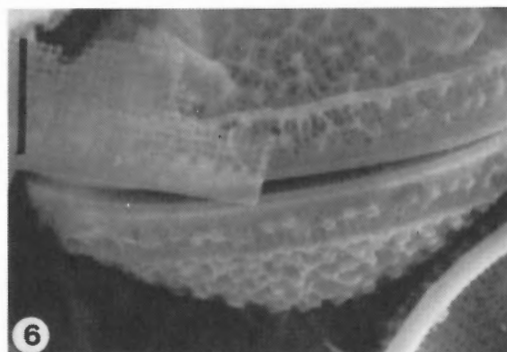
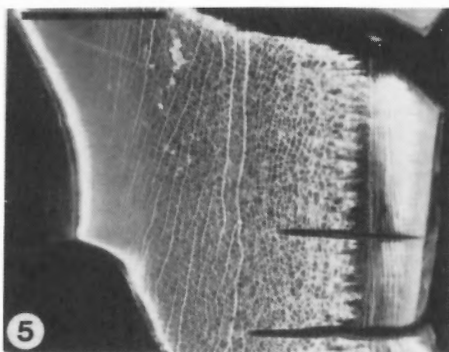


**Plate 6.9 (cont'd)**

Figure 5 Well-preserved bone fragment from an olive-brown lamina at 206.5cm. AGC # 1137.17; bar = 100 $\mu$ m.

Figure 6, 7 and 8 Diatoms from a set of light brown to white microlaminae from 209-211.5cm. Figure 6: lateral view of a diatom resting spore (?*Goniothecium* sp.) showing the excellent preservation of small diatoms. AGC # 1139.7; bar = 5 $\mu$ m. Figure 7: oblique surface view of *Coscinodiscus lineatus*, showing a thin patchy film of silica. AGC # 1139.3; bar = 10 $\mu$ m. Figure 8: frustule of *Hemiaulus* sp., showing overgrowth of MnO<sub>2</sub>. AGC # 1139.1; bar = 3 $\mu$ m.

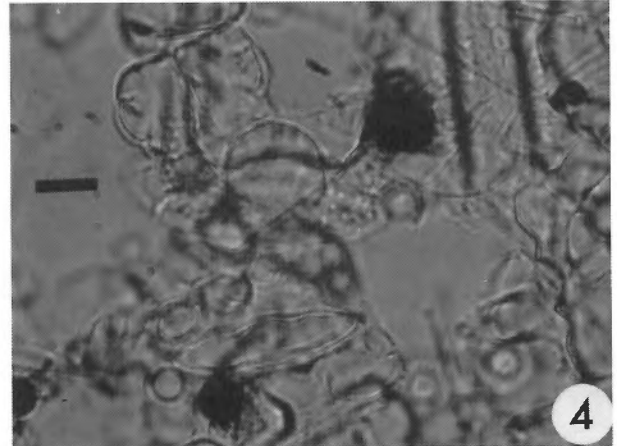
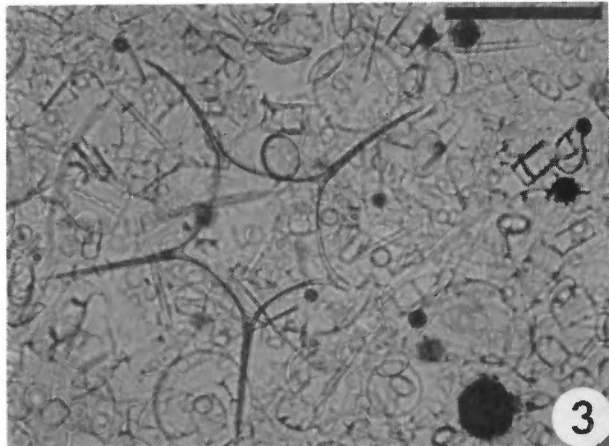
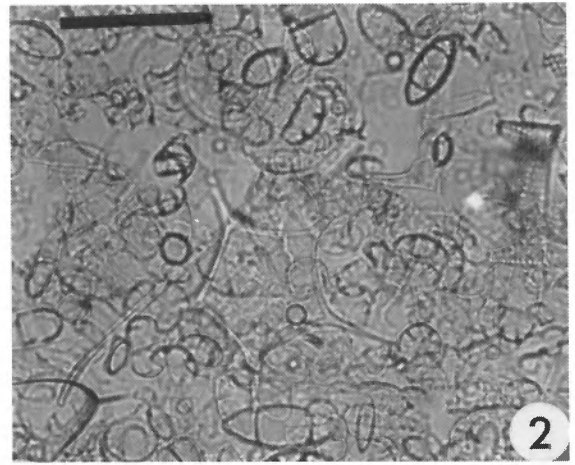
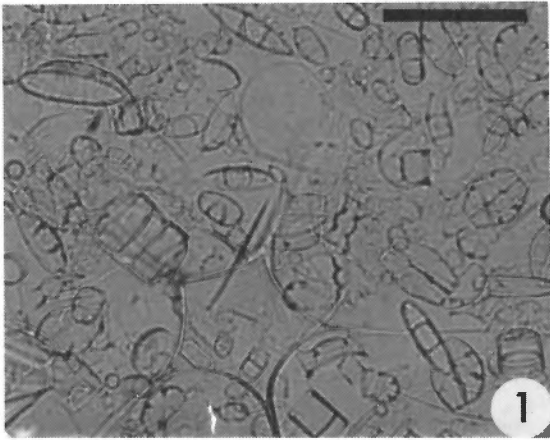


#### Plate 6.10

Smear slide samples of sediment from light and dark laminae, CESAR 6. Light photomicrographs; magnification  $\times 400$  except for Figure 4, 7 and 8 which are  $\times 1000$ ; bar scale =  $50\mu\text{m}$ . Photographs by P.J. Mudie, AGC.

- Figure 1 White lamina at 214.3cm, showing *Vallacerta siderea* and various diatoms, and near-absence of clay-sized particulates. Photo # 840126.12.
- Figure 2 Pale brown lamina at 214cm, unburrowed area, showing *Vallacerta siderea*, *Lynamula burchardae* and various diatoms in a matrix of silt – clay sized particles. Photo # 840126.14.
- Figure 3 Sediment from black "micronodule" at 214cm, showing *Vallacerta siderea*, numerous small diatoms and scattered black FeMn-rich particulates. Photo # 840126.03.
- Figure 4 Enlargement ( $\times 1000$ ) of small "micronodule" and diatom spores shown in figure 3. Photo # 840126.04.

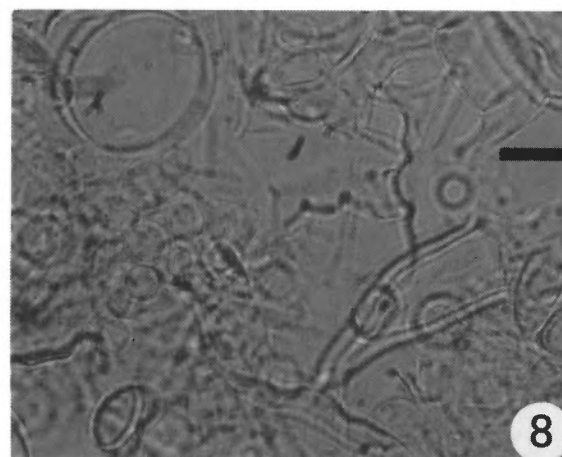
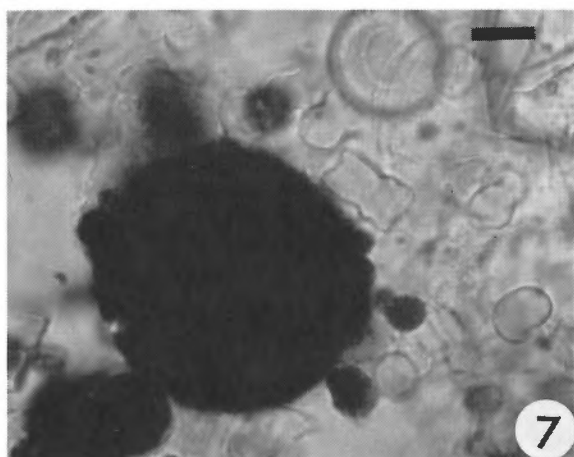
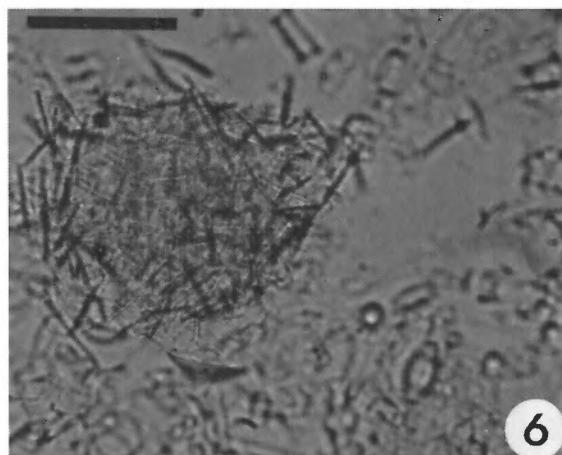
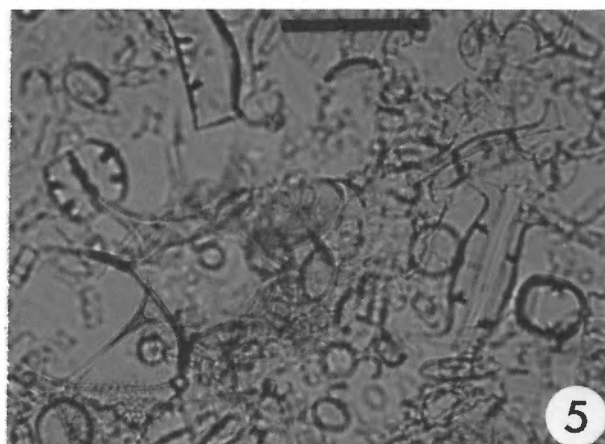


**Plate 6.10 (cont'd)**

- Figure 5 Darker brown lamina at 213.7cm, showing general similarity to lighter laminae shown in figure 1 and 2. Photo # 840126.13.
- Figure 6 White lamina at 226cm, showing "floc" containing abundant biosiliceous spicules and background of abundant small diatoms. Photo # 840126.08.
- Figure 7 Enlargement ( $\times 1000$ ) of FeMn-rich particulates from a dark brown "micro-nodule" in the white lamina at 226cm. Photo # 840126.10.
- Figure 8 Enlargement ( $\times 1000$ ) of small diatoms and resting spores in background of Figure 6. Photo # 840126.02.

## REFERENCES

- Aksu, A.E.  
1983: Holocene and Pleistocene dissolution cycles in deep-sea cores of Baffin Bay and Davis Strait; paleoceanographic implications; *Marine Geology*, v.53, p.331-348.
- 1985a: Paleomagnetic stratigraphy of the CESAR cores; in *Initial Geological Report on CESAR — the Canadian Expedition to Study the Alpha Ridge, Arctic Ocean*, ed. H.R. Jackson, P.J. Mudie and S.M. Blasco; Geological Survey of Canada, Paper 84-22, report 7.
- 1985b: Planktonic foraminiferal and oxygen isotopic stratigraphy of CESAR cores 102 and 103: preliminary results; in *Initial Geological Report on CESAR — the Canadian Expedition to Study the Alpha Ridge, Arctic Ocean*, ed. H.R. Jackson, P.J. Mudie and S.M. Blasco; Geological Survey of Canada, Paper 84-22, report 8.
- Barron, J.A.  
1985: Diatom biostratigraphy of the CESAR 6 core; in *Initial Geological Report on CESAR — the Canadian Expedition to Study the Alpha Ridge, Arctic Ocean*, ed. H.R. Jackson, P.J. Mudie and S.M. Blasco; Geological Survey of Canada, Paper 84-22, report 10.
- Berger, W.H. and Roth, P.H.  
1975: Oceanic micropaleontology; progress and prospect; *Reviews of Geophysics and Space Physics*, v.13, p.561-636.
- Berger, W.H. and Winterer, E.L.  
1974: Plate stratigraphy and the fluctuating carbonate line; in *Pelagic Sediments on Land and Under the Sea*: ed. K.J. Hsü and J.C. Jenkyns; Special Publication No. 1 of the International Association of Sedimentologists, p.11-48, Blackwell Scientific Publications, Oxford.
- Blasco, S.M., Bornhold, B.D., and Lewis, C.F.M.  
1979: Preliminary results of surficial geology and geomorphology studies of the Lomonosov Ridge, central Arctic Basin; in *Current Research, Part C*, Geological Survey of Canada, Paper 79-1C, p.73-83.
- Bukry, D.  
1981: Cretaceous arctic silicoflagellates; *Geo-Marine Letters*, v.1, p.57-63.
- Bukry D.  
1985: Correlation of Late Cretaceous silicoflagellates from Alpha Ridge; in *Initial Geological Report on CESAR — the Canadian Expedition to Study the Alpha Ridge, Arctic Ocean*, ed. H.R. Jackson, P.J. Mudie and S.M. Blasco; Geological Survey of Canada, Paper 84-22, report 9.
- Clark, D.L.  
1977: Climatic factors of the Late Mesozoic and Cenozoic Arctic Ocean; in *Polar Oceans*, ed. M.J. Dunbar; Arctic Institute of North America, Calgary, Alberta, p.603-613.
- 1982: Origin, nature and world climate effect of Arctic Ocean ice-cover; *Nature*, v.300, p.321-325.
- Clark, D.L., Whitman, R.R., Morgan, K.A., and Mackey, S.D.  
1980: Stratigraphy and glacial-marine sediments of the Amerasian Basin, central Arctic Ocean; *Geological Society of America, Special Paper 181*, 57p.
- Harland, W.B., Cox, A.V., Llewellyn, P.G., Pickton, C.A.G., Smith, A.G., and Walters, R.  
1982: *A Geological Time Scale*; Cambridge University Press, Cambridge, U.K., 131p.
- Heezen, B.C. and Hollister, C.D.  
1971: *The Face of the Deep*; Oxford University Press, New York, 659p.
- Hein, J.R. and Karl, S.M.  
1983: Comparisons between open-ocean and continental margin chert sequences; in *Siliceous Deposits in the Pacific Region*, ed. A. Iijima, J.R. Hein and R. Siever; *Developments in Sedimentology*, v.36, Elsevier Scientific Publishing Co., Amsterdam, p.25-43.
- Herman, Y.  
1974: Arctic Ocean sediments, microfauna, and the climatic record in Late Cenozoic time; in *Marine Geology and Oceanography of the Arctic Seas*, ed. Y. Herman; Springer-Verlag, New York, p.283-348.
- 1983: Baffin Bay; present-day analog of the central Arctic during Late Pliocene and mid-Pleistocene time; *Geology*, v.11, p.356-359.
- Iijima, A. and Utada, M.  
1983: Recent developments in the sedimentology of siliceous deposits in Japan; in *Siliceous Deposits in the Pacific Region*, ed. A. Iijima, J.R. Hein and R. Siever; *Developments in Sedimentology*, v.36, p.45-64.
- Isaacs, C.M.  
1981: Porosity reduction during diagenesis of the Monterey Formation, Santa Barbara coastal area, California; in *The Monterey Formation and Related Siliceous Rocks of California*, ed. R.E. Garrison et al.; Special Paper of the Society of Economic Paleontologists and Mineralogists, p.257-271.
- Jackson, H.R.  
1985: Seismic reflection results from CESAR; in *Initial Geological Report on CESAR — the Canadian Expedition to Study the Alpha Ridge, Arctic Ocean*, ed. H.R. Jackson, P.J. Mudie and S.M. Blasco; Geological Survey of Canada, Paper 84-22, report 3.
- Jodrey, F. and Heffler, D.  
1985: Piston coring on CESAR; in *Initial Geological Report on CESAR — the Canadian Expedition to Study the Alpha Ridge, Arctic Ocean*, ed. H.R. Jackson, P.J. Mudie and S.M. Blasco; Geological Survey of Canada, Paper 84-22, report 12.
- Kitchell, J.A. and Clark, D.L.  
1982: Late Cretaceous-Paleozoic paleogeography and paleocirculation; evidence of North Polar upwelling; *Paleogeography, Paleoclimatology, Paleocology*, v.40, p.135-165.
- Marincovich, L., Brouwers, E.M., and Hopkins, D.M.  
1983: Paleogeographic affinities and endemism of Cretaceous and Paleogene marine faunas in the Arctic; *U.S. Geological Survey Polar Research Symposium, Abstracts with Program*, p.45-46; Geological Survey Circular 911.
- Miall, A.D.  
1979: Mesozoic and Tertiary geology of Banks Island, Arctic Canada; The history of an unstable craton margin; *Geological Survey of Canada, Memoir 387*, 235p.



- Minicucci, D.A. and Clark, D.L.  
1983: A Late Cenozoic stratigraphy for glacial-marine sediments of the eastern Alpha Cordillera, central Arctic Ocean; *in* Glacial-marine Sedimentation, ed. B.F. Molnia; Plenum Publishing Corp., New York and London, p.331-365.
- Mudie, P.J. and Aksu, A.E.  
1984: Paleoclimate of Baffin Bay: 300 000 yr. record of foraminifera, dinoflagellates and pollen; *Nature*, v. 312, p. 630-634.
- Mudie, P.J., Piper, D.J.W., Rideout, K., Robertson, K.R., Schafer, C.T., Vilks, G., and Hardy, I.A.  
1984: Standard methods for collecting, describing and sampling Quaternary sediments at the Atlantic Geoscience Centre; Geological Survey of Canada, Open File 1044, 39 p.
- Mudie, P.J.  
1985: Palynology of the CESAR cores, Alpha Ridge; *in* Initial Geological Report on CESAR — the Canadian Expedition to Study the Alpha Ridge, Arctic Ocean, ed. H.R. Jackson, P.J. Mudie and S.M. Blasco; Geological Survey of Canada, Paper 84-22, report 11.
- Nisbet, E.G. and Price, I.  
1974: Siliceous turbidites: bedded chert as redeposited, ocean ridge-derived sediments; *in* Pelagic Sediments; On Land and Under the Sea, ed. K.J. Hsu and H.C. Jenkyns; Special Publications of the International Association of Sedimentologists, v.1, p.351-366.
- Plauchut, B.P. and Jutard, G.G.  
1976: Cretaceous and Tertiary stratigraphy, Banks and Eglinton islands and Anderson Plain (N.W.T.); *Bulletin of Canadian Petroleum Geology*, v.24, p.321-371.
- Schnitker, D., Mayer, L.M., and Norton, S.  
1980: Loss of calcareous fossils from sediments through gypsum formation; *Marine Geology*, v.36, p.M35-M44.
- Siever, R.  
1983: Evolution of chert at active and passive continental margins; *in* Siliceous Deposits in the Pacific Region, ed. A. Iijima, J.R. Hein and R. Siever; *Developments in Sedimentology*, v.36, p.7-24, Elsevier Scientific Publishing Co., Amsterdam.
- Soutar, A., Johnson, S.R., and Taylor, E.  
1982: X-radiography of Hole 480, procedures and results: Initial Reports of the Deep Sea Drilling Project, v.64, part 2, U.S. Government Printing Office, Washington, p. 1183-1190.
- Thiede, J., Dean, W.E., and Claypool, G.E.  
1982: Oxygen-deficient depositional paleoenvironments in the mid-Cretaceous tropical and subtropical Pacific Oceans; *in* Nature and Origin of Cretaceous Carbon-Rich Facies, ed. S.O. Schlanger and M.B. Cita; Academic Press, London and New York, p.79-100.
- Vincent, J.S., Ochietti, S., Rutter, N., Lortie, G., Gilbault, J.P., and De Boutray, B.  
1983: The Late Tertiary-Quaternary stratigraphic record of the Duck Hawk Bluffs, Banks Island, Canadian Arctic Archipelago; *Canadian Journal of Earth Sciences*, v.20, p.1694-1712.



## PALEOMAGNETIC STRATIGRAPHY OF THE CESAR CORES

A.E. Aksu<sup>1</sup>

Dalhousie University, Centre for Marine Geology

Aksu, A.E. *Paleomagnetic stratigraphy of the CESAR cores; in Initial Geological Report on CESAR — the Canadian Expedition to Study the Alpha Ridge, Arctic Ocean*, ed. H.R. Jackson, P.J. Mudie and S.M. Blasco; Geological Survey of Canada, Paper 84-22, p. 101-114, 1985.

### Abstract

Three cores of Cenozoic-Recent sediment from the Alpha Ridge cordillera of the Arctic Ocean have been studied paleomagnetically. Plots of stable inclinations versus depth in the cores show the presence of distinctive normal and reverse polarity chrons resembling those observed elsewhere, and correlation with the accepted paleomagnetic stratigraphy is attempted. An average sedimentation rate of 1.00 mm/1000 years is calculated, based on the Brunhes-Matuyama and Matuyama-Gauss transitions. The oldest sediments represented in these cores were deposited between 4.5 and 4.2 Ma BP.

Four major lithostratigraphic units are present in CESAR core 83-6. Paleomagnetic study of the Cretaceous-Paleocene pelagic siliceous section of unit 4 yielded a sequence of magnetic polarity zones that may be correlated with the marine magnetic anomaly profiles. This unit is characterized by two reversed chrons (A- and C-) and a shorter positive chron (B+). B+ may be correlated with anomaly 29 or 30 plus 31. In both cases, the magnetic data disagree with the Campanian age assigned by diatom data, and partially agree with the Maastrichtian age suggested by silicoflagellate data. Correlation of the magnetic data from units 1, 2 and 3 is uncertain because these sediments are devoid of diagnostic microfossils. However, the short reversed polarity zone at the upper part of the core suggests a minimum age of 0.73 Ma (older than Brunhes normal polarity chron) for the core top.

### Résumé

Des études paléomagnétiques ont été effectuées sur trois carottes de sédiments d'âge cénozoïque et holocène provenant de la cordillère de la dorsale Alpha dans l'océan Arctique. Les graphiques des inclinaisons stables par rapport à la profondeur font voir des chronnes caractéristiques à polarité directe et inversée similaires à ceux qui ont été observés ailleurs; l'auteur tente de les mettre en corrélation avec la stratigraphie paléomagnétique acceptée. La vitesse de sédimentation moyenne, fondée sur les transitions de Brunhes-Matuyama et de Matuyama-Gauss, est de 1,00 mm/1 000 ans. La mise en place des sédiments les plus anciens trouvés dans ces carottes a eu lieu il y a entre 4,5 et 4,2 millions d'années.

La carotte CESAR 83-6 contient quatre grandes unités lithostratigraphiques. L'étude paléomagnétique de la section siliceuse pélagique de l'unité 4 (Crétacé-Paléocène) a donné une séquence de zones à polarité magnétique susceptibles d'être mises en corrélation avec les profils des anomalies magnétiques marines. La présence de deux chronnes inversés (A- et C-) et d'un chronne positif plus court (B+) caractérise cette unité. Le chronne B+ peut être mis en corrélation avec l'anomalie 29 ou les anomalies 30 plus 31. Dans les deux cas, les données magnétiques ne concordent pas avec l'âge campanien indiqué par les diatomées, mais coïncident partiellement avec l'âge maastrichtien suggéré par les silicoflagellés. La corrélation des données magnétiques provenant des unités 1, 2 et 3 est incertaine puisque ces sédiments sont dépourvus de microfossiles caractéristiques. Toutefois, la courte zone à polarité inversée dans la partie supérieure de la carotte semble indiquer que cette partie de l'échantillon date au moins de 0,73 Ma (âge plus ancien que le chronne de Brunhes à polarité directe).

<sup>1</sup>Now at Department of Earth Sciences, Memorial University of Newfoundland, St. Johns, Newfoundland A1B 3X5

## INTRODUCTION

Over the past two decades, a limited number of cores from the Arctic Ocean have been the subject of detailed paleoclimatic and oceanographic studies by Y. Herman (e.g. Herman, 1974; Herman and Hopkins, 1980; Herman, 1983) and D. Clark (e.g. Clark et al., 1980; Clark, 1982). In these studies, the magnetic stratigraphy has been used as a tool to establish time frameworks. However, different interpretations of the magnetic record and the poor knowledge of the modern Arctic fauna have led to conflicting chronologies for the sediments involved. It has not yet been possible to correlate satisfactorily the Neogene record of Clark with that of Herman, primarily because few magnetic data were published in these studies other than summary polarity columns.

About 20 long piston and gravity cores were collected from the Alpha Ridge cordillera from the CESAR ice station. It is the purpose of this paper to describe the paleomagnetic data from four of these cores. The objectives are: 1) to establish a chronostratigraphic framework in which faunal and sedimentological histories can be determined, and 2) to show some of the sources of inconsistencies that limit interpretation of the results.

## ACKNOWLEDGMENTS

The laboratory work was supported by DSS contract #OSC83-00399. I thank Linda Dobbin, Kathy McKinnon, Charlie Walls and Mario Justino for their work in sampling and preliminary measurements. The manuscript was reviewed by James Hall, and Edward Irving has made valuable comments on the data. This paper is Publication No. 9, Centre for Marine Geology, Dalhousie University.

## CESAR CORES 83-14, 83-102 AND 83-103

### *Material and techniques*

The following three cores were selected for detailed magnetic studies: CESAR 83-14, 83-102 and 83-103. Figure 7.1 shows the location of the cores. These cores represent typical lithostratigraphic sequences for the last 1 to 4 Ma of the Arctic Ocean sediments. Gravity cores 83-102 (= CESAR 102) and 83-103 (= CESAR 103) were selected to estimate the amount of sediment missing from the tops of the piston cores, e.g. CESAR 83-14 (= CESAR 14). Core recovery, and lithological description of cores are given by Mudie and Blasco (1985). All cores were stored in a vertical position at 4°C at the Bedford Institute of oceanography (BIO) core repository until they were split. The plastic liners were cut longitudinally with a rotary saw, and the sediment was split with nylon fishing line. All cores were subsequently X-radiographed. Paleomagnetic samples were taken with a plastic cylinder (2.5 cm in diameter and height) by pushing the sample holders into the split core sections. Cores were sampled at an average of every 2.5 cm. Care was exercised to avoid disturbance of sediment during this process. The samples were taken with their cylindrical axes accurately positioned perpendicular to the split longitudinal face of the core sections, in order to preserve orientation with respect to the horizontal and relative azimuth in each core section. The core-top direction was carefully recorded on each sample holder. All samples were taken from the centre of the cores to avoid erroneous results originating from the distorted outer edges. The samples were subsequently placed in plastic vials with a moistened sponge at the bottom and were stored within Helmholtz coils for at least 15 days before measurements.

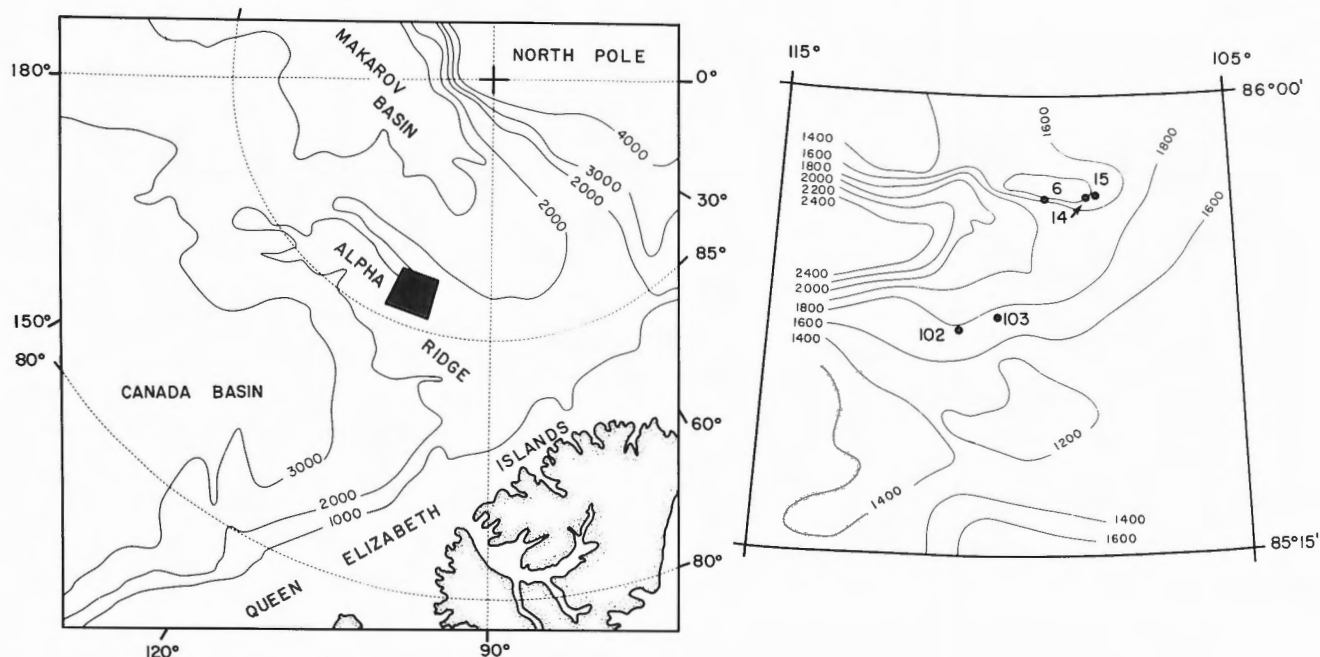


Figure 7.1 Bathymetry of the Alpha Ridge, showing major structural features of the Arctic Ocean (left), and detailed bathymetry of the study area and core locations (right).

## Magnetic measurements

Measurements of the remanent magnetization were performed using a Schonstedt DSM-I Digital Spinner Magnetometer and a 400 Hz alternating field demagnetization unit. The intensities of the natural remanent magnetization (NRM) ranged from  $0.1 \times 10^{-5}$  emu/cm<sup>3</sup> in normally magnetized samples to  $0.5 \times 10^{-6}$  emu/cm<sup>3</sup> in reverse magnetized samples. Measurements of the natural magnetization were made after alternating field (AF) demagnetization steps until the intensity values were reduced to 15% of the NRM.

The cores were not oriented with regard to azimuth; thus, the true declination of the remanence could not be determined. At high latitudes, however, the steep inclination ( $I = 80^\circ$ ) of the geomagnetic field is dominantly along the axis of the cores, and remanence azimuth is not expected to relate strongly to polarity, which is best determined by study of the remanence inclination.

## Results

Figure 7.2 illustrates examples of the normalized intensity and directional response to AF demagnetization observed in the core samples. Some samples showed a steady decrease in intensity with demagnetization, accompanied by very little directional response. This behaviour was typical of normally magnetized zones in the cores (also see Fig. 7.4). In other samples the NRM was initially positive but gradually changed to negative values with progressive removal of the over-printed viscous remanent magnetization (VRM) after treatment at 100 to 200 Oe. The steady decrease in normalized intensity values of these samples (Fig. 7.2) suggested that the reverse stable remanence intensity was weaker than the VRM. These samples were typical of reverse magnetized zones. For some samples from CESAR 83-14 (*s* and *r* in Fig. 7.2), the intensity progressively increased on treatment at 100 or 200 Oe, then showed a steady decrease on demagnetization to 500 or 1000 Oe. The removal of VRM caused very little directional response in these samples. This behaviour was observed in about 20% of the samples from the reversely magnetized zone in core 83-14 (179 to 240cm), and indicates that the reverse stable remanence intensity was stronger than the VRM. Progressive removal of the soft VRM component(s) caused an initial increase in the resultant magnetization until only the reverse stable remanence component remained; the intensity then decreased with further demagnetization.

The direction of magnetization was considered stable when the averages of directions at several successive steps varied less than  $6^\circ$ . Preliminary results indicated that most samples were stably magnetized with a median destructive field ranging from 300 to 400 Oe. However, as a precaution against possible loss of information through too intense demagnetization, all samples were treated at 25, 50, 75, 100, 150, 200, 250, 300, 350 and 400 Oe. A few samples were further demagnetized to 1000 Oe. Histograms of the inclination values of samples from core 83-14 during this treatment are plotted in Figure 7.3. Most normal and reverse stable remanence directions had associated precision parameters,  $k$ ,

greater than 200 and 50, with corresponding semi-cones of confidence,  $\alpha_{95}$ , being less than  $3^\circ$  and  $5^\circ$  respectively.

In core 83-14, the inclinations of samples from the positive polarity chrons, Brunhes and Gauss (Fig. 7.4; 0-52cm and 240-300cm respectively) were highly skewed towards positive NRM values and showed very little displacement with stepwise demagnetization (Fig. 7.3). It is noted that the mean inclination direction for the Gauss chron is slightly shallower than that for the Brunhes chron. The NRM inclination of samples from the intervening reversed Matuyama polarity chron (Fig. 7.4; 52-240cm), showed a slight skewness towards positive values in the NRM, gradually displacing towards the negative values with progressive demagnetization to form a well defined peak at ca.  $-45$  to  $-75^\circ$  by 400 Oe (Fig. 7.3). This behaviour demonstrated the successful removal of low coercivity downward normal components, and the isolation of high coercivity reversed polarity components. Samples below 300cm (Gilbert reverse polarity chron) showed a very strong soft positive VRM superimposed on a much weaker negative initial magnetization. Through the demagnetization steps performed it was not always possible to determine a stable phase of magnetization direction. However, the gradual displacement of inclinations towards negative values indicated that the actual polarity during the deposition of these sediments was reversed and that the initial magnetizing field direction was probably steeper than the magnetization observed in the samples.

## Paleomagnetic stratigraphy

The plots of the stable inclinations versus depth in the cores (Fig. 7.4) showed the presence of distinctive normal and reverse polarity chrons resembling those observed in the generally accepted paleomagnetic stratigraphy (e.g. Mankinen and Dalrymple, 1979; Harland et al., 1982). A summary polarity log was constructed for each core based on all polarity changes that exceed  $30^\circ$  positive or negative on their stable inclinations, even if only one sample is involved. Inclination values of  $30$  to  $-30^\circ$  are indicated as transitional. Detailed inspection of the upper sections of the cores suggests that the Brunhes/Matuyama boundary occurs around 71-77cm in core 83-103 and 50-55cm in core 83-14 (Fig. 7.5); in core 83-102 the boundary is at 85-90cm (Fig. 7.4). In all cases this transition is associated with a large decrease in intensity of  $0.8 \times 10^{-6}$  emu/cm<sup>3</sup> and occurred in the middle of lithofacies K. The Matuyama/Gauss transition is identified between 239 and 244cm depth in core 83-14 (Fig. 7.5). Within the Matuyama reverse chron, four major positive polarity sub-chrons are identified in core 83-14, whereas only two are seen in the short gravity cores. In all cases the polarity changes are accompanied by large changes in intensity values. The most prominent of these sub-chrons (135 to 161cm in core 83-14), which occurs from the middle of lithofacies G to uppermost DE, is tentatively correlated with the Olduvai normal event. In the central Arctic Ocean, the Olduvai event is identified within the lower part of lithofacies G and upper F (Clark et al., 1980; Gilbert and Clark, 1983). Two relatively short positive events are identified immediately below the Brunhes/Matuyama boundary,



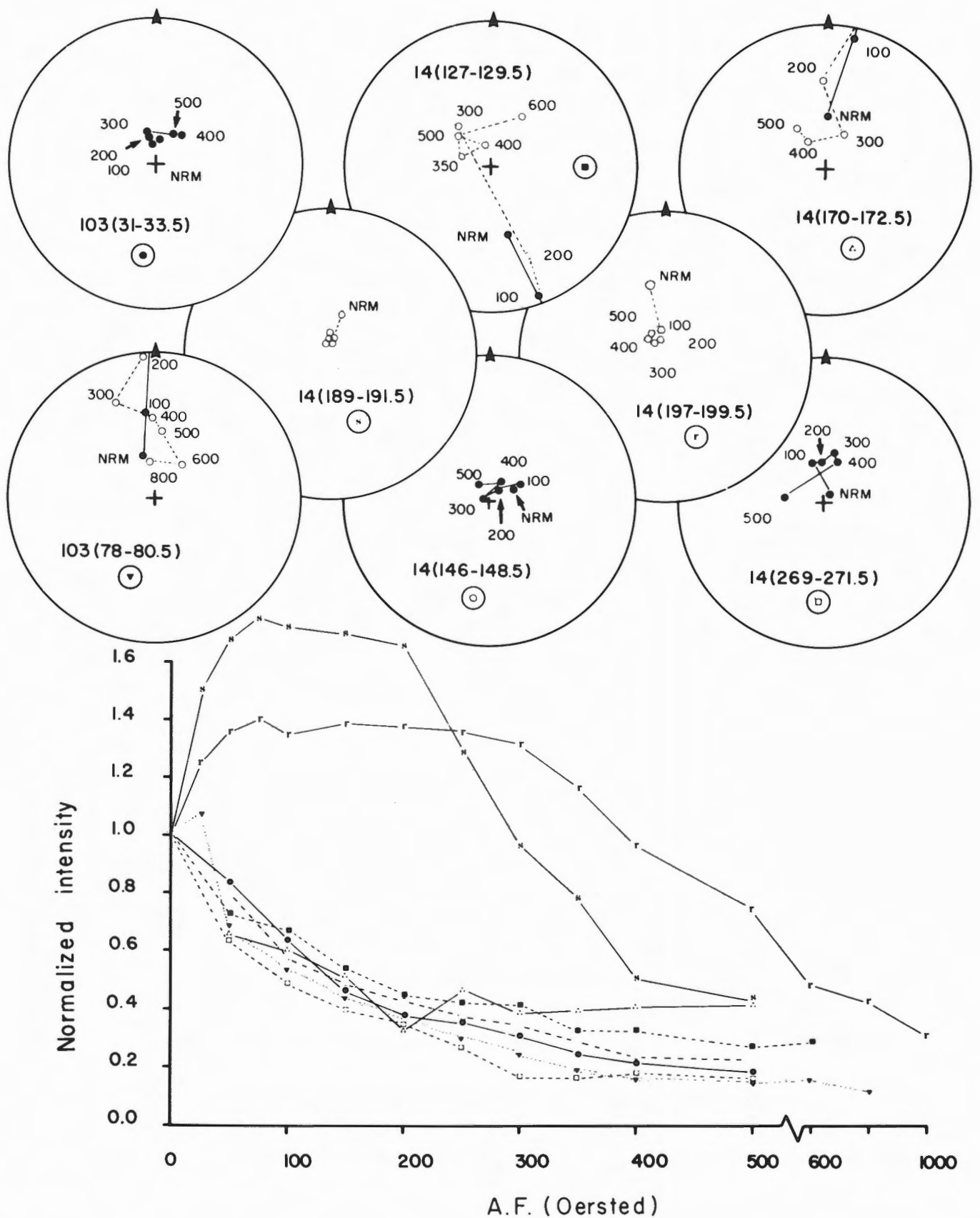


Figure 7.2 Examples of directional response to AF demagnetization are shown in the large circles above, and the normalized intensity response of AF demagnetization for these samples is plotted in the graph below. Different samples for the core intervals shown in the circles are represented by dots, squares, triangles etc. in the graph. Solid circles represent positive inclinations, and open circles are negative inclinations for the demagnetization field values in Oersteds.

occurring near the unit K-J and J-I transitions respectively. These are tentatively correlated with the Jaramillo event. The Jaramillo is thought to occur near the unit J-I transition by Clark et al. (1980, p. 22, Fig. 32) and near the unit K-J transition in Gilbert and Clark (1983, p. 388, Fig. 2). The least clearly correlated of these four events is that identified between 102 and 109cm depth in core 83-14, occurring within the lowermost part of the lithofacies I (Fig. 7.4). This event has not been previously reported from the Arctic Ocean and may represent i) a split Olduvai with the lower part occurring between 135 and 161m depth in core 83-14, or ii) a separate event (?Gilsa). Work in progress on the nearby core 83-15 may resolve the status of this event.

The transition from the Gauss normal to Gilbert reverse polarity chrons was inconspicuous in core 83-14. The stable inclination values oscillated between 60 and 75° from 245 to 299cm depth in the core. At around 300cm, a 70° shift (from +38 to -32°) is observed, below which very few samples yielded clearly defined stable remanence directions. It may be significant that this transition is associated with the transition from core section 3 to 4. However, careful examination of X-radiographs from this transition showed no sign of sediment

disturbance resulting from the coring operation and no primary sedimentary structures indicative of displaced sediments, although significant increase in bioturbation does occur at this level. The effects of faunal activity on paleomagnetic data is well known (e.g. Watkins, 1968). However, unless an organic process could create larger domains in the original ferromagnetic material, the redeposited sediment would record the ambient magnetic field following the bioturbation with essentially the same precision as during the initial sedimentation; therefore, bioturbation cannot obviously account for many shallow stable inclinations in the 300-385cm interval. As discussed earlier (Fig. 7.3), it is believed that the polarity during the deposition of these sediments was reversed, and the direction of the magnetizing field was steeper than is observed. The Gauss/Gilbert transition is tentatively placed at around 300cm depth in core 83-14, pending further investigation. It is important to note that the Kaena and Mammoth reverse polarity sub-chrons are not observed in the inferred Gauss chron. The two positive polarity events identified at 388-391cm and 415-423cm depth in core 83-14 are tentatively correlated with the Cochiti and Nunivak positive sub-chrons within the Gilbert chron.

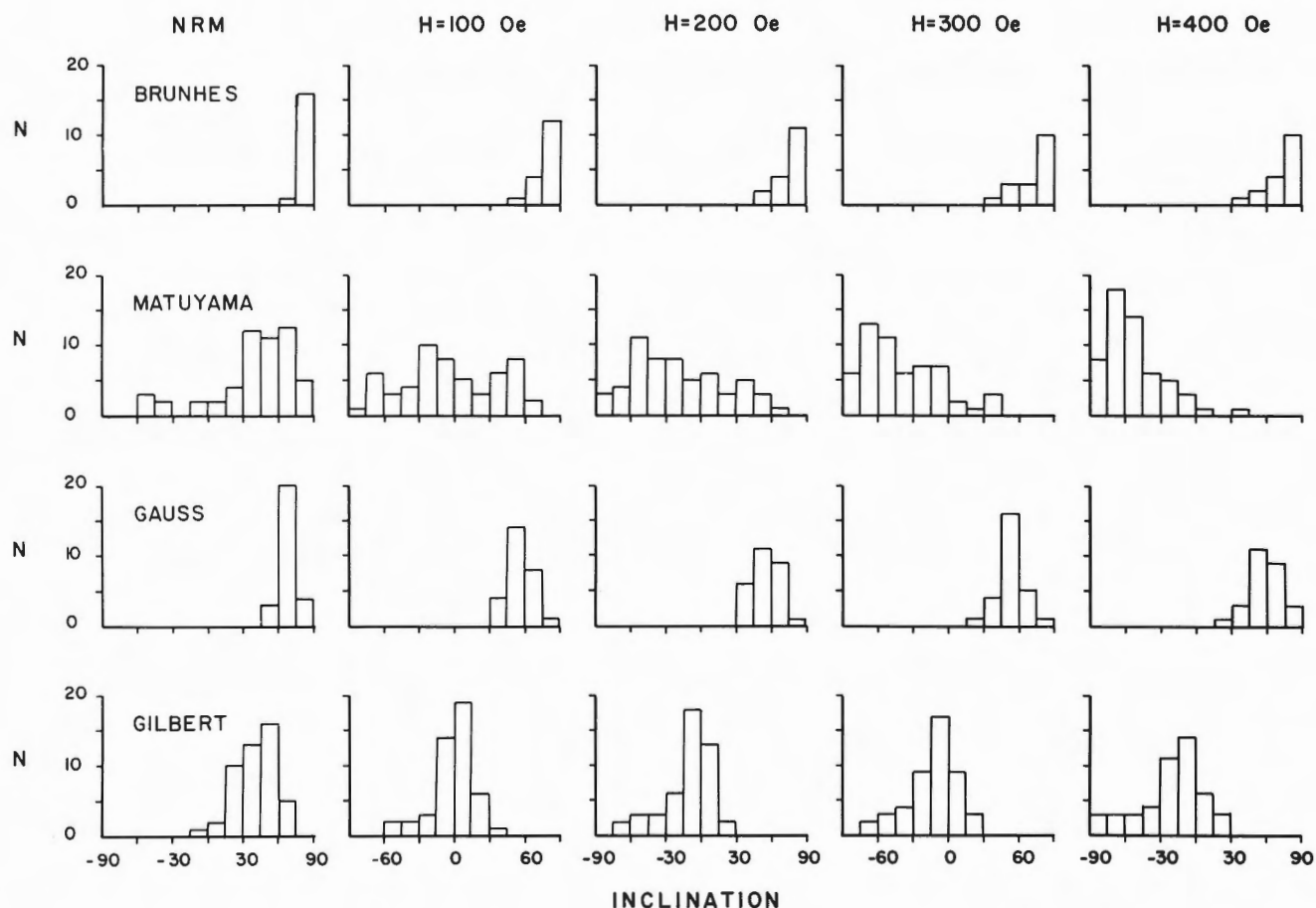


Figure 7.3 Histograms of inclination values from major magnetic polarity chrons for CESAR core 83-14. N = number of samples.

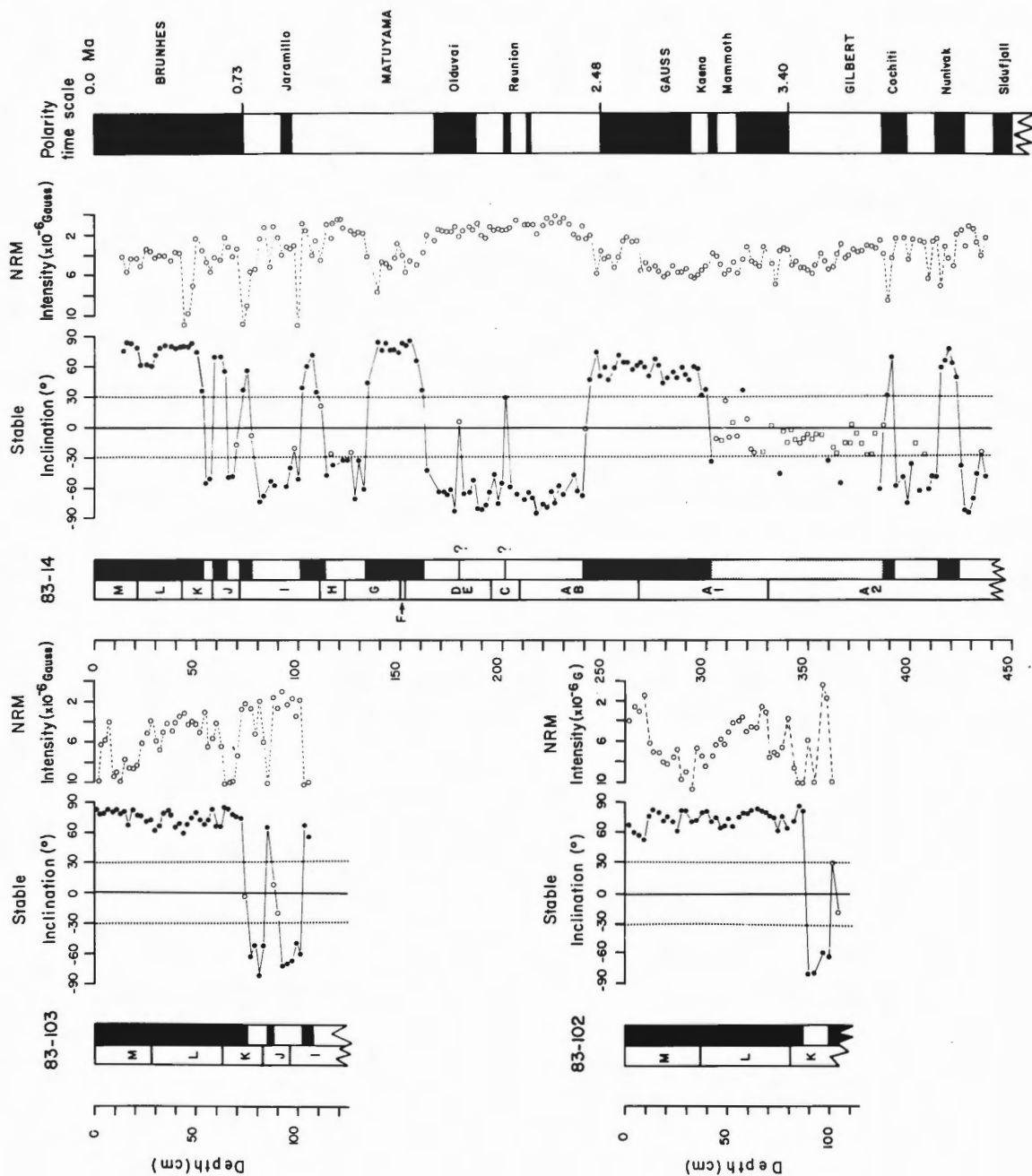


Figure 7.4 Downcore plots of stable inclinations (solid circles) and NRM intensities. Open circles represent transition zones, open squares indicate samples in which a stable phase of magnetization direction was not achieved. A2 to M are lithostratigraphic units of Clark et al. (1980) and of Mudie and Blasco (1985). Summary polarity columns are shown next to the cores. Polarity time scale (right) is from Harland et al. (1982).

## Sedimentation rate

Before the rate of deposition can be calculated for the core sites, an indication of the age of sediment is necessary. This can be done by correlating the magnetic signatures of the cores with the accepted paleomagnetic reversal time scale. This process, however, assumes that the acquisition of magnetization direction took place syndepositionally as the ferromagnetic particles settled and oriented themselves according to the geomagnetic field direction. This assumption is generally correct for basins where the sedimentation rate is high and bioturbation is negligible; but it is not necessarily correct for basins with slower rate of deposition and higher bioturbational reworking. Previous studies indicated that the rate of sediment deposition is an order of magnitude lower in the Arctic Ocean than it is in most oceans in the world (Herman, 1983; Clark et al., 1980). Examination of X-radiographs of the cores showed that most units showed some bioturbational mixing of sediments but their magnetic values do not differ significantly from adjacent unmixed sediments.

Therefore, for simplicity, it can be assumed that postdepositional changes had very little effect on the magnetization direction recorded during the deposition. It should be noted, however, that this process of acquisition can take place during the early stage of dewatering as well as following bioturbation. All these processes would depress a particular magnetic boundary as much as the depth required for peak dewatering or the depth of organic activity, thus giving apparent local perturbation to the rate of deposition.

Figures 7.4 and 7.6 illustrate the chronology assigned for the cores. One notable shortcoming of the piston coring process is that the sediment-water interface is commonly destroyed. This can be compensated by using a short gravity corer as a trigger weight. Comparison of the two cores then gives an estimate of the amount of section missing from the piston core. During most of the CESAR piston coring operations, no gravity core trigger weight was used (Mudie and Blasco, 1985). However, comparison between the gravity core 83-103 and piston core 83-14 suggested that the top 22cm of

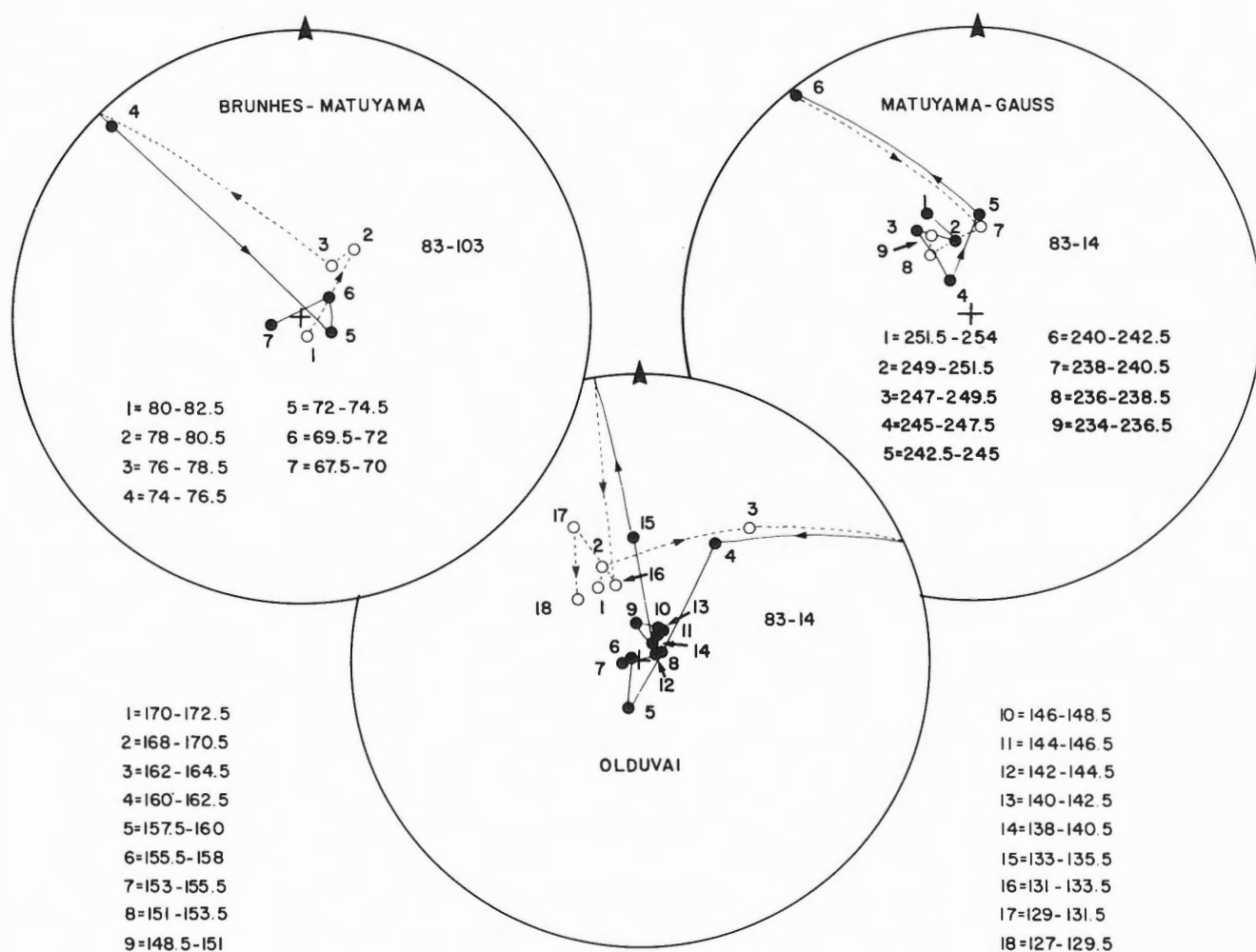


Figure 7.5 Path of magnetic vector in Matuyama-Brunhes transition, Matuyama-Olduvai-Matuyama transitions and Gauss-Matuyama transition. Solid circles represent positive inclinations, open circles negative inclinations.

the piston core is missing. Figure 7.6 illustrates the sedimentation rate calculated for two of the core sites. The straight line assumes a variable rate of deposition of 1.03mm, 1.06mm, 1.42mm and 1.51mm per 1000 years for Brunhes, Matuyama, Gauss and Gilbert polarity chrons respectively. The dashed line assumes an average of 1.00 mm per 1000 years sedimentation rate. If this is correct, the basal age of core CESAR 83-14 should be older than 4.2 Ma.

#### Comments on the records

Figure 7.7 illustrates the summary magneto/lithostratigraphy of the Alpha Ridge cordillera as described by D. Clark and his co-workers (e.g. Steuerwald et al., 1968; Clark et al., 1980; Gilbert and Clark, 1983; Minicucci and Clark, 1983) and that observed in CESAR core 83-14. There is no major difficulty of correlating the stratigraphy of the upper 2 Ma or so. For example, in both cases the Brunhes-Matuyama boundary occurs in the middle of lithofacies K. Even though differences exist in the finer scale correlations, a similar situation is evident for Jaramillo and Olduvai subchrons. However, there is a significant discrepancy in the correlation of the sediments older than 2 Ma. Clark et al. (1980) indicated that the Matuyama-Gauss boundary occurs near the middle of lithofacies D (DE in Minicucci and Clark, 1983), whereas this polarity transition is near the middle of

lithofacies AB in core 83-14. The first question is "How reliable are the lithofacies described in core 83-14?". Fortunately, D. Clark was present during the splitting of the CESAR cores and he delimited those lithofacies corresponding to the lithostratigraphic scheme of Clark et al. (1980). Therefore, it is very unlikely that the discrepancy observed in Figure 7.7 arises from misidentification of lithofacies. However, three new lithostratigraphic units A1, A2 and A3 were recovered in core 83-14, which have not been previously described. The Gauss-Gilbert transition is seen within the newly described unit A1 in core 83-14. However, Clark et al. (1980) put this boundary near the uppermost part of unit A in their cores; furthermore, they indicated that the Gilbert to magnetic anomaly 3A (ca. 5.41 to 5.70 Ma) transition also occurs in unit A.

In Minicucci and Clark (1983), however, the Gauss/Gilbert transition is indicated near the base of lithofacies AB, which correlates with lower A of Clark et al. (1980). Evaluation of this apparent discrepancy is complicated primarily because no solid paleomagnetic data have been published by Clark and his co-workers. In most papers discussing the Late Cenozoic magnetic stratigraphy of Arctic Ocean cores, only a summary polarity stratigraphy is presented (e.g. Steuerwald et al., 1968; Clark, 1970; Clark et al., 1980; Gilbert and

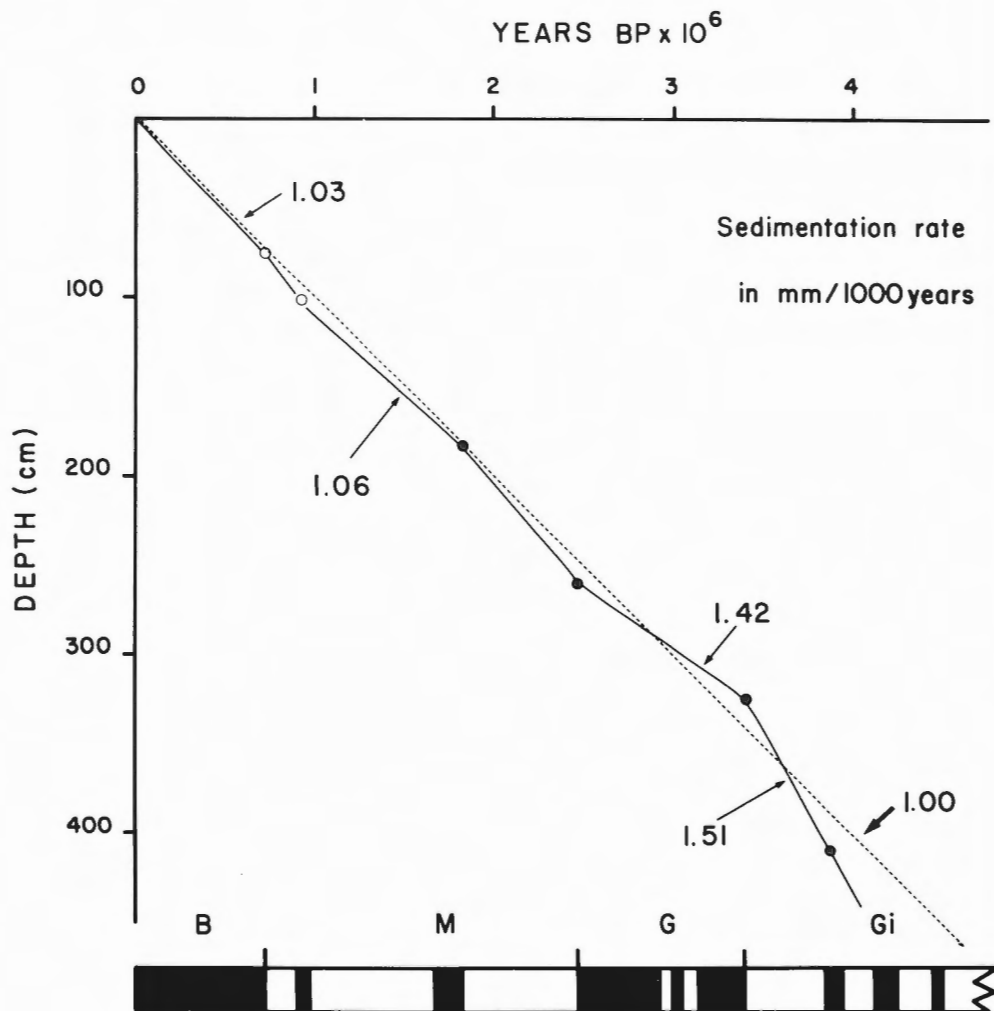
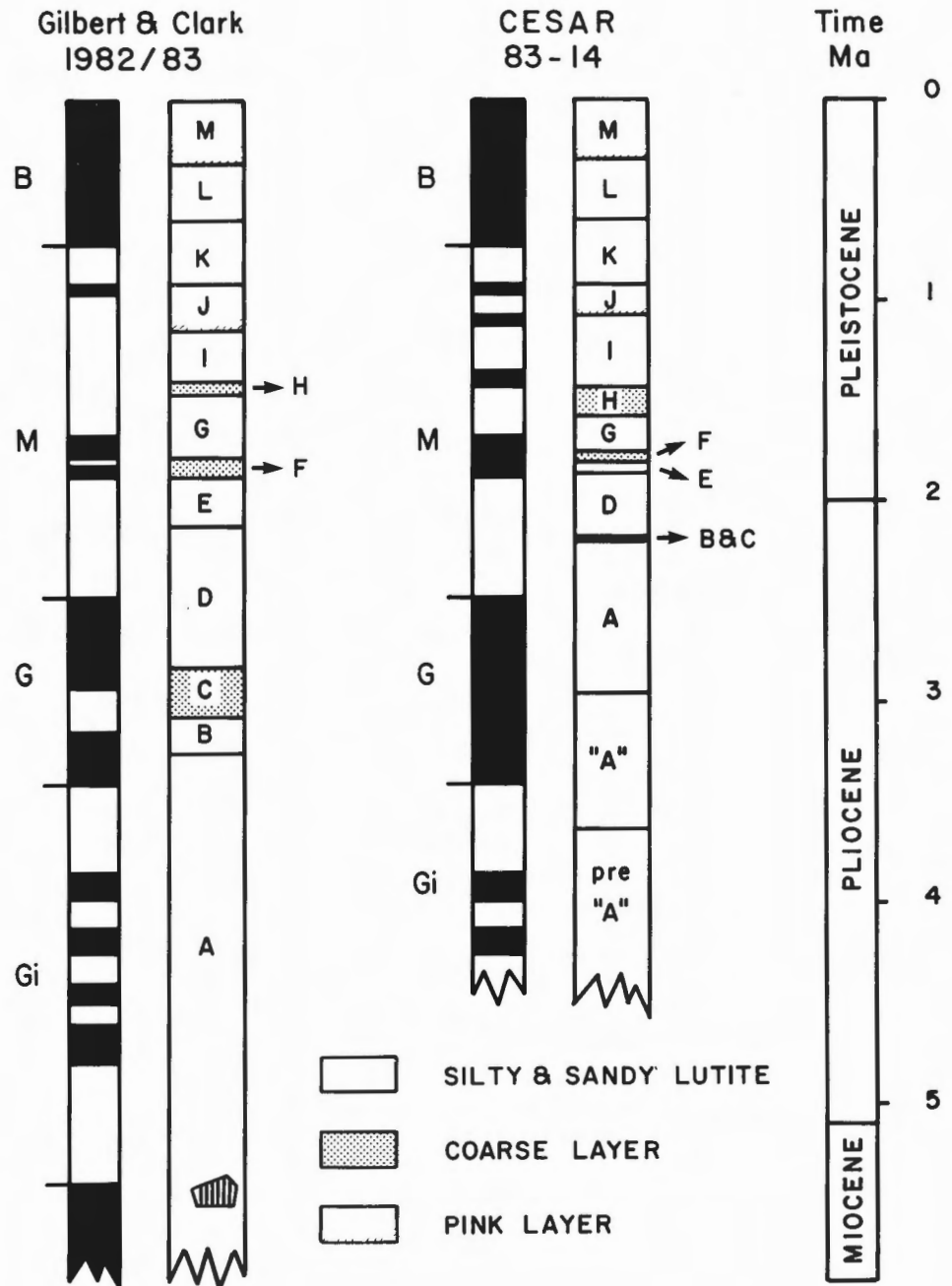


Figure 7.6 Ages inferred for key polarity chrons by comparison with the polarity time scale (bottom) from Harland et al., 1982. Open circles represent core 83-103 and solid circles core 83-14. Solid line assumes variable rate of deposition, dashed line assumes a uniform rate.



Figure 7.7 Summary stratigraphy of the Alpha Ridge cordillera (left) from Clark et al. (1980) and Gilbert and Clark (1983), redrawn; compared with the stratigraphy of CESAR core 83-14 (centre). Lithostratigraphic units (A3 to M) are those of Clark et al. (1980) and described by Mudie and Blasco (1985). Hatched symbol near the base of column 1 indicates the glacial erratics described by Clark et al. (1981). Time scale (right) is from Harland et al. (1982).



Clark, 1983). The problem is further complicated by the reciprocal polarities assigned in these papers; e.g. in Steuerwald et al. (1968, p. 81, Fig. 2), the Brunhes normal polarity chron carries a negative sign and the Matuyama reversed polarity chron carries a positive sign. A similar situation exists in Clark et al. (1980, p. 19, Fig. 29). Therefore, because the actual paleomagnetic data were not reported, a detailed evaluation of these data is not possible.

The knowledge of the timing of the initial freezing of the Arctic Ocean and the precise chronology of the initial ocean-

atmosphere cooling (?pre-Pleistocene onset of continental glacial) is crucial for global paleoclimate modelling and a fundamental parameter for the understanding of the factors involved in the initiation of glacial-interglacial cycles. The most widely accepted basis for the chronology of the Arctic Ocean sediments lies in the interpretation of the paleomagnetic stratigraphy. Therefore, despite the fact that this type of paleomagnetic work brings very little new information for the magnetic reversal theory, more data is needed to resolve the chronostratigraphy of the Arctic Ocean sediments. Utmost care should be exercised in the acquisition and publication of future paleomagnetic work.

## Conclusions

1. Despite the very slow rate of deposition (about 1mm per 1000 years), the Arctic Ocean sediments carry the fine scale magnetic signature of the earth's polarity history.
2. There is a discrepancy in the interpretation of paleomagnetic records between D. Clark and this study. Further work is needed to resolve the chronology of the Arctic Ocean sediments.
3. If the chronology presented here is correct, reinterpretation of the previously published paleoclimatic and paleoceanographic data may be required.

## CESAR CORE 83-6

### Introduction

Core 83-6 (= CESAR 6) is from the northern part of a fault-bounded structural high (see Fig. 6.9 of Mudie and Blasco, 1985). The presence of chaotic seismic sequences between sites 83-6 and 83-7, as well as a thick depositional prism showing roll-over toward the normal fault down-dip from the core site 83-6, suggest that a considerable amount of sediment has been stripped off from the high, exposing a much older sedimentary sequence at the core site.

The core includes four distinct lithofacies referred to as units 1 to 4 (Mudie and Blasco, 1985). Unit 1 (0-99cm) is composed of brown silty muds with occasional silt laminae and scattered coarse sand/gravel. A limited number of samples examined from this interval contained only Cretaceous-Recent microfossils; therefore no precise age can be assigned to the unit. Unit 2 (99-111 cm) consists of grey silty muds. A hard reddish friable mud is distinguished as unit 3 (111-127cm). Both units 2 and 3 contained no calcareous or siliceous microfossils. Unit 4 (127-305cm) is composed of soft, pale yellow laminated siliceous ooze, with discontinuous horizontal dark streaks. Silicoflagellate data suggest that this unit is uppermost Campanian to Maastrichtian in age (Bukry, 1985). The diatom stratigraphy, however, indicates a slightly older age of mid- to late-Campanian (Barron, 1985). Visual examination of CESAR 83-6 suggests the presence of three major lithostratigraphic breaks, possibly corresponding to three major unconformities.

Core 83-6 was sampled for detailed paleomagnetic measurements. The 305cm section yielded 122 samples from four lithological units. Methods of sampling and magnetic measurement are the same as those described earlier in this report. In addition, seven samples were taken from unit 4 for Curie temperature analysis. The aims of this paleomagnetism study are: 1) to determine whether or not an independent age could be assigned to units, particularly units 1 to 4; and 2) to resolve whether the origin of the laminated couplets in unit 4 (see Mudie and Blasco, 1985) is due to rapid deposition (i.e. annual varves) or is the result of slow cyclical pelagic sedimentation.

## Remanent magnetization

The intensities of the natural remanent magnetization (NRM) in CESAR 83-6 were weak, ranging from  $2.9 \times 10^{-7}$  emu/cm<sup>3</sup> to  $9.9 \times 10^{-6}$  emu/cm<sup>3</sup> in samples from units 2 to 4, and from  $2.3 \times 10^{-6}$  emu/cm<sup>3</sup> to  $9.8 \times 10^{-6}$  emu/cm<sup>3</sup> in samples from unit 1. After demagnetization in a peak alternating magnetic field of 400 Oe, the remanent intensities of samples from unit 4 were generally less than 40% of the NRM intensities (Fig. 7.8). In samples from unit 1, the NRM included a significant soft component which was easily removed by an alternating field ranging from 100 to 250 Oe. The median destructive field (MDF) varied between 200 to 400 Oe in these samples from unit 1. Following the removal of the viscous unstable component, sample remanence was relatively stable against further alternating field (AF) demagnetization. In samples from units 2 and 3, the NRM contained a very large viscous component. The MDF in these samples ranged between 50 and 100 Oe, at which point the anhysteretic magnetization became a serious problem making further demagnetization in higher AF impractical. In most samples from units 2 and 3, the AF demagnetization to 100 Oe erased more than 80% of the NRM intensities.

Samples from unit 4 included an extremely small soft component that was generally removed by 100 Oe AF and which also erased less than 10% of the NRM intensities. The stable remanence in these samples persisted for at least a few hundred oersteds against AF demagnetization (Fig. 7.8.). The inclination of the stable remanent vector in successive AF demagnetization varied less than 2°; similarly the declination varied between 10 and 20°.

## Magnetic minerals

The pelagic sediments in most of unit 4 include more than 95% of siliceous biogenic skeletal tests (see Mudie and Blasco, 1985). They were deposited presumably in deep and tranquil conditions of the early Arctic Ocean. The matrix is mostly opaline silica but also includes very small amounts of silicoclastic debris, including clay minerals and a minute fraction of mafic minerals, which would have acquired the paleomagnetic field direction during the early postdepositional stage (Kent, 1973). Several attempts were made to extract magnetic minerals from the siliceous ooze. Because a large amount of sediment is required to extract a sufficient amount of magnetic minerals, we could not justify the destruction of sections of this core. As an alternative, Curie temperature analysis of bulk sediment were carried out on seven selected samples. Preliminary examination of smear slides indicated that mafic mineral concentrations (which are not necessarily all magnetic) were generally less than 1%. In three samples, the thermomagnetic curves showed relatively well defined single Curie points ranging from 540 to 550°C. The magnetic minerals in these samples are probably mostly magnetite. The thermomagnetic curves in the remaining four samples were noisy and only two curves gave reliable results,

with double Curie points at 640 and 560°C corresponding to hematite and magnetite respectively.

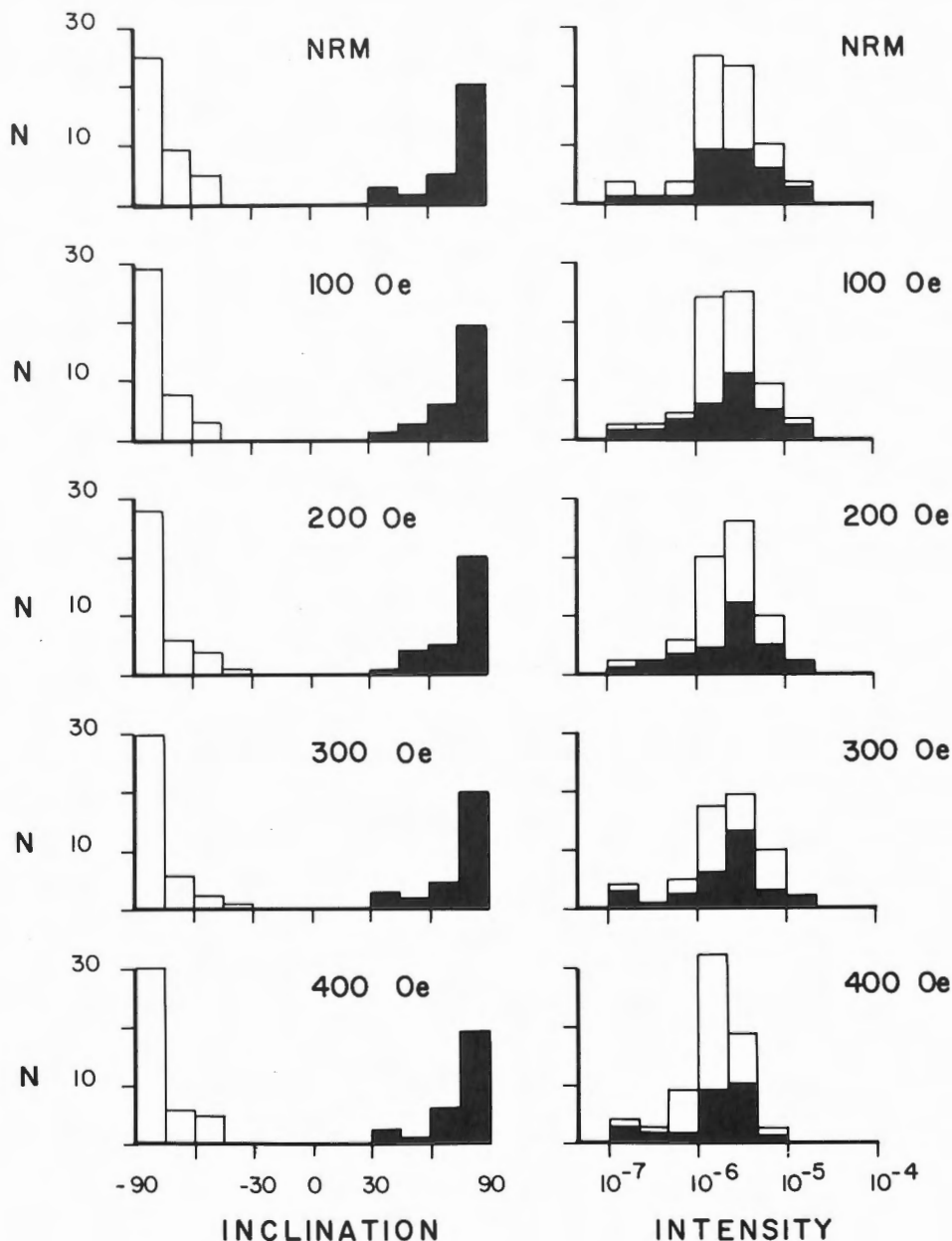
The thermomagnetic analysis of the bulk sediments in unit 4 generally suggest that the primary magnetic mineral is magnetite with varying proportions of hematite. because hematite is generally an oxidation product of primary magnetic minerals (i.e. magnetite) in marine sediments, if the NRM is carried by hematite in the samples, it is questionable that it represents primary remanence. It is therefore possible that the unit 4 sediments may exhibit a combination of primary and secondary magnetization vectors. On the other hand, if the hematization occurred sometime after the acquisition of primary remanence and it did not completely

replace the original magnetite, then the primary magnetization may be preserved largely unaltered in direction. Further work is needed to quantitatively determine the magnetic mineralogy and the timing of remanence acquisition. The following discussion assumes that 1) the remanence is relatively contemporaneous with the sedimentation and 2) hematization has not appreciably altered the remanent magnetization direction.

### Results

Unit 4: Five normal and six reversed zones are delimited (Fig. 7.9). For reference purposes they are named by letters in ascending alphabetical order, with normal intervals dis-

Figure 7.8 CESAR core 83-6, unit 4: histograms of NRM inclinations (left) and intensities (right), and inclinations and intensities after AF demagnetization in demagnetization fields of 100, 200, 300 and 400 Oe. N = number of samples.



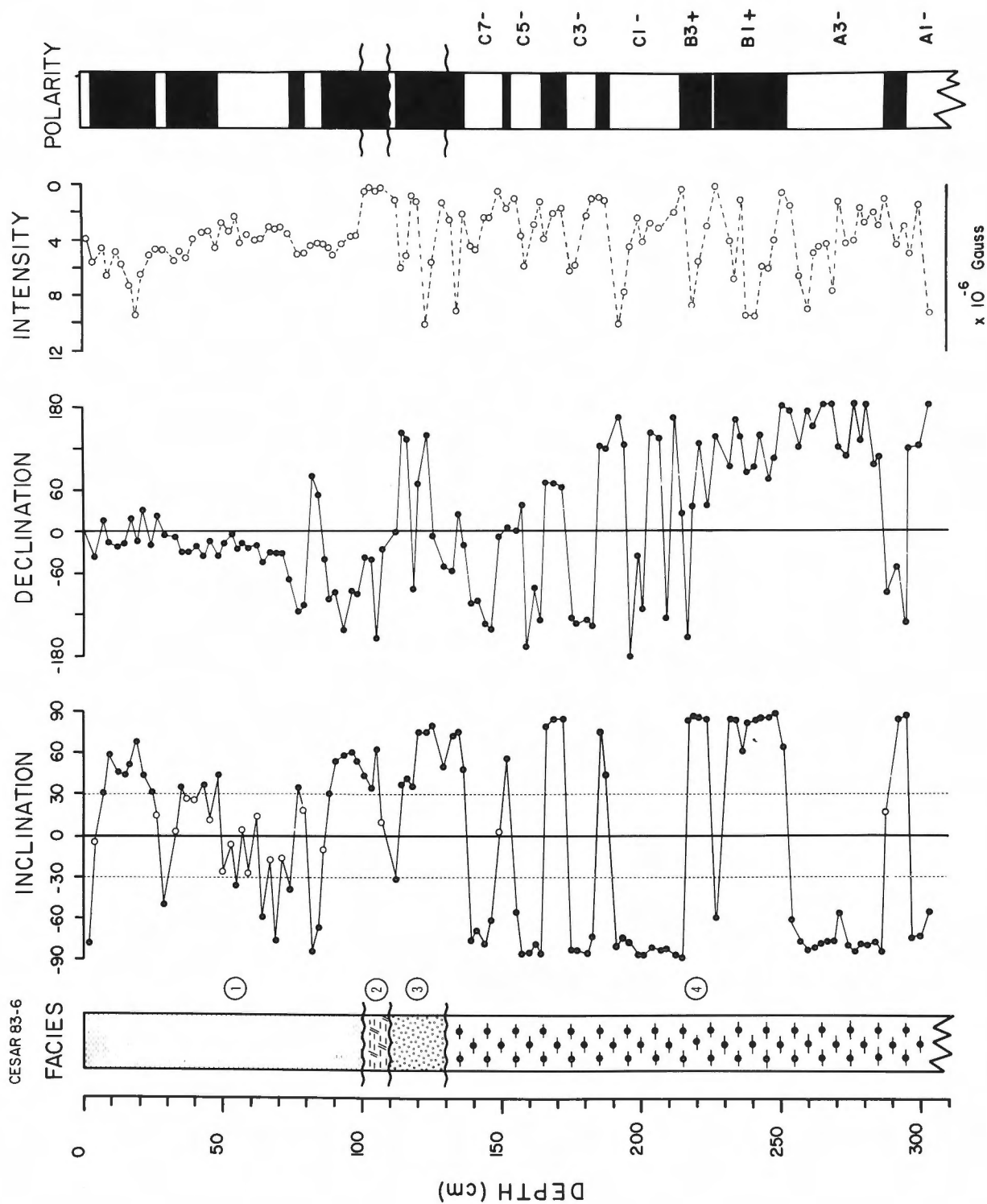


Figure 7.9 CESAR core 83-6: downcore plots of stable inclinations, declinations and NRM intensities. Inclination transition zones are indicated by open circles. Lithostratigraphic units 1 to 4 explained in Mudie and Blasco (1985). Magnetostratigraphic units A-, B+ and C- are explained in the text.

tinguished by “+” and reversed zones by “-”. Assuming that the rate of deposition was constant, the paleomagnetic record from unit 4 can be divided into three magnetostratigraphic units: 1) A- is a reversed chron with a short positive sub-chron A2+; 2) a positive chron, B+, appears to be interrupted by a small negative sub-chron B2-; and 3) C- is a negative chron, which includes three short positive sub-chrons C2+, C4+ and C6+. Because the micropaleontological data cannot unequivocally date the sediments in unit 4 (see Bukry, 1985; Barron, 1985), no one-to-one correlation can be made with the previously published magnetostratigraphies. The diatom data assign a mid to late Campanian age to unit 4 (Barron, 1985). Most magnetostratigraphies (marine and terrestrial) from the mid-upper Campanian epoch include a long and uninterrupted normal zone, otherwise known as the Long Normal episode of the Cretaceous, which also corresponds to marine magnetic anomaly 33 (Harland et al., 1982). The predominantly reversed paleomagnetic signature of unit 4 disagrees with the Campanian age. Silicoflagellate data (Bukry, 1985) and palynological data (Mudie, 1985) indicate a younger age of at least uppermost Campanian to Maastrichtian. There are three major reversed chrons in the Maastrichtian: marine magnetic anomalies 32r, 31r and 29r (Harland et al., 1982). Because the rate of deposition is unknown, the paleomagnetic data cannot be used to precisely correlate the record of unit 4 with the standard Maastrichtian magnetostratigraphy. However, the following scenarios and correlations are conceivable.

1) If the sedimentation rate is relatively high (3mm/1000 years), continuous sampling in unit 4 would record a very detailed magnetic signature of one of these Maastrichtian reversed chrons. The shortcoming of this scenario is that all three reversed chrons have been studied in considerable detail in the Upper Cretaceous-Paleocene Gubbio section (Alvarez et al., 1977) which showed no indication of positive sub-chrons. Similarly, no large scale perturbations can be seen in the Late Cretaceous marine magnetic anomaly profiles (see Lowrie and Alvarez, 1977).

2) If the sedimentation rate is very slow (<1 mm/1000 years), the record may include two or more of the Maastrichtian reverse chrons. If indeed the reverse polarity chron B+ correlates with marine magnetic anomalies 30 and 31, the Maastrichtian-Paleocene boundary can be placed at around 200cm depth in the core. However, if B+ is correlated with anomaly 29, the Cretaceous-Paleocene boundary may be as low as 270cm depth in the core, placing most sediments in unit 4 within the Paleocene. This will disagree with both sets of microfossil data but can be accommodated by the palynological data.

The paleomagnetic data provide no clear cut resolution of this discrepancy, and independent absolute dating is needed to determine the chronostratigraphy. The paleomagnetic data also fall short in resolving the origin of lamination in unit 4. If indeed the lamination represents annual varves, the published paleomagnetic stratigraphies from the Upper Cretaceous would not have the resolution needed for correlation with CESAR core 6.

Units 3 and 2 are both bounded by sharp sedimentary breaks possibly representing major unconformities. Very lit-

tle information can be gained from their magnetic stratigraphies. Unit 1 is characterized by a normal polarity chron which includes four shorter reversed sub-chrons. Because no definitive biostratigraphic data are available from this unit, the magnetic record cannot be unambiguously correlated with the Tertiary magnetostratigraphies. The core top however, includes a reversed interval which suggests that the uppermost sample is older than 0.72 Ma (older than Brunhes/Matuyama boundary). This interpretation agrees with conclusions obtained from lithological and palynological studies of CESAR core 83-6 (see Mudie and Blasco, 1985; and Mudie, 1985, respectively).

## REFERENCES

- Alvarez, W., Arthur, M.A., Fisher, A.G., Lowrie, W., Napoleone, G., Silva, I.P., and Roggenthen, W.M.  
1977: Upper Cretaceous-Paleocene magnetic stratigraphy at Gubbio, Italy, Part V; type section for the Late Cretaceous-Paleocene geomagnetic reversal time scale; Geological Society of America, Bulletin, v. 88, p. 383-389.
- Barron, J.A.  
1985: Diatom biostratigraphy of the CESAR 6 core; in Initial Geological Report on CESAR — the Canadian expedition to Study the Alpha Ridge, Arctic Ocean, ed. H.R. Jackson, P.J. Mudie and S.M. Blasco; Geological Survey of Canada, Paper 34-22, report 10.
- Bukry, D.  
1985: Correlation of Late Cretaceous silicoflagellates from Alpha Ridge; in Initial Geological Report on CESAR — the Canadian Expedition to Study the Alpha Ridge, Arctic Ocean, ed. H.R. Jackson, P.J. Mudie and S.M. Blasco; Geological Survey of Canada, Paper 84-22, report 9.
- Clark, D.L.  
1970: Magnetic reversals and sedimentation rates in the Arctic Ocean; Geological Society of America, Bulletin, v. 81, p. 3129-3134.  
1982: Origin, nature and world climate effect of Arctic Ocean ice-cover; Nature, v. 300, p. 321-325.
- Clark, D.L., Whitman, R.R., Morgan, K.A., and Mackey, S.D.  
1980: Stratigraphy and glacial-marine sediments of the Amerasian Central Arctic Ocean; Geological Society of America, Special Paper 181, 57 p.
- Gilbert, M.W. and Clark, D.L.  
1983: Central Arctic Ocean paleoceanographic interpretations based on Late Cenozoic calcareous dinoflagellates; Marine Micropaleontology, v. 7, p. 385-401.
- Harland, W.B., Cox, A.V., Llewellyn, P.G., Pickton, C.A.G., Smith, A.G., and Walters, R.  
1982: A Geologic Time Scale; Cambridge University Press, Cambridge, U.K., 131 p.
- Herman, Y.  
1974: Arctic Ocean sediments, microfauna, and the climatic record in Late Cenozoic time; in Marine Geology and Oceanography of the Arctic Seas, ed. Y. Herman; Springer-Verlag, New York, p. 283-348.  
1983: Baffin Bay; present day analog of the central Arctic during the Late Pliocene and mid-Pleistocene time; Geology, v. 11, p. 356-359.



- Herman, Y. and Hopkins, D.M.  
1980: Arctic oceanic climate in Late Cenozoic time; *Science*, v. 209, p. 557-562.
- Kent, D.V.  
1973: Post-depositional remanent magnetization in deep sea sediments; *Nature*, v. 246, p. 32-34.
- Lowrie, W. and Alvarez, W.  
1977: Upper Cretaceous-Paleocene magnetic stratigraphy at Gubbio, Italy, Part III; Upper Cretaceous magnetic stratigraphy; *Geological Society of America, Bulletin*, v. 88, p. 374-377.
- Mankinen, E.A. and Dalrymple, G.B.  
1979: Revised geomagnetic polarity time scale for the interval 0-5 My BP; *Journal of Geophysical Research*, v. 84(B2), p. 615-626.
- Minicucci, D.A. and Clark, D.L.  
1983: A Late Cenozoic stratigraphy for glacial-marine sediments of the eastern Alpha Cordillera, Central Arctic Ocean; *Glacial-marine Sedimentation*, ed. B.F. Molnia; Plenum Publishing Corporation, p. 331-365.
- Mudie, P.J.  
1985: Palynology of the CESAR cores, Alpha Ridge; *in* Initial Geological Report on CESAR — the Canadian Expedition to Study the Alpha Ridge, Arctic ocean, ed. H.R. Jackson, P.J. Mudie and S.M. Blasco; *Geological Survey of Canada, Paper 84-22*, report 11.
- Mudie P.J. and Blasco, S.M.  
1985: Lithostratigraphy of the CESAR cores; *in* Initial Geological Report on CESAR — the Canadian Expedition to Study the Alpha Ridge, Arctic Ocean, ed. H.R. Jackson, P.J. Mudie and S.M. Blasco; *Geological Survey of Canada, paper 84-22*, report 6.
- Steuerwald, B.A., Clark, D.L., and Andrew, J.A.A.  
1968: Magnetic stratigraphy and faunal patterns in Arctic ocean sediment; *Earth and Planetary Science Letters*, v. 5, p. 79-85.
- Watkins, N.D.  
1968: Short period geomagnetic polarity event in deep sea sedimentary cores; *Earth and Planetary science Letters*, v. 4, p. 341-349.

## PLANKTONIC FORAMINIFERAL AND OXYGEN ISOTOPIC STRATIGRAPHY OF CESAR CORES 102 AND 103: PRELIMINARY RESULTS

A.E. Aksu<sup>1</sup>

Dalhousie University, Centre for Marine Geology

Aksu, A.E., *Planktonic foraminiferal and oxygen isotopic stratigraphy of CESAR cores 102 and 103: preliminary results*: in *Initial Geological Report on CESAR — the Canadian Expedition to Study the Alpha Ridge, Arctic Ocean*, ed. H.R. Jackson, P.J. Mudie and S.M. Blasco; Geological Survey of Canada, Paper 84-22, p. 115-124, 1985.

### Abstract

Two gravity cores from the eastern Alpha Ridge, Arctic Ocean, include a continuous sedimentary record of the last 1 Ma. In most sample intervals, planktonic foraminifera are the dominant component of the biogenic skeletal debris in the  $>63\mu\text{m}$  sediment fraction, with pteropods, benthic foraminifera, ostracods and pelecypods not exceeding 2%. *Neogloboquadrina pachyderma* (left and right coiled) and *Neogloboquadrina cryophila* are the major planktonic foraminifera; *Neogloboquadrina polusi*, *Globigerina quinqueloba*, *Globigerina egelida* and *Globigerina bulloides* are secondary in abundance. Oxygen isotopic composition of *Neogloboquadrina pachyderma* together with the foraminiferal data suggest the following paleoenvironmental conditions.

Large scale decreases in planktonic foraminiferal abundances reflect: i) dilution of the surface waters by increased runoff, during marine isotopic stage 3 and for part of lithofacies L; ii) increased calcium carbonate dissolution on the seafloor, as indicated by very low total foraminiferal counts near the base of core 83-103; and iii) intervals of thicker sea ice, which would decrease primary productivity. Sediment intervals with high abundances of foraminifera strongly suggest relatively high productivity in the water column, but there is no evidence in the faunal or isotopic record of the gravity cores to suggest pack-ice free conditions during the past 1 Ma.

### Résumé

Deux carottes prélevées par carotteuse à chute libre dans la partie est de la dorsale Alpha, dans l'océan Arctique, présentent un enregistrement continu de l'histoire sédimentaire de la région au cours du dernier million d'années. Dans la plupart des intervalles échantillonnés, les foraminifères planctoniques sont la composante dominante des débris squelettiques de nature organogène dans la fraction de  $>63\mu\text{m}$ , la quantité de ptéropodes, de foraminifères benthiques, d'ostracodes et de pélecypodes ne dépassant pas 2 %. *Neogloboquadrina pachyderma* (enroulement senestre et dextre) et *Neogloboquadrina cryophila* sont les foraminifères planctoniques les plus nombreux; parmi les espèces moins abondantes, on compte *Neogloboquadrina polusi*, *Globigerina quinqueloba*, *Globigerina egelida* et *Globigerina bulloides*. La composition des isotopes d'oxygène dans *Neogloboquadrina pachyderma* ainsi que les données sur les foraminifères permettent de tirer les conclusions suivantes sur les conditions paléoenvironnementales.

Les réductions marquées dans l'abondance des foraminifères planctoniques sont dues à: i) la dilution des eaux de surface par le ruissellement accru au cours de l'étage 3 des isotopes marins et pour une partie du lithofaciès L; ii) la dissolution accrue du carbonate de calcium sur le fond océanique, comme l'indique le très petit nombre total de foraminifères près de la base de la carotte 83-103; et iii) des intervalles caractérisés par une plus forte épaisseur de glace marine qui réduirait la productivité primaire. La présence de sections de sédiments renfermant un très grand nombre de foraminifères semble fortement indiquer que la productivité était relativement élevée dans la colonne d'eau, mais il n'existe aucune indication dans les rapports d'observations fauniques ou isotopiques des carottes prélevées par chute libre qui laisse supposer que le milieu était libre de banquise au cours du dernier million d'années.

<sup>1</sup>Now at Department of Earth Sciences, Memorial University of Newfoundland, St. Johns, Newfoundland A1B 3X5

## INTRODUCTION

The climatic and oceanographic history of the Arctic Ocean, the timing of initial sea-ice formation and its role in global climatic cycles have been the subject of controversial debates for the last two decades (Clark et al., 1980; Herman, 1974, 1983). In these studies the chronology of the Arctic ocean sediments was based on scanty paleomagnetic data, and the age of oldest Cenozoic sediments is still the subject of dispute (see Aksu, 1985). Except for Herman (1974) and Hunkins et al. (1971), few detailed micropaleontological data exist from the deep-sea region other than gross foraminiferal abundance estimates (e.g. Clark, 1971). From these data, however, it is evident that planktonic foraminifera show large scale variations in abundance during the last 730,000 years and foraminifera are generally absent in older sediments. The environmental significance of the foraminifera barren zones is poorly understood. The absence of foraminifera has been variously ascribed to the following factors: thicker sea ice (Clark, 1971; Clark et al., 1980); carbonate dissolution (Hunkins et al., 1971) and both dissolution and salinity reductions in surface waters (Herman, 1974). Whichever of these explanations is valid for foraminifera, none can explain the concurrent variations in dinoflagellates (see Mudie, 1985).

The purpose of this paper is: i) to provide a detailed account of the taxonomic, oxygen and carbon isotopic variations in planktonic foraminifera; and ii) to illustrate the effects of some of the environmental parameters that contribute to the total foraminiferal abundance.

## ACKNOWLEDGMENTS

The laboratory work was supported by DSS contract # OSC83-00399. I thank Oliver Maass, Department of Geology, University of Toronto, for his assistance with sampling and initial laboratory procedures. Thanks are extended to Bahn Deonarine, Atlantic Geoscience Centre, for his help in SEM photography. The manuscript was critically read by Peta J. Mudie, whose helpful comments are gratefully acknowledged.

## MATERIALS AND TECHNIQUES

CESAR cores 83-102 (=CESAR 102) and 83-103 (=CESAR 103) were selected for detailed biostratigraphic studies (Fig. 8.1). The core collection, description and storage are described in Mudie and Blasco (1985). In order to determine the abundance and vertical distribution of foraminifera in the cores, about 10cc samples were taken each centimetre down-core. Samples were dried in an oven at approximately 40°C for 24 hours, and the initial dry weights were recorded. Subsequently, the sediment was dispersed in distilled water with about 20cc of 1% Calgon solution. All samples were wet sieved through a  $>63\mu\text{m}$  screen, the coarse fractions were dried in an oven and their dry weights recorded. The finer than  $63\mu\text{m}$  fractions were stored for future work. The percentage of the  $63\mu\text{m}$  and  $375\mu\text{m}$  fraction was calculated for each sample. Foraminifera were studied in the  $63\mu\text{m}$  fraction according to standard micropaleontological procedures. In about 40% of the samples, for-

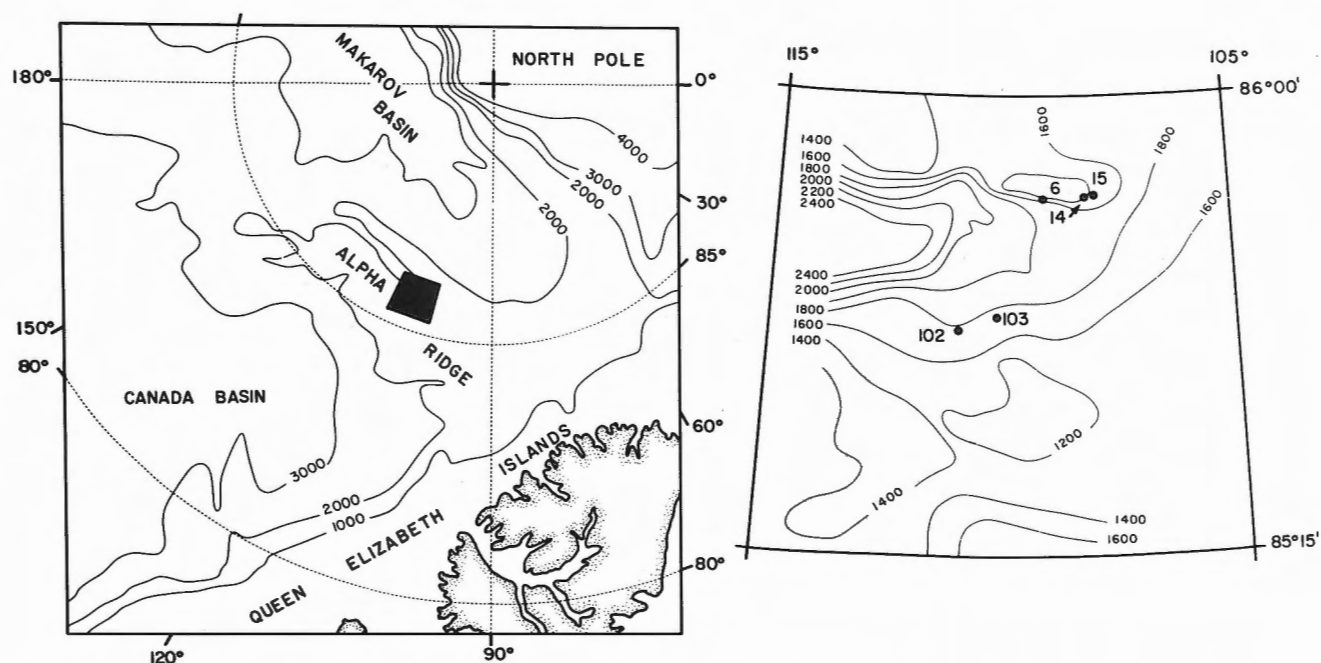


Figure 8.1 Map of the Arctic Ocean showing the major physiographical features. Inset shows the bathymetry of the Alpha Ridge core locations.

aminifera were concentrated by flotation in carbon tetrachloride (specific gravity = 1.59). Large samples required splitting several times to obtain a workable population. About 300 to 500 specimens were counted in each sample, and the results were converted to "foraminifera per gram dry weight sediment". Following the faunal study, about 200 to 500 specimens of planktonic foraminifera *Neogloboquadrina pachyderma* were picked and stored for oxygen and carbon isotopic analysis.

## TAXONOMIC NOTES

Planktonic foraminifera are the dominant component of the biogenic skeletal debris in the samples, accompanied by pteropods and calcareous benthic foraminifera. Sporadic occurrence of ostracods, pelecypods, arenaceous benthic foraminifera, sponge spicules and other biogenic remains never exceeded 2% of the fauna. The abundance of planktonic and benthic foraminifera are shown in Figures 8.2 and 8.3. Plates 8.1 and 8.2 illustrate the most common planktonic foraminifera in the cores. *Neogloboquadrina pachyderma*, *Neogloboquadrina cryophila*, *Neogloboquadrina polusi*, *Globigerina quinqueloba*, *Globigerina egelida* and *Globigerina bulloides* constitute more than 98% of the planktonic foraminiferal population; the rest were too small or broken for clear identification, and were thus classified as *Globigerina* sp. The author believes the *Neogloboquadrina cryophila* (Plate 8.1, Fig. 5-8) is conspecific with *Neogloboquadrina pachyderma* (Plate 8.1, fig. 1-4) and it shows large morphologic variations. However, as a precaution against possible loss of information and for comparison purpose with Herman (1974), these species were counted separately. Admittedly, a degree of uncertainty exists in the identification of *Neogloboquadrina cryophila* because of its transitional forms. *Neogloboquadrina polusi* (Plate 8.1, fig. 9-12) is distinguished from *Neogloboquadrina pachyderma* by its more numerous subspherical chambers, by the position of the aperture (umbilical-extraumbilical) and by the characteristic umbilically extended chambers in the larger forms; and by the high, arch-shaped aperture showing a secondary opening on the dorsal side in similar forms. Saito et al. (1981) consider this species as an ecologic variant of *Neogloboquadrina pachyderma*. *Globigerina egelida* (previously described as *Globigerina exumbilicata* by Herman, 1974) is distinguished from *Globigerina quinqueloba* by its spherical last chamber, well developed deep umbilicus, higher spire and larger test size (Plate 8.2, fig. 5-8). The final chamber of *Globigerina quinqueloba* is also diagnostic as it typically partially or completely covers the umbilicus (Plate 8.2, fig. 1-4). *Globigerina bulloides* (Plate 8.2, fig. 9-11) is only seen in few samples, with abundances never exceeding 3%. Both sinistrally and dextrally coiled specimens were observed in *Globigerina egelida*, *Globigerina quinqueloba*, *Neogloboquadrina pachyderma*, *Neogloboquadrina cryophila* and *Neogloboquadrina polusi*, but only the relative proportions of the dextral forms in *Neogloboquadrina pachyderma* are recorded.

## OXYGEN AND CARBON ISOTOPES

The oxygen and carbon isotopic variations of *Neogloboquadrina pachyderma* (sinistral) were examined in cores 83-102 and 83-103 (Fig. 8.2, 8.3). All samples analyzed contained more than 0.5 mg carbonate (200 specimens). The foraminiferal shells were ultrasonically cleaned in distilled water; subsequently, each sample was washed twice with distilled water and oven dried at 90°C. Samples were then roasted for 60 minutes at 400°C under vacuum. Tests were acidified with 100% phosphoric acid at 50°C and the water in the evolved CO<sub>2</sub> was trapped in a -85°C bath. The purified CO<sub>2</sub> was analyzed in a V.G. Micromass 602D mass spectrometer. Duplicate analyses of the standards as well as samples show that the reproducibility is subject to a variation of  $\pm 0.04\text{‰}$ . The isotopic ratios are expressed as per mil (‰) difference between the <sup>18</sup>O/<sup>16</sup>O and <sup>13</sup>C/<sup>12</sup>C in the samples and that in the laboratory standard "Carrara Marble". The latter deviates from the Chicago PDB-1 standard by -1.19‰ in  $\delta^{18}\text{O}$  and +2.79‰ in  $\delta^{13}\text{C}$ , where  $\delta = 1000 \text{ (R of sample - R of standard) / (R of standard)}$  and R stands for the <sup>18</sup>O/<sup>16</sup>O or <sup>13</sup>C/<sup>12</sup>C ratios.

Figure 8.4 illustrates the oxygen and carbon isotopic composition in CESAR 102 and 103, and the oxygen isotopic variations in the equatorial Pacific core V28-239 (data from Shackleton and Opdyke, 1976). Core V28-239 is re-plotted, taking the Brunhes-Matuyama boundary as a reference datum to allow stage by stage comparison with the CESAR cores. The upper 40cm of the CESAR 103 record is characterized by four light and three heavy isotopic zones. From about 40 to 63cm and from 94 to 107cm depth, there were not enough foraminifera in the samples to carry out isotopic analyses. Between 63 and 94cm depth, the record includes two isotopically light and two heavy intervals.

The average rate of deposition in the CESAR cores is calculated to be approximately 1 mm per 1000 years based on the Brunhes-Matuyama boundary (Aksu, 1985). If this rate is representative for the entire Brunhes normal polarity chron, the ages of the heavy isotopic stages identified between 1.5 and 4cm and 12 to 15cm are 15,000-40,000 and 120,000-150,000 years BP respectively. These age estimates are comparable with the glacial isotopic stages 2 and 6 (13,000-32,000 and 128,000-195,000 years BP; Shackleton and Opdyke, 1976). Linear extrapolation estimates the heavy isotopic stage between 25 and 31cm depth to be 250,000 to 310,000 years BP. This zone can be tentatively correlated with isotopic stage 8 which occurs between 251,000 and 297,000 years BP in V28-239. The Brunhes-Matuyama boundary is found near a glacial to interglacial transition in CESAR 103. This boundary occurs within the lower part of glacial isotopic stage 20 in core V28-239. Therefore, the heavy isotopic interval between 68 and 74cm depth in CESAR 103 may correlate with stage 20.

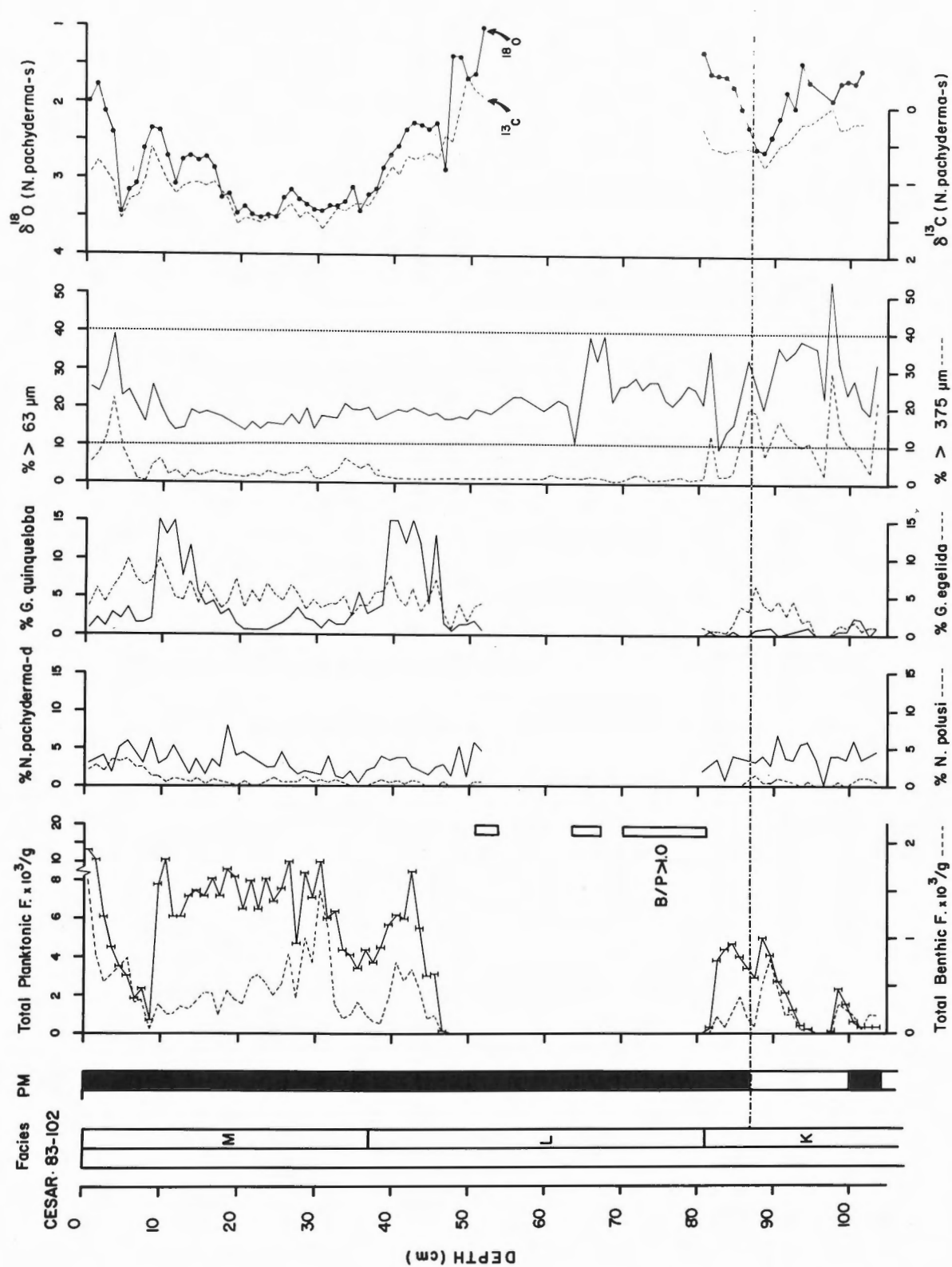


Figure 8.2 Foraminiferal abundance versus depth in CESAR core 83-102. K to M are lithostratigraphic units of Clark et al. (1980); summary polarity scale (PM) after Aksu (1985); F = foraminifera per gram sediment; % = percentage of total planktonic foraminiferal assemblages or percentage of larger than  $63\mu\text{m}$  and  $375\mu\text{m}$  fractions (column 6). Oxygen and carbon isotopic composition of *Neogloboquadrina pachyderma* (sinistral) expressed as ‰ deviation from Chicago PDB-1 standard. B/P = ratio of benthic to planktonic forams; rectangles indicate intervals of low total foraminifera in which B/P is greater than 1.0.



There are several striking features of the CESAR record which warrant further discussion. Most importantly, there are large differences in the amplitude of the  $^{18}\text{O}$  values in the interglacial stages. For example, stages 1, 3, 5, 7 and 9 exhibit minimum  $^{18}\text{O}$  values of 1.8, 1.4, 1.9, 2.4 and 1.8‰, with interstadial stage 3 showing maximum depletion in  $^{18}\text{O}$ . Large differences in  $^{18}\text{O}$  values are also observed between stages 2, 6 and 8. The record does not show a clear isotopic stage 4. Despite these peculiarities, there are indications of a cyclicity in the  $^{18}\text{O}$  record. This first order cyclic character of the isotopic record with about 100,000 periodicity suggests that the Arctic Ocean record carries the imprint of the global ice-volume fluctuations driven by orbital variations (Berger, 1978).

The oxygen isotopic fluctuations in the cores are controlled primarily by glacial to interglacial changes in (i) continental ice-volume and (ii) isotopic composition of Arctic Ocean surface water mass due to changing patterns of evaporation, precipitation and, most importantly, changes in discharge patterns of large rivers from Siberia and northern Canada. Other factors such as glacial-interglacial temperature changes and depth habitat of foraminifera are believed to have little effect on the  $^{18}\text{O}$  variations.

Bioturbational mixing of sediment is known to be an effective process which reduces the time resolution and amplitude of the oxygen isotopic record (Duplessy, 1978). All CESAR cores examined showed secondary sedimentary structures typical of bioturbation. Because the rate of deposition is very slow, even a small population of benthic macro-organisms had ample time for bioturbation. The smooth nature of the oxygen isotopic record in both cores may be partly the result of bioturbational mixing.

Fluctuations in the  $^{13}\text{C}$  record of *Neogloboquadrina pachyderma* exhibit cycles very similar to those of  $^{18}\text{O}$ , with a maximum change from heavy to light values of about 1.5‰. With few exceptions, there is a striking linear relationship (correlation coefficient  $r=0.92$ ) between the  $^{18}\text{O}$  and  $^{13}\text{C}$ . In general, the surface waters in the oceans are enriched in  $^{13}\text{C}$  which reflects the isotopic exchange with the atmosphere  $\text{CO}_2$  but also reflects preferential removal of  $^{12}\text{C}$  by organisms. The degree of this enrichment is proportional to the magnitude of biomass present in the surface waters. The carbon of *Neogloboquadrina pachyderma* shells is depleted in  $^{13}\text{C}$  relative to the calcite precipitated in isotopic equilibrium with the ambient total  $\text{CO}_2$  (Williams et al., 1977), suggesting that this species incorporates  $^{13}\text{C}$  depleted (about -25‰) metabolic  $\text{CO}_2$  in their calcite tests. Therefore, the light  $^{13}\text{C}$  zones corresponding with light  $^{18}\text{O}$  values may represent periods of higher primary and secondary production.

## FORAMINIFERAL ABUNDANCE AND COMPOSITION

In CESAR 103, the foraminiferal data exhibit large variations in abundance from 10 to 10,000 specimens per gram sediment (Fig. 8.2). In general, this abundance curve may represent the superimposed effects of: i) different sedimentation rates during different periods; ii) changes in the preservation state of calcareous biogenic debris on the sea-

floor; and iii) changes in climate and oceanic circulation patterns accompanied by changes in biological productivity. In order to make accurate paleoenvironmental interpretations, it is essential to delineate the effects of these variables on the faunal data. Careful examinations of X-radiographs and the split cores indicated that sediments in both cores are predominantly hemipelagic, augmented by a nearly constant proportion of ice-rafted debris as suggested by the  $>63\mu\text{m}$  and  $>375\mu\text{m}$  fractions (Fig. 8.2, 8.3). The primary and secondary internal sedimentary structures do not indicate large fluctuations in the rate of deposition. Therefore, smaller scale variations of the sedimentation rate probably have a minimal effect on the observed foraminiferal data.

The ratio of benthic to planktonic foraminifera (B/P) is an effective parameter that semiquantifies the preservation state of foraminifera on the seafloor (Thunell, 1976). Briefly, the technique assumes that the benthic foraminifera are not susceptible to dissolution, that the initial B/P is constant through time and that this ratio is only affected by dissolution of planktonics. The B/P ratio is 1 from 94 to 110cm depth in CESAR 103, suggesting substantial loss of foraminifera to dissolution. The synchronous disappearance of both benthic and planktonic foraminifera between 37.5 and 62.5cm depth in the core is conspicuous and can be partially explained by dissolution, as suggested by B/P ratios greater than 1. More data are needed to determine the precise nature of this zone.

It is concluded that the faunal data mainly reflect the productivity history of the Alpha Ridge cordillera and that except for the two intervals discussed above, the record is not affected by dissolution and differential sedimentation rate. The cores can be divided into four foraminiferal zones as described below.

*Zone I (0-37.5cm)* is generally characterized by high abundances of benthic and planktonic foraminifera. This zone closely correlates with lithofacies M of Clark et al. (1980; also see Mudie and Blasco, 1985), and includes isotopic stages 1 through 9. Five subzones are distinguished: Subzone Ia (0-3.5cm) includes very high total planktonic and benthic foraminifera. The planktonic foraminifera are mostly composed of *Neogloboquadrina pachyderma* sinistral, with up to 10% of *Neogloboquadrina pachyderma* dextral, *Neogloboquadrina polusi*, *Globigerina quinqueloba* and *Globigerina egelida*. This subzone corresponds to isotopic stages 1 and 2. Subzone Ib (3.5-9cm) is characterized by an order of magnitude decrease in both total benthic and planktonic foraminifera, and lower percentages of *Globigerina quinqueloba* and *Globigerina egelida*. It is correlated with isotopic stage 3. Subzones Ic to Ie are defined on the basis of total planktonic foraminiferal abundances; in these intervals, the benthic foraminifera show very little variation, fluctuating between 100 and 400 specimens per gram sediment. The uppermost part of subzone Ic (9-24cm) contains between 10 and 20% of *Globigerina quinqueloba* and *Globigerina egelida*, with an average of 2% *Globigerina bulloides*, and it correlates with isotopic stage 5. The fauna in the lower part of the subzone is similar to that of subzone Ia, and includes isotopic stages 6 and 7. Subzones Id (24-31cm) and Ie (31-37.5cm) are similar to subzones Ib and Ic and correlate with isotopic stages 8 and 9 respectively.

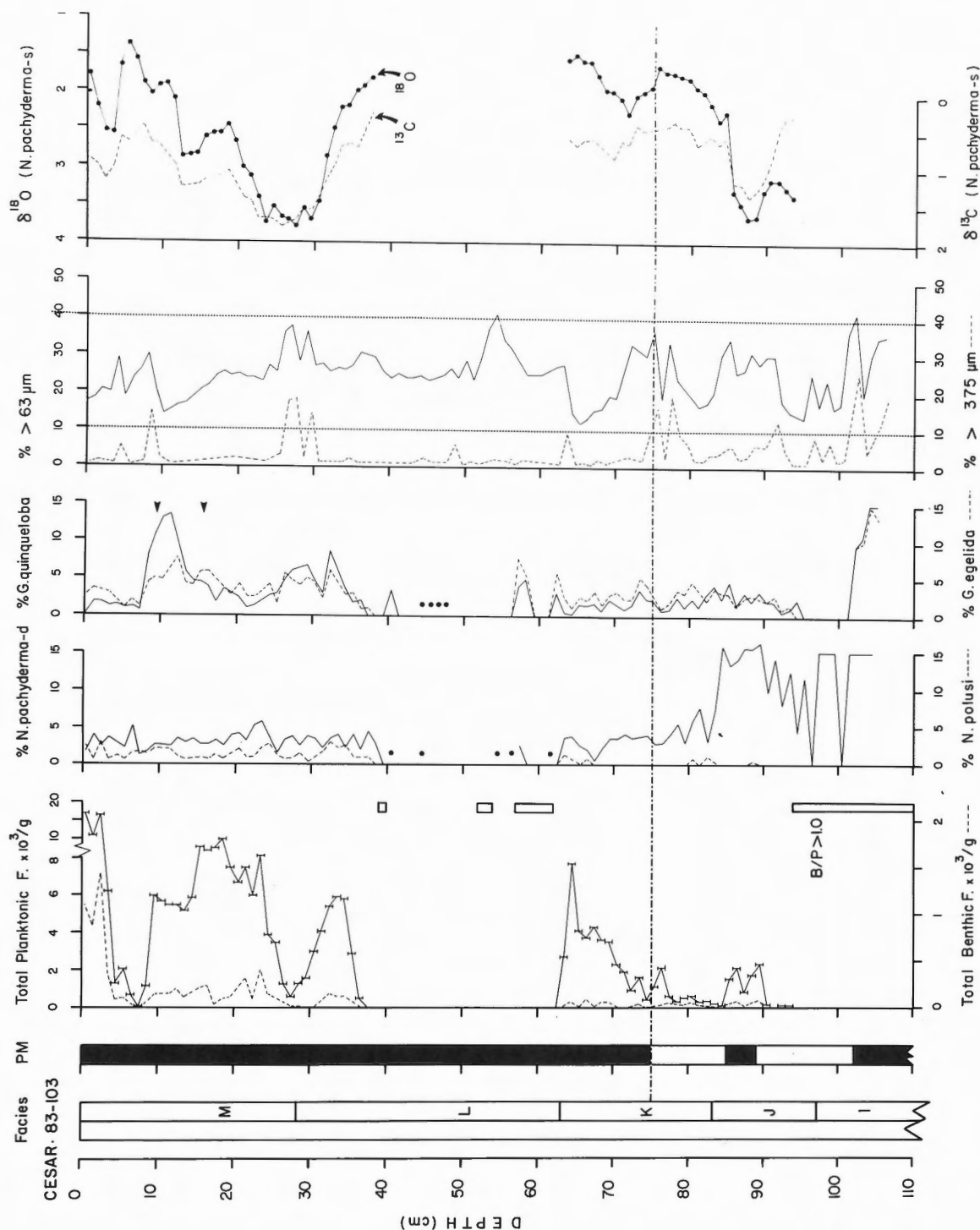


Figure 8.3 Foraminiferal abundance versus depth in CESAR core 83-103. I to M are lithostratigraphic units of Clark et al. (1980); Summary polarity scale (PM) after Aksu (1985); F = foraminifera per gram sediment; % = percentage of total planktonic foraminiferal assemblages (column 4 and 5) or percentage of larger than 63µm and 375µm fractions (column 6). Dots (column 6 and 5) indicate presence of *Neogloboquadrina pachyderma* (dextral) and *Globigerina bulloides*. Oxygen and carbon isotopic composition of *Neogloboquadrina pachyderma* (sinistral) expressed as ‰ deviation from Chicago PDB-1 standard. B/P = ratio of benthic to planktonic forams; rectangles indicate intervals of low total foraminifera in which B/P is greater than 1.0.

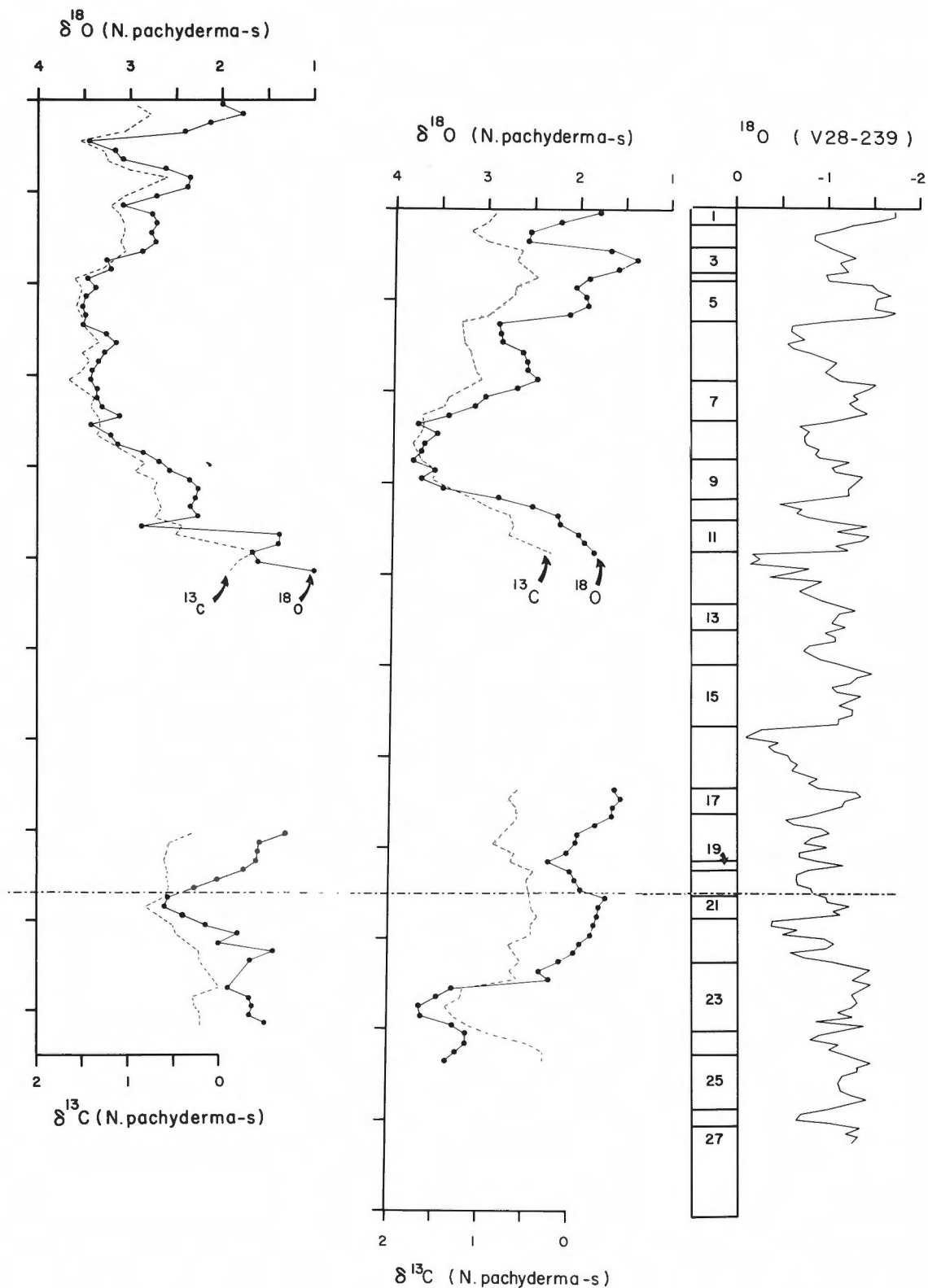
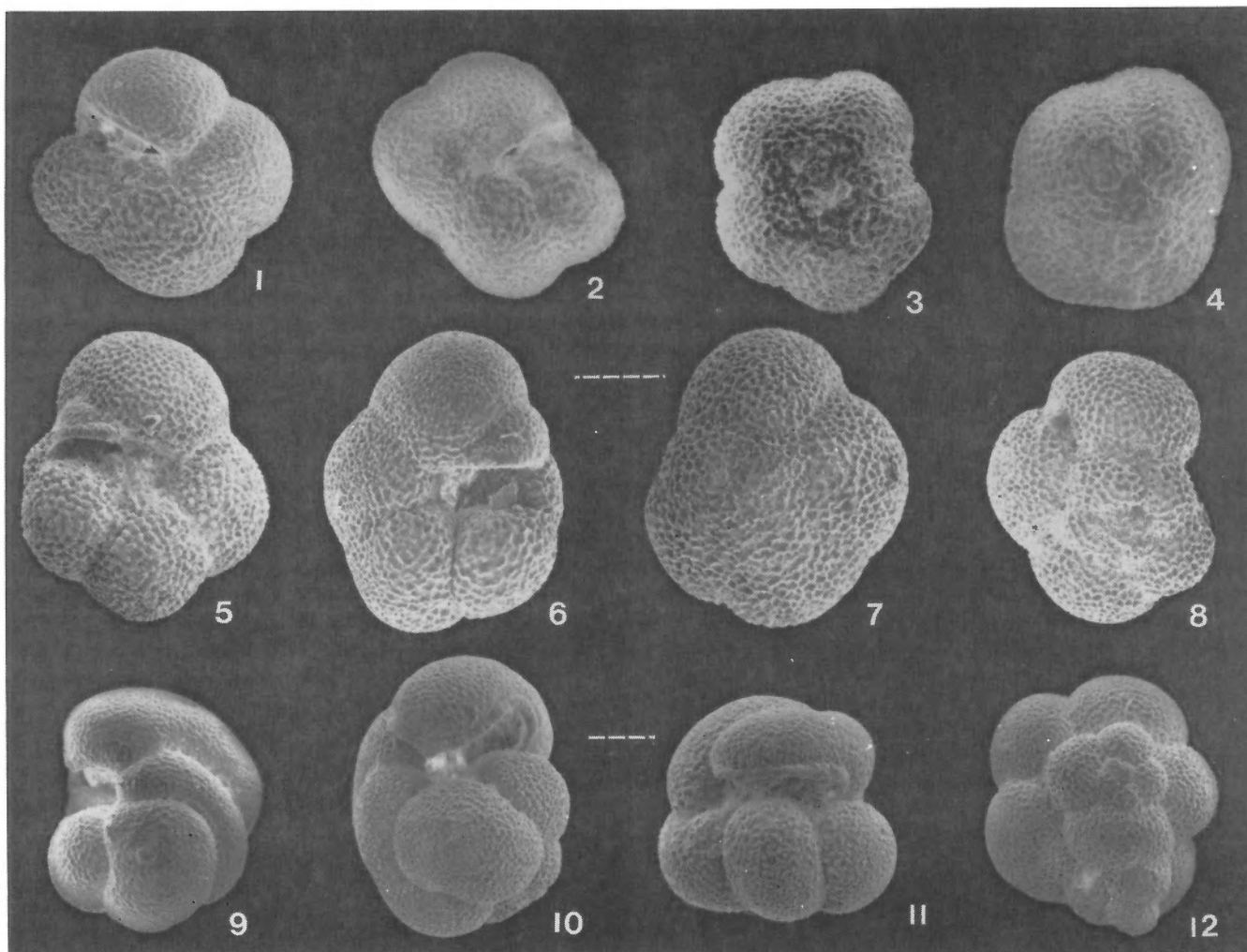
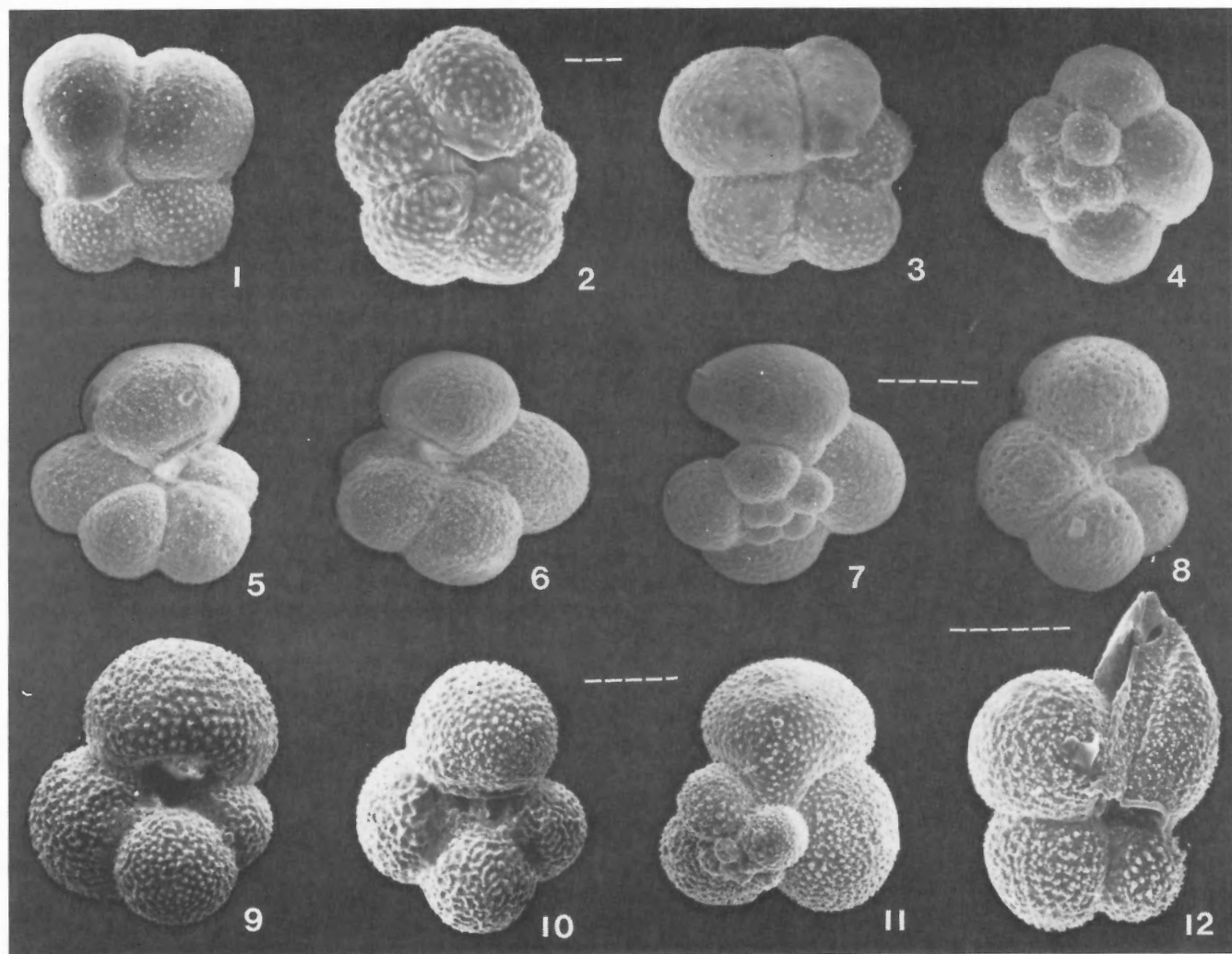


Figure 8.4 Isotopic records of CESAR 83-102 and 83-103 compared with the isotopic record of Pacific core V28-239 (Shackleton and Opdyke, 1976). Oxygen and carbon isotope values are expressed as ‰ deviation from Chicago PDB-1 standard.



**Plate 8.1**

- Figures 1-4 *Neogloboquadrina pachyderma* (Ehrenberg). Dextral specimen, umbilical view (1), dorsal view (4); sinistral specimen, umbilical view (2), dorsal view (3). Bar scale = 100 $\mu$ m.
- Figures 5-8 *Neogloboquadrina cryophila* (Herman). Dextral specimen, umbilical view (5), dorsal view (8); sinistral specimen, umbilical view (6), dorsal view (7). Bar scale = 100 $\mu$ m.
- Figures 9-12 *Neogloboquadrina polusi* (Androsova). Side view (9), umbilical view (10 and 11), dorsal view (12). Bar scale = 100 $\mu$ m.



# **Plate 8.2**

- Figures 1-4 *Globigerina quinqueloba* (Natland). Dextral specimen, umbilical view (1); sinistral specimen, umbilical view (2 and 3), dorsal view (4). Bar scale = 30 $\mu$ m.
- Figures 5-8 *Globigerina egelida* (Cifelli and Smith). Sinistral specimen, umbilical view (5 and 8); dextral specimen, umbilical view (6), dorsal view (7). Bar scale = 30 $\mu$ m.
- Figures 9-11 *Globigerina bulloides* (d'Orbigny). Umbilical view (9 and 10), dorsal view (11). Bar scale = 100 $\mu$ m.
- Figure 12 *Globigerina* species. Bar scale = 30 $\mu$ m.



Zone II (37.5-63cm) is characterized by very low total benthic and planktonic foraminifera, and correlates with the lithofacies L.

Zone III (63-94cm) is similar to Zone I except it contains lower total benthic and planktonic foraminifera. It includes the lithofacies K and upper J. Below the Brunhes-Matuyama boundary, a gradual increase in *Neogloboquadrina pachyderma* dextral is observed, reaching between 15-25% of the total planktonic foraminiferal fauna. This zone is correlated with isotopic stages 19 through 22. Zone IV (94-107cm) is similar to zone II in containing very low abundances of foraminifera.

Preliminary inspection of the faunal and isotopic data suggests the following salient conclusions:

1) The large scale decreases in the planktonic foraminiferal abundances may be the result of: a) intense dilution of the surface waters by increased runoff as suggested by the  $^{18}\text{O}$  data (e.g. stage 3). If the surface salinity decreased below the tolerance level of planktonic foraminifera, this would be reflected as low total foraminiferal counts in sediments regardless of the primary productivity in the water column and regardless of climate (e.g. subzone Ib); b) increased calcium carbonate dissolution on the seafloor would also give lower total foraminiferal counts regardless of climate and production, as seen near the base of CESAR 103; and c) thicker sea ice may decrease the primary productivity and result in lower foraminiferal counts. Subzone Id which is correlated with the heaviest isotopic stage 8 (?coldest) interval, may be an example of this kind.

2) The absence or very low numbers of foraminifera in the Arctic Ocean sediments does not necessarily indicate lower primary/secondary productivity but a high abundance of foraminifera in the sediments strongly suggests higher productivity in the water column.

3) There is no evidence in the faunal record of the core to suggest pack-ice free conditions during the last 1 Ma BP.

## REFERENCES

- Aksu, A.E.  
1985: Paleomagnetic stratigraphy of the CESAR cores; in Initial Geological Report on CESAR — the Canadian Expedition to Study the Alpha Ridge, Arctic Ocean, ed. H.R.J. Jackson, P.J. Mudie and S.M. Blasco; Geological Survey of Canada, Paper 84-22, report 7.
- Berger, A.L.  
1978: Long-term variations of caloric insolation resulting from the Earth's orbital elements; *Quaternary Research*, v.9, p.139-167.
- Clark, D.L.  
1971: Arctic Ocean Ice Cover and its Late Cenozoic History; *Geological Society of America, Bulletin*, v.82, p.3313-3324.
- Clark, D.L., Whitman, R.R., Morgan, K.A. and MacKey, S.D.  
1980: Stratigraphy and glacial-marine sediments of the Amerasian Basin, Central Arctic Ocean; *Geological Society of America, Special Paper* 181, 57p.
- Duplessy, J.C.  
1978: Isotope studies; in *Climatic Change*, J. Gribbin, ed.; Cambridge University Press, p.46-67.
- Herman, Y.  
1974: Arctic Ocean sediments, microfauna, and the climatic record in Late Cenozoic time; in *Marine Geology and Oceanography of the Arctic Seas*, Y. Herman, ed.; Springer Verlag, New York, p.283-348.
- Herman, Y.  
1983: Baffin Bay; present-day analog of the central Arctic during Late Pliocene to mid-Pleistocene time; *Geology*, v.11, p.356-359.
- Hunkins, K., Be, A.W.H., Opdyke, N.D. and Mathieu, G.  
1971: The Late Cenozoic History of the Arctic Ocean; in *The Late Cenozoic Ages*, ed. K.K. Turekian; New Haven, Yale University Press, p.215-237.
- Mudie, P.J.  
1985: Palynology of the CESAR cores; in Initial Geological Report on CESAR — the Canadian Expedition to Study the Alpha Ridge, Arctic Ocean, ed. H.R. Jackson, P.J. Mudie and S.M. Blasco; Geological Survey of Canada, Paper 84-22, report 11.
- Mudie, P.J. and Blasco, S.M.  
1985: Lithostratigraphy of the CESAR cores, Alpha Ridge; in Initial Geological Report on CESAR — the Canadian Expedition to Study the Alpha Ridge, Arctic Ocean, ed. H.R. Jackson, P.J. Mudie and S.M. Blasco; Geological Survey of Canada, Paper 84-22, report 6.
- Saito, T., Thompson, P.R. and Breger, D.  
1981: Systematic Index of Recent and Pleistocene Planktonic Foraminifera; University of Tokyo Press, 190p.
- Shackleton, N.J. and Opdyke, N.D.  
1976: Oxygen-isotope and paleomagnetic stratigraphy of Pacific Core V28-239 Late Pliocene to Latest Pleistocene; in *Investigation of Late Quaternary Paleoclimatology and Paleoclimatology* R.M. Cline and J.D. Hays, eds.; Geological Society of America, Memoir 145, p.449-464.
- Thunell, R.C.  
1976: Calcium carbonate dissolution in Late Quaternary deep-sea sediments, western Gulf of Mexico; *Quaternary Research*, v.6, p.281-297.
- Williams, D.F., Michael, A. and Sommer, I.I.  
1977: Carbon isotopic composition of recent planktonic foraminifera of the Indian Ocean; *Earth and Planetary Science Letters*, v.36, p.391-403.

## CORRELATION OF LATE CRETACEOUS ARCTIC SILICOFLAGELLATES FROM ALPHA RIDGE

David Bukry<sup>1</sup>

United States Geological Survey

Bukry D., *Correlation of Late Cretaceous Arctic silicoflagellates from Alpha Ridge; in Initial Geological Report on CESAR — the Canadian Expedition to Study the Alpha Ridge, Arctic Ocean*, ed. H.R. Jackson, P.J. Mudie and S.M. Blasco; Geological Survey of Canada, Paper 84-22, p. 125-135, 1985.

### Abstract

Late Cretaceous silicoflagellates are abundant and well preserved in core CESAR 6 from the Arctic Ocean. A probable Middle or Late Maastrichtian age is suggested for the core because the most widespread, long-ranged, and abundant Cretaceous silicoflagellate (*Lynamula furcula*), which is known from the Santonian-Campanian to the Late Maastrichtian, disappeared in both cores CESAR 6 and FI-437 on the Alpha Ridge. Partial isolation of the Arctic basin in the Maastrichtian because of shoaling or tectonic uplift of previous seaway connections could have contributed to the disappearance of *Lynamula furcula*. Comparisons with other Cretaceous silicoflagellate localities show the unique character of the Alpha Ridge assemblages with abundant *Vallacerta siderea*, sparse to common *Lynamula burchardae* and *Lynamula deflandrei*, sparse *Lynamula porta*, but no *Corbisema*, *Cornua trifurcata*, or *Vallacerta tumidula* which characterize Campanian and Maastrichtian elsewhere. The provincial character of the assemblages on Alpha Ridge probably is the result of ecologic factors such as differences in high-latitude sunlight, nutrient circulation, and possibly salinity.

### Résumé

Les silicoflagellés du Crétacé récent sont abondants et bien conservés dans la carotte CESAR 6 prélevée dans le fond de l'océan Arctique. Les sédiments de cette carotte datent vraisemblablement du Maastrichtien moyen ou récent vu l'absence, dans les carottes CESAR 6 et FI-437 de la dorsale Alpha, de *Lynamula furcula*, silicoflagellé crétacé non seulement le plus abondant et le plus répandu géographiquement et stratigraphiquement, mais également reconnu du Santonien-Campanien au Maastrichtien récent. L'isolation partielle du bassin Arctique au cours de Maastrichtien, provoquée par la réduction de la profondeur ou le soulèvement tectonique de passages marins antérieurs, pourrait avoir contribué à la disparition de cette espèce. Une comparaison avec d'autres lieux d'où proviennent des silicoflagellés crétacés montre la nature unique des assemblages de la dorsale Alpha, source d'échantillons abondants de *Vallacerta siderea*, d'échantillons épars à communs de *Lynamula burchardae* et de *Lynamula deflandrei* et d'échantillons épars de *Lynamula porta* mais dépourvue d'échantillons de *Corbisema*, de *Cornua trifurcata* ou de *Vallacerta tumidula*, espèces caractéristiques du Campanien et du Maastrichtien ailleurs. La nature locale des assemblages de la dorsale Alpha est vraisemblablement le résultat de facteurs écologiques comme les variations de l'ensoleillement aux hautes latitudes, de la circulation des éléments nutritifs et possiblement du degré de salinité.

### INTRODUCTION

A distinctive laminated Cretaceous biosiliceous sediment from the Alpha Ridge in the Arctic Ocean was obtained as part of the CESAR study. Cretaceous silicoflagellates are abundant in the diatom-rich sediment which occurs in core CESAR 6 (latitude 85°50'0.41"N, longitude 109°01'05.2"W, depth 1365m). This location is very near a previously cored

Cretaceous silicoflagellate-rich section in USGS core FI-437 (latitude 85°58.87'N, longitude 129°58.76"W, depth 1584m). These similar biosiliceous-rich buff sediments contain similar arrays of Cretaceous species which are distinctive and are not recorded at any other Cretaceous localities. Correlation with other areas is dubious because the present limited data do not allow definite discrimination of ecologic effects from evolutionary succession. Provincialism in the

<sup>1</sup>Scripps Institution of Oceanography, La Jolla, California 92093

known silicoflagellate assemblages limits precise dating of the Alpha Ridge Cretaceous strata, but the disappearance of cosmopolitan *Lyamula furcula* in both Alpha Ridge cores is a key event.

## ACKNOWLEDGMENTS

I thank Peta J. Mudie, Geological Survey of Canada, and John A. Barron, U.S. Geological Survey, for helpful discussions during the study of core CESAR 6. Constructive reviews of the paper were provided by Paula J. Quintero and John A. Barron, U.S. Geological Survey. I thank Dorothy L. Blackstock for typing and proofing the manuscript.

## METHODS

Owing to the rich biosiliceous content of CESAR 6 samples from 134 to 320cm, smear slides of unprocessed sediment could be used to study the silicoflagellate assemblages. Species identification and enumeration were done by light microscopy at 250 to 500X magnification using mechanical stage traverses. Counts of the first 300 specimens per sample were used to calculate percentages. Specimen breakage is minor (<5%) and partial specimens were combined into composite whole specimens for counting purposes.

## BIOSTRATIGRAPHY

Late Cretaceous silicoflagellates are abundant and well preserved in samples from 134 to 320cm in CESAR 6. The majority of the silicoflagellate assemblages are predominated by *Vallacerta siderea*. *Lyamula* species are dominant in only two parts of the core, where *Lyamula deflandrei* and *Lyamula burchardae* are most abundant. Several species of *Lyamula* are restricted to the basal part of the core, suggesting a stratigraphic division; however, the major biostratigraphic units in CESAR 6 are based on obvious shifts in the abundance of *Vallacerta*.

Four biostratigraphic units are identified for the Cretaceous part of CESAR 6 by shifts in *Vallacerta* abundance. These units are labeled A1, A2, A3, and B (Table 9.1). Unit B (298 to 320cm) at the base of the core, has very low *Vallacerta* percentages, ranging from 6 to 46%. This is a distinct contrast with the next higher unit where *Vallacerta* percentages are consistently high, between 78 and 92%. *Lyamula* is predominant in unit B. A small variety of *Lyamula deflandrei* is abundant and essentially restricted to unit B. The greatest diversity of *Lyamula* (8 taxa) for CESAR 6 occurs in unit B. *Lyamula furcula*, the dominant species in many Late Cretaceous assemblages outside of Alpha Ridge, is sparse and occurs only in unit B and in the basal sample of unit A3.

Adjacent dark and light sedimentary laminae were examined separately for the sample at 298 to 300cm. The quantitative results (Table 9.1) show a practically identical assemblage of silicoflagellates according to species and abundance.

Unit A3 (250 to 292cm) is characterized by consistently high percentages of *Vallacerta*, between 78 and 92%. *Lyamula burchardae* and *Lyamula deflandrei* are sparse but consistently present through unit A3. The highest stratigraphic occurrence of *Lyamula arctica* and *Lyamula furcula* is in the basal sample (290 to 292cm).

The assemblages of unit A2 (157 to 232cm) are variegated, with generally high *Vallacerta* abundance (up to 58%) for *Lyamula burchardae*. Wide fluctuations in the abundance of *Lyamula burchardae* (3 to 58%), *Lyamula deflandrei* (7 to 25%), and *Vallacerta siderea* (29 to 85%) characterize unit A2. *Arctyochoa* sp. first occurs and is sparse at 170cm, persisting up into the base of unit A1. The predominant Cretaceous silicoflagellate, *Lyamula furcula* is missing from unit A2.

Two samples are assigned to unit A1 (134 to 152cm) which is characterized by the high abundance of *Vallacerta siderea* (88 to 95%). Unit A1 is also distinguished by the very low abundance of *Lyamula burchardae* relative to underlying unit A2. The assemblages of unit A1 are very similar to older unit A3.

## CORRELATION

*Lyamula furcula* is the most cosmopolitan silicoflagellate of the Late Cretaceous. It is present or predominant at all known localities ranging from south of New Zealand in DSDP 275 (latitude 50°S) to the Arctic Ocean in core FI-437 (latitude 86°N). The age and correlation of the new Arctic Ocean CESAR 6 silicoflagellates are based on the occurrence of sparse (1 to 4%) specimens of *Lyamula furcula* in the lower part of the core. Nearby FI-437 has sparse to common *Lyamula furcula* in the lower and middle part of that core. Because both Arctic Ocean cores lack *Lyamula furcula* in the upper part of the core they both have sampled the disappearance of the most abundant and widespread Cretaceous species. Silicoflagellate assemblages with abundant *Lyamula furcula* have been correlated by calcareous nannofossils as Late Maastrichtian at DSDP 216 (latitude 1°N) (Bukry, 1974a), by foraminifers as Middle or Late Maastrichtian at the Moreno Formation (Cornell, 1972), and by several microfossil groups as latest Campanian or Early Maastrichtian at DSDP 275 (Kennett et al., 1975). The persistence of *Lyamula furcula* through the Maastrichtian followed by its disappearance near the Maastrichtian/Danian boundary in California and DSDP 216 (Bukry, 1981a), suggests that Arctic cores CESAR 6 and FI-437 are Middle or Late Maastrichtian and partly correlative.

Arctic Ocean assemblages contain especially abundant *Vallacerta siderea* and *Lyamula burchardae* but lack *Vallacerta hortonii* and *Vallacerta tumidula* and *Corbisema*. These assemblages are distinctive and suggest partial isolation from other assemblages by solid or ecologic barriers, possibly shifting the extinction time of *Lyamula furcula* somewhat. An alternative that these Alpha Ridge assemblages contain distinctive species arrays because they are much older or younger than known Late Cretaceous assemblages seems implausible because of the presence and

Table 9.1 Occurrence of Cretaceous silicoflagellates in Arctic Ocean core CESAR 6 recorded as percents. Four silicoflagellate biostratigraphic units are delineated. The relative abundance of the distinctive Cretaceous diatom *Gladius* is also given for comparison (Bukry, 1981b). DK = subsample of a dark brown sediment layer.

LT = subsample of a light tan sediment layer.

CC = Core-catcher sample from the base of the cored interval.

Age	Biostratigraphic unit	Core CESAR-6 sample depth (cm)	Note	Total specimens	<i>Arctocytha</i> sp. A	<i>Cornua</i> sp. A	<i>Lyramula arctica</i>	<i>L. burchardae</i>	<i>L. deflandrei</i> [small, like <i>L. minor</i> ]	<i>L. deflandrei</i>	<i>L. furcula</i>	<i>L. minor</i>	<i>L. porta</i> s. ampl.	<i>L. spp.</i>	<i>Vallacerta siderea</i>	<i>V. siderea</i> (4-spined)	<i>V. siderea</i> (6-spined)	<i>V. siderea</i> (7- or 8-spined)	<i>Gladius</i> per 100 silicoflagellates
-	-	0-2		0															
		127-129		0															
Late Cretaceous	A1	134-136		300				2		9				1	84	3	1		2
		150-152		300	<1	<1		1		3					83	9	3		4
	A2	157-158		300	2	1		18		8					68	2	<1		3
		167-168		300		1		36		7					56	1			5
		170-172		300	<1	1		9		24			1		63	1	1		5
		184-185		300		2		58	1	10					28	1	<1		7
		190-192		300				24		8					65	2	1		1
		204-205		300				3		11			1		81	4	<1		2
		210-212		300		<1		19	1	14			<1		62	1	1		4
		230-232		300		<1		5		25			<1		67	1	1		4
	A3	250-252		300		<1		2		10					84	3	1		10
		260-261		300		<1		1		16					77	3	3		3
		270-272		300		<1		2		9					79	6	3	<1	1
		280-281		300		<1		1		7					82	6	4		1
		290-292		300		1	<1	4		16	1				75	1	2	<1	2
	B	298-300	DK	300				1	84	3	1	1			10	<1	1		1
		298-300	LT	300			<1		88	3		2	<1	1	6				1
		305		200				8	31	26	2	<1	8	3	21		1	1	16
		305-320	CC	100			1	3	22	22	4		1		46		1		2

disappearance of cosmopolitan *Lynamula furcula* in these cores. This event should occur near the end of the Maastrichtian. Because of the unique assemblage and short core coverage the *Lynamula furcula* populations might represent a short-term incursion by this cosmopolitan form. An exotic presence would hinder correlation.

Specific correlation between CESAR 6 (Table 9.2) and FI-437 (Bukry, 1981b) on Alpha Ridge is keyed by the disappearance of long-ranging *Lynamula furcula* within these cores prior to the decline of other Cretaceous silicoflagellates and prior to the appearance of any Paleocene guide species. The *Lynamula furcula* disappearances are assumed to represent the same ecologic or evolutionary event. Other similarities between these two cores include the dominance of *Lynamula burchardae* and *Lynamula deflandrei* in all but the lower part of FI-437, the persistence of *Lynamula burchardae* and *Lynamula deflandrei* after the disappearance of *Lynamula furcula*, and the predominance of *Vallacerta* in the upper part of the core after the removal of *Lynamula furcula*. *Lynamula furcula* is less abundant at CESAR 6 (1 to 4%) than at FI-437 (2 to 43%) and disappears much lower in the core. Therefore, the section at CESAR 6 may be partly equivalent to FI-437, but the upper part is probably younger.

## DIFFICULTIES IN CORRELATION

Because the small amount of data about Cretaceous silicoflagellates has been accumulated at different times (Hanna, 1928; Schulz, 1928; Deflandre, 1950; Mandra, 1960, 1968; Glezer, 1966; Cornell, 1972; Bukry, 1974a; Perch-

Nielsen, 1975; Bukry, 1981b) using different nomenclatural systems, direct comparisons may be difficult, unless assemblages are re-examined. For example, *Lynamula furcula* var. *minor* Deflandre was originally described as a normal Y-shaped form distinguished by small size. Mutant forms with a third or extra branch to the Y were also included. Some later workers used the variety *Lynamula minor* as a species for the mutant morphology (Cornell, 1972), others used the name for the normally-formed holotype (Deflandre, 1950). Perch-Nielsen and Edwards in Perch-Nielsen (1975) gave the mutant morphology an independent name, *Lynamula deflandrei*. Bukry (1975) tabulated normal mutant morphologies together as *Lynamula furcula* s. ampl. Glezer (1966) found no mutant forms of *Lynamula* from the Urals, and she indicated that the separation of small forms of *Lynamula furcula*, as *Lynamula minor*, was unjustified because of wide variation in *Lynamula furcula*. Therefore, a common nomenclature has not been available for direct interpretations of paleoecologic and biostratigraphic correlation. Re-examination of DSDP, California, and Arctic assemblages has been done. For example, DSDP 275 has 2% *Lynamula deflandrei* among the *Lynamula furcula* s. ampl. of Bukry (1975).

Another difficult aspect involving correlation of *Lynamula furcula* could be the Arctic Ocean freshening event postulated to have occurred in the Late Maastrichtian (Gartner and Keany, 1978; Thierstein and Berger, 1978). If *Lynamula furcula* is accepted as a robust, cosmopolitan species able to survive at the most polar sites we know, then its disappearance from the Alpha Ridge may reflect an ecologic

Table 9.2 Comparison of silicoflagellate species arrays at documented Cretaceous localities (Bukry, 1974a, 1975, 1981b; Cornell, 1972; Glezer, 1966; Hajos, 1975; Perch-Nielsen, 1975).

	Arctic		Asian	Indo-Pacific		
	Alpha Ridge	Canadian Arctic Islands*	Ural Mountains	California	DSDP 216	DSDP 275
<i>Arctyochoa quadralta</i>			X	X		X
A. sp. A	X					?
<i>Corbisema apiculata</i>			X	X		
<i>C. archangelskiana</i>			X		X	X
<i>C. geometrica</i>				X	X	X
<i>C. lateradiata</i>			X	X		X
<i>C. spp.</i>		X				
<i>Cornua trifurcata</i>			X		X	X
<i>C. spp.</i>	X	X	X		X	X
<i>Lynamula arctica</i>	X					
<i>L. burchardae</i>	X					
<i>L. deflandrei</i>	X			X	X	X
<i>L. furcula</i>	X	X	X	X	X	X
<i>L. minor</i>	X		X	X		X
<i>L. porta</i>	X					
<i>L. simplex</i>	?		X	X		X
<i>Vallacerta hannai</i>				X		X
<i>V. hortonii</i>			X	X	X	X
<i>V. siderea</i>	X	?				?
<i>V. simplex</i>			X			
<i>V. tumidula</i>		X	X		X	X

\*Preliminary study.



control, other than temperature. The postulated lowering of marine salinities by surface freshening may have locally debilitated *Lynamula furcula*. This would not need to be a complete freshening, but perhaps a partial lowering of salinities by 20 to 40% which could be tolerated by some taxa better than *Lynamula furcula*. The basin closing for such an event may have been near the end of the Maastrichtian (Gartner and Keany, 1978). Therefore, because *Lynamula furcula* is robust and dissolution-resistant, its ecologic disappearance from Alpha Ridge should be in the Middle or Late Maastrichtian if it is linked to a freshening event.

Since the reference localities for Late Cretaceous silicoflagellates are so few so far apart, the discrimination of ecologic from evolutionary changes is difficult. Therefore, although the general age of Late Cretaceous is established by the presence of Cretaceous genera *Lynamula* and *Vallacerta* in CESAR 6 and by the absence of Early Paleocene guide taxa, such as *Corbisema hastata*, the absence of the genus *Corbisema* throughout CESAR 6 suggests that special ecologic conditions, not simple age differences are involved. Both California and Ural Mountains Cretaceous assemblages contain *Corbisema*. Although abundances are not predominant, all the Indo-Pacific and Arctic Islands localities that have been studied contain *Corbisema* (Bukry, 1981b). Because of this widespread occurrence in the Late Cretaceous and predominance in the Paleocene (Bukry, 1981b), the exclusion of *Corbisema* from Alpha Ridge cores CESAR 6 and FI-437 must result from different ecology, making biostratigraphic insights for Alpha Ridge more speculative.

Three significant species from Alpha Ridge, *Lynamula deflandrei*, *Lynamula furcula*, and *Vallacerta siderea* are long-ranging. All three are recorded from DSDP 275 which has been correlated as latest Campanian or Early Maastrichtian. If the Alpha Ridge cores were the same age, then the exclusion of *Corbisema geometrica*, *Vallacerta hortonii*, and *Vallacerta tumidula*, which do occur at DSDP 275, would be ecologic.

Another problem of analysis is the much greater abundance of *Vallacerta hortonii* and *Vallacerta siderea* at DSDP 275. Because *Vallacerta siderea* is listed as rare, and the only specimens illustrated have obscured centres, these *Vallacerta siderea* may be only poorly developed variants of *Vallacerta tumidula*. Without this occurrence, *Vallacerta siderea* would then be limited to its original locality (southern Baltic area) and to the immense populations of the Alpha Ridge.

Considering the uncertainty over the evolutionary sequence between the three species of *Vallacerta*, and the documented long ranges of *Vallacerta hortonii* and *Vallacerta tumidula*, I prefer to consider *Vallacerta siderea* a later development of the group. Also, the prominence of the complex form, *Lynamula burchardae*, is considered an advancement over the less complicated shapes in the genus, such as *Lynamula deflandrei*, *Lynamula furcula*, and *Lynamula simplex*. The most probable correlation by silicoflagellates is that the Alpha Ridge assemblage is ecologically specialized and probably Middle or Late Maastrichtian.

## LATE CRETACEOUS PROVINCIAL SILICOFAGELLATE ASSEMBLAGES

In comparing the species arrays of Late Cretaceous silicoflagellates from different parts of the world, Glezer (1966) suggested environmental conditions were very similar between the Santonian-Campanian seas of the Urals and the Maastrichtian sea of California because the abundance of dominant taxa, such as *Lynamula furcula*, *Lynamula simplex*, and *Vallacerta hortonii* were similar and the form of *Vallacerta hortonii* was very similar. The main differences between the Urals assemblages and the California assemblage are the more common *Corbisema geometrica* and *Dictyocha* of California and the more common *Cornua trifurcata* of the Urals. Although the assemblages described from the Urals are assigned a Santonian-Campanian age, they may not all be the same age. Some may even be Maastrichtian because ages of fossil groups, such as silicoflagellates, that are not present in European type stages must be correlated indirectly through other groups or physical stratigraphic techniques. Do all Cretaceous silicoflagellate localities of similar latest Campanian or Maastrichtian age represent different ecological provinces, or are they all different ages to account for the distinctive species arrays (Table 9.2)? Most seem to be associated with similar shallow marine plateau or shelf areas with abundant diatoms, so the generally low total diversity of silicoflagellates may be related to their development during a short time span (Late Campanian to Maastrichtian = 7 Ma) or to limiting oceanic conditions that were augmented by increased volcanic activity and silica availability in the Late Campanian and Maastrichtian (Axelrod, 1981; Wall, 1975). Calcareous nannoplankton, among the golden-brown algae with which silicoflagellates are classified, did show cold- and warm-favoring arrays of species in the Late Maastrichtian (Worsley and Martini, 1970; Bukry, 1974b; Thierstein, 1981). Therefore, silicoflagellate populations were likely to have been ecologically partitioned into different provincial assemblages during the Late Cretaceous.

The major taxonomic distinctions of Late Cretaceous silicoflagellate provinces are summarized in Table 9.2 which shows the distribution of typical species. Large abundances of *Vallacerta siderea* and *Lynamula burchardae* distinguish Alpha Ridge assemblages. The Canadian Arctic Islands are under study and contain several new taxa, but the presence of *Corbisema* spp., *Lynamula furcula*, and *Vallacerta tumidula* var. *quadrata* suggests closer affinity to Indo-Pacific assemblages than to those on Alpha Ridge.

DSDP site 275 on the Campbell Plateau, southeast of New Zealand, contains a short section of silicoflagellates that is predominated by *Lynamula furcula*. The abundance of this species combined with *Corbisema geometrica*, *Corbisema lateradiata*, *Lynamula deflandrei*, and *Vallacerta tumidula*, accounts for about 98% of the population throughout the section (Bukry, 1975).

The identification of *Vallacerta tumidula* var. *quadrata* by Hajos (1975) at DSDP 275 is significant because this variety also occurs in the Canadian Arctic Islands (Bukry,

unpublished data, 1983), and helps to show the Indo-Pacific affinities of some Arctic assemblages outside the Alpha Ridge.

At DSDP 216, east of Sumatra, *Lynamula furcula* predominates in a Late Maastrichtian section, as correlated by the coccolith *Nephrolithus frequens* Zone (Bukry, 1974b). Other silicoflagellates present suggest similarities to the Ural Mountains (*Cornua* sp. cf. *Cornua trifurcata* and *Vallacerta tumidula*) and California (*Corbisema geometrica*, *Lynamula deflandrei*, and *Vallacerta hortonii*).

The Alpha Ridge province lacks most of the key species in common between the other provinces. Most of the characteristic species at the Alpha Ridge, *Lynamula burchardae*, *Lynamula porta*, and *Vallacerta siderea*, are missing or only sparse in the other provinces. *Lynamula furcula* is the only species found on Alpha Ridge which is common (up to 43% at FI-437) both there and elsewhere (86% at DSDP 275). To a lesser extent *Lynamula deflandrei* (up to 26% at CESAR 6 and 75% in California) is also a link between the Indo-Pacific localities (Cornell, 1972; Perch-Nielsen, 1975) and the Alpha Ridge. Because *Lynamula furcula* is the most widespread Late Cretaceous silicoflagellate, its disappearance from the Alpha Ridge, without other substantial addition or subtraction of taxa, is believed to represent a restriction of conditions (such as normal salinity) which particularly favoured *Lynamula furcula* in the Arctic. This would assume that the subsequent provincial extinction of *Lynamula furcula* on Alpha Ridge in the mid or Late Maastrichtian presaged the final extinction at other localities. Whatever the precise time of the disappearance of *Lynamula furcula* from Alpha Ridge ultimately proves to be, the upper assemblages of cores FI-437 and CESAR 6 are distinctive and effectively isolated from other localities in space or time. The presence of a partly restricted basin at high latitude, where annual sunlight incidence could require special adaptations, is easily responsible for an ecologically distinct provincial assemblage. But this same distinctness makes biostratigraphic correlation for these assemblages speculative. Paleomagnetic and geochemical study of the Alpha Ridge cores is needed to help resolve the correlation of the unique silicoflagellate assemblages.

## CONCLUSION

Cretaceous silicoflagellates from Alpha Ridge core CESAR 6 are similar in all respects to the assemblages of core FI-437 from Alpha Ridge. The distinctive species array at Alpha Ridge is believed to result from progressive ecological restriction (reduced diversity upwards in the cores) probably during the Middle or Late Maastrichtian. A correlation earlier in the Cretaceous cannot be ruled out, because there is a lack of high-latitude reference localities which would permit distinction of ecological and evolutionary changes. But the disappearance of long-ranged, cosmopolitan *Lynamula furcula* and the subsequent prominence of more complex companion species, such as *Lynamula burchardae*, is suggestive of a Maastrichtian age, because tectonic activity was isolating the Arctic Basin during the Maastrichtian (Gartner and Keany, 1978; Williams and Stelck, 1975). If these were older assemblages, they should

have some of the other widespread taxa, such as *Vallacerta hortonii* and *Vallacerta tumidula*, as a result of more open-marine communication during Santonian and Campanian (Jeletzky, 1970, 1978).

The fundamental differences between assemblages at Alpha Ridge and the Canadian Arctic Islands result from different ecology and age and suggest that additional studies in the Arctic Basin will yield much new information on tectonics, paleoceanography, and paleontology.

## SYSTEMATIC PALEONTOLOGY FOR CESAR 6 TAXA

### Genus ARCTYOCHA Bukry, n. gen.

Type species: *Dictyocha quadrata* Hanna, 1928, p.261, pl.41, fig.3.

Description: *Arctyocha*, unlike *Dictyocha*, has no basal pikes. The basal ring outlines, typically, have four, five, or six corners with moderate-length spines. The interspine sides of the ring are typically indented but may be straight. Various patterns of bars and struts compose the apical structures which rise above the plane of the basal ring.

Remarks: *Arctyocha* may have developed from *Corbisema* but it lacks basal pikes. *Arctyocha* is separated from *Dictyocha* by several structural and lineal barriers. *Dictyocha* has Miocene *Dictyocha fibula* as the type species (Loeblich et al., 1968). This and related Neogene species have basal pikes. The earliest Cenozoic forms resembling *Dictyocha*, in the Paleocene, have septate spines and were probably derived from coeval *Corbisema* species having septate spines. Compare *Dictyocha prearentis* and *Corbisema glezeriae* (Bukry, 1976). Triangular *Corbisema* is much more prevalent in the Paleocene and Late Cretaceous than *Dictyocha*-like (quadrate or pentagonal) specimens. This, together with the absence of *Dictyocha* in many Lower Miocene assemblages (Bukry, in press), suggests that there is no direct generic connection between Late Cretaceous specimens of *Arctyocha* and the more dominant and continuous members of *Dictyocha* found in the Middle Miocene and higher.

*Arctyocha* sp. A  
(Plate 9.1, fig. 1-3)

Remarks: An *Arctyocha* population predominated by pentagonal specimens with moderate to long spines occurs in upper core CESAR 6. Sparse forms with higher symmetry occur, but no quadrate specimens occur. The apical structures are lower than for specimens from site DSDP 275 and the spines are longer than for specimens from core FI-437.

### Genus CORNUA Schulz, 1928

*Cornua* sp. A  
(Plate 9.1, fig. 4-5)

Remarks: *Cornua* sp. A has a bar that bifurcates at each end. The bifurcations are angled in the same direction, resembling a saw-horse, and are ornamented with several small projections.

## Genus LYRAMULA Hanna, 1928

*Lynamula arctica* Bukry  
(Plate 9.1, fig. 6)

*Lynamula arctica* Bukry, 1981b, p.60, fig.2-3.

Remarks: *Lynamula arctica* has a wide open Y-shape, instead of the more curved shape of *Lynamula furcula*.

*Lynamula burchardae* Bukry  
(Plate 9.1, fig. 7, 9)

*Lynamula burchardae* Bukry, 1981b, pl.61, fig.4-5

Remarks: *Lynamula burchardae* is distinguished from *Lynamula deflandrei* by having four major spines instead of three. The specimens in CESAR 6 are also larger, more robust, and more flared-out at the tips than *Lynamula deflandrei*.

*Lynamula deflandrei* Perch-Nielsen and Edwards  
(Plate 9.1, fig. 8, 10)

*Lynamula furcula* var. *minor* Deflandre, 1940 (in part), p.509, fig.7-9 (not 10).

*Lynamula minor* (Deflandre) Deflandre, 1950 (in part), p.99.

*Lynamula minor* (Deflandre) Cornell, 1972, p.149, pl.1, fig.2.

*Lynamula furcula* var. *minor* Deflandre, Ling et al., 1973, p.1361, fig.g.

*Lynamula deflandrei* Perch-Nielsen and Edwards in Perch-Nielsen, 1975, p.688, pl.9, fig.8-17.

*Lynamula deflandrei* n. sp. Hajos, 1975, p.968, pl.16, fig.1-2.

Remarks: *Lynamula deflandrei* is a small three-pronged species originally described by Deflandre and by Cornell from the California Moreno Formation. The species was named from specimens present at DSDP 275 southeast of New Zealand. Specimens from Alpha Ridge cores CESAR 6 and FI-437 are sparse to common and are generally smaller and less robust than *Lynamula burchardae*. Re-examination of samples from FI-437 showed sparse specimens of *Lynamula deflandrei*, but *Lynamula furcula* and *Lynamula burchardae* are more numerous. A small, crescent-shaped variety of *Lynamula deflandrei* is predominant in the lower samples from CESAR 6. This variety closely resembles *Lynamula minor* s. str. in size and form and indicates that *Lynamula deflandrei* may be a phenotypic expression for several species of *Lynamula*.

*Lynamula furcula* Hanna  
(Plate 9.1, fig. 11)

*Lynamula furcula* Hanna, 1928, p.262, pl.41, fig.4-5.

*Lynamula furcula* Hanna, Deflandre, 1940, p.509, fig.4.

*Lynamula furcula* Hanna, Ling et al., 1973, p.1361, fig.f.

Remarks: The type species of *Lynamula* has a moderate to large Y-shaped skeleton with the apical spine being the shortest. There is variation in length and curvature of the three elements (Hanna, 1928) which may be extensive (Glezer, 1966). This is a cosmopolitan species which is dominant at Indo-Pacific sites DSDP 216, DSDP 275, and California.

*Lynamula minor* (Deflandre) Deflandre  
(Plate 9.1, fig. 12)

*Lynamula furcula* var. *minor* Deflandre, 1940, p.509, fig.7-10.

*Lynamula minor* (Deflandre) Deflandre, 1950, p.99.

*Lynamula minor* (Deflandre) Perch-Nielsen, 1975, p.688, pl.9, fig.1-7.

Remarks: *Lynamula minor* was effectively emended by Perch-Nielsen and Edwards in Perch-Nielsen (1975) to be the small normal forms typified by the holotype and which resemble *Lynamula furcula*. These smaller more rounded forms can also be seen with *Lynamula deflandrei*-like three-armed format in lower core CESAR 6. These forms were tabulated as *Lynamula deflandrei* (small, like *Lynamula minor*), but they indicate that *Lynamula deflandrei* is probably just a phenotypic variant of both small *Lynamula minor* and *Lynamula furcula*. Therefore, this new occurrence, at Alpha Ridge, of three-armed variants, resembling *Lynamula minor*, supports Deflandre's original viewpoint that three-armed forms were mutants. But larger species such as *Lynamula arctica*, *Lynamula furcula*, and *Lynamula porta* tend not to produce three-spined forms. The division of Perch-Nielsen (1975) between *Lynamula deflandrei* and *Lynamula minor* is used for this report, but reconsideration of this nomenclature may be needed in view of the assemblages recovered from CESAR 6.

*Lynamula porta* Bukry s. ampl.  
(Plate 9.2, fig. 1-2)

*Lynamula porta* Bukry, 1981b, p.61, fig.6-8.

Remarks: The sparse specimens tabulated as *Lynamula porta* s. ampl. lack the curvature of *Lynamula furcula*, or the wide open Y-shape of *Lynamula arctica*, but do not fully match the symmetry of the original specimens from core FI-437. One side may not show the dog-leg bend that brings the two sides of the Y-shape into subparallel alignment.

*Lynamula* spp.  
(Plate 9.2, fig. 3)

Remarks: Irregular, tilted, or obscured specimens which are not assignable to recognized species are tabulated as *Lynamula* spp.

## Genus VALLACERTA Hanna, 1928

*Vallacerta siderea* (Schulz) Bukry  
(Plate 9.2, fig. 4-8)

*Dictyocha siderea* Schulz, 1928, p.284, fig.81a-b.

*Vallacerta siderea* (Schulz) Bukry, 1981b, p.62, fig.1.

Remarks: *Vallacerta siderea* is the pre-eminent silico-flagellate of CESAR 6. Sizes are uniform and preservation is excellent everywhere but the highest sample (134 to 136cm) where both small and normal specimens are mixed and where rimless, spineless, and fragmented specimens occur.

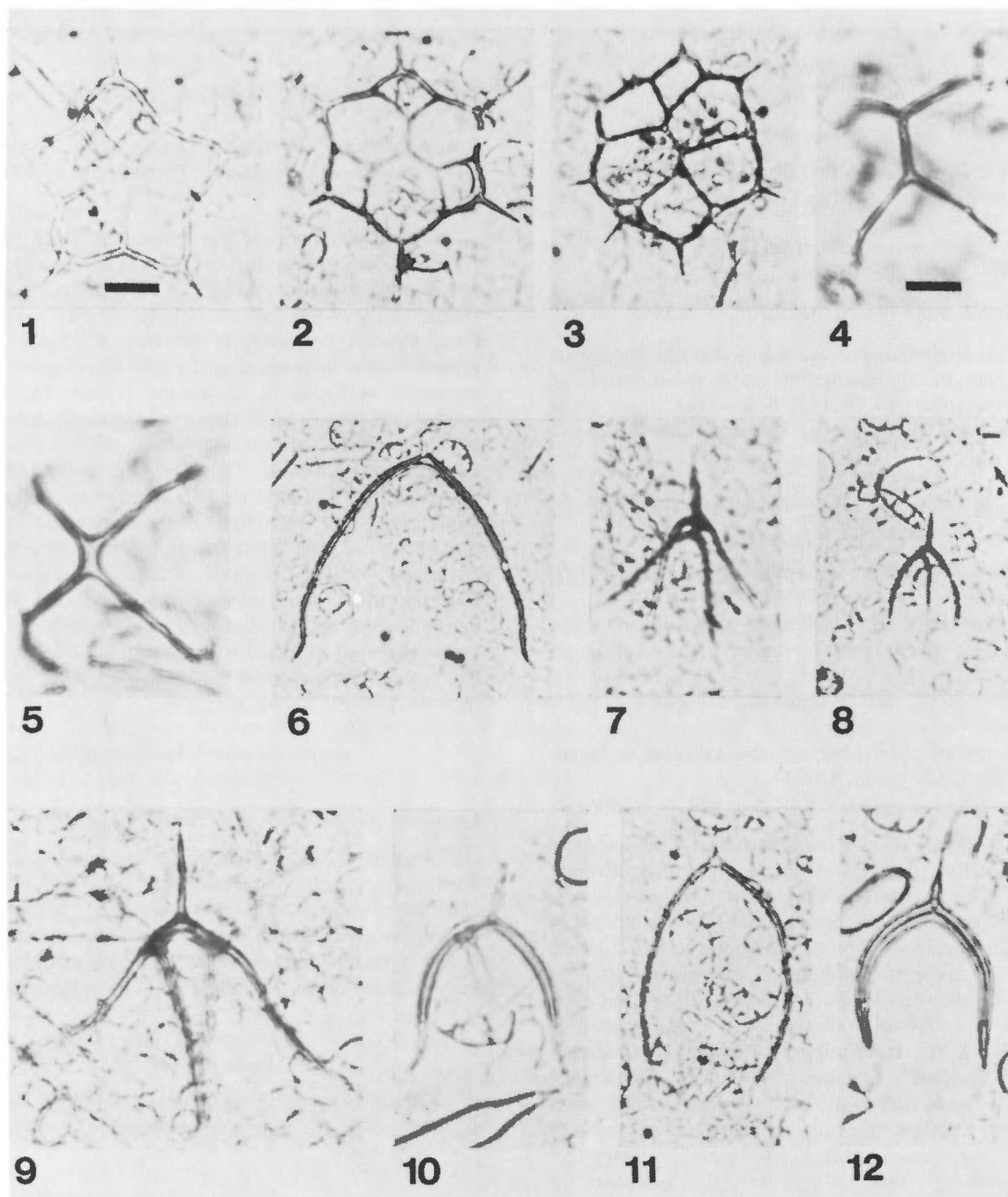


**Plate 9.1**

Cretaceous silicoflagellates from CESAR 6. Scale bar = 20  $\mu\text{m}$  for figures 1-3, 6-8 and 11. Scale bar = 10  $\mu\text{m}$  for figures 4, 5, 9, 10 and 12.

Figures 1-3 *Arctyochoa* sp. A (1, 3) Sample 157-158cm. (2) Sample 150-152cm.

Figure 4 and 5 *Cornua* sp. A Sample 157-158cm.

Figure 6 *Lyrarnula arctica* Bukry Sample 298-300cm, LT.

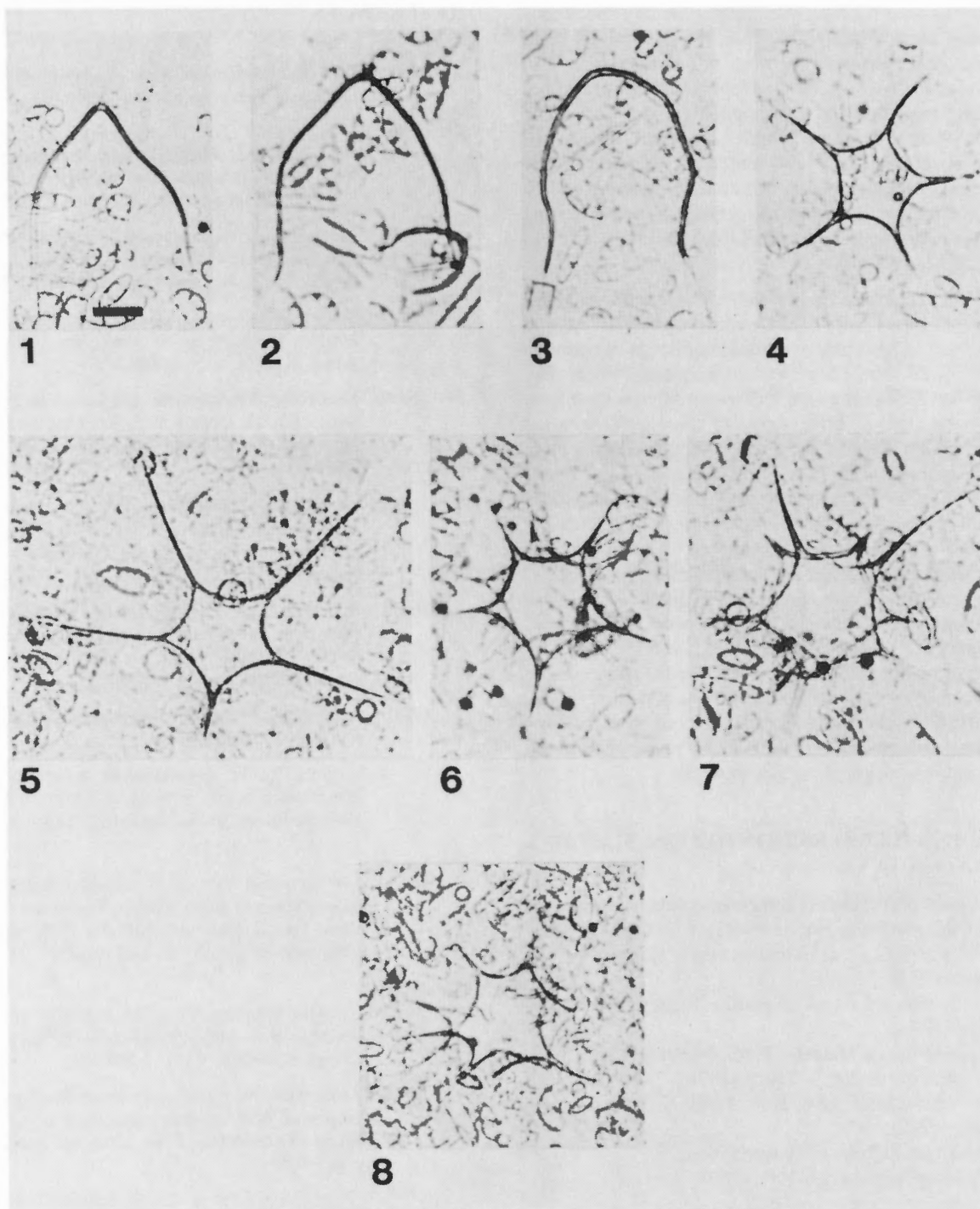
Figure 7 and 9 *Lyrarnula burchardae* Bukry (7) Sample 210-212cm. (9) Sample 167-168cm.

Figure 8 and 10 *Lyrarnula deflandrei* Perch-Nielsen and Edwards (8) Sample 210-212cm. (10) Small variety, sample 305cm.

Figure 11 *Lyrarnula furcula* Hanna Sample 305cm.

Figure 12 *Lyrarnula minor* (Deflandre) Deflandre Sample 305cm.





### Plate 9.2

Cretaceous silicoflagellates from CESAR 6. Scale bar = 20  $\mu$ m.

Figure 1 and 2 *Lyrarnula porta* Bukry (1) Sample 305cm. (2) Core-catcher sample, with small variety of *Lyrarnula deflandrei* Perch-Nielsen and Edwards at right.

Figure 3 *Lyrarnula* sp. Sample 305cm.

Figure 4-8 *Vallacerta siderea* (Schulz) Bukry (4) Sample 157-158cm. (5) Sample 134-136cm. (6) Paired skeletons, core-catcher sample. (7) Paired skeletons, sample 210-212cm. (8) Paired skeletons, irregular, hexagonal, sample 270-272cm.



Variations within *Vallacerta siderea* include specimens with different numbers of spines than the five-spined main population. Quadrate forms are most numerous (up to 9%) followed by hexagonal (up to 4%). Heptagonal and octagonal forms are extremely rare and no triangular variants occur. The abundances of these variants is high only where the normal pentagonal specimens are most abundant. Therefore, they represent a low-level member of the natural population and do not become abnormally abundant or rare where the normal population is periodically reduced (Table 9.1, samples 184 to 185cm or 298 to 300cm).

The *Vallacerta siderea* populations are noteworthy for the presence of intact pairs of skeletons between 157cm and the core bottom. These pairs are most numerous in samples 210 to 212cm, 230 to 232cm, and core-catcher, where they account for 7 to 22% of the total *Vallacerta siderea* skeletons. Because of the shallow bowl shape of the central area (or plate), overlapping and nesting of two skeletons during slide preparation or during original sedimentation would be possible. But the *Vallacerta siderea* pairs in CESAR 6 are believed to be of biologic origin because of two lines of evidence. In sample 270 to 272cm a pair composed of two irregular hexagonal *Vallacerta siderea* occurs (Plate 9.2, fig. 8). Hexagonal variants are so rare that there is small likelihood a random juxtaposition between two independent, irregular, hexagonal specimens would be observed in routine counts. A second line of evidence is in the core-catcher sample where the abundance (46%) of *Vallacerta siderea* is relatively low, but 22% of these specimens are encountered in pairs. This slide preparation is sufficiently thin that secondary juxtaposition of so many specimens seems unlikely.

#### AUTHOR AND ILLUSTRATION REFERENCES FOR OTHER CITED TAXA

- Arctyochoa quadralta* (Hanna) Bukry, n. comb.—Basionym: *Dictyochoa quadralta* Hanna (1928), p.261, pl.41, fig.3.  
*Corbisema apiculata* (Lemmermann) Hanna—Perch-Nielsen (1975).  
*Corbisema archangelskiana* (Schulz) Frenguelli—Perch-Nielsen (1975).  
*Corbisema geometrica* Hanna—Perch-Nielsen (1975).  
*Corbisema gelzeri* Bukry—Bukry (1976).  
*Corbisema lateradiata* (Schulz) Perch-Nielsen—Perch-Nielsen (1975).  
*Cornua trifurcata* Schulz—Glezer (1966).  
*Dictyochoa fibula* Ehrenberg—Bukry (1980).  
*Dictyochoa precarentis* Bukry—Bukry (1976).  
*Lyrarnula simplex* Hanna—Ling et al. (1973).  
*Vallacerta hannai* Deflandre—Deflandre (1944).  
*Vallacerta hortonii* Hanna—Perch-Nielsen (1975).  
*Vallacerta simplex* Jousé—Jousé (1949).  
*Vallacerta tumidula* Glezer—Perch-Nielsen (1975).  
*Vallacerta timidula* var. *quadrata* Hajos—Hajos (1975).

#### REFERENCES

- Axelrod, D.I.  
 1981: Role of volcanism in climate and evolution; Geological Society of America, Special Paper 185, 59p.
- Bukry, D.  
 1974a: Coccolith and silicoflagellate stratigraphy, eastern Indian Ocean, Deep Sea Drilling Project Leg 22; Deep Sea Drilling Project Initial Reports, v.22, p.601-607.  
 1974b: Cretaceous and Paleogene coccolith stratigraphy, Deep Sea Drilling Project Leg 26; Deep Sea Drilling Project Initial Reports, v.26, p.669-673.  
 1975: Silicoflagellate and coccolith stratigraphy, Deep Sea Drilling Project Leg 29; Deep Sea Drilling Project Initial Reports, v.29, p.845-872.  
 1976: Cenozoic silicoflagellate and coccolith stratigraphy, South Atlantic Ocean, Deep Sea Drilling Project Leg 36; Deep Sea Drilling Project Initial Reports, v.35, p.885-917.  
 1980: Miocene *Corbisema triacantha* Zone phytoplankton from Deep Sea Drilling Project Sites 415 and 416, off northwest Africa; Deep Sea Drilling Project Initial Reports, v.50, p.507-523.  
 1981a: Synthesis of silicoflagellate stratigraphy for Maastrichtian to Quaternary marine sediment; Society of Economic Paleontologists and Mineralogists, Special Publication 32, p.433-444.  
 1981b: Cretaceous Arctic silicoflagellates; Geo-Marine Letters, v.1, p.57-63.  
 — Tropical Pacific silicoflagellate zonation and paleotemperature trends of the Late Cenozoic; Deep Sea Drilling Project Initial Reports, v.85 (in press).
- Cornell, W.C.  
 1972: Chrysomonad cysts and silicoflagellates from the Marca Shale Member, Moreno Formation (Maastrichtian), Fresno County, California; Ph.D. dissertation, University of California, Los Angeles, 235p.
- Deflandre, G.  
 1940: L'origine phylogénétique des *Lyrarnula* et l'évolution des Silicoflagellidées; Academie des Sciences, Paris, Comptes Rendus, v.211, p.508-510.  
 1944: Remarques sur l'évolution des Silicoflagellidées, à propos de deux espèces crétaciques nouvelles; Academie des Sciences, Paris, Comptes Rendus, v.219, p.463-465.  
 1950: Contribution à l'étude des Silicoflagellidées actuels et fossiles; Microscopie, v.2, p.72-108, 117-142, 191-210.
- Gartner, S. and Keany, J.  
 1978: The terminal Cretaceous event; a geologic problem with an oceanographic solution; Geology, v.6, p.708-712.

- Glezer, Z.I.  
1966: Silicoflagellatophyceae; in *Cryptogamic plants of the U.S.S.R.*: ed. M.M. Gollerbakh; Akademia Nauk SSSR, V.A. Komarova Botanicheskii Institut (Translated from Russian by Israel Program for Scientific Translations Ltd., Jerusalem, 1970), v.7, p.1-363.
- Hajos, M.  
1975: Late Cretaceous Archaeomonadaceae, Diatomaceae, and Silicoflagellatae from the South Pacific Ocean, Deep Sea Drilling Project Leg 29, Site 275; Deep Sea Drilling Project Initial Reports, v.29, p.913-1009.
- Hanna, G.D.  
1928: Silicoflagellata from the Cretaceous of California; *Journal of Paleontology*, v.1, p.259-263.
- Jeletzky, J.A.  
1970: Marine Cretaceous biotic provinces and paleogeography of Western and Arctic Canada; Illustrated by a detailed study of ammonites: Geological Survey of Canada, Paper 70-22, 92p.  
1978: Causes of Cretaceous oscillations of sea level in Western and Arctic Canada and some general geotectonic implications; Geological Survey of Canada, Paper 77-18, 44p.
- Jousé, A.P.  
1949: Algae diatomaceae aetatis supernecretaceae ex arenis argillaceis systematis fluminis bolschoy aktay in declivitate oriental Ural borealis; Akademia Nauk SSSR, Botanicheskii Institut, Botanicheskii Materialy, Otdel Sporovyykh Rastenii, v.6, p.65-78.
- Kennett, J.P., Houtz, R.E., Andrews, P.B., Edwards, A.R., Gostin, V.A., Hajos, M., Hampton, M., Jenkins, D.G., Margolis, S.V., Owenshine, A.T., Perch-Nielsen, K., Wilson, G.J., and Pessagno, E.  
1975: Site 275; Deep Sea Drilling Project Initial Reports, v.29, p.19-35.
- Ling, H.Y., McPherson, L.M. and Clark, D.L.  
1973: Late Cretaceous (Maastrichtian?) silicoflagellates from the Alpha Cordillera of the Arctic Ocean; *Science*, v.180, p.1360-1361.
- Loeblich, A.R., III, Loeblich, L.A., Tappan, H., and Loeblich, A.R. Jr.  
1968: Annotated index of fossil and recent silicoflagellates and ebridians with descriptions and illustrations of validly proposed taxa; Geological Society of America, Memoir 106, 319p.
- Mandra, Y.T.  
1960: Fossil silicoflagellates from California, U.S.A.; International Geological Congress, 21st, Copenhagen 1960, part 6, p.77-89.  
1968: Silicoflagellates from the Cretaceous, Eocene, and Miocene of California, U.S.A.; California Academy of Science, Proceedings, v.36, p.231-277.
- Perch-Nielsen, K.  
1975: Late Cretaceous to Pleistocene silicoflagellates from the southern southwest Pacific, Deep Sea Drilling Project Leg 29; Deep Sea Drilling Project Initial Reports, v.29, p.677-721.
- Schulz, P.  
1928: Beiträge zur Kenntnis fossiler und rezenter Silicoflagellaten; *Botanisches Archiv*, v.21, p.225-292.
- Thierstein, H.R.  
1981: Late Cretaceous nannoplankton and the change at the Cretaceous-Tertiary boundary; Society of Economic Paleontologists and Mineralogists, Special Publication 32, p.355-394.
- Thierstein, H.R. and Berger, W.H.  
1978: Injection events in ocean history; *Nature*, v.276, p.461-466.
- Wall, J.H.  
1975: Diatoms and radiolarians from the Cretaceous system of Alberta; a preliminary report; in *Cretaceous System in the Western Interior of North America*, ed. W.G.E. Caldwell; Geological Association of Canada, Special Paper 13, p.391-410.
- Williams, G.D. and Stelck, C.R.  
1975: Speculations on the Cretaceous palaeogeography of North America; in *Cretaceous System in the Western Interior of North America*, ed. W.G.E. Caldwell; Geological Association of Canada, Special Paper 13, p.1-20.
- Worsley, T.R. and Martini, E.  
1970: Late Maastrichtian nannoplankton provinces; *Nature*, v.255, p.1242-1243.



## DIATOM BIOSTRATIGRAPHY OF THE CESAR 6 CORE, ALPHA RIDGE

John A. Barron<sup>1</sup>

United States Geological Survey

Barron, J.A., *Diatom biostratigraphy of the CESAR 6 core; in Initial Geological Report on CESAR — the Canadian Expedition to Study the Alpha Ridge, Arctic Ocean*, ed. H.R. Jackson, P.J. Mudie and S.M. Blasco; Geological Survey of Canada, Paper 84-22, p. 137-148, 1985.

### Abstract

The CESAR 6 core, from the flank of the Alpha Ridge in the Arctic Ocean, contains a diverse, well-preserved diatom assemblage of probable Late Campanian (Late Cretaceous) age. Thirty-three diatom taxa were recorded in 10 samples from a 165 cm thick section of the core. The diatom assemblage resembles closely Late Campanian diatom assemblages from the northern Ural Mountains in western Siberia and differs markedly from known Maastrichtian diatom assemblages. The abundance of diatom resting spores and lack of shallow water diatoms suggest that deposition occurred near a shelf or bank edge which was distant from the shoreline.

### Résumé

La carotte CESAR 6, prélevée sur le versant de la dorsale Alpha dans l'océan Arctique, contient un assemblage varié et bien conservé de diatomées datant vraisemblablement du Campanien récent (Crétacé récent). Trente-trois taxons de diatomées sont identifiés dans dix échantillons provenant d'un segment de carotte de 165 cm. L'assemblage de diatomées ressemble étroitement à ceux du Campanien récent de la partie nord des monts Oural dans l'ouest de la Sibérie; il diffère grandement des assemblages de diatomées connus du Maastrichtien. L'abondance des spores en sommeil de diatomées et l'absence de diatomées d'eau peu profonde semblent indiquer que la sédimentation a eu lieu en marge d'une plate-forme ou d'un banc situés à quelque distance du littoral.

## INTRODUCTION

The CESAR 6 core, collected by the Geological Survey of Canada from the flank of the Alpha Ridge in the Arctic Ocean (85°50'0.41"N, 109°01'05.2"W, water depth 1365m), contains abundant, very well-preserved diatoms in unit 4 (134-310cm) referable to the Upper Cretaceous. Correlation of the diatoms is hindered by the relatively poor stratigraphic and geographic coverage of published studies on Cretaceous diatoms. Nevertheless, it is possible to make comparisons of the CESAR 6 diatoms with published studies on Late Cretaceous diatoms.

The most extensive and best documented studies of Late Cretaceous diatoms are those of Long et al. (1946) on the Marca Shale of California, Strelnikova (1974) on diatomites from the northern Ural Mountains in western Siberia, and Hajos and Stradner (1975) on DSDP site 275 southeast of New Zealand.

Long et al. (1946) listed 116 diatom taxa from the Marca Shale Member of the Moreno Formation in central California. Many of these taxa were illustrated by them and by Hanna (1927, 1934). The most diverse genera (in terms of numbers of species) listed by Long et al. (1946) include: *Actinopterychus* (7 species), *Aulacodiscus* (14 taxa), *Auliscus* (10 species), *Biddulphia* (10 species), *Coscinodiscus* (18 species), and *Triceratium* (10 species).

The Marca Shale was assigned to the Late Maastrichtian by Lewis (1964) on the basis of benthic foraminifers. Cornell (1972) accepted a Middle to Late Maastrichtian age for the Marca Shale in his study of the silicoflagellate assemblages. Pessagno (1976) assigned the Marca Shale radiolarian assemblages to his *Orbiculiforma renillaeformis* Zone which he considered to be either Early to Middle Maastrichtian (based on planktonic foraminifers) or Late Maastrichtian (based on benthic foraminifers) in age. For the purpose of this report, the Marca Shale assemblages will be considered to be undifferentiated Maastrichtian in age.

<sup>1</sup>345 Middlefield Road, Menlo Park, California 94025

Strelnikova (1974) tabulated 145 diatom taxa from three Campanian and one Maastrichtian?–Danian? diatom complexes from the pre-Polar and Muzinsk Urals (60° to 68°N) in western Siberia. She recorded the diatoms in 45 samples from a thickness of over 200m of diatomites, and illustrated them on 57 plates. Dominant diatom genera include: *Aulacodiscus* (10 species and varieties), *Biddulphia* (7 species), *Coscinodiscus* (9 species), *Hemiaulus* (15 species), *Pterotheca* (7 species), *Stephanopyxis* (12 species), and *Triceratium* (16 species).

Strelnikova's (1974) Campanian diatom complexes were dated by radiolarians, benthic foraminifers, and molluscs, and she listed the radiolarian genus *Prunobrachium* as being typical of the deposits. According to C.D. Blome of the United States Geological Survey (oral communication, 1983) *Prunobrachium* is a good Campanian marker genus.

Hajos and Stradner (1975) tabulated 124 diatom taxa from cores 1 and 2 of DSDP site 275 (50°26.34'S, 176°18.99'E, water depth 2800m) on the Campbell Plateau southeast of New Zealand. Hajos and Stradner (1975) recorded 11 species and varieties of *Hemiaulus*, 13 species of *Triceratium* and 8 species of *Trinacria* in their assemblages, which they considered to be Late Campanian to Maastrichtian on the basis of comparison with other Cretaceous diatom assemblages. Pessagno (1975), on the other hand, assigned the same cores to his latest Campanian *Patulibracchium dickinsoni* Zone of radiolarians, noting similarities with radiolarian assemblages from California. Because Late Cretaceous radiolarian stratigraphy is more refined than Late Cretaceous diatom stratigraphy, a Late Campanian age will be accepted for the DSDP site 275 diatom assemblages.

## ACKNOWLEDGMENTS

I thank the Geological Survey of Canada and particularly Peta J. Mudie for providing the CESAR 6 material for study. David Bukry and Jack G. Baldauf of the United States Geological Survey provided helpful discussion during this study. I acknowledge the reviews of Louie Marincovich, Charles A. Repenning, and Jack G. Baldauf of the United States Geological Survey.

## METHODS

Unprocessed strew slides were prepared for 10 samples from unit 4 of the CESAR 6 core and mounted in Hyrax (n = 1.65). The abundance and excellent preservation of the diatoms and the lack of terrigenous material in unit 4 made chemical processing of the material unnecessary. Additional slides were studied from unit 1 (0–2cm) and unit 3 (127–129cm); but the former was barren of diatoms, and the latter contained only sparse diatoms reworked from unit 4. One entire slide (cover glass size 22 × 22mm) was examined under the light microscope at 500× with identifications checked at 1250×. The abundance of diatoms in unit 4 resulted in at least 2000 diatoms examined per sample. Relative abundance of taxa encountered during mechanical traverses of the slides were estimated as follows: abundant, two or more specimens in a field of view at 500× (442 μm diameter); common, one or more specimens seen after exam-

ination of two fields of view; few, one specimen seen in each vertical traverse; and rare, for sparser occurrences.

## RESULTS

Table 10.1 lists the 33 diatom taxa which were recorded from the 10 samples examined from unit 4. Most of these taxa are illustrated in Plates 10.1 – 10.3. The most abundant taxa present in the CESAR 6 core include: *Anaulus sibiricus* Strelnikova, *Hemiaulus gleseri* Hajos, *Hemiaulus tumidicornis* Strelnikova, *Rhizosolenia* sp. (thin form), and *Skeletonema polychaetum* Strelnikova. Most of the diatom taxa range throughout unit 4, although *Hemiaulus rossicus* Pantocsek, *Hemiaulus polymorphus* var. *frigida* Grunow, *Rhizosolenia cretacea* Hajos and Stradner, and *Sceptroneis dimorpha* Strelnikova are absent from the upper two samples, 134–136cm and 150–152cm. *Skeletonema polychaetum* is abundant to common throughout unit 4 except in sample 298–300cm, the lowermost sample examined, where it is rare. The lowermost sample is also distinguished by a greater relative abundance of *Actinopterychus simbirskianus* A. Schmidt, *Hemiaulus polymorphus* var. *frigida*, and *Rhizosolenia cretacea* than other samples from unit 4.

Diatom resting spores, including *Goniothecium*, *Pseudopyxilla*, spores of *Hemiaulus*, and small, plain, round forms not recorded on Table 10.1, are abundant throughout unit 4. Their abundance suggests proximity of the site of deposition to the shelf edge or a bank top, as only meroplanktonic diatoms form resting spores in the modern ocean. Shallow water diatoms such as *Aulacodiscus*, *Auliscus*, and *Melosira*, which are common in other Late Cretaceous diatom assemblages, however, are lacking from the CESAR 6 assemblages. The lack of terrigenous material and displaced shallow water diatoms in unit 4 suggest a site of deposition on an outer slope or in an outer basin which was isolated from downslope transport. The excellent preservation of the diatoms is evidence for little, if any, transport.

## CORRELATION

Table 10.2 shows the occurrence of CESAR 6 diatoms in Late Cretaceous diatom assemblages described from western Siberia by Strelnikova (1974), from DSDP site 275 by Hajos and Stradner (1975), and from the Marca Shale of California by Long et al. (1946). I examined three strew slides from two samples from the Marca Shale to supplement the lists of Long et al. (1946). Table 10.2 incorporates broad species concepts, and taxa illustrated in the earlier reports that resemble CESAR 6 diatoms have been included for comparison (marked with "cf.").

The CESAR 6 diatom assemblage is most similar to the middle and upper diatom complexes (Late Campanian) of Strelnikova (1974) from western Siberia. Accepting rather broad species concepts, 29 out of 33 of the CESAR 6 diatoms are present in either the middle or upper complex of Strelnikova (1974). The presence of *Skeletonema polychaetum*, *Coscinodiscus circumspectus* (*Coscinodiscus solidus* of Strelnikova, 1974), and *Hemiaulus tumidicornis* suggest correlation with Strelnikova's (1974) middle complex. *Hemiaulus antiquus* Jousé, *Stephanopyxis turris* (Greville



Table 10.1. Occurrence of diatoms in unit 4 of the CESAR 6 core. A = abundant, C = common, F = few, R = rare.

SPECIES \ INTERVAL	134-136cm	150-152cm	170-172cm	190-192cm	210-212cm	230-232cm	250-252cm	270-272cm	290-292cm	298-300cm
<i>Anaulus sibiricus</i>	C	A	F	A	A	A	A	A	C	A
<i>Actinoptychus simbirskianus</i>	R	R	R	F	R	R	R	F	F	C
<i>A. tenuis</i>	R	R	R	-	-	R	R	-	-	R
<i>Coscinodiscus circumspectus</i>	F	F	R	F	F	R	F	R	F	F
<i>C. sibiricus</i>	-	-	-	R	R	-	R	-	-	-
<i>C. symbolophorus</i>	-	-	-	-	-	-	-	-	-	R
<i>C. wittianus</i>	R	R	R	R	R	R	R	R	-	R
<i>Gladius pacificus</i>	R	R	R	R	R	R	R	F	R	R
<i>G. speciosus</i> f. <i>speciosus</i>	R	R	-	R	R	R	-	R	R	R
<i>Goniothecium odontellum</i>	R	A	R	F	R	R	R	R	R	F
<i>Hemiaulus antiquus</i>	R	R	F	C	F	F	F	F	F	F
<i>H. elegans</i>	R	R	R	R	R	F	R	F	R	R
<i>H. gleseri</i>	F	F	F	C	F	F	C	C	F	F
<i>H. cf. includens</i>	F	R	-	R	R	R	R	-	R	R
<i>H. kittoni</i>	R	R	R	F	R	R	F	F	R	R
<i>H. polymorphus</i> var. <i>frigida</i>	-	-	R	-	R	R	R	-	-	C
<i>H. rossicus</i>	-	-	R	R	R	R	R	-	R	R
<i>H. tumidicornis</i>	F	A	A	C	C	A	A	A	A	F
<i>H. sp. 1</i>	-	R	F	R	R	R	R	R	F	-
<i>Pseudopyxilla americana</i>	R	-	-	-	R	R	R	R	-	R
<i>P. russica</i>	F	F	F	R	R	F	F	R	F	R
<i>Pterotheca</i> ? sp. of Strelnikova (1974)	R	-	R	-	R	R	R	-	-	-
<i>Rhizosolenia cretacea</i>	-	-	-	R	-	R	R	-	-	F
<i>R. sp. (thick form)</i>	F	R	R	R	F	R	R	R	R	F
<i>R. sp. (thin form)</i>	A	C	A	C	C	C	C	C	C	A
<i>Sceptroneis dimorpha</i>	-	-	R	R	-	R	R	R	R	-
<i>S. sp. of Strelnikova</i> (1974)	-	R	-	-	-	-	-	-	-	-
<i>Skeletonema polychaetum</i>	A	A	A	C	C	C	A	A	A	R
<i>Stephanopyxis turris</i>	F	-	R	R	R	R	R	R	R	R
<i>Triceratium indefinitum</i>	C	R	R	F	C	R	F	F	R	R
<i>T. planum</i>	R	-	R	R	F	R	R	R	-	R
<i>T. tessela</i>	R	F	F	-	-	R	R	R	-	-
<i>Trinacria acutangulum</i>	R	-	-	R	R	R	-	-	-	R

and Arnott) Ralfs, *Triceratium tessela* (Krotov) Strelnikova, and *Sceptroneis* sp. of Strelnikova (1974) all have their first occurrences in Strelnikova's (1974) middle complex and provide further constraint on the correlation. *Pseudopyxilla russica* (Pantocsek) Forti and *Triceratium planum* Strelnikova suggest correlation with the upper complex; however, Strelnikova (1974) lists *Gladius speciosus* f. *aculeolatus* Strelnikova and *Gladius speciosus* f. *poratus* Strelnikova as being typical of her upper complex, and neither were observed in the CESAR 6 core.

Harland et al. (1982) report a 10 Ma duration for the Campanian (83-73 Ma BP) and divide the Campanian equally into the Early and Late Campanian. Consequently, the Late Campanian can be considered to be approximately 5

Ma in duration. It is unlikely that unit 4 of the CESAR 6 core represents the entire Late Campanian, because no diatom evolution was observed, in contrast to the evolution reported by Strelnikova (1974) in her Late Campanian diatom assemblages. Similarly, the abundant diatom resting spores in unit 4 suggest a highly productive environment, which ordinarily would mean higher sedimentation rates (at least  $10 \times \text{M.Ma}^{-1}$ ). Therefore, it is possible that the laminae reported in unit 4 (Mudie and Blasco, 1985) may be seasonal in origin.

Correlations with the Late Campanian assemblages of DSDP site 275 are also relatively strong in that 21 of the 33 CESAR 6 diatoms are also present in DSDP site 275. In contrast, only 11 of the CESAR 6 diatoms occur in the undifferentiated Maastrichtian Marca Shale and only 12 of

Table 10.2. Occurrence of CESAR 6 diatom taxa in diatom assemblages from western Siberia (Strelnikova, 1974), Deep Sea Drilling Program site 275, southeast of New Zealand (Hajos and Stradner, 1975), and the Marca Shale of California (Long et al., 1946; and the author's notes). cf. = similar species.

	Western Siberia				SW Pacific	California
	CAMPANIAN				CAMPANIAN	MAASTRICT.
	low.	upper			upper	
	1. Lower complex	2. Middle complex	3. Upper complex	4. Maastrichtian?-Danian?	5. DSDP site 275	6. Marca Shale
<i>Anaulus sibiricus</i>	X	X	X	-	cf.	cf.
<i>Actinoptychus simbirskianus</i>	X	X	X	-	cf.	cf.
<i>A. tenuis</i>	X	X	X	-	-	cf.
<i>Coscinodiscus circumspectus</i>	-	X	-	-	X	X
<i>C. sibiricus</i>	X	X	X	-	-	cf.
<i>C. symbolophorus</i>	X	X	X	X	-	-
<i>C. wittianus</i>	X	X	X	-	X	X
<i>Gladius pacificus</i>	?	?	?	?	X	cf.
<i>G. speciosus</i> f. <i>speciosus</i>	X	X	X	X	X	X
<i>Goniothecium odontellum</i>	X	X	X	X	X	X
<i>Hemiaulus antiquus</i>	-	X	X	-	-	-
<i>H. elegans</i>	X	X	X	-	cf.	-
<i>H. glezeri</i>	-	-	-	-	X	-
<i>H. cf. includens</i>	X	X	X	X	-	-
<i>H. kittoni</i>	X	X	X	X	cf.	-
<i>H. polymorphus</i> var. <i>frigida</i>	X	X	X	-	cf.	-
<i>H. rossicus</i>	X	X	X	X	cf.	-
<i>H. tumidicornis</i>	-	X	-	-	-	-
<i>H. sp. 1</i>	-	-	-	-	-	-
<i>Pseudopyxilla americana</i>	X	X	X	X	X	-
<i>P. russica</i>	-	-	X	X	X	-
<i>Pterotheca</i> ? sp. of Strelnikova	X	X	X	-	-	-
<i>Rhizosolenia cretacea</i>	-	-	-	-	X	-
<i>R. sp. (thick form)</i>	-	cf.	cf.	-	-	-
<i>R. sp. (thin form)</i>	-	-	-	-	-	-
<i>Sceptroneis dimorpha</i>	X	X	X	-	cf.	-
<i>S. sp. of Strelnikova</i>	-	X	X	-	cf.	-
<i>Skeletonema polychaetum</i>	-	X	-	-	cf.	-
<i>Stephanopyxis turris</i>	-	X	X	X	X	X
<i>Triceratium indefinitum</i>	X	X	X	X	cf.	-
<i>T. planum</i>	-	-	X	X	-	cf.
<i>T. tessela</i>	-	X	X	-	-	-
<i>Trinacria acutangulum</i>	X	X	X	X	cf.	-

the CESAR 6 taxa were recorded by Strelnikova (1974) in her Maastrichtian?-Danian? complex.

Although the Marca Shale diatoms (35°N) undoubtedly occupied a warmer environment than the CESAR 6 flora, the differences in the two assemblages are too great to be explained by ecology alone. For example, Long et al. (1946) record 10 species of *Triceratium* in the Marca Shale, but only one of these species occurs in the CESAR 6 core. Species of *Triceratium*, however, are also common in the high-latitude western Siberian assemblages of Strelnikova (1974), so *Triceratium* cannot be considered a dominantly warm water genus in the Late Cretaceous.

In order to consider the CESAR 6 diatom assemblages Maastrichtian in age, one must account for the great differences between the CESAR 6 assemblages and the Marca Shale assemblages of known Maastrichtian age. Admittedly, no unequivocal Maastrichtian assemblages have been described from higher latitudes (north of 60°N). Strelnikova's (1974) Maastrichtian?-Danian? diatom complex lacks age documentation from other fossil groups. Strelnikova (1975) considered that the great differences between her western Siberian Late Cretaceous assemblages and the Marca Shale assemblages of California were due mainly to differing paleobiogeography. However, the Late Campanian assemblages

from western Siberia are more similar to the Late Campanian assemblages from DSDP site 275 (50°S) of Hajos and Stradner (1975) than they are to the Maastrichtian Marca Shale assemblages, and a strong bipolarity of Late Cretaceous diatom assemblages would have to be invoked. A simpler solution is to consider that the major differences in the assemblages reflect differences in age rather than ecology. Consequently, the similarities of the CESAR 6 assemblages to the Late Campanian assemblages of DSDP site 275 and western Siberia imply a Late Campanian age for unit 4.

The resemblance of the CESAR 6 diatom assemblages to those of the western Siberian diatomites is to be expected as a seaway through western Siberia to the Arctic Ocean existed during at least part of the Late Cretaceous (Vinogradov, 1967-1969).

## FLORAL REFERENCE LIST

- Anaulus sibiricus* Strelnikova, 1974, p. 104, pl. 52, fig. 1-5 (Plate 10.2, fig. 10)
- Actinoptychus simbirskianus* Schmidt, 1875, pl. 29, fig. 11 – Strelnikova, 1974, p. 68, pl. 15, fig. 1-7 (Plate 10.1, fig. 8)
- Actinoptychus tenuis* Strelnikova, 1974, p. 67, pl. 14, fig. 1-4 (Plate 10.1, fig. 7)
- Coscinodiscus circumspectus* Long, Fuge and Smith, 1946, p. 102, pl. 15, fig. 12 – Hajos and Stradner, 1975, p. 927, pl. 1, fig. 1
- Coscinodiscus solidus* Strelnikova, 1974, p. 63, pl. 10, fig. 1-5 (Plate 10.1, fig. 1)
- Coscinodiscus sibiricus* Strelnikova, Strelnikova, 1974, p. 64, pl. 11, fig. 1-4 (Plate 10.1, fig. 6)
- Coscinodiscus symbolophorus* Grunow, Strelnikova, 1974, p. 63, pl. 12, fig. 1-7 (Plate 10.1, fig. 9)
- Coscinodiscus wittianus* Pantocsek, Gleser et al., 1974, pl. 8, fig. 8
- Coscinodiscus lineatus* Ehrenberg, Strelnikova, 1974, p. 62, pl. 9, fig. 3-12 – Hajos and Stradner, 1975, p. 927, pl. 3, fig. 1-3; pl. 38, fig. 1
- Remarks: Late Cretaceous diatoms referred to *Coscinodiscus lineatus* Ehrenberg must be renamed because *Coscinodiscus lineatus* Ehrenberg is a synonym of *Thalassiosira leptopus* (Grunow) Hasle and Fryxell, which is a Late Cenozoic diatom. *Coscinodiscus wittianus* Pantocsek sensu Gleser et al. (1974) appears to be the earliest available name for such forms and has been used in this report (Plate 10.1, fig. 5)
- Gladius pacificus* Hajos in Hajos and Stradner, 1975, p. 933, pl. 11, fig. 1-2; pl. 26, fig. 2 (Plate 10.2, fig. 15)
- Gladius speciosus* Schulz f. *speciosus* Strelnikova, 1974, p. 104, pl. 49, fig. 2-11, 14-15, 18, 20-21; pl. 50, fig. 1, 4 (Plate 10.2, fig. 15)
- Goniothecium odontellum* Ehrenberg, Hajos and Stradner, 1975, p. 935, pl. 10, fig. 11-12 – Strelnikova, 1974, p. 116, pl. 55, fig. 1-12; pl. 56, fig. 1-5 (Plate 10.2, fig. 13)
- Hemiaulus antiquus* Jousé, Strelnikova, 1974, p. 101, pl. 46, fig. 1-14 (Plate 10.2, fig. 4)
- Hemiaulus elegans* (Heiberg) Grunow, Strelnikova, 1974, p. 98, pl. 44, fig. 1-17 (Plate 10.2, fig. 3)
- Hemiaulus gleseri* Hajos in Hajos and Stradner, 1975, p. 931, pl. 5, fig. 20; pl. 7, fig. 6-7 (Plate 10.2, fig. 1, 2)
- Hemiaulus* sp. cf. *Hemiaulus includens* (Ehrenberg) Grunow, Strelnikova, 1974, p. 101, pl. 48, fig. 1-6
- Remarks: The specimens figured here are probably resting spores of *Hemiaulus* (Plate 10.2, fig. 7)
- Hemiaulus kittoni* Grunow, Strelnikova, 1974, p. 96, pl. 42, fig. 12-24 (Plate 10.2, fig. 8)
- Hemiaulus polymorphus* var. *frigida* Grunow, Strelnikova, 1974, p. 103, pl. 45, fig. 1-19
- Hemiaulus rossicus* Pantocsek, Strelnikova, 1974, p. 102, pl. 43, fig. 1-18
- Hemiaulus tumidicornis* Strelnikova, Strelnikova, 1974, p. 102, pl. 47, fig. 17-25 (Plate 10.2, fig. 5-6, 12?)
- Hemiaulus* sp. 1
- Remarks: Probably a resting spore (Plate 10.2, fig. 9)
- Pseudopyxilla americana* (Ehrenberg) Forti, Strelnikova, 1974, p. 112, pl. 54, fig. 1-15
- Pseudopyxilla russica* (Pantocsek) Forti, Strelnikova, 1974, p. 111, pl. 56, fig. 6-8
- Pterotheca*? sp. of Strelnikova, 1974, p. 116, pl. 57, fig. 33-34 (Plate 10.2, fig. 11)
- Rhizosolenia cretacea* Hajos and Stradner, 1975, p. 929, pl. 7, fig. 1; pl. 31, fig. 4-6 (Plate 10.3, fig. 1)
- Rhizosolenia* sp. (thick form)
- Remarks: This form resembles *Rhizosolenia pokrovskajae* (Jousé) Strelnikova but lacks well-developed surficial septae and has a less prominent apex (Plate 10.3, fig. 2)
- Rhizosolenia* sp. (thin form)
- (Plate 10.3, fig. 3)
- Sceptroneis dimorpha* Strelnikova, 1974, p. 110, pl. 54, fig. 18-30 (Plate 10.3, fig. 4)
- Sceptroneis* sp. of Strelnikova, 1974, p. 110, pl. 53, fig. 8-9
- Skeletonema polychaetum* Strelnikova, Strelnikova, 1974, p. 54, pl. 3, fig. 3-7 (Plate 1, fig. 2-4)
- Stephanopyxis turris* (Greville and Arnott) Ralfs, Strelnikova, 1974, p. 59, pl. 8, fig. 1-13 (Plate 10.3, fig. 5)
- Triceratium indefinitum* (Jousé) Strelnikova, 1974, p. 82, pl. 30, fig. 1-29; pl. 31, fig. 1-6 (Plate 10.3, fig. 11, 12)
- Triceratium planum* Strelnikova, 1974, p. 87, pl. 29, fig. 12-17 (Plate 10.3, fig. 7)
- Triceratium tessela* (Krotov) Strelnikova, 1974, p. 84, pl. 29, fig. 8-11 (Plate 10.3, fig. 10)
- Trinacria acutangulum* (Strelnikova) Barron, n. comb.
- Triceratium acutangulum* Strelnikova, 1974, p. 83, pl. 32, fig. 1-10
- Remarks: The markedly elevated apices of this form are typical of *Trinacria* (Plate 10.3, fig. 6, 8-9)

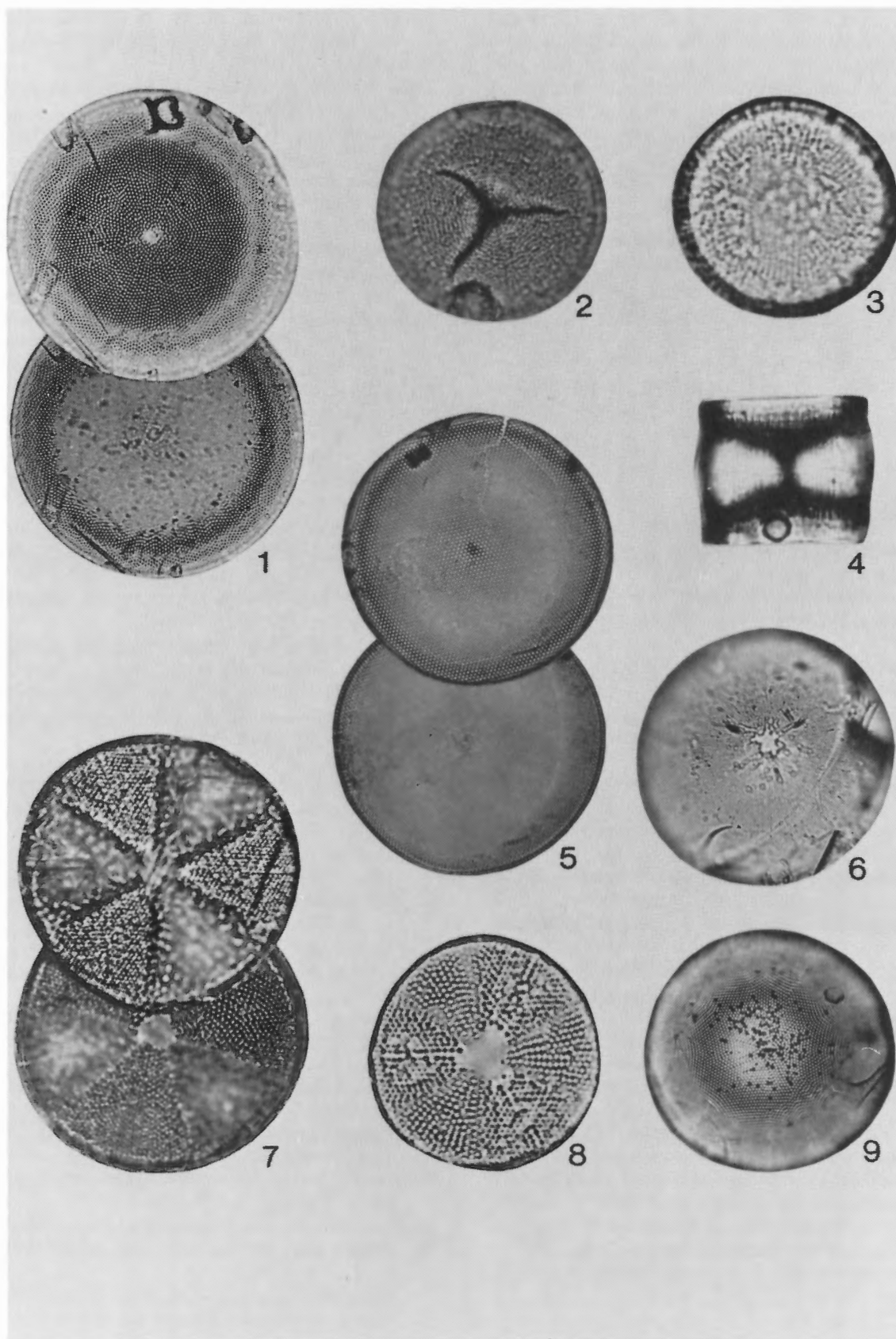


**Plate 10.1 (opposite)**

- Figure 1 *Coscinodiscus circumspectus* Long, Fuge and Smith. High and low focus. Sample 150-152cm. Diameter 75 $\mu$ m.
- Figures 2-4 *Skeletonema polychaetum* Strelnikova. 2. Sample 250-252cm. Diameter 29 $\mu$ m. 3. Sample 250-252cm. Diameter 22 $\mu$ m. 4. Sample 230-232cm. Diameter 27 $\mu$ m. View of margin.
- Figure 5 *Coscinodiscus wittianus* Pantocsek. High and low focus. Sample 290-292cm. Diameter 137 $\mu$ m.
- Figure 6 *Coscinodiscus sibiricus* Strelnikova. Sample 290-292cm. Diameter 60 $\mu$ m.
- Figure 7 *Actinoptychus tenuis* Strelnikova. Low and high focus. Sample 298-300cm. Diameter 43 $\mu$ m.
- Figure 8 *Actinoptychus simbirskianus* A. Schmidt. Sample 250-252cm. Diameter 27 $\mu$ m.
- Figure 9 *Coscinodiscus symbolophorus* Grunow. Sample 298-300cm. Diameter 106 $\mu$ m.



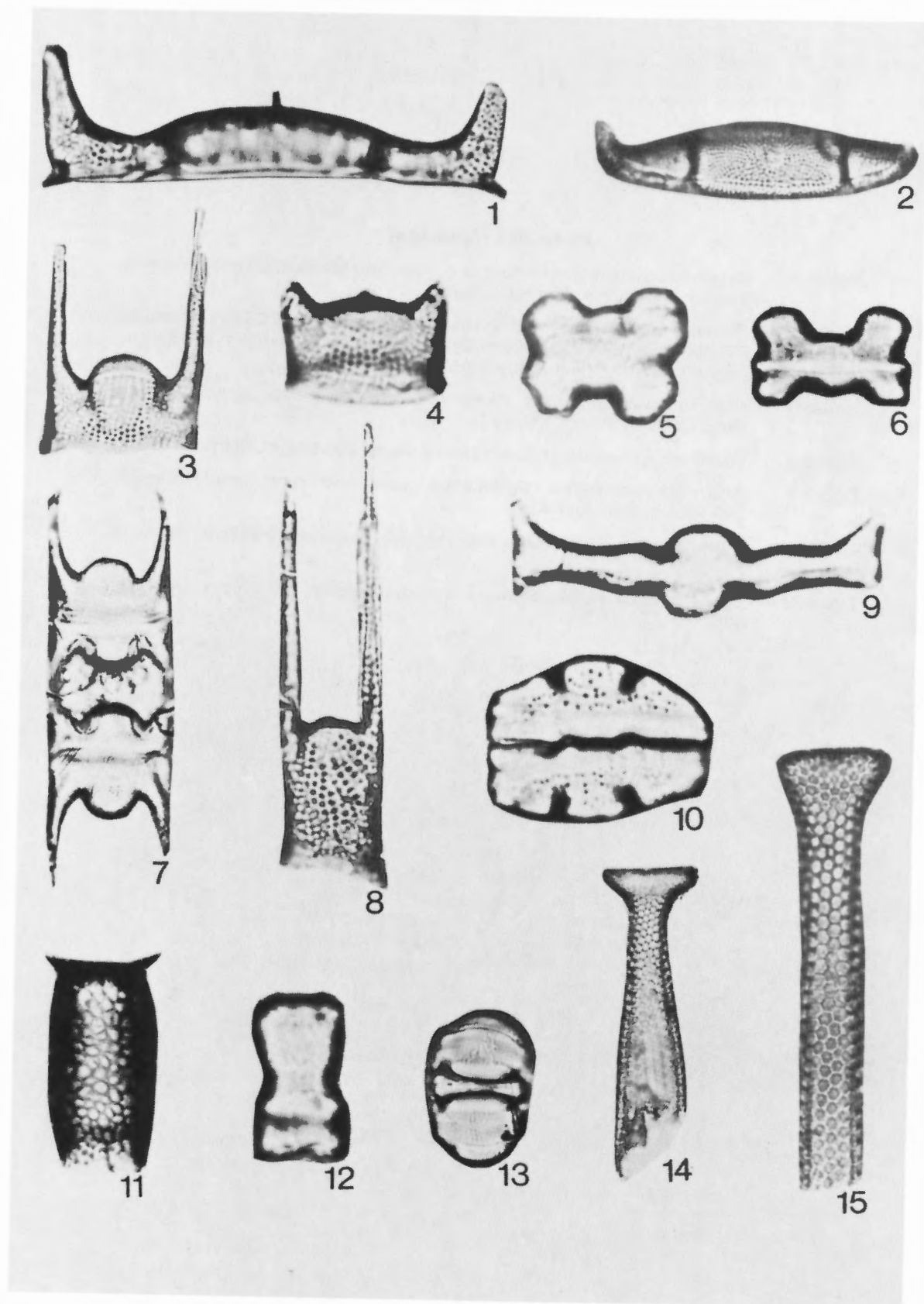


**Plate 10.2 (opposite)**

- Figures 1-2 *Hemiaulus gleseri* Hajos. Sample 250-252cm. Length of base 57 $\mu$ m (fig. 1) and 56 $\mu$ m (fig. 2).
- Figure 3 *Hemiaulus elegans* (Heiberg) Grunow. Sample 250-252cm. Length of base 24  $\mu$ m.
- Figure 4 *Hemiaulus antiquus* Jousé. Sample 250-252cm. Length of base 15 $\mu$ m.
- Figures 5-6 *Hemiaulus tumidicornis* Strelnikova. 5. Sample 250-252cm. Length of base 13 $\mu$ m. 6. Sample 230-232cm. Length of base 17 $\mu$ m.
- Figure 7 *Hemiaulus* sp. cf. *Hemiaulus includens* (Ehrenberg) Grunow. Chain. Sample 298-300cm. Length of base 41 $\mu$ m.
- Figure 8 *Hemiaulus kittoni* Grunow. Sample 250-252cm. Height 41 $\mu$ m.
- Figure 9 *Hemiaulus* sp. 1. Sample 250-252cm. Length of base 30 $\mu$ m.
- Figure 10 *Anaulus sibiricus* Strelnikova. Sample 190-192cm. Length of base 24 $\mu$ m.
- Figure 11 *Pterotheca?* sp. of Strelnikova (1974). Sample 230-232cm. Height 33 $\mu$ m.
- Figure 12 *Hemiaulus* sp. cf. *Hemiaulus tumidicornis* Strelnikova. Sample 250-252cm. Height 12 $\mu$ m.
- Figure 13 *Goniothecium odontellum* Ehrenberg. Sample 298-300cm. Length of base 28 $\mu$ m.
- Figure 14 *Gladius speciosus* f. *speciosus* Schulz. Sample 250-252cm. Length 88 $\mu$ m.
- Figure 15 *Gladius pacificus* Hajos. Sample 250-252cm. Length 75 $\mu$ m.

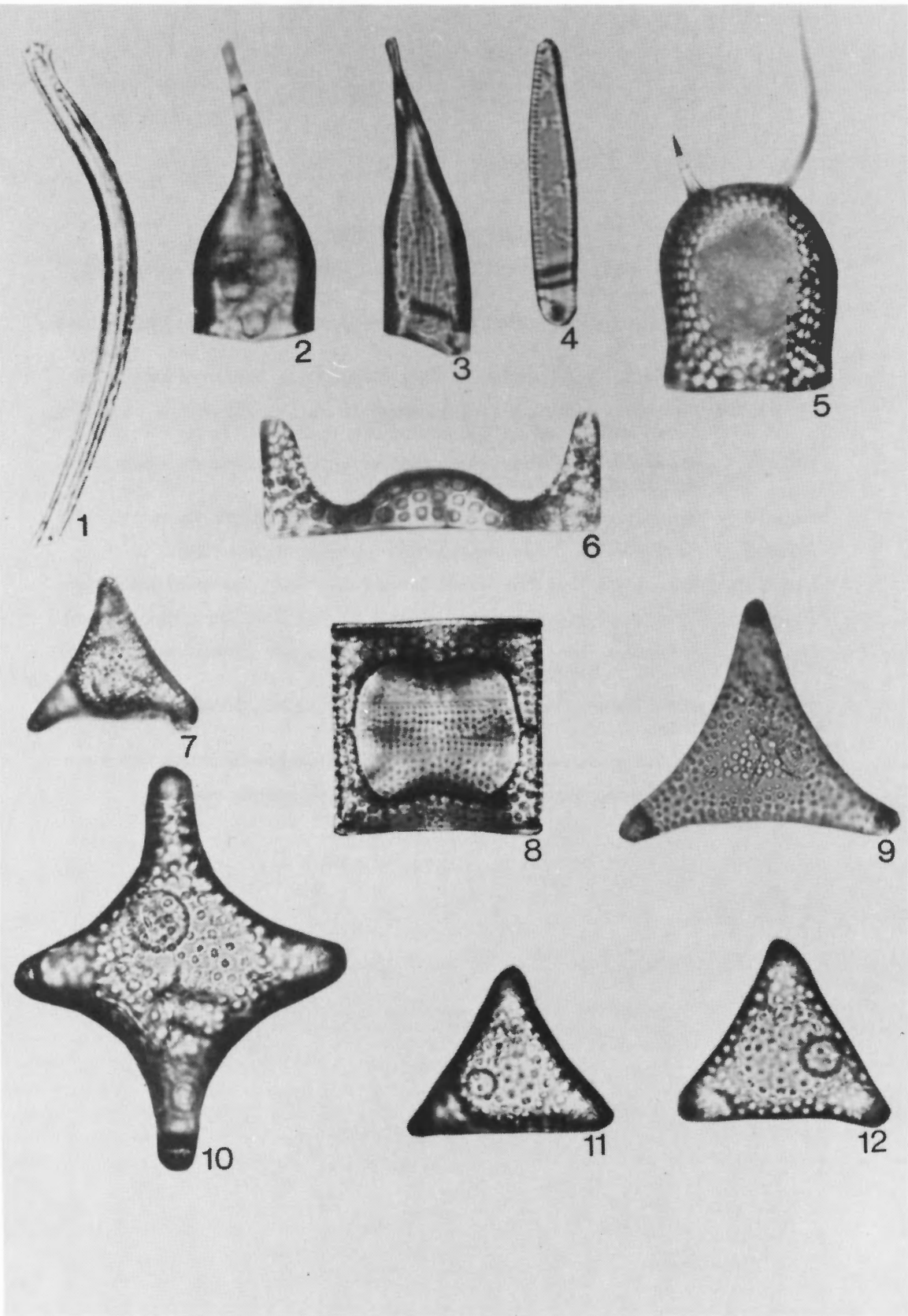


**Plate 10.3 (opposite)**

- Figure 1 *Rhizosolenia cretacea* Hajos and Stradner. Sample 298-300cm. Length 66 $\mu$ m.
- Figure 2 *Rhizosolenia* sp. (thick form). Sample 250-252cm. Length 57 $\mu$ m.
- Figure 3 *Rhizosolenia* sp. (thin form). Sample 230-232cm. Length 29 $\mu$ m.
- Figure 4 *Sceptroneis dimorpha* Strelnikova. Sample 250-252cm. Length 21 $\mu$ m.
- Figure 5 *Stephanopyxis turris* (Greville and Arnott) Ralfs. Sample 230-232cm. Width 24 $\mu$ m.
- Figures 6,8,9 *Trinacria acutangulum* (Strelnikova) Barron, n. comb. 6. Margin view. Sample 134-136cm. Length of base 42 $\mu$ m. 8. Margin view. Sample 298-300cm. Length of base 30 $\mu$ m. 9. Valve view. Sample 250-252cm. Length of base 51 $\mu$ m.
- Figure 7 *Triceratium planum* Strelnikova. Sample 250-252cm. Length of base 41 $\mu$ m.
- Figure 10 *Triceratium tessela* (Krotov) Strelnikova. Sample 170-172cm. Length 55 $\mu$ m.
- Figures 11,12 *Triceratium indefinitum* (Jousé) Strelnikova. 11. Sample 230-232cm. Length of base 26 $\mu$ m. 12. Sample 250-252cm. Length of base 27 $\mu$ m.

## REFERENCES

- Cornell, W.C.  
1972: Chrysomonad cysts and silicoflagellates from the Marca Shale Member, Moreno Formation (Maastrichtian), Fresno County, California; Ph.D. dissertation, University of California, Los Angeles, 235p.
- Gleser, Z.I., Jousé, A.J., and Makarova, I.V. (ed.)  
1974: Diatoms of the U.S.S.R., Fossil and Recent, Volume I; Nauka, Leningrad, 403p. (in Russian).
- Hajos, M.  
1975: Late Cretaceous *Archaeomonadaceae*, *Diatomaceae*, and *Silicoflagellatae* from the South Pacific Ocean, Deep Sea Drilling Project Leg 29, Site 275; In J.P. Kennett, R.E. Houtz *et al.*: Deep Sea Drilling Projects Initial Reports, v.29, p.913-1009.
- Hanna, G.D.  
1927: Cretaceous diatoms from California; California Academy of Sciences, Occasional Papers, v.13, p.5-39.  
1934: Additional notes on diatoms from the Cretaceous of California; Journal of Paleontology, v.8, p.352-355.
- Harland, W.B., Cox, A.V., Llewellyn, P.G., Pickton, C.A.G., Smith, A.G., and Walters, R.  
1982: A Geologic Time Scale; Cambridge University Press, Cambridge, 131p.
- Lewis, M.  
1964: Upper Cretaceous and Lower Tertiary foraminifera from Fresno County, California; Jahrbuch der Geologischen Bundesanstalt, v.9, p.129.
- Long, J.A., Fuge, D.P., and Smith, J.  
1946: Diatoms of the Moreno Shale; Journal of Paleontology, v.20, p.89-118.
- Mudie, P.J. and Blasco, S.M.  
1985: Lithostratigraphy of the CESAR cores, Alpha Ridge; in Initial Geological Report on CESAR — The Canadian Expedition to Study the Alpha Ridge, Arctic Ocean, ed. H.R. Jackson, P.J. Mudie and S.M. Blasco; Geological Survey of Canada, Paper 84-22, report 6.
- Pessagno, E.A. Jr.  
1975: Upper Cretaceous *Radiolaria* from Deep Sea Drilling Project Leg 29, Site 275. In J.P. Kennett, R.E. Houtz *et al.*: Deep Sea Drilling Project Initial Reports, v.29, p.1011-1029.  
1976: Radiolarian zonation and stratigraphy of the Upper Cretaceous portion of the Great Valley Sequence of California; Micropaleontology, Special Publications 2, Micropaleontology Press, New York, 95p.
- Schmidt, A.  
1875-1959: Atlas der Diatomaceenkunde (Begun by A. Schmidt, continued by Schmidt, M., Fricke, F., Muller, O., Heiden, H. and Hustedt, F.); O.R. Reisland, Leipzig, Berlin, 480 plates.
- Strelnikova, N.I.  
1974: Late Cretaceous diatoms of western Siberia; Academie Nauk, SSSR, Roy. 8, 202p. (in Russian).  
1975: Diatoms of the Cretaceous Period; Beih. Nova Hedwigia, v.53, p.311-321.
- Vinogradov, A.P.  
1967-1969: Atlas of the lithological-paleogeographical maps of the U.S.S.R.; Minist. Geol. U.S.S.R. and Acad. Sci. U.S.S.R., Moscow, 255 plates (in Russian).



## PALYNOLOGY OF THE CESAR CORES, ALPHA RIDGE

P.J. Mudie<sup>1</sup>

Geological Survey of Canada

Mudie, P.J., *Palynology of the CESAR cores, Alpha Ridge; in Initial Geological Report on CESAR — the Canadian Expedition to Study the Alpha Ridge, Arctic Ocean*, ed. H.R. Jackson, P.J. Mudie and S.M. Blasco; Geological Survey of Canada, Paper 84-22, p. 149-174, 1985.

### Abstract

Biostratigraphic and paleoecological studies were made of pollen, spores, dinoflagellates, algal spores and palynodebris types in CESAR cores 103, 14 and 6 from the Alpha Ridge, central Arctic Ocean. Palynomorph concentrations are low in all these deep-sea cores, but the stratigraphic ranges of selected taxa can be correlated with established age ranges of North American and European circumpolar pollen genera and with dinoflagellate ranges documented for deep-sea cores in the Bering and Norwegian seas. These palynological data confirm the Pliocene-Recent age assigned to CESAR 103 and 14 by paleomagnetic data and the late Campanian-Paleogene age assigned to the siliceous ooze in CESAR 6, based on silicoflagellate and paleomagnetic data. In the late Cenozoic core, CESAR 103, fluctuations in ratios of arctic- to temperate-climate palynomorphs broadly correspond to global variations in  $^{18}\text{O}$  values reflecting ice volume changes during the past 1 Ma. Changes in concentrations of phytoliths, algal spores, and reworked Paleozoic or Mesozoic palynomorphs suggest that the predominantly arenaceous lithofacies I and L reflect intervals of increased eolian and fluvial terrigenous sediment influx, while the carbonate lithofacies in units J, K and M reflect increased iceberg debris transport. In CESAR 6, very low dinoflagellate concentrations in the Cretaceous-Tertiary siliceous sediments suggest low oceanic productivity; low pollen concentrations also suggest that aerial and fluvial transport of sediment from the circumpolar continental region was minimal during this period.

### Résumé

L'auteur a étudié la biostratigraphie et la paléoécologie des pollens, des spores, des dinoflagellés, des spores d'algues et des types de débris palynologiques trouvés dans les carottes CESAR 103, 14 et 6 de la dorsale Alpha dans la partie centrale de l'océan Arctique. Les concentrations de microfossiles organiques sont faibles dans toutes ces carottes prélevées en eau profonde, mais les répartitions stratigraphiques de certains taxons peuvent être mises en corrélation avec la chronologie établie de divers genres polliniques trouvés dans les régions circumpolaires nord-américaines et européennes et avec les répartitions stratigraphiques de dinoflagellés identifiés dans les carottes prélevées en eau profonde dans les mers de Béring et de Norvège. Les données palynologiques confirment l'âge Pliocène-Holocène donné aux sédiments des carottes CESAR 103 et 14 et établi en fonction des données paléomagnétiques, et l'âge Campanien récent-Paléogène donné à la boue siliceuse dans la carotte CESAR 6 et établi en fonction des silicoflagellés et des données paléomagnétiques. Dans la carotte CESAR 103 (Cénozoïque récent), les variations des proportions de microfossiles organiques arctiques et de microfossiles de climat tempéré correspondent en gros aux variations globales de la teneur en  $^{18}\text{O}$  que reflètent les changements dans les volumes de glace au cours du dernier million d'années. Les variations dans la concentration de phytolithes, de spores d'algue et de microfossiles organiques remaniés d'âge paléozoïque ou mésozoïque semblent indiquer que les lithofaciés surtout arénacées des unités I et L représentent des intervalles caractérisés par un apport accru de sédiments terrigènes fluviaux et éoliens, tandis que les lithofaciés carbonatés des unités J, K et M représentent une période de transport accru des débris par les icebergs. Dans la carotte CESAR 6, les très faibles concentrations de dinoflagellés dans les sédiments siliceux d'origine crétacée et tertiaire attestent d'une période de faible productivité océanique; les faibles concentrations polliniques semblent également indiquer que le transport aérien et fluvial des sédiments à partir de la région continentale circumpolaire était minimal au cours de cette période.

<sup>1</sup>Atlantic Geoscience Centre, Bedford Institute of Oceanography, Box 1006, Dartmouth, Nova Scotia, B2Y 4A2

## INTRODUCTION

Few palynological studies have been made of deep-sea sediments in the Arctic Ocean. Herman (1974) demonstrated the occurrence of plant debris in several cores of Pliocene-Pleistocene sediment from the western Alpha Ridge (ca. 84-85°N, 167-168°W) and noted that intervals of frequent palynodebris occurrence corresponded to zones of low foraminiferal abundance. Initial studies of Fletcher Ice Island cores (Clark, personal communication, 1983) revealed no palynomorphs other than *Thoracosphaera*, a calcareous dinoflagellate. J.P. Bujak (see Blasco et al., 1979) studied the palynomorphs in 5cm long sample intervals from a Lomonosov Ridge core, LOREX B25 (89°10'N, 170°W). Quaternary palynomorphs (mainly bisaccate pollen) were very rare but relatively large numbers of Cretaceous spores and dinoflagellates, and Devonian spore fragments were found, which probably indicate a large amount of sediment redeposition on this ridge. Pleistocene sediments from DSDP Leg 38 in the Norwegian Sea (68-71°N) also contained rare palynomorphs and abundant altered kerogen (Simoneit, 1976), the origin of which was attributed to ice-rafting.

Very low pollen concentrations are expected for modern Arctic Ocean sediments because of 1) the extensive ice cover; 2) predominantly centripetal (southward flowing) polar air movement; and 3) large areas of submerged continental shelves that trap fine grained terrigenous sediments. However, occasional pollen and spore influxes probably do occur as shown by air sample data (Polunin, 1955) collected on Spitsbergen (78°44'N), Jan Mayen Island (71°N) and near Point Barrow, Alaska (71°20'N), and as indicated by snow or ice samples collected from the Canadian Arctic Islands and Greenland (Lichti-Federovich, 1974; J. Bourgeois, Polar Continental Shelf Project, personal communication, 1983). The slow sedimentation rates measured for the Pleistocene CESAR cores (Aksu, 1985a) also increases the likelihood of recovering pollen deposited sporadically over a long period of time. Furthermore, the Cretaceous sediment in CESAR 6 should contain abundant pollen if the hypothesis of Kitchell and Clark (1982) is correct in predicting a warm Arctic Ocean with a seasonally centrifugal (monsoon-type) air circulation pattern.

Palynological studies of two late Cenozoic CESAR cores and CESAR 6 were carried out, with the primary aim being to provide dating control and paleoenvironmental data for sediment intervals lacking calcareous and siliceous microfossils. A secondary aim was to gain insight to the dominant environmental parameters associated with major fluctuations in Cenozoic planktonic foraminiferal populations (see Aksu, 1985b). For example, palynological data could resolve questions about periods of increased freshwater runoff vs. increased ice cover, and acid-resistant palynomorphs may provide evidence pertaining to the oceanographic conditions prevailing during postulated intervals of carbonate dissolution (Herman, 1983). The locations of the core sites are shown in Figure 11.1; the lithology of the cores is described by Mudie and Blasco (1985).

## ACKNOWLEDGMENTS

I thank G.L. Williams and E.H. Davies, Atlantic Geoscience Centre, for their assistance with the identification of CESAR 6 palynomorphs; also Judi Lentin (L.I.B. Consultants Ltd.) for her notes on the Cretaceous dinoflagellates and Elliott Burden (Memorial University of Newfoundland) for his help with Cretaceous pollen taxonomy. I am also grateful to David L. Clark, University of Wisconsin, for providing me with samples from USGS cores FL 437 and FL 422. E.H. Davies reviewed this paper and provided much constructive criticism.

## METHODS

The small sediment sample size (5-10cm<sup>3</sup>) available from the CESAR cores and the expected low palynomorph concentrations required the use of special palynological processing methods. Two methods were tested: 1) processing as described by Barss and Williams (1973); and 2) acid treatment with cold 10% HCl, followed by 52% HF in an ice bath to reduce frothing. Only the latter method yielded residues containing palynomorphs; therefore, this method was routinely used although it was usually impossible to remove the fine clays and amorphous organics which adhered to the palynomorphs despite the use of Darvan and other detergents. Similar palynomorph extraction problems were reported by Manum (1976) for Cenozoic deep-sea sediments from high latitude sites in the Norwegian Sea. Most of the residues extracted from the CESAR samples were so small that they could be mounted on a single slide. Grain counts were made for about half of each slide and the rest was scanned for additional species occurrences. Estimates of total abundances per cm are based on the ratio of the fossil grains counted to a known number of added modern *Eucalyptus* pollen, following the method of Stockmarr (1971).

## RESULTS FROM LATE CENOZOIC CORES

### CESAR 103

Figure 11.2 summarizes the main palynological features of the Cenozoic sediments in CESAR 103, which was sampled throughout at intervals of 1-2.5cm. A list of the main taxa is given at the end of this report. Concentrations of all types of palynomorphs are very low, including pollen and terrestrial plant spores, dinoflagellates, algal spores and phytoliths. Fluctuations in relative abundances of individual taxa are therefore of doubtful significance and the main emphasis has been placed on illustrating major down-core changes in broad taxonomic categories, e.g. percentage of total tree pollen and percentage of subarctic dinoflagellates. It should also be noted that the most common pollen genera (*Pinus* and *Picea*) and dinoflagellate species (*Operculodinium centrocarpum* and *Spiniferites ramosus*) have long stratigraphic ranges (at least Miocene to Holocene); hence, there is some

uncertainty regarding their primary deposition in the Alpha Ridge sediments. However, the stratigraphic ranges of certain pollen taxa (Figure 11.3) that have well-known last occurrences in northwestern Europe (van der Hammen et al., 1971) and Alaska (Leopold, 1969) agree reasonably well with the magnetostratigraphy and  $^{18}\text{O}$  chronology of CESAR 103, and the combined data strongly suggest that most of the palynomorphs reflect penecontemporary deposition during the past 1 Ma. Morphologically distinct reworked pre-Quaternary palynomorphs are rare in most of the core, as shown by the PQ (pre-Quaternary) Index in Figure 11.2. Late Cenozoic index species and the most common palynomorphs in Cenozoic sediments are illustrated in Plate 11.1.

Total concentrations of pollen and spores range from ca. 10 to 430 grains per gram wet sediment, with major peaks

roughly corresponding to isotopic stages 5 (74-128 Ka), stages 11 and 12 (367-478 Ka) and stage 15 (542-592 Ka), according to the time scale of Shackleton and Opdyke (1976). These intervals also correspond to peaks in tree pollen abundances in CESAR 103 (Fig. 11.2) and suggest periods of maximum forest expansion into the regions flanking the Arctic Ocean. Other tree pollen percentage peaks are found, however, which also correspond to warm isotopic stages (e.g. 7, 9, 17, 21, 23) but are not matched by abundance increases; instead, these peaks coincide with spikes in phytolith concentrations, which suggests that they represent intervals of increased eolian transport from arid circumpolar environments.

In the upper half of CESAR 103 (0-55cm), *Pinus* and *Picea* are the main pollen species (ca. 50% total pollen). Rare

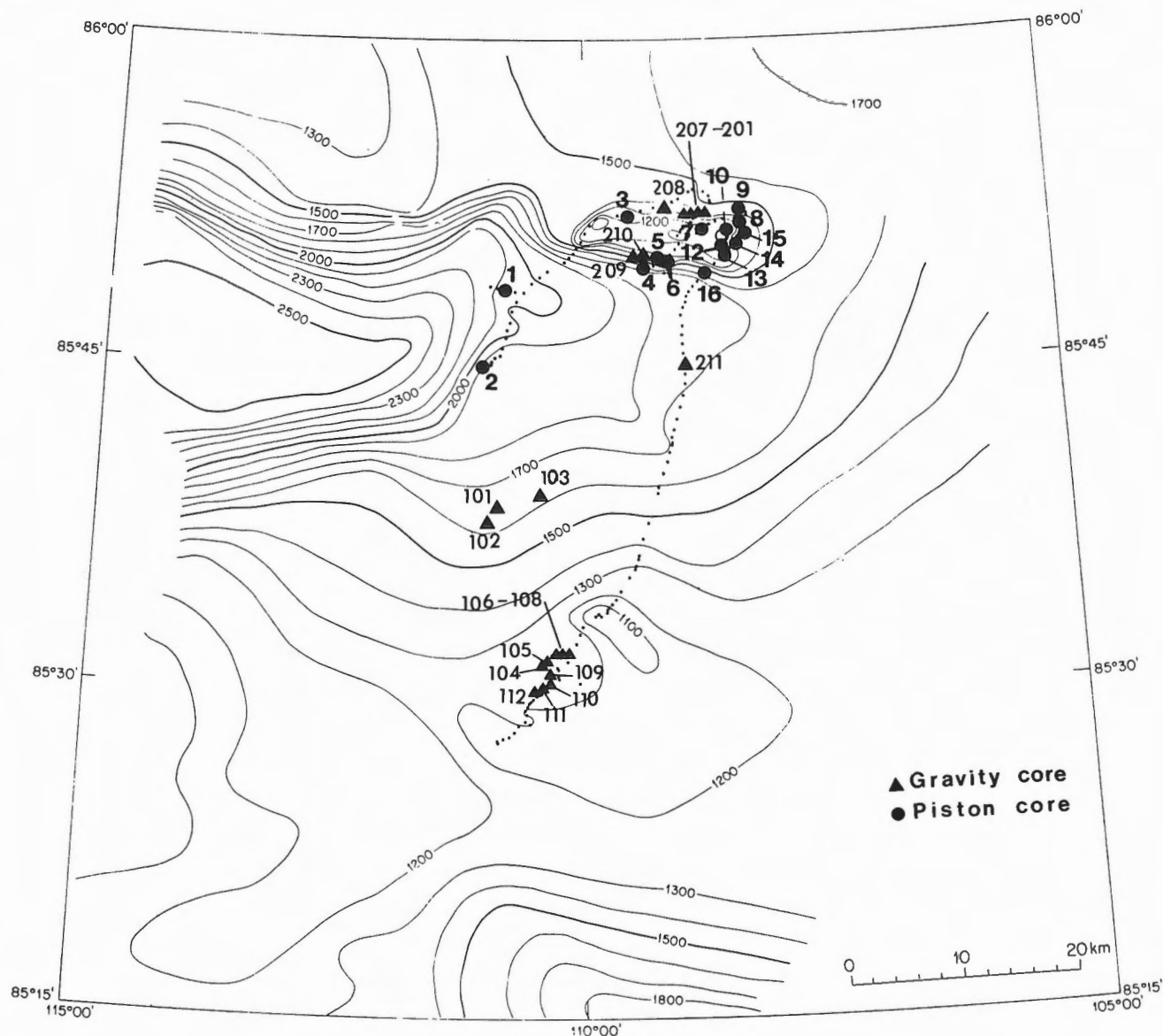


Figure 11.1 Bathymetric map of the eastern Alpha Ridge and locations of the core sites; fine dotted line is the drift track of the CESAR main camp.

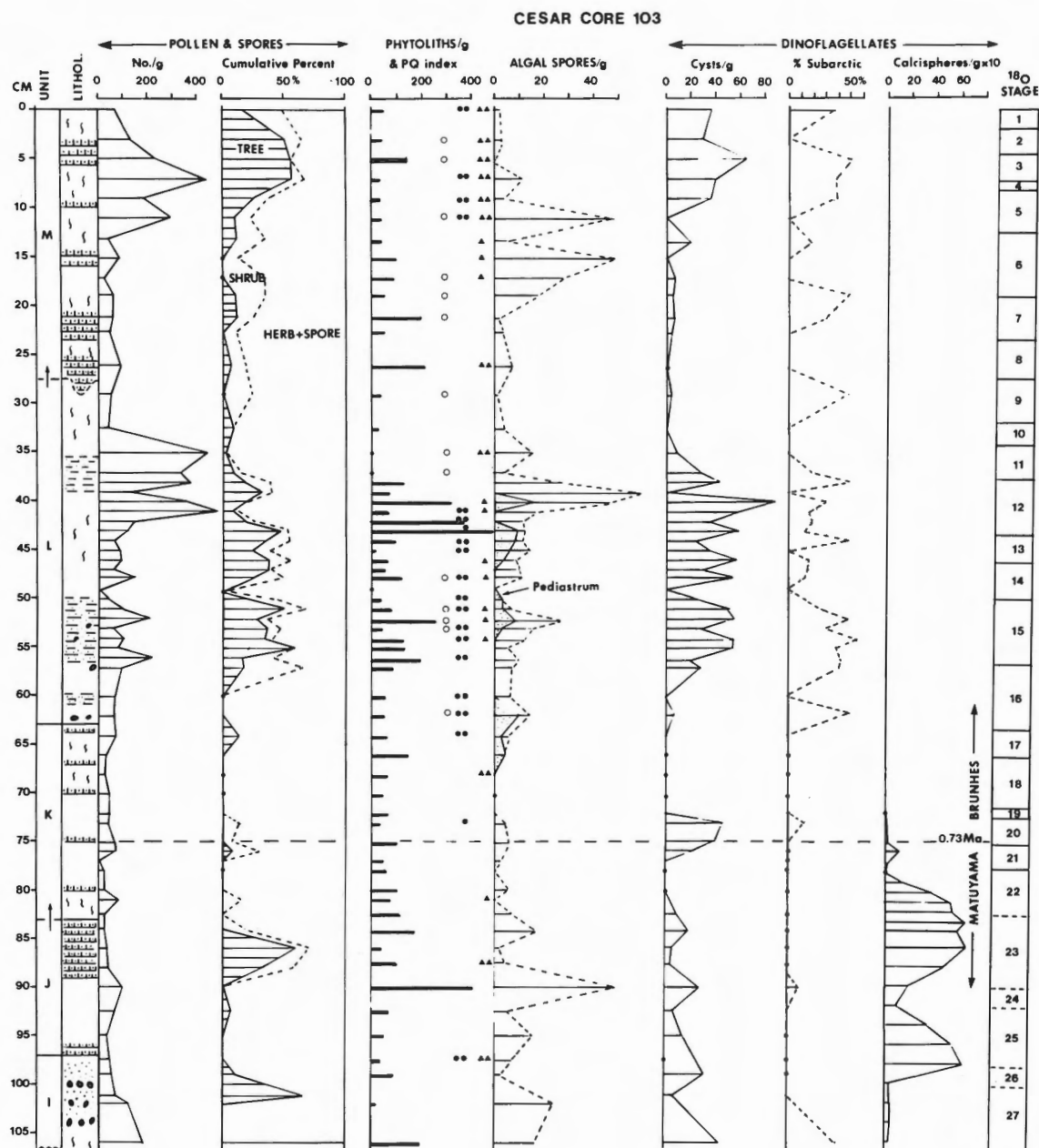


Figure 11.2 Summary diagram of palynomorph distribution in CESAR 103, showing the relationship to lithofacies, and to oxygen isotopic stages of Shackleton and Opdyke (1976) as calculated by Aksu (1985b). PQ index denotes the presence of pre-Quaternary palynomorphs as follows: open circle = Paleozoic acritarch; closed circle = Mesozoic dinoflagellate; triangle = Paleozoic-Mesozoic spores; one symbol = present but rare; two symbols = common. Dashed horizontal line indicates Brunhes-Matuyama boundary as determined from paleomagnetic data of Aksu (1985a).

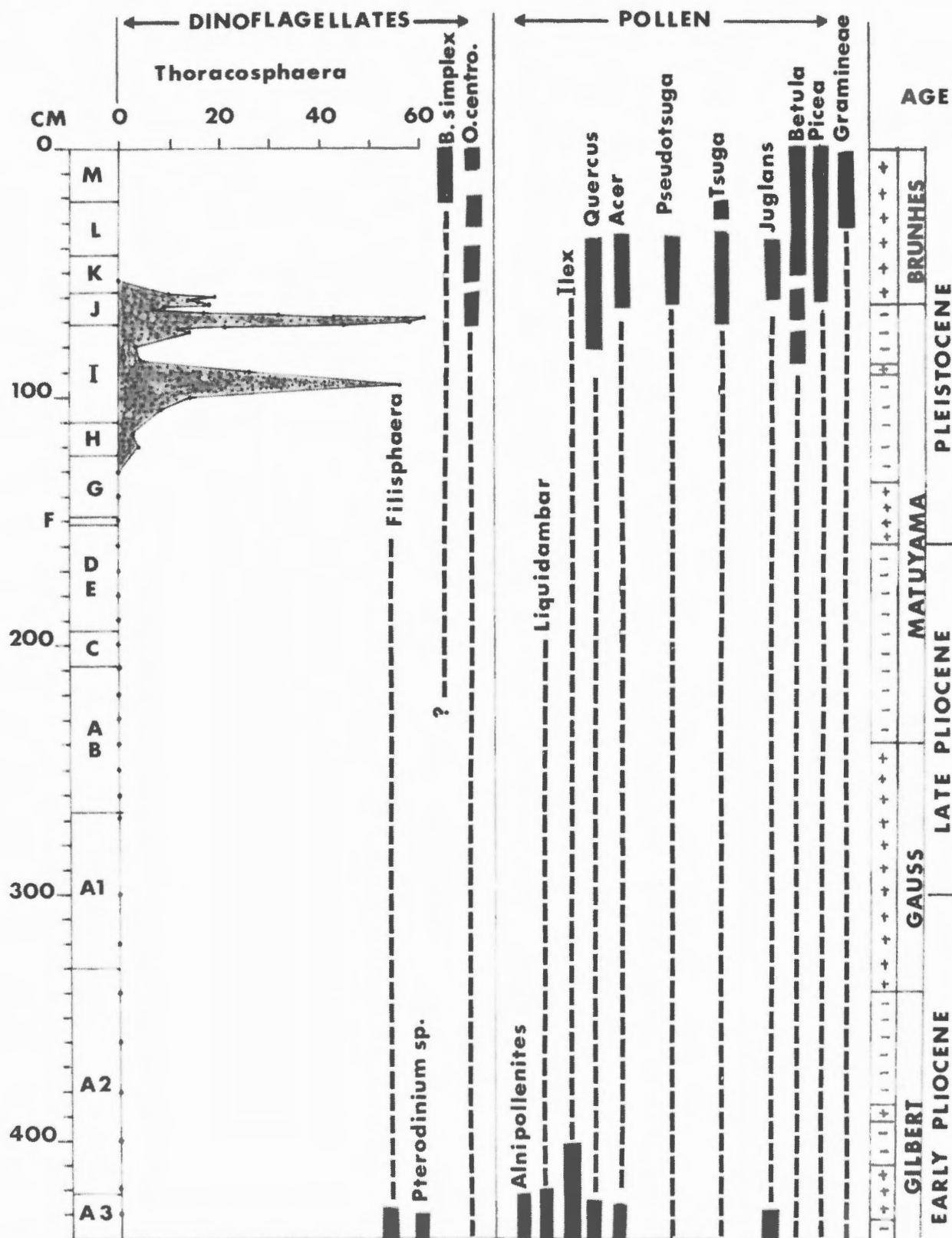
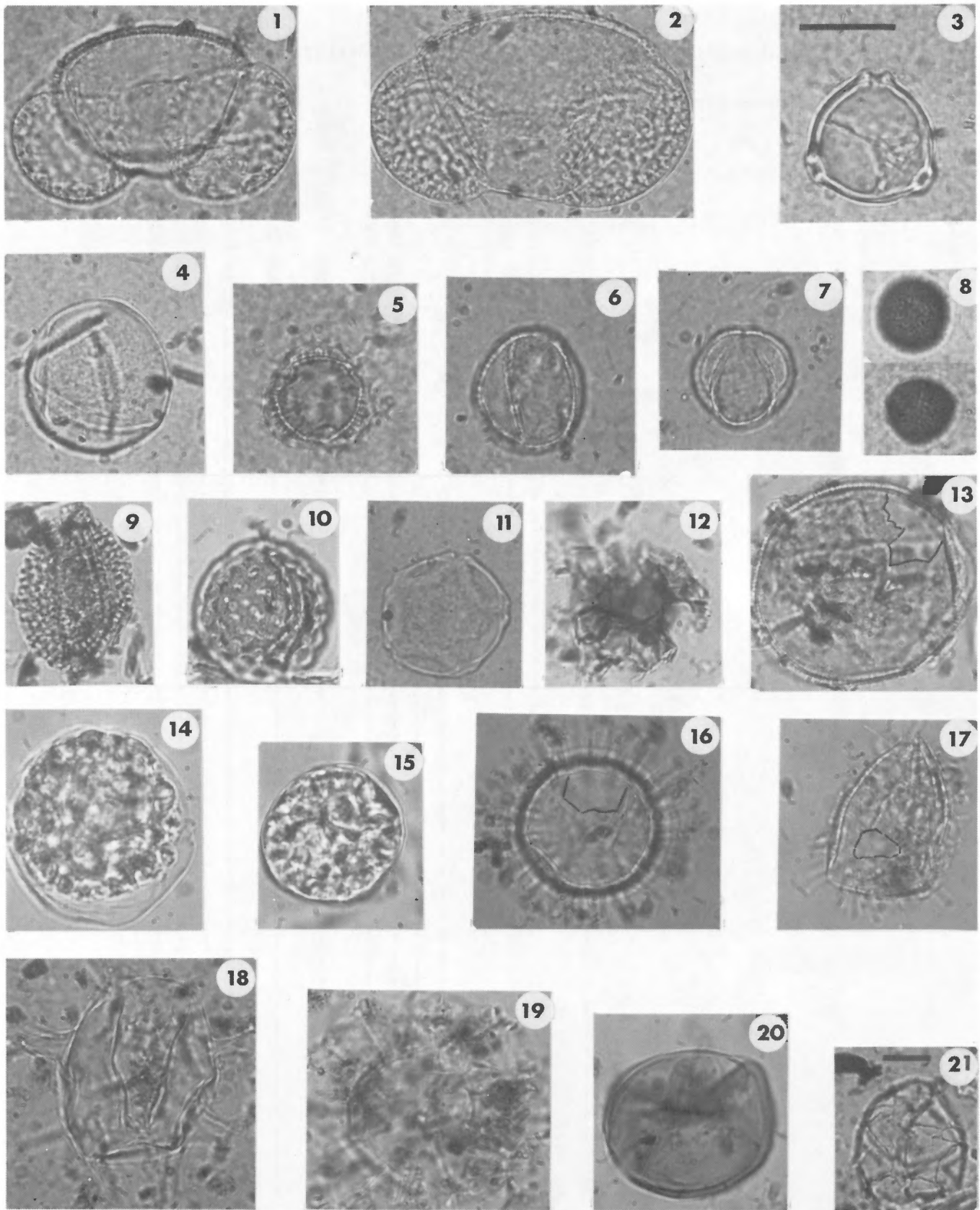


Figure 11.3 Stratigraphic ranges of selected dinoflagellates and pollen compiled using data from CESAR 103 (units M-I) and CESAR 14 (units 1-A3). Time scale is from paleomagnetic data of Aksu (1985a). Solid bars show observed ranges in the CESAR cores; dashed lines show known ranges reported for dinoflagellates by Bujak (1984) for Bering Sea DSDP sites or by Manum (1976) for Norwegian Sea DSDP sites; and ranges of pollen taxa in the Arctic circumpolar region (Leopold, 1969). Presence of *Thoracosphaera arctica* is shown as number per 10g sediment dry weight.





### Plate 11.1 (opposite)

Most common or diagnostic organic-walled palynomorphs found in late Cenozoic-Holocene sediments on Alpha Ridge. Zeiss Universal microphotographs; scale bar = 25  $\mu\text{m}$  for Fig. 3 and Fig. 21; Figs. 1-20 are all the same magnification. Alphanumeric code = England Finder co-ordinates; # = EMG photo negative.

- Figures 1-8 Pollen and spores from CESAR dredge sample 10A. Figure 1: *Pinus* cf. *sylvestris*, oblique ventral view showing subsphaerical sacci constricted at base; exine not verrucate; Z 32/3; # 84427-7. Figure 2: *Picea* cf. *omorika*, T 19/0; # 84427-14. Figure 3: *Betula* cf. *humilis*, exine smooth; grain slightly damaged; Y 41/4; # 84427-9. Figure 4: *Gramineae* sp., slightly folded, with weakly annulate pore in focus; W 45/4; # 84427-12. Figure 5: *Liguliflorae* sp., equatorial focus; Z 26/4; # 84427-8. Figure 6: *Quercus* sp., equatorial view showing relatively long furrows and finely granulate exine; R 35/0; # 84427-17. Figure 7: *Acer* cf. *negundo*, showing faintly granulostriate exine; R 41/3; # 84427-16. Figure 8: Fungal spores, cf. *Ustilago* sp., surface focus; V 29/0; # 84427-13 and 13A.
- Figures 9-13 Pollen and dinoflagellates from CESAR 14, unit A3. Figure 9: *Ilex* sp., equatorial view; T 58/3; # 84427-3. Figure 10: *Liquidambar* sp., surface focus; X 21/2; # 84427-4. Figure 11: *Alnipollenites* sp. 1; D 51/4; # 84427-25. Figure 12: *Pterodinium* sp., showing apical archeopyle; P 50/0; # 84427-5. Figure 13: *Filisphaera filifera*, with archeopyle outline emphasized by ink line; K 40/4; # 84427-6.
- Figures 14-15 Brown ice from LOREX station 112. Figure 14: ?*Gymnodinium* sp., with epitheca opening along the cingulum to release membrane enclosed non-pigmented cell contents; Y 24/4; # 84427-2. Figure 15: *Botryococcus*-type "algal spore"; Z 28/3; # 84427-1.
- Figure 16 *Operculodinium centrocarpum* from DSDP site 611, 4H-2, 48-50cm; F 46/1; # 84427-23; archeopyle outline emphasized by ink lines.
- Figures 17-21 Dinoflagellate cysts from FRAM III, core 9, 0-1cm. Figure 17: *Operculodinium centrocarpum*, showing typical crumpled appearance of Arctic Ocean specimens; archeopyle outline emphasized by ink lines; F 33/0; # 84427-22. Figure 18: *Spiniferites ramosus*, with body and processes slightly folded; Q 34/1; # 84427-20. Figure 19: *Nematosphaeropsis labyrinthea*, with surface trabeculae and epiphragm obscured by clay flocs; N 45/2. Figure 20: *Brigantedinium simplex*, with operculum attached on one edge of archeopyle; O 39/3; # 85527-18. Figure 21: *Impagidinium* cf. *patulum*, ventral surface in focus, hypotheca torn at base; J 37/2; # 84427-21.

amounts of other pollen (*Abies*, *Tsuga*, *Acer* and *Quercus*) occur sporadically in the pollen abundance peaks below 20cm core-depth. Most of the shrub pollen are *Betula*, *Alnus* and *Salix* species; these may be of regional circumpolar origin or may be transported from farther south. *Gramineae*, *Cyperaceae*, *Rumex* and *Artemisia* are the most common herb pollen and are probably of Arctic origin. The largest spore component consists of very small brown fungal spores (Plate 11.1, fig. 9, 10) which resemble those of the grass smut, *Ustilago* (see Bassett et al., 1978). In general, the pollen composition in the surface sediment is similar to that obtained by air pollen traps in Spitsbergen during summer (Polunin, 1955). At this site, the influx of about 1 grain of *Pinus* and *Picea* per cm<sup>2</sup> per year was associated with strong winds from northern Europe. On the Alpha Ridge, the deposition rate of these pollen types is ca. 1 grain per cm per 1000 years; this lower pollen influx is generally consistent with a deep-sea site located more than 200km offshore (Mudie, 1982). Similar low pollen deposition rates are also found in surface sediments from Fram Strait, ca. 250km north of Spitsbergen (Mudie, unpublished data).

In the lower half of CESAR 103 (55-107cm), relative abundances of *Pinus* and *Picea* decrease, and the representation of *Tsuga* and *Quercus* increases. This change appears to be consistent with pollen profiles from pre-Cromerian (0.7 Ma) sediments in northwest Europe (van der Hammen et al., 1971). The predominance (ca. 50%) of thermophilous tree pollen *Tsuga*, *Pseudotsuga*, *Juglans*, *Acer*, *Quercus* and *Ilex* in sediments of the upper Matuyama – lower Brunhes magnetostratigraphic zones of CESAR 103 (Fig. 11.3) suggests that aerial influx of pollen was also from northwest Europe during the middle Pleistocene because these taxa disappeared from the North American circumpolar region by the mid-Pliocene or earlier (Leopold, 1969). Alternatively, these thermophilous tree pollen might reflect stronger meridional air influx from more southerly regions of North America during the mid-Pleistocene; however, the relatively high percentages of *Pinaceae* and *Gramineae* pollen which dominate the boreal-temperate North American floras (Leopold, 1969) makes this a less likely explanation for the mid-Pleistocene Alpha Ridge assemblages.

Phytoliths are mineral-impregnated plant cells which are most commonly produced by herbs (especially grasses) that grow in arid or saline regions (Baker, 1959). Their presence in marine sediments is considered to be a good index of aerial transport from large deserts (Melia, 1982) although transport by runoff and/or ice is also possible. In CESAR 103, peaks in phytolith abundance often coincide with intervals of increased numbers of reworked (PQ) palynomorphs, particularly Mesozoic pollen and dinoflagellates, and Paleozoic spores. The correspondence between reworked palynomorphs and phytoliths suggest stronger current erosion of Arctic slope sediments during periods of intensified polar winds. In contrast, Ordovician-Devonian acritarchs in unit M (0-35cm core depth) are correlated with detrital carbonate layers, suggesting transport by icebergs from the extensive carbonate formations of Ellesmere Island (see Amos, 1985). The arenaceous unit L, however, contains a mixture of acritarchs, PQ dinoflagellates and spores. This

interval corresponds closely to the common occurrence of *Pediastrum* coenobia which usually denote the proximity of large rivers (Chowdhury, 1982), hence a possible fluvial source for the sediments in unit L.

The algal spores shown in Figure 11.2 are of uncertain origin, and they are probably derived from several phyla. Some of these spores resemble resting spores of blue-green algae (Cyanophyta) or small coenobia of the colonial alga *Botryococcus* (Chlorophyta). Their environmental significance in the Alpha Ridge sediments is not clear but it is known that most Cyanophyta are nitrogen-fixing plants; these algae and *Botryococcus* thrive in fresh-water or saline lakes where low nitrogen or other limiting conditions restrict the growth of other algae (Tappan, 1980). Other taxa included with these algal spores are similar to cyst-like bodies associated with a non-pigmented dinoflagellate (?*Gymnodinium* sp.) which is common in samples of "brown ice" obtained during LOREX (see Plate 11.1); these spores may be indicative of ice algae blooms. In CESAR 103, the peaks of algal spores commonly coincide with glacial isotopic stages and they continue to be strongly represented in units J and I below the level (ca. 95cm) at which calcareous dinoflagellates and planktonic foraminifera diminish in abundance.

Late Cenozoic dinoflagellate cysts are poorly represented in the Alpha Ridge cores: their numbers are generally very low and they are mostly poorly preserved compared to specimens from the North Atlantic (see Plate 11.1). In surface samples from the Arctic Ocean, the abundance and preservation state of dinocysts decreases rapidly with distance away from the Norwegian Sea and Fram Strait (see Plate 11.1, fig. 16, 17) and it is not clear if they are formed in situ in the Alpha Ridge area. Bursa (1961) also noted that dinoflagellates are rare in the Canadian Arctic and that cysts were formed by only 3 out of 32 species found at Igloodik (ca. 70°N). In CESAR 103, however, the dinocyst peaks coincide with intervals of increased pollen influx, i.e. during the global warm climatic intervals, at which time there was probably more river discharge containing humic compounds that are required for blooms of gonyaulacoid species (Prakash, 1967). Despite the low total dinocyst concentrations, it is also notable that peaks of common subarctic taxa (*Operculodinium centrocarpum*, *Spiniferites ramosus*, *Tectatodinium pellitum*) generally coincide with warm isotopic stages. This may indicate intervals of increased advection of Atlantic and Pacific water through Fram Strait and Bering Strait during sea level maxima.

In CESAR 103, there is a notable decrease in the frequency of subarctic cyst occurrences below unit L (63cm depth) which corresponds to the top of an interval containing common calcareous-walled dinoflagellates (calcspheres of Gilbert and Clark, 1982). The calcspheres in the CESAR cores (Plate 11.2) and other Arctic cores resemble the planktonic stages of *Thoracosphaera heimii* (Lohmann) Kamptner described by Tangen et al. (1982) but Gilbert and Clark (1982) described the larger thicker-walled Arctic taxon as the resting stage of an endemic species, *Thoracosphaera arctica*. This difference in interpretation of the taxonomy and life stage is important to resolve in light of the correlation between calcspheres and planktonic foram abundances in

sediments below unit K of the Alpha Ridge cores (see fig. 11.2, 11.3). If the calcispheres are cysts requiring high calcium concentrations for their formation and preservation, their occurrence may coincide with carbonate dissolution cycles in the mid-early Pleistocene Arctic Ocean. Alternatively, if the calcispheres are vegetative stages similar to *Thoracosphaera heimii*, they suggest warm, ice-free surface water conditions. Suture-like external and internal wall structures in *Thoracosphaera arctica* specimens from CESAR 14 (Plate 11.2) are more similar to cyst morphologies than those in vegetative cells of *Thoracosphaera heimii*.

## CESAR 14

Palynological studies were carried out on samples from CESAR 14, with the following specific aims: 1) to confirm the apparent stratigraphic continuity between sediments at the base of the gravity core CESAR 103 (units J-I) and units I-A3 in the piston core, CESAR 14; 2) to evaluate the early Pliocene age assigned to unit A3 based on paleomagnetic studies (Aksu, 1985a).

Figure 11.3 shows the frequency distribution of *Thoracosphaera arctica* in the 63-125  $\mu\text{m}$  size fraction of samples from intervals spaced 2.5-20 cm apart in CESAR 14. The frequency of cysts per gram in units K-I is very similar to that found in CESAR 103 (Fig. 11.2) and supports the concept of stratigraphic continuity of the cores. The peak abundances of calcispheres near the top of the Matuyama magnetochron in CESAR 14 also agrees with the data of Gilbert and Clark (1982) who assigned an age range of 2.0-0.7 Ma to *Thoracosphaera arctica*.

Eight samples from units A3 and the base of A2 in CESAR 14 were examined for organic-walled palynomorphs and palynodebris types. These samples were either barren or they contained very low numbers (<100/g) of pollen and algal spores, and rare dinoflagellates (<20/g), together with common, well-preserved phytoliths and wood fibres. All samples also contained abundant highly altered coal fragments; however, reworked Mesozoic or older palynomorphs were not found. The most common pollen are *Quercus* and *Acer*. The sparseness of conifer tree pollen, *Betula* and *Gramineae* is conspicuous relative to the late Quaternary sediments in CESAR 103 and surface samples from ten other CESAR cores (Mudie, unpublished data). In general, the palynomorph assemblages at the base of CESAR 14 are similar to those at the base of CESAR 103, but unit A3 contains 3 pollen taxa (*Alnipollenites*, *Liquidambar* and *Ilex*) and two dinoflagellate species (*Pterodinium* sp. and *Filisphaera filifera*) that are not present in sediments of the Brunhes-upper Matuyama magnetochron (see Fig. 11.3). According to Leopold (1969), the stratigraphic tops of *Liquidambar* and *Ilex* in northern North America and Europe are at or below the Pliocene-Pleistocene boundary. The *Pterodinium* sp. with an apical archeopyle (Plate 11.1, fig. 12) closely resembles *Dinocyst* sp. V of Manum (1976) which has a late Oligocene to mid-Miocene range in DSDP cores from the Norwegian Sea and is common in early Pliocene sediments of DSDP site 611, south of Iceland (Mudie, unpublished data). The only other dinocyst present in unit A3

(Plate 11.1, fig. 13) resembles *Filisphaera filifera* Bujak (1984) which has a late Miocene-early Pleistocene range in DSDP cores from the Bering Sea. The combined palynomorph data from the base of CESAR 14 indicate a minimum early Pleistocene age for unit 3 and they do not conflict with the early Pliocene age assignment based on paleomagnetic data.

## RESULTS FROM CESAR CORE 6

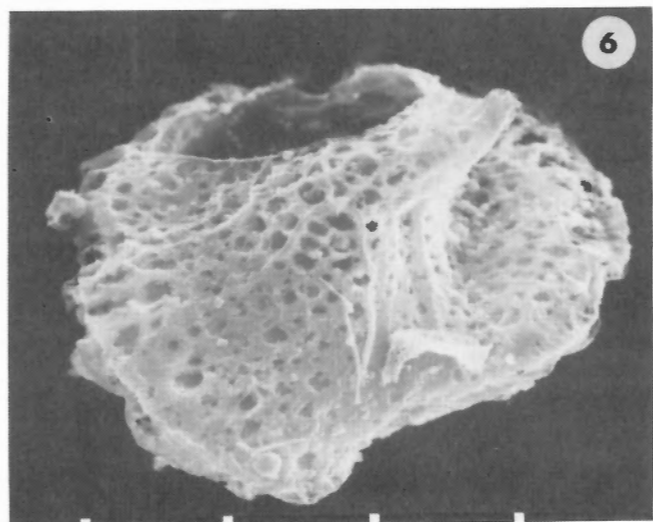
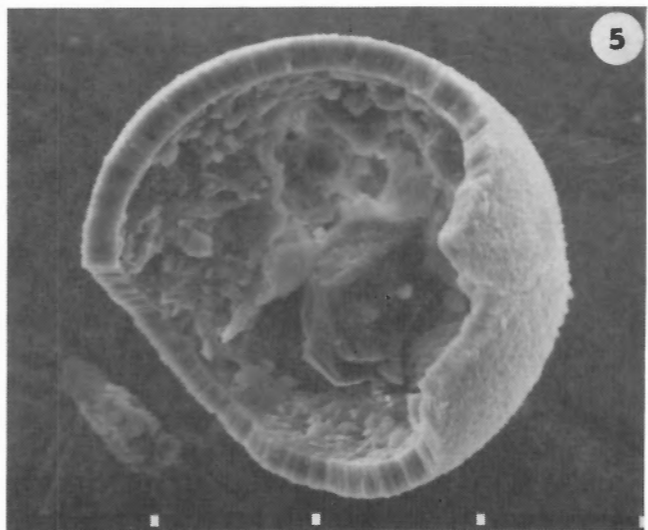
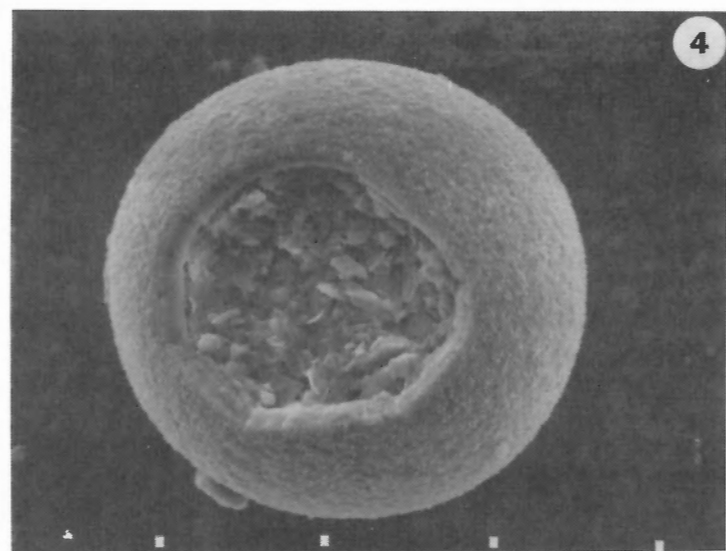
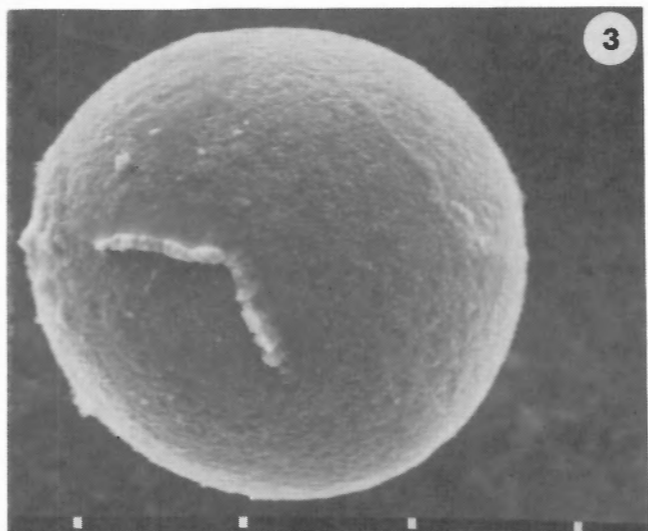
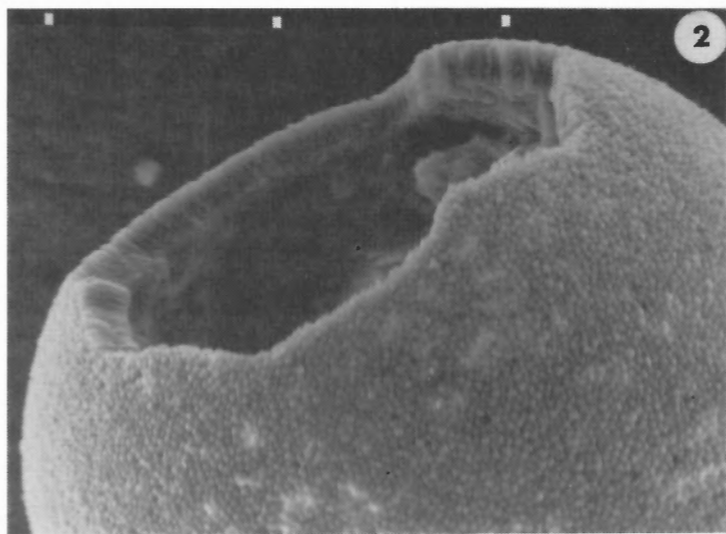
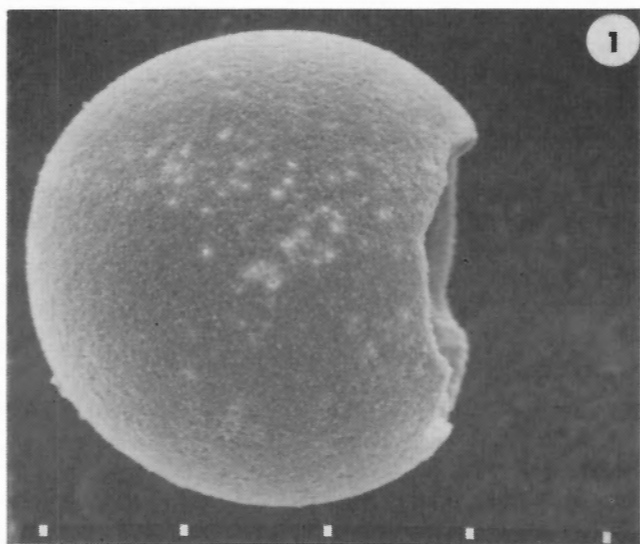
Thirty samples from Cretaceous-late Cenozoic sediments in CESAR 6 were processed for palynological study (Table 11.1). In addition, samples of late Mesozoic-early Cenozoic biosiliceous sediments (Clark, 1974; Bukry, 1984) from Alpha Ridge USGS cores FL 437 (Late Cretaceous) and FL 422 (Middle Eocene) were studied in an attempt to correlate the Arctic Ocean palynomorph assemblages of the laminated siliceous sediment in CESAR 6, unit 4 (see Mudie and Blasco, 1985). One sample from the inner core of a volcanic rock dredged from the Alpha Ridge (see Jackson, 1985) was also studied in an attempt to provide a minimum age for the rock exposed at the ridge crest.

Almost all of the above samples contained very low numbers of palynomorphs although unaltered wood fragments and phytoliths were common (Table 11.1). However, samples from the core catcher of CESAR 6 and from the USGS cores contained common-abundant pollen, spores and acritarchs, and occasional dinoflagellates. Preliminary analyses were made of these samples by G.L. Williams (AGC, Dartmouth), J.K. Lentin (L.I.B. Consultants Ltd., Calgary) and Elliott Burden (MUN, Newfoundland); however, paleoenvironmental interpretations are those of the author. A list of Mesozoic-Paleogene taxa is given at the end of this report; for simplicity, the names of diagnostic taxa cited by Doerenkamp et al. (1976) for the Canadian Arctic Islands region are used here and in Table 11.2.

### Microplankton Biostratigraphy

Table 11.1 shows that dinoflagellates and acritarchs are rare or absent in units 1-3 of CESAR 6. Table 11.2 lists the dinoflagellates and acritarchs which have been identified from CESAR 6, unit 4. This table also shows the occurrence of these or morphologically very similar taxa in core FL 422, the Canadian Arctic Islands, and other regions which may have been linked by major seaways to the Mesozoic-Paleogene Arctic Ocean. Most of these taxa are illustrated in Plate 11.3. It should be noted, however, that two stratigraphic guide taxa, *Spongodinium* cf. *delitiense* (Plate 11.2, 11.3) and *Paleoperidinium* cf. *pyrophorum* (Plate 11.3), of the Alpha Ridge cores may not be conspecific with the Arctic Islands and North Atlantic taxa (Lentin, personal communication, 1984). Central Arctic Ocean floral endemism is discussed by Bukry (1985), but following the lead of both Bukry (1985) and Barron (1985), it is assumed that the two Alpha Ridge dinocyst taxa noted above are closely related to, and of approximately the same age as, *Spongodinium delitiense* and *Paleoperidinium pyrophorum*, respectively.







The main features that emerge from Table 11.2 are summarized as follows. 1) Most of the microplankton appear to be of Maastrichtian-Paleocene age, with a strong Canadian Arctic Islands affinity. 2) Some older late Cretaceous taxa are also present but these are confined to samples from the core-catcher and subunit 4C (see Mudie and Blasco, 1985) which contain abundant coaly particles (Plate 11.4) and several dark, poorly preserved Albian-Cenomanian spores (see Plate 11.5) which suggest that the lowest part of CESAR 6 includes some older reworked sediment. 3) The most common microplankton in CESAR 6, unit 4, are also present in FL 422 which has a Paleogene or Eocene age based on silicoflagellates (Clark, 1974; Bukry, 1984).

Unfortunately, the most common taxa in CESAR 6 are acritarchs or other algae, such as *Palambages*, which are of uncertain phylogenetic and paleoecological affinity. The sparseness of dinoflagellates above unit 4C in CESAR 6, and in cores FL 437 and FL 422 is enigmatic, and it is presently unclear whether this reflects poor preservation (pollen, however, are mostly well preserved) or unfavourable paleoenvironmental conditions. Lack of dinoflagellate data from high latitude Cretaceous-Tertiary deep-sea sites strongly constrains interpretation. It is notable, however, that Eocene sediments in the Bering Sea (Bujak, 1984) also contain few dinoflagellate species (including *Impagidinium vellorum* which is present in most of the Alpha Ridge siliceous sediments). Dinoflagellate species diversity in the North Pacific increases in proportion to diatom diversity in the late Miocene, however, and Bujak (1984) suggested that this change reflects increased upwelling and nutrient availability.

By analogy, then, it is suggested that the low diversity Alpha-Ridge dinoflagellate assemblages reflect a low productivity oceanic environment.

### Pollen Stratigraphy

Table 11.1 shows the relative abundances of pollen and spores in samples from CESAR 6 and other Alpha Ridge samples examined. The most important pollen and spores are illustrated in Plates 11.5 and 11.6. In general, pollen concentrations are low (<10/g); most grains, however, appear fairly well preserved although samples from unit 4B show some oxidation. Dark, thermally altered pollen and spores are rare and are mostly confined to unit 4C and unit 1; these palynomorphs appear to be reworked from pre-Campanian Mesozoic sediments.

Table 11.3 shows the occurrences of the pollen taxa identified in CESAR 6. Four palynozones are tentatively delimited as described below.

**Zone 1 (core catcher).** This assemblage is marked by the frequent occurrence of Cretaceous bisaccate and vestibulate pollen which have range tops in the late Campanian of North America (Tschudy, 1973), including *Alisporites bilateralis*, *Cedripites cretaceus*, *Phyllocladites microreticulatus* and *Triatriopollenites costatus*. This assemblage is generally similar to that of the Late Campanian-Maastrichtian Horton River section (District of Mackenzie) described by McIntyre (1974), except for the presence of several *Ulmoideipites* species and the absence of *Aquilapollenites* species. The latter may reflect differential sorting of large taxa which are not

### Plate 11.2 (opposite)

SEM photographs of dinoflagellate cysts from CESAR cores. Figures 1-5 show *Thoracosphaera arctica* from CESAR 14, 64-65cm core depth (from B. Deonarine, AGC); figure 6 shows *Spongodinium* cf. *delitiense* from CESAR 6, core catcher (from F.E. Cole, AGC). Scale marks = 30µm intervals; # = EMG SEM sample number.

- Figure 1 Specimen of *Thoracosphaera arctica* with Type I morphology, showing uniformly fine grained surface and irregular ?pentagonal aperture, with V-shaped notches possibly reflecting plate boundaries; # 1148-04.
- Figure 2 Specimen of *Thoracosphaera arctica*, tilted to show details of wall structure and ?excystment aperture; # 1148-05.
- Figure 3 Specimen of *Thoracosphaera arctica* with more irregular Type II surface texture and with smooth-edged V-shaped sutures perhaps marking paraplate boundaries in at the start of excystment; # 1148-03.
- Figure 4 Specimen of *Thoracosphaera arctica* with Type II surface texture, showing a less angular aperture, possibly due to post-excystment loss of the angular plate delimited in figure 3. Specimen is infilled by clay; # 1148-02.
- Figure 5 Specimen of *Thoracosphaera arctica* broken to show apparently ridged inner wall morphology which does not resemble that of *Thoracosphaera heimii* vegetative cells; # 1148-01.
- Figure 6 Apical view of *Spongodinium* cf. *delitiense*, showing the concave ventral surface and epicyst plates, and the dorsal archeopyle formed by loss of paraplate 3"; # 1120-1.

Table 11.1 Distribution of palynomorphs and palynodebris types in CESAR 6. A = abundant (>50); C = common (15-50); O = occasional (5-14); R = rare (1-5); DR = reworked.

	Pollen and spores	Dinocysts and acritarchs	Coal	Phytoliths and wood	Amorphogen	Algal spore	Foram lining	Faecal pellet
Core top 0-1cm	barren							→
3-4	—	DR	O	R	—	R		
6-7	O	-	C	R	—	R		
9-10	—	—	—	O	—	—		
12-13	R	DR	—	R	—	R		
15-16	R	—	O	R		R		
18-19	—	R	C	R		R		
21-22	barren							→
Unit 1 0-2	DR	—	A	—	—	R		
3-6	←			barren	—			→
8-11	←			barren	—			→
96-98	DR	DR	C	C	—	O	—	
Unit 2 99-101	R	DR	C	A	—	O	—	
Unit 3 120-123	DR	—	—	O	+	O	R	
Unit 4 127-129	O	R		A	—	—	—	
134-136	R	—	R	A	—	R	R	
150-152	R	R	—	A	—	C	—	
170-172	C	R	—	A	A	R	—	
190-192	—	R		C	—	O	—	
210-212	R	R	—	A	—	R	—	
230-232	O	R	—	C	—	R	—	
250-252	barren							→
270-272	C	R	—	C	O	C	—	+
290-292	C	—	—	O	R	R	R	+
298-300	C	O	C	C	C	R	—	+
(dark) 302-304A	R	C	C	C	A	—	—	+
(light) 302-304B	O	C	—	C	R	—	—	+
Core 366-340A	C	C	—	R	A	—	R	+
Catcher 366-340B	C	O	—	R	A	—	—	+
FL 437 seg. 11	C	R	R	O	A	C	—	+
FL 422 seg. 13	C	C	—	R	A	C	—	+
Volcanic rock core	R	—	—	O	—	R	—	—

likely to be transported to a deep-water offshore location such as the Alpha Ridge. However, *Aquilapollenites* is rarely found in northeastern parts of North America (Norris et al., 1975); therefore, a more Atlantic provenance may be indicated. Furthermore, the presence of Ulmaceae pollen may indicate a younger (Late Maastrichtian-Paleocene) age.

**Zone 2 (304-270cm).** This zone is characterized by the presence of *Wodehousia gracile* which has a restricted middle Maastrichtian age range in the Kanguk Formation of the Canadian Arctic (Doerenkamp et al., 1976). This zone is also marked by the lowest occurrence of *Pistillipollenites mcgregorii* and by *Nyssapollenites* sp. A of Rouse (1977) which have a Paleocene-Eocene range in the Canadian Arctic Islands. Other taxa in Zone 2, e.g. *Classopollis* and *Podocarpites*, have Middle to Late Cretaceous range tops in northern

North America and are probably reworked. Zone 2 closely corresponds to subunit 4C in CESAR 6 and appears to represent assemblages transitional from the Late Cretaceous to Paleocene.

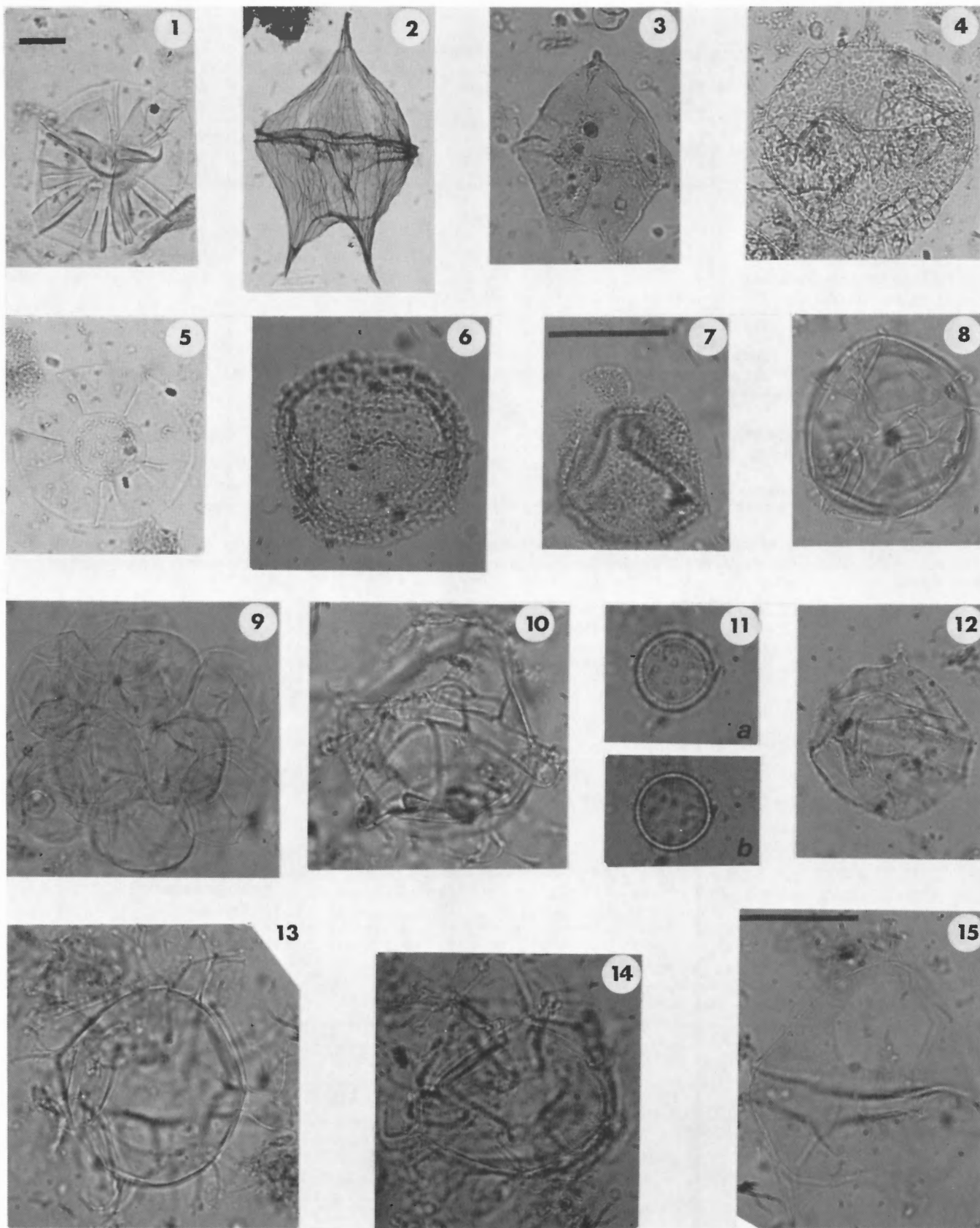
**Zone 3 (250-135cm).** This zone contains relatively few pollen and spores, and includes barren intervals at 250 and 190cm core depth; it is the least clearly defined of the four zones. It is marked, however, by the last occurrences of several typical conifer and reticulate tricolpate pollen types that characterize the Late Cretaceous pollen floras of North America (see Singh, 1975). The top of the zone is placed just below the base of the first appearance of typical *Platycarya*-type triatriate taxa which characterize the Paleogene floras of North America (Rouse, 1977). The top of this zone also corresponds closely to the top of subunit 4B in CESAR 6.

Table 11.2 Microplankton taxa in CESAR 6, unit 4 and occurrences of these or closely related taxa in other geographical regions as reported by 1) Doerenkamp et al., 1976; 2) Bujak, 1984; 3) Williams and Bujak, 1977; 4) Stover, 1977.

Alpha Ridge, CESAR 6	Canadian Arctic Islands <sup>1</sup> :			Alpha Ridge	N. Pacific <sup>2</sup>	N.W. Atlantic	
	Horton Fm	Kanguk Fm	Eureka Sound Fm	FL 422	DSDP sites 183-192	Eastern Canada <sup>3</sup>	Eastern U.S.A. <sup>4</sup>
	Albian	Maastrichtian - Danian	Paleocene	Eocene	Eocene-Oligocene	Maastrichtian - Paleocene	Eocene-Oligocene
<i>Cleistosphaeridium aciculare</i>	+						
" <i>Deflandrea</i> " <i>diebeli</i>		+				+	
<i>Gonyaulacysta</i> sp. B						+	
<i>Impagidinium vellorum</i>				+	+		
<i>Kallosphaeridium biornatum</i>							+
" <i>Kalyptea</i> " <i>aceras</i>	+						
" <i>Lejeunia</i> " <i>kozłowski</i>							
<i>Microdinium ornatum</i>	+						
<i>Micrystridium</i> sp.				+			
<i>Palambages</i> f. A		+	+	+		?	
? <i>Palaeoperidium pyrophorum</i>	+	+		?		+	
<i>Pterodinium aliferum</i>	+						
<i>Pterospermopsis australiensis</i>	+						
<i>Pterospermopsis ginginensis</i>				?			
<i>Spiniferites ramosus</i>			+	+		+	
<i>Spongodinium</i> cf. <i>S. delitiense</i>		+	+				

Table 11.3 Occurrences of pollen and spores in CESAR 6, core catcher, unit 4 (127-304cm), unit 3 (120cm) and unit 2 (100cm). + indicates present but rare; ++ indicates common. Systematic listing of pollen and spores is given at the end of this report.

Core catcher	CORE-DEPTH (cm)														
	304	300	290	270	250	230	210	190	170	150	135	127	120	100	
++															Alisporites bilateralis
++															Cedripites cretaceus
+															Phyllocladites microreticulatus
+															Triatriopollenites costatus
++-----++															Podocarpites multesimus
++-----+															Ulmoideipites spp.
++-----+-----+															Classopollis sp.
++-----+-----+-----+															Triporopollenites bituitus
++-----++-----+															Tricolpites spp.
++-----+-----+-----+-----+															Abietinaepollenites
++-----+-----+-----+															Fraxinoipollenites
++-----+-----+-----+															Taxodium sp.
++-----+-----+-----+-----+-----+															Tricolporopollenites sp.
-----++-----++-----++-----+															Wodehousia gracile
++-----+-----+-----+															Nyssapollenites sp. A
++-----++-----++-----+-----+															Paraalnipollenites confusus
++-----+-----+-----+-----+															?Quercoidites sp.
++-----+-----+-----+-----+-----+															Alnipollenites spp.
++-----+-----+-----+-----+-----+															Pistillipollenites mcgregorii
++-----+-----+-----+-----+-----+															Tricolporate sp. A
++-----+-----+-----+-----+-----+															Kurtzipites sp.
++-----+-----+-----+-----+-----+															Monosulcites sp.
++-----+-----+-----+-----+-----+															Glyptostrobus vacuipites
++-----+-----+-----+-----+-----+															?-----Platycaryapollenites
++-----+-----+-----+-----+-----+															+-----Compositoipollenites
++-----+-----+-----+-----+-----+															+-----Caryapollenites
++-----+-----+-----+-----+-----+															+-----Picea sp.
++-----+-----+-----+-----+-----+															?-----Podocarpites parvus
++-----+-----+-----+-----+-----+															+-----Tilia crassipites
Zone 1	Zone 2				Zone 3					Zone 4					



### Plate 11.3 (opposite)

Dinoflagellate cysts, acritarchs and other organic-walled microfossils from CESAR 6. Transmitted light photographs, Zeiss Universal. Scale bar = 20µm for figures 1-6; scale bar = 25µm figs 7-15; c.c. = core catcher sample; alphanumeric codes = England Finder co-ordinates; # = EMG photo negative.

- Figure 1 *Impagidinium vellorum*, showing distinctive high membranous sutural crests with smooth distal margins; c.c. sample CESAR 6B, Q 13/4; # 84409-19.
- Figure 2 "*Lejeunea*" *koslowski*, a morphotype similar to that in the Kanguk Formation (Doerenkamp et al., 1976); c.c. sample CESAR 6B, 63-125µm fraction, P 32/2; # 88417-8.
- Figure 3 *Palaeoperidinium* cf. *pyrophorum*, a morphotype with visible panda-sutural lines and granules on the endocyst; c.c. sample CESAR 6B, M 25/0; # 84409-16.
- Figure 4 *Spongodinium* cf. *delitiense*, showing vesicular ornament and well developed antapical lobes; c.c. sample CESAR 6B, G 15/2; AGC # 84409-3.
- Figure 5 *Pterospermopsis australiensis*; c.c. sample CESAR 6B, G 48/2; # 84409-1.
- Figure 6 Dinocyst species 1; CESAR 6, 230-232cm, U 9/0; # 84329-36.
- Figure 7 *Kallosphaeridium biornatum*; c.c. sample CESAR 6B, F 42/3; # 84409-8.
- Figure 8 ?*Microdinium ornatum*; c.c. sample CESAR 6B, E 50/1; # 84409-10.
- Figure 9 *Palambages* form A; c.c. sample CESAR 6B, F 33/4; # 84409-6.
- Figure 10 ?*Pterodinium aliferum*, morphotype with weakly developed tubular gonol processes and connecting membranous septa; c.c. sample CESAR 6B, M 28/0; # 84409-15.
- Figure 11 *Cymatiosphaera punctifera*; c.c. sample CESAR 6B, E 50/1; # 84409- 10. a) surface focus; b) equatorial focus, showing pentagonal fields bounded by low membranes, each field with a prominent central thickening.
- Figure 12 ?*Gonyaulacysta* sp. B; CESAR 6, 230-232cm.
- Figure 13 *Spiniferites* sp., possibly *Spiniferites ramosus*, but with spines much longer, thinner and more branched than in modern Arctic sediment; c.c. sample CESAR 6B, L 6/1; # 84409-18.
- Figure 14 *Achomosphaera* sp. like *Achomosphaera ramulifera* of Manum (1976), with long, weak multifurcate processes ending in rosette-like complexes in the paracingular region; adjacent spines sometimes touching, but not interconnected by trabeculae; FL 422, R 47/1; # 84411-4.
- Figure 15 ?*Deflandrea* sp. 1, archeopyle in focus; FL 422, Y 54/1; # 84411-1.



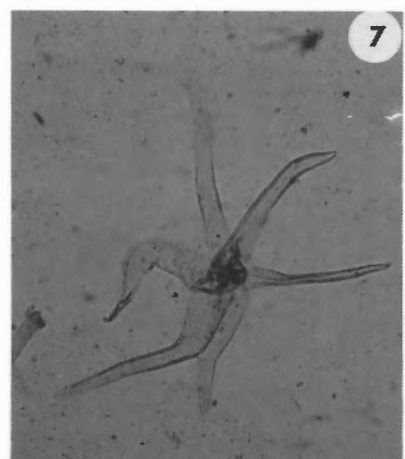
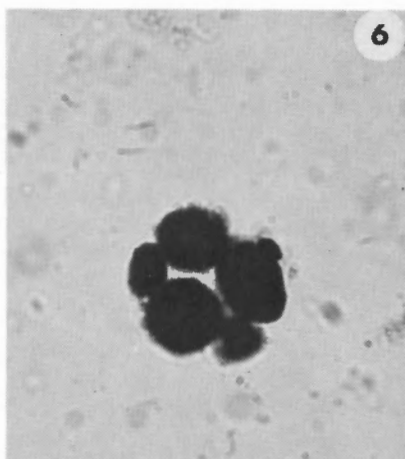
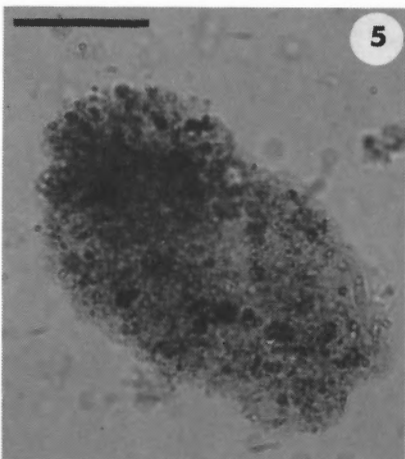
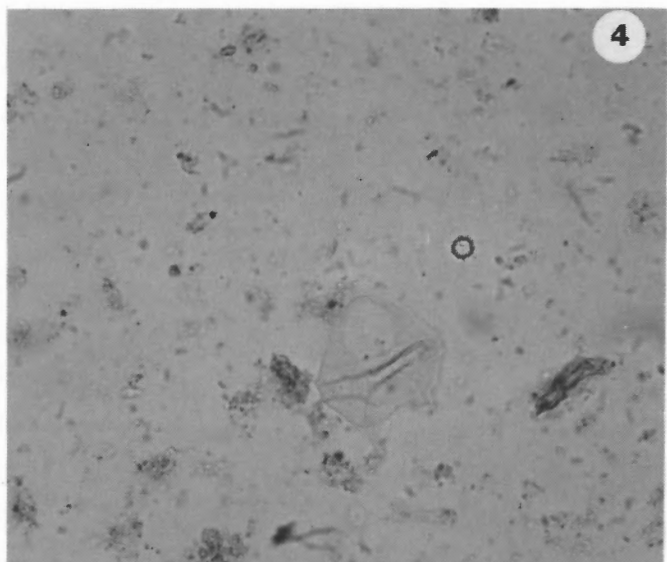
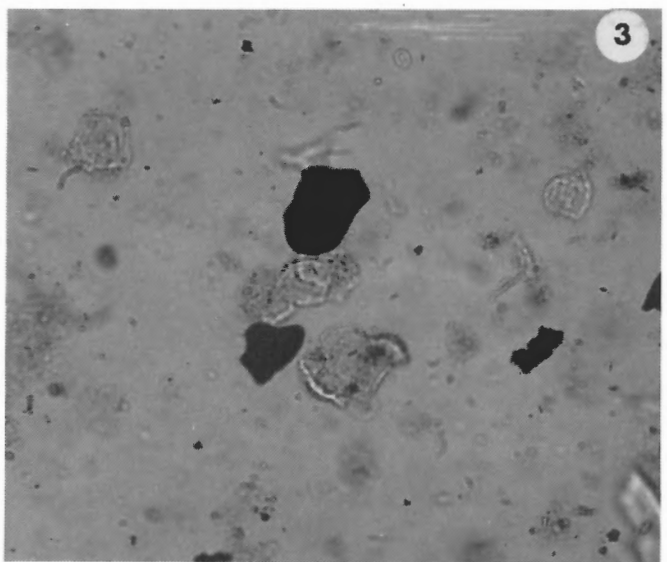
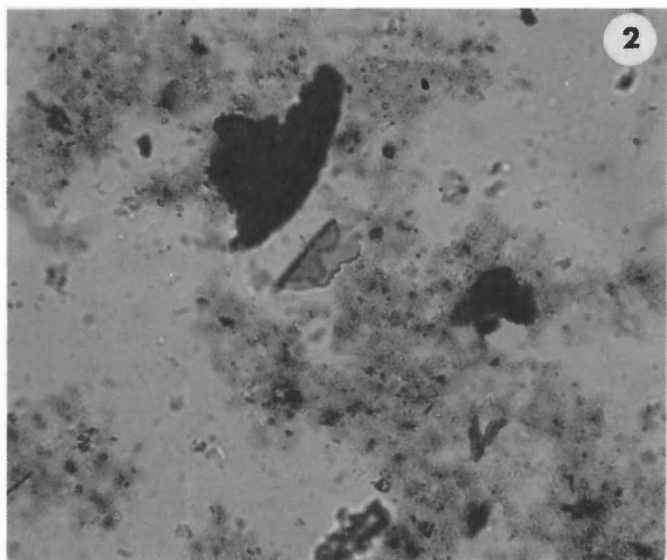
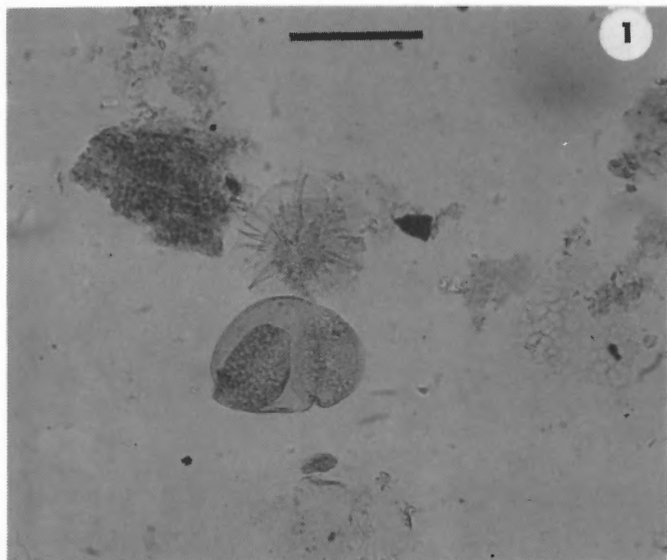


**Plate 11.4 (opposite)**

Palynodebris types, laminated sediment from cores CESAR 6 and USGS FL 422. Transmitted light photomicrographs; scale bar = 80  $\mu\text{m}$  for figures 1-4; scale bar = 50  $\mu\text{m}$  for figures 5-7; # = EMG photo negative.

- Figure 1 Core catcher sample 6B-2, showing large flocs of amorphous kerogen, bisaccate pollen, and dinoflagellates (*Impagidinium vellorum* and isolated plate of *Spongodinium delitiense*); # 84329-13.
- Figure 2 CESAR 6, unit 4C, light brown laminae from 301.5-304cm, showing large flocs of amorphous kerogen and imbedded clay-sized iron particles, brown wood fragments and fragments of highly altered (dark brown to black) large spores; # 84329-21.
- Figure 3 CESAR 6, unit 4C, brown laminae from 298-300cm, showing small flocs of amorphous kerogen, coal particles and poorly preserved (highly oxidized) spores; # 84329-33.
- Figure 4 Fletchers Ice Island core FL 422, segment 13, showing well dispersed amorphous flocs, large thin-walled (?oxidized) dinoflagellate (*Palaeoperidinium* cf. *pyrophorum*) and small acritarch (*Cymatiosphaera* sp. 1); # 84411-2.
- Figure 5 CESAR 6, 301.5-304cm, faecal pellet containing abundant biosiliceous fragments; AGC 84329-24.
- Figure 6 CESAR 6, 301.5-304cm, coiled structure resembling foraminiferal organic lining infilled by pyrite; # 84329-20.
- Figure 7 Dredge rock sample; CESAR rock 1 core; multicellular structure, resembling a stellate epidermal hair of Malvaceae; x160; # 84409-28.

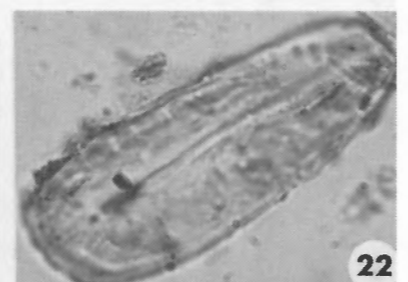
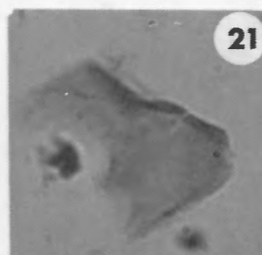
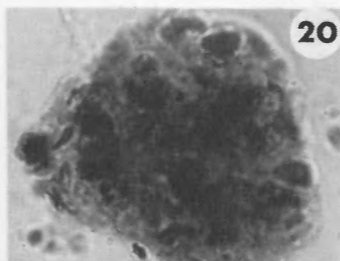
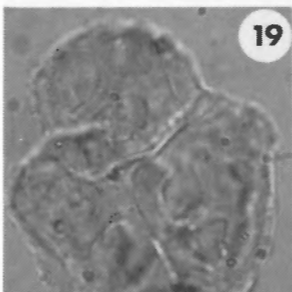
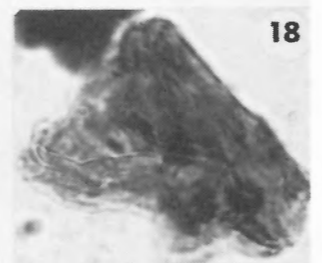
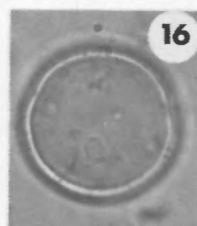
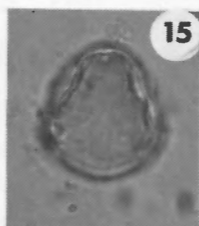
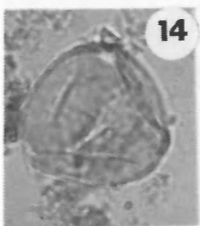
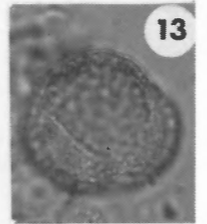
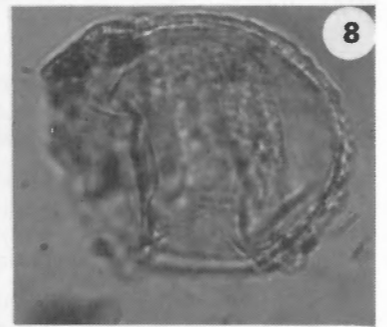
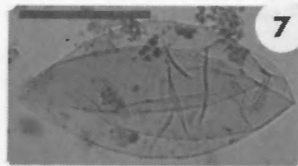
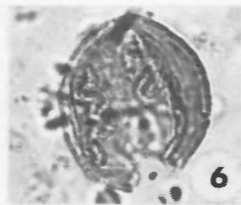
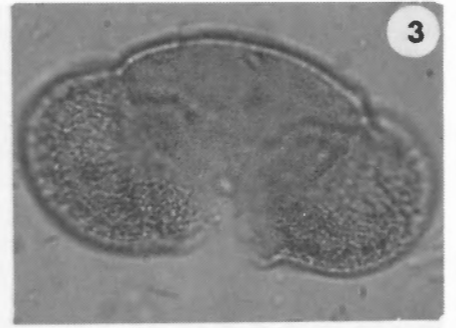
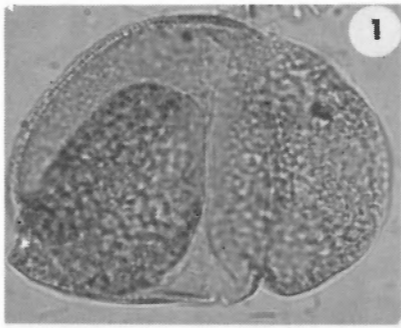


### Plate 11.5 (opposite)

Pollen and spores from core catcher and unit 4C of CESAR 6. Zeiss Universal photomicrographs; scale bar = 25µm for all figures except figure 7, where the scale bar = 50µm; sample number is followed by England Finder co-ordinates for the specimen; # = EMG photo negative.

- Figure 1 *Abietinaepollenites* sp., with subsphaerical sacchi slightly smaller than the corpus, but the cappa not thickened as in *Cedrus* or *Abies*; sample CESAR 6B-2, Y 11/2; # 84329-12.
- Figure 2 *Alisporites bilateralis*; sample CESAR 6B-2, X 11/3; # 84329-8.
- Figure 3 *Cedripites cretaceus*; sample CESAR 6B-2, G 14/2; # 84409-5.
- Figure 4-5 *Podocarpites multesimus*; sample CESAR 6B-2. Figure 4: specimen N 40/4; # 84409-14. Figure 5: specimen G 10/1; # 84409-4.
- Figure 6 *Phyllocladites microreticulatus*; sample CESAR 6B, M 9/1; # 84409-17.
- Figure 7 *Laricoidites magnus*; sample CESAR 6, 301.5-304cm, L 49/2; # 84329-23.
- Figure 8 *Pristinuspollenites sulcatus*; sample CESAR 6, 298-300cm, P 8/4; # 84329-30.
- Figure 9 *Triatriopollenites costatus*; sample CESAR 6B, E 54/2; # 84409-9.
- Figure 10 *Triporopollenites bituitus*; sample CESAR 6B-2, Y 13/1; # 84329-10.
- Figure 11 ?*Tricolporopollenites* sp., type A of Rouse et al., 1970; sample CESAR 6, 301.5-304cm, M 47/1; # 84329-17.
- Figure 12 *Tricolpites* sp. 1 of McIntyre, 1974; sample CESAR 6, 301.5-304cm, J 6/4; a) high focus; # 84329-25; b) equatorial focus; # 84329-26.
- Figure 13 *Fraxinoipollenites* cf. *pachyexinous*, grain shape is more rotund than in type material of *Fraxinoipollenites pachyexinous*; sample CESAR 6B-1, M 44/3; # 84409-20.
- Figure 14 *Ulmipollenites* sp. A, with a verrucate exine and weakly defined arci; sample CESAR 6B-1, T 36/2; # 84409-21.
- Figure 15 *Ulmoideipites krempii*, showing weakly defined annuli continuous with thickened arci; sample CESAR 6B, D 14/2; # 84409-11.
- Figure 16 ?*Classopollis* sp., a thin-walled taxon not forming tetrads as in Late Cretaceous material of Penny (1969); sample CESAR 6, 301.5-304cm, V 18/1; # 84329-16.
- Figure 17 *Monosulcites* sp.; sample CESAR 6B-2; # 84329-11.
- Figure 18 *Expressipollenites accuratus*; sample CESAR 6, 298-300cm, V 19/1; # 84329-34.
- Figure 19 *Alnipollenites* sp. of McIntyre, 1974; most grains single, but some in loose tetrads as shown here; sample CESAR 6, 298-300cm, Q 4/0; # 84329-32.
- Figure 20 *Verrucosisporites* sp.; sample CESAR 6, 298-300cm, N 18/3; # 84329-28.
- Figure 21 Fragment of *Expressipollis sibiricus*; sample CESAR 6, 301.5-304cm, L 21/4; # 84329-19.
- Figure 22 *Wodehousia gracile*; sample CESAR 6, 301.5-304cm, V 47/3; # 84329-15B.

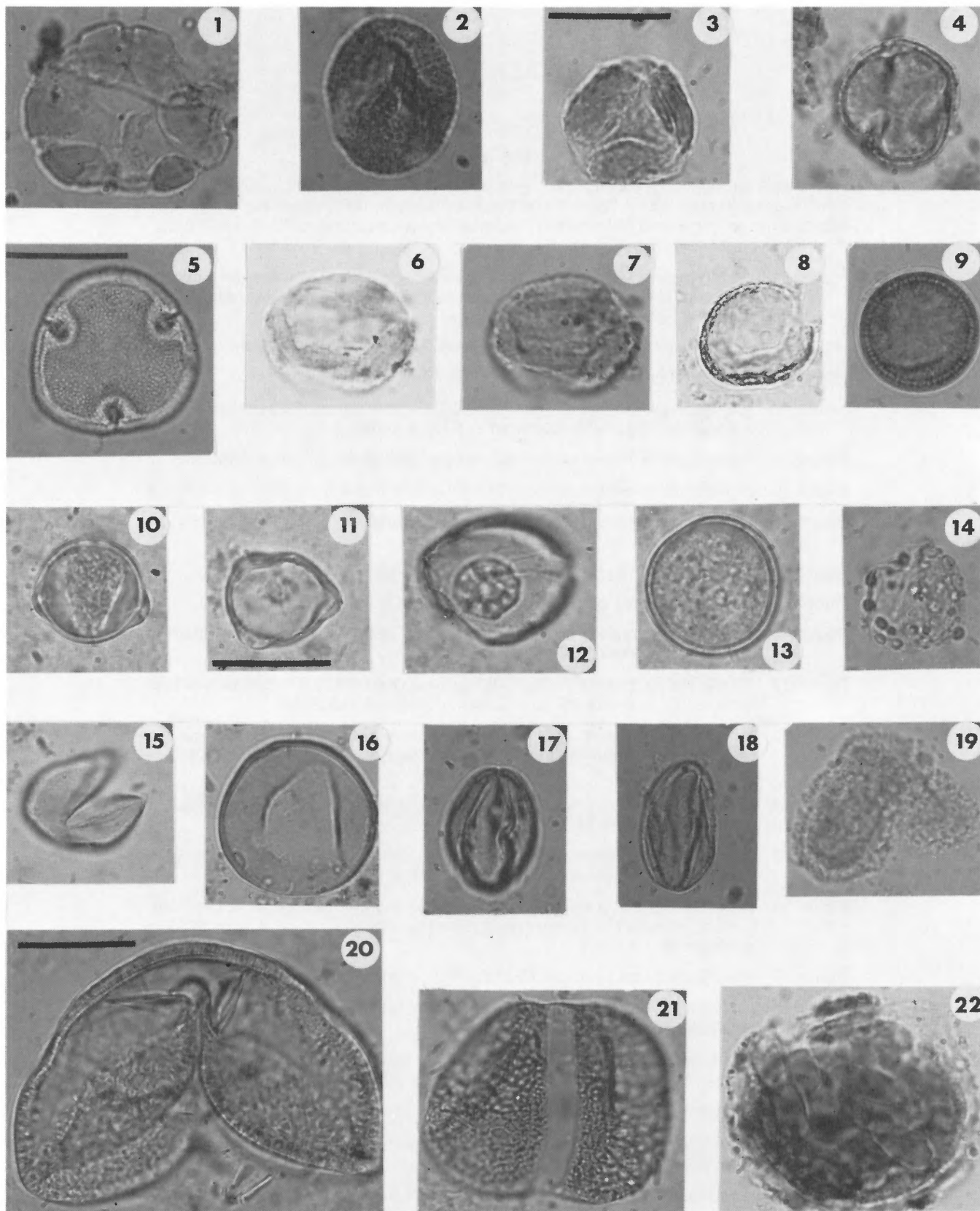




**Plate 11.6 (opposite)**

Pollen and spores from CESAR 6, USGS 6 FL 422 and a volcanic rock dredged from the Alpha Ridge crest during CESAR. Scale bar = 25µm for all figures; alphanumeric codes are England Finder co-ordinates; # = EMG photo negatives.

- Figure 1 *Alnipollenites* sp. 2, a large hexaporate species with wide irregular-shaped atria; sample CESAR 6, 298-300cm, N 23/4; # 84329-29.
- Figure 2 *Tricolporopollenites* sp. A, showing thick, granulo-striate exine and narrow colpi with thickened pore margins as in Cenomanian species of Singh (1975); sample CESAR 6, 298-300cm, V 51/3; # 84329-35.
- Figure 3 *?Grewipollenites canadensis*; sample CESAR 6, 298-300cm, Q 4/0; # 84329-31.
- Figure 4 *Nyssapollenites* sp. A; sample CESAR 6, 170-172cm, S 54/3; # 84329-9.
- Figure 5 *Tilia crassipites*; sample CESAR 6, 127-129cm, S 15/2; # 84329-2.
- Figure 6-7 Monosulcate pollen-type 1, showing the granulo-reticulate exine and sulcus with an irregular, almost denticulate margin; sample CESAR 6, 120-122cm, C 19/2. Figure 6: Sulcul (ventral?) view; # 84329-6. Figure 7: Dorsal view; # 84329-5.
- Figure 8 Monosulcate pollen-type 1; sample FL 422, X 24/3; # 84411-3.
- Figure 9 Tasmanaceae spore (similar to *Discoidea*, Habib, 1970); sample CESAR 6, 270-272cm, Z 15/0; # 84411-15.
- Figure 10 *?Kurtzipites* sp., showing atriate pores and short meridionally oriented colpi; sample CESAR DR-10B, Q 41/4; # 84409-29.
- Figure 11 *Casuarinidites convexus*; sample CESAR DR-10B, P 38/2; # 84409-30.
- Figure 12 *Platycaryapollenites platycaryoides*; sample CESAR DR-10B, X 33/3; # 84409-24.
- Figure 13 *Monoporopollenites* sp.; sample CESAR DR-10B, X 36/2; # 84409-22.
- Figure 14 *Pistillipollenites mcgregorii*; sample FL 422, Y 47/4; # 84417-4.
- Figure 15 *Glyptostrobus vacuipites*; sample FL 422, G 42/0; # 84417-1.
- Figure 16 *Caryapollenites prodromus*; sample FL 422, C 55/4; # 84417-17.
- Figure 17 *Aesculiidites* sp.; sample FL 422, E 35/2; # 84411-6.
- Figure 18 *Quercoidites* sp.; sample FL 422, F 40/1; # 84411-7.
- Figure 19 *?Aquilapollenites* sp.; sample FL 422, W 21/3; # 84417-7.
- Figure 20 *Podocarpites* sp.; sample CESAR DR-10B, V 15/4; # 84409-25.
- Figure 21 *Picea* sp.; sample FL 422, Z 37/4; # 84417-3.
- Figure 22 *?Pesavis* sp., resembling the multicellular fruiting body of *Pesavis tagluensis*, but apparently without a distinct stalked central cell and with a membranous outer layer enclosing the septate hypha-like filaments; sample CESAR 6, 270-272cm; # 84409-25.

**Zone 4 (135-100cm).** This zone is characterized by a predominance of Paleogene triporate species and smooth-walled tricolporates which are typical of late Paleocene-Eocene floras in the Canadian Arctic (Rouse, 1977). The most conspicuous of these pollen-types is *Tilia crassipites* (Plate 11.5, fig. 5) which has an Early Eocene first occurrence in northern North America according to Rouse (1977). There are no unequivocal Mesozoic taxa in this zone.

The flora in Zone 4 of CESAR 6 is very similar to that in the Middle Eocene sample from core FL 422, which contains many pollen grains. This correlation strongly suggests an early Tertiary (Eocene-Oligocene) age for the top of the siliceous sediment unit and for the volcanic ash units in CESAR 6. A similar flora was also found in a sample from the centre of a volcanic rock dredged from the crest of Alpha Ridge. The latter assemblage contains very well preserved palynomorphs which show no visible sign of thermal alteration; therefore, the pollen probably postdate the time of volcanic activity. It is notable, however, that the volcanic rock contained no coalified organic material such as found in and around the Thingmuli volcanic centres of Iceland (Mudie, unpublished data); this suggests that the volcanic sediment cooled rapidly.

The low numbers of pollen and spores in most samples from CESAR 6 preclude detailed paleoclimatic analysis of the Cretaceous-Tertiary circumpolar environment. However, some tentative conclusions may be drawn regarding two postulated climatic models. The dominant polar cyclonic air circulation pattern suggested by Kitchell and Clark (1982) should direct air masses, hence pollen and spores, to the Arctic, and pollen influx would be expected to be higher than during the late Cenozoic. Likewise, increased freshwater runoff associated with a monsoonal rainfall pattern (Kitchell and Clark, 1982) should be accompanied by higher pollen influx. Data from CESAR 6 support these predictions only for the oldest (core-catcher) sediments, which also contain the largest amount of amorphogen commonly associated with high marine productivity. An alternative Cretaceous paleoclimatic reconstruction (Barron, 1983), which postulates a relatively weak latitudinal thermal gradient and meridional circulation of air, is more compatible with the CESAR pollen data. Furthermore, if this climatic scenario was also accompanied by increased cloud-cover over lowlying circumpolar continental regions (Barron, 1983), then pollen transport by both air and runoff would be minimal. A combination of these climatic conditions and a southward flowing drainage pattern due to Maastrichtian uplift along the outer Sverdrup Basin (Miall, 1981) best accounts for the low pollen influx to the Alpha Ridge, given the ample evidence for a warm late Cretaceous climate in the Canadian Arctic Islands (e.g. Hopkins and Balkwill, 1973).

## ALPHABETICAL LIST OF TAXA

### *Dinoflagellates, Acritarchs and other Algae*

<i>Achomosphaera</i> sp.	Plate 11.3, figure 14
<i>Brigantadinium simplex</i> (Wall)	
Reid, 1977	Plate 11.1, figure 20
<i>Botryococcus</i> -type "algal spore"	Plate 11.1, figure 15

<i>Cymatiosphaera punctifera</i>	Plate 11.3, figure 11
Deflandre and Cookson, 1955	Plate 11.4, figure 4
<i>Cymatiosphaera</i> sp. 1	
" <i>Deflandrea</i> " <i>diebeli</i> of	
Doerenkamp et al., 1976	Plate 11.3, figure 15
? <i>Deflandrea</i> sp. 1	Plate 11.4, figure 4
Dinocyst sp. 1	Plate 11.3, figure 6
<i>Filisphaera filifera</i> Bujak, 1984	Plate 11.1, figure 13
? <i>Gonyaulacysta</i> sp. B of Williams	
and Brideaux, 1975	Plate 11.3, figure 12
? <i>Gymnodinium</i> sp.	Plate 11.1, figure 14
<i>Impagidinium patulum</i> (Wall)	
Stover and Evitt, 1978	Plate 11.1, figure 21
<i>Kallosphaeridium biornatum</i>	
Stover, 1977	Plate 11.3, figure 7
" <i>Lejeunea</i> " <i>koslowki</i> of	
Doerenkamp et al., 1976	Plate 11.3, figure 2
<i>Nematosphaeropsis labyrinthea</i>	
(Ostenfeld) Reid, 1974	Plate 11.1, figure 19
? <i>Microdinium ornatum</i> Cookson	
and Eisenack, 1960	Plate 11.3, figure 8
<i>Michrystidium</i> spp.	
<i>Operculodinium centrocarpum</i>	
Deflandre and Cookson, 1955	Plate 11.1, figures 16,17
<i>Palambages</i> form A of	
Doerenkamp et al., 1976	Plate 11.3, figure 9
<i>Palaeoperidinium</i> cf. <i>pyrophorum</i>	
(Ehrenberg) Sarjeant, 1967	Plate 11.3, figure 3
<i>Pediastrum</i> spp.	
? <i>Pterodinium aliferum</i> Eisenack,	
1958	Plate 11.3, figure 10
<i>Pterodinium</i> sp.	Plate 11.1, figure 12
<i>Pterospermopsis australiensis</i>	
Deflandre and Cookson, 1955	Plate 11.3, figure 5
<i>Pterospermopsis ginginensis</i>	
Deflandre and Cookson, 1955	
<i>Spiniferites ramosus</i> (Ehrenberg)	
Loeblich and Loeblich, 1966	Plate 11.1, figure 18
<i>Spiniferites</i> sp.	Plate 11.3, figure 13
<i>Spongodinium</i> cf. <i>delitiense</i>	
(Ehrenberg) Deflandre, 1936	Plate 11.2, figure 6
Tasmanaceae-type spore cf	
<i>Discoidella</i> Habib, 1970	Plate 11.6, figure 9
<i>Thoracosphaera arctica</i> Gilbert	
and Clark, 1982	Plate 11.2, figures 1-5

### *Fungal Spores*

<i>Ustilago</i> spp. of Bassett et al.,	
1978	Plate 11.1, figure 8
? <i>Pesavis</i> sp.	Plate 11.6, figure 22

### *Pollen and Spores*

<i>Abietinaepollenites</i> sp. of McIntyre,	
1974	Plate 11.5, figure 1
<i>Acer</i> cf. <i>negundo</i> (see Bassett et	
al., 1978)	Plate 11.1, figure 7
<i>Aesculiidites</i> A of Rouse, 1977	Plate 11.6, figure 17
<i>Alnipollenites</i> sp. of McIntyre,	
1974	Plate 11.5, figure 19
<i>Alnipollenites</i> sp. 1	Plate 11.1, figure 11
<i>Alnipollenites</i> sp. 2	Plate 11.6, figure 1
<i>Alisporites bilateralis</i> Rouse 1959	Plate 11.5, figure 2
? <i>Aquilapollenites</i> sp.	Plate 11.6, figure 19
<i>Betula</i> cf. <i>humilis</i> (see Erdtman,	
1943)	Plate 11.1, figure 3

- Caryapollenites prodromus* Nichols and Ott, 1978 Plate 11.6, figure 16
- Casuarinidites convexus* (Groot and Groot) Frederiksen and Christopher, 1978 Plate 11.6, figure 11
- Cedripites cretaceus* Pocock, 1962 Plate 11.5, figure 3
- ?Classopollis* sp. of Penny, 1969, Pl.16-1, Fig.11 Plate 11.5, figure 16
- Expressipollenites accuratus* Chlonova, 1961 Plate 11.5, figure 18
- ?Expressipollis sibiricus* (Bondarenko) Felix and Burbridge, 1973 Plate 11.5, figure 21
- Fraxinoipollenites pachyexinous* Leffingwell 1970 Plate 11.5, figure 13
- Glyptostrobus vacuipites* Wodehouse 1933 Plate 11.6, figure 15
- Gramineae* sp. Plate 11.1, figure 4
- ?Grewipollenites canadensis* Srivastava, 1969 Plate 11.6, figure 3
- Ilex* sp. Plate 11.1, figure 9
- ?Kurtzipites* sp. of Leffingwell, 1970 Plate 11.6, figure 10
- Laricoidites magnus* (Potonié) Potonié et al., 1950 Plate 11.5, figure 7
- Liguliflorae* sp. Plate 11.1, figure 5
- Liquidambar* sp. Plate 11.1, figure 10
- Monoporopollenites* sp. Plate 11.6, figure 13
- Monosulcate pollen-type 1 Plate 11.6, figures 6-8
- Monosulcites* sp. of Penny, 1969 Plate 11.5, figure 17
- Nyssapollenites* sp. A of Rouse, 1977 Plate 11.6, figure 13
- Paraalnipollenites confusus* (Zaklinskaia) Hills and Wallace, 1969
- Picea omorika* (see Erdtman, 1943) Plate 11.1, figure 2
- Picea* sp. of Leopold in Penny, 1969 Plate 11.6, figure 21
- Phyllocladites microreticulatus* Brenner, 1963 Plate 11.5, figure 6
- Pinus* cf. *sylvestris* (see Erdtman, 1943) Plate 11.1, figure 1
- Pistillipollenites mcgregorii* (Rouse) Elsik, 1968 Plate 11.6, figure 14
- Platycaryapollenites platycaryoides* (Roche) Frederiksen and Christopher, 1978 Plate 11.6, figure 12
- Podocarpites multesimus* (Bolchovitina) Pocock, 1962 Plate 11.5, Figures 4-5
- Podocarpites* sp. Plate 11.6, figure 20
- Pristinuspollenites sulcatus* (Pierce) Tschudy, 1973 Plate 11.5, figure 8
- Quercoidites* A Rouse, 1977 Plate 11.66, figure 18
- Quercus* sp. Plate 11.1, figure 6
- Tilia crassipites* Wodehouse, 1933 Plate 11.6, figure 5
- Triatriopollenites costatus* Norton in Norton and Hall, 1969 Plate 11.5, figure 9
- Tricolpate* sp. (see *Quercoidites*) Plate 11.6, figure 18
- Tricolpites* sp. 1 of McIntyre, 1974 Plate 11.5, figure 12
- Tricolporate* sp. (see *Aesculiidites*) Plate 11.6, figure 17
- ?Tricolporopollenites* sp. of Singh, 1975 Plate 11.6, figure 2
- Tricolporopollenites* sp. type A of Rouse et al., 1970 Plate 11.5, figure 11
- Triporopollenites bituitus* (Potonié) Elsik, 1968 Plate 11.5, figure 10
- Ulmipollenites* sp. A Plate 11.5, figure 14
- Ulmoideipites krempii* Anderson, 1960 Plate 11.5, figure 15
- Verrucosisporites* sp. Plate 11.5, figure 20
- Wodehousia gracile* (Samoilovitch) Pokrovskaya, 1966 Plate 11.5, figure 22

## REFERENCES

- Aksu, A.E.  
1985a: Paleomagnetic stratigraphy of the CESAR cores; in Initial Geological Report on CESAR — The Canadian Expedition to Study the Alpha Ridge, Arctic Ocean, ed. H.R. Jackson, P.J. Mudie, and S.M. Blasco; Geological Survey of Canada, Paper 84-22, report 7.  
1985b: Planktonic foraminiferal and oxygen isotopic stratigraphy of CESAR cores 102 and 103: preliminary results; in Initial Geological Report on CESAR — The Canadian Expedition to Study the Alpha Ridge, Arctic Ocean, ed. H.R. Jackson, P.J. Mudie, and S.M. Blasco; Geological Survey of Canada, Paper 84-22, report 8.
- Amos, C.L.  
1985: Bottom photography and sediment analyses on CESAR; in Initial Geological Report on CESAR — The Canadian Expedition to Study the Alpha Ridge, Arctic Ocean, ed. H.R. Jackson, P.J. Mudie and S.M. Blasco; Geological Survey of Canada, Paper 84-22, report 4.
- Anderson, R.Y.  
1960: Cretaceous-Tertiary palynology, eastern side of the San Juan Basin, New Mexico; New Mexico Institute of Mining Technology, Memoir 6, p.20.
- Baker, G.  
1959: Opal phytoliths in some Victorian soils and "red rain" residues; Australian Journal of Botany, v.7, p.64-87.
- Barron, E.J.  
1983: A warm, equable Cretaceous; the nature of the problem; Earth-Science Reviews, v.19, p.305-338.
- Barron, J.A.  
1985: Diatom biostratigraphy of the CESAR 6 core, Alpha Ridge; in Initial Geological Report on CESAR — The Canadian Expedition to Study the Alpha Ridge, Arctic Ocean, ed. H.R. Jackson, P.J. Mudie and S.M. Blasco; Geological Survey of Canada, Paper 84-22, report 10.
- Barss, M.S. and Williams, G.L.  
1973: Palynology and nannofossil processing techniques; Geological Survey of Canada, Paper 73-26, 25p.
- Bassett, I.J., Crompton, C.W. and Parmelee, J.A.  
1978: An atlas of airborne pollen grains and common fungus spores of Canada; Canada Department of Agriculture, Monographs No. 18; Supply and Services Canada, Hull, Quebec, 321 p.
- Blasco, S.M., Bornhold, B.D., and Lewis, C.F.M.  
1979: Preliminary results of surficial geology and geomorphology studies of the Lomonosov Ridge, Central Arctic Basin; in Current Research, Part C, Geological Survey of Canada, Paper 79-1C, p.73-83.
- Brenner, G.  
1963: The spores and pollen of the Potomac Group of Maryland, Baltimore; Maryland Department of Geology, Mines and Water Resources, Bulletin, v.27, p.1-215.

- Bujak, J.P.  
1984: Cenozoic dinoflagellate cysts and acritarchs from the Bering Sea and northern North Pacific; *Micropaleontology*, v.30, p.250-265.
- Bukry, D.  
1984: Paleogene paleoceanography of the Arctic Ocean is constrained by the middle or late Eocene age of USGS Core FL-422: evidence from silicoflagellates; *Geology* v.12, p.199-201.  
1985: Correlation of Late Cretaceous silicoflagellates from Alpha Ridge; in *Initial Geological Report on CESAR — The Canadian Expedition to Study the Alpha Ridge, Arctic Ocean*, ed. H.R. Jackson, P.J. Mudie and S.M. Blasco; Geological Survey of Canada, Paper 84-22, report 9.
- Bursa, A.S.  
1961: The annual oceanographic cycle at Igloolik in the Canadian Arctic. II. The phytoplankton; *Fisheries Research Board of Canada, Journal* v.18, p.563-615.
- Chlonova, A.F.  
1961: Spores and pollen of the upper half of the Upper Cretaceous in the eastern part of the Western Siberian lowland; *Pollen et Spores*, v.4, p.279-309.
- Chowdhury, K.R.  
1982: Distribution of Recent and fossil palynomorphs in the southeastern North Sea (German Bay); *Senckenbergiana maritima*, v.14, p.79-145.
- Clark, D.L.  
1974: Late Mesozoic and early Cenozoic sediment cores from the Arctic Ocean; *Geology*, v.2, p.41-44.
- Cookson, I.C. and Eisenack, A.  
1960: Microplankton from Australian Cretaceous sediments; *Micropaleontology* v.6, p.1-18.
- Deflandre, G.  
1936: Microfossils de silex cétacés; Première partie, Généralités Flagelles; *Annales paléontologie*, v.25, p.151-191.
- Deflandre, G. and Cookson, I.C.  
1955: Fossil microplankton from Australian late Mesozoic and Tertiary sediments; *Australian Journal of Marine and Freshwater Research*, v.6, p.242-313.
- Doerenkamp, A., Jardine, S., and Moreau, P.  
1976: Cretaceous and Tertiary palynomorph assemblages from Banks Island and adjacent areas (N.W.T.); *Bulletin of Canadian Petroleum Geology*, v.24, p.372-417.
- Eisenack, A.  
1958: Mikroplankton aus dem norddeutschen Apt.; *Neues Jahrbuch für Geologie und Paläontologie, Abhandlungen*, v.106, p.383-422.
- Elsik, W.C.  
1968: Palynology of a Paleocene Rockdale lignite, Milam County, Texas. II. Morphology and taxonomy (end); *Pollen et Spores*, v.10, no.3, p.599-664.
- Erdtman, G.  
1943: *An Introduction to Pollen Analysis*; Ronald Press Co., New York, 239p.
- Felix, C.J. and Burbridge, P.P.  
1973: A Maastrichtian-age microflora from Arctic Canada; *Geoscience and Man*, v.7, p.1-29.
- Frederiksen, N.O. and Christopher, R.A.  
1978: Taxonomy and biostratigraphy of late Cretaceous and Paleogene triporate pollen from South Carolina; *Palynology*, v.2, p.113-145.
- Gilbert, M.W. and Clark, D.L.  
1982: Central Arctic Ocean paleoceanographic interpretations based on late Cenozoic calcareous dinoflagellates; *Marine Micropaleontology*, v.7, p.385-401.
- Habib, D.  
1970: Middle Cretaceous palynomorph assemblages from clays near the Horizon Beta deep-sea outcrop; *Micropaleontology*, v.16, p.345-379.
- Herman, Y.  
1974: Arctic Ocean sediments, microfauna, and the climatic record in late Cenozoic time; in *Marine Geology and Oceanography of the Arctic Seas*, ed. Y. Herman; Springer Verlag, New York, p.283-348.  
1983: Baffin Bay; present-day analog of the central Arctic during late Pliocene to mid-Pleistocene time; *Geology*, v.11, p.356-359.
- Hills, L.V. and Wallace, S.  
1969: *Paraalnipollenites*, a new form genus from uppermost Cretaceous and Paleocene rocks of Arctic Canada and Russia; *Geological Survey of Canada, Bulletin* 132, p.139-145.
- Hopkins, W.S. Jr. and Balkwill, H.R.  
1973: Description, palynology and paleoecology of the Hassel Formation (Cretaceous) on eastern Ellef Ringnes Island, District of Franklin; *Geological Survey of Canada, Paper* 72-37, 31p.
- Jackson, H.R.  
1985: Seismic reflection results from CESAR; in *Initial Geological Report on CESAR — The Canadian Expedition to Study the Alpha Ridge, Arctic Ocean*, ed. H.R. Jackson, P.J. Mudie and S.M. Blasco; Geological Survey of Canada, Paper 84-22, report 3.
- Kitchell, J.A. and Clark, D.L.  
1982: Late Cretaceous-Paleogene paleogeography and paleocirculation; evidence of north polar upwelling; *Palaeogeography, Palaeoclimatology, Palaeoecology*, v.40, p.135-165.
- Leffingwell, H.A.  
1970: Palynology of the Lance (late Cretaceous) and Fort Union (Paleocene) formations of the type Lance area, Wyoming; in *Symposium on Palynology of the Late Cretaceous and Early Tertiary*, ed. R.M. Kosanke and A.T. Cross; Geological Society of America, Special Paper 127, p.1-64.
- Leopold, E.B.  
1969: Late Cenozoic palynology; in *Aspects of Palynology*, ed. R.H. Tschudy and R.A. Scott; Wiley Interscience, New York, p.377-438.
- Lichti-Federovich, S.  
1974: Pollen analysis of surface snow from the Devon Island ice cap; in *Report of Activities, Part A, Geological Survey of Canada, Paper* 74-1, p.197-199.
- Loeblich, A.R. Jr. and Loeblich, A.R. III.  
1966: Index to the genera, subgenera and sections of the Pyrrhophyta; *Studies in Tropical Oceanography*, Miami, no.3, 94p.

- Manum, S.B.  
1976: Dinocysts in Tertiary Norwegian-Greenland Sea sediments (Deep Sea Drilling Project Leg 38), with observations on palynomorphs and palynodebris in relation to environment; in Initial Reports of the Deep Sea Drilling Project, v.38, ed. M. Talwani, G. Udintsev *et al.*; U.S. Government Printing Office, Washington, p.897-919.
- McIntyre, D.J.  
1974: Palynology of an upper Cretaceous section, Horton River, District of Mackenzie, N.W.T.; Geological Survey of Canada, Paper 74-14, 85p.
- Melia, M.B.  
1982: The distribution and relationship between palynomorphs in aerosols and deep-sea sediments off the coast of northwest Africa; *Palynology*, v.6, p.285.
- Miall, A.D.  
1981: Late Cretaceous and Paleogene sedimentation and tectonics in the Canadian Arctic Islands; Geological Association of Canada, Special Paper 23, p.221-272.
- Mudie, P.J.  
1982: Pollen distribution in recent marine sediments, eastern Canada; *Canadian Journal of Earth Sciences*, v.19, p.729-747.
- Mudie, P.J. and Blasco, S.M.  
1985: Core recovery and lithostratigraphy on CESAR; in Initial Geological Report on CESAR — The Canadian Expedition to Study the Alpha Ridge, Arctic Ocean, ed. H.R. Jackson, P.J. Mudie and S.M. Blasco; Geological Survey of Canada, Paper 84-22, report 6.
- Nichols, D.J. and Ott, H.L.  
1978: Biostratigraphy and evolution of the *Momipites-Caryapollenites* lineage in the early Tertiary in the Wind River Basin, Wyoming; *Palynology*, v.2, p.93-145.
- Norris, G., Jarzen, D.M., and Awai-Thorne, B.V.  
1975: Evolution of the Cretaceous terrestrial palynoflora in western Canada; in *The Cretaceous System in the Western Interior of North America*, ed. W.G.E. Caldwell; Geological Association of Canada, Special Paper 13, p.333-364.
- Norton, N.J. and Hall, J.W.  
1969: Palynology of the Upper Cretaceous and Lower Tertiary in the type locality of the Hell Creek Formation, Montana, U.S.A.; *Palaeontographica*, B, v.125, 64p.
- Penny, J.S.  
1969: Late Cretaceous and early Tertiary palynology; in *Aspects of Palynology*, ed. R.H. Tschudy and R.A. Scott; Wiley Interscience, p.331-376.
- Pocock, S.A.  
1962: Microfloral analysis and age determinations of strata at the Jurassic-Cretaceous boundary in western Canada; *Palaeontographica*, v.111, sec.B, p.10-195.
- Pokrovskaya, I.M.  
1966: Pollen of Angiospermae of unestablished systematic position; in I.M. Pokrovskaya, *Paleopalynology, Methods of Paleopalynologic Investigations and Morphology of Some Fossil Spores, Pollen and Other Plant Microfossils*, I.M. Pokrovskaya, ed., Trudy Vses. Nauchn.-Issled. Geol. Inst. v.141, p.301-321.
- Polunin, N.  
1955: Arctic aeropalynology; *Canadian Journal of Botany*, v.55, p.401-415.
- Potonié, R., Thomson, P.W., and Thiergart, F.  
1950: Zur Geologie der rheinischen Braunkohle; I. Zur Nomenklatur und Klassifikation der neogenen Sporomorphae (Pollen und Sporen); *Geologisches Jahrbuch*, v.65, p.35-69.
- Prakash, A.  
1967: Growth and toxicity of a marine dinoflagellate, *Gonyaulax tamarensis*; Fisheries Research Board of Canada, Journal v.24, p.1589-1606.
- Reid, P.C.  
1974: Gonyaulacacean dinoflagellate cysts from the British Isles; *Nova Hedwigia*, v.25, p.579-637.  
1977: Peridiniacean and Glenodiniacean dinoflagellate cysts from the British Isles; *Nova Hedwigia*, v.29, p.429-463.
- Rouse, G.E.  
1959: Plant microfossils from Kootenay coal-measures Strata of British Columbia; *Micropaleontology* v.5, p.303-324.  
1977: Paleogene palynomorph ranges in western and northern Canada; American Association of Stratigraphic Palynologists, Contribution Series No. 5A; Contributions of Stratigraphic Palynology, v.1, Cenozoic Palynology, p.48-65.
- Rouse, G.E., Hopkins, W.S., and Piel, K.M.  
1970: Palynology of some Late Cretaceous and Early Tertiary deposits in British Columbia and adjacent Alberta; in *Symposium on Palynology of the Late Cretaceous and Early Tertiary*, ed. R.M. Kosanke and A.T. Cross; Geological Society of America, Special Paper 127, p.213-246.
- Sarjeant, W.A.S.  
1967: The genus *Palaeoperidium* Deflandre (Dinophyceae); *Grana Palynologica*, v.7, p.243-258.
- Shackleton, N.J. and Opdyke, N.D.  
1976: Oxygen-isotope and paleomagnetic stratigraphy of Pacific Core V28-239, late Pliocene to latest Pleistocene; in *Investigation of Late Quaternary Paleoenvironment and Paleoclimatology*, ed. R.M. Cline and J.D. Hays; Geological Society of America, Memoir 145, p.449-464.
- Simoneit, B.R.  
1976: Sources of the solvent-soluble organic matter in the glacial sequence of DSDP samples from the Norwegian-Greenland Sea, Leg 38; Deep Sea Drilling Program Initial Report, v.38, p.805-806.
- Singh, C.  
1975: Stratigraphic significance of early Angiosperm pollen in the mid-Cretaceous strata of Alberta; in *The Cretaceous System in the Western Interior of North America*, ed. W.G.E. Caldwell; Geological Association of Canada, Special Paper 13, p.365-389.
- Srivastava, S.K.  
1969: Some angiosperm pollen from the Edmonton Formation (Maastrichtian), Alberta, Canada; in J. Sen Memorial Volume; Botanical Society Bengal, p.47-67.



- Stockmarr, J.  
1971: Tablets with spores used in absolute pollen analysis; *Pollen et Spores*, v.13, p.615-621.
- Stover, L.  
1977: Oligocene and early Miocene dinoflagellates from Atlantic corehole 5/5B, Blake Plateau; *in* Contributions of Stratigraphic Palynology, v.1, Cenozoic Palynology, ed. W.C. Elsik; American Association of Stratigraphic Palynologists, Contribution Series 5A, p.66-89.
- Stover, L.E. and Evitt, W.R.  
1978: Analyses of pre-Pleistocene organic-walled dinoflagellates; Stanford University Publications in Geological Sciences, v.15, 300p.
- Tangen, K., Brand, L.E., Blackwelder, P.L., and Guillard, R.R.  
1982: *Thoracosphaera heimii* (Lohmann) Kamptner is a dinophyte; observations on its morphology and life cycle; *Marine Micropaleontology*, v.7, p.193-212.
- Tappan, H.  
1980 *The Paleobiology of Plant Protists*; W.H. Freeman and Co, San Francisco, 1028p.
- Tschudy, B.D.  
1973 Palynology of the upper Campanian (Cretaceous) Judith River Formation, North Central Montana; U.S. Geological Survey, Professional Paper 770, 42p. + 11 plates.
- van der Hammen, T., Wijmstra, T.A., and Zagwijn, W.H.  
1971: The floral record of the late Cenozoic of Europe; *in* The late Cenozoic Ages, ed. K.K. Turekian; Yale University Press, New Haven and London, p.391-424.
- Williams, G.L. and Brideaux, W.W.  
1975: Palynological analyses of Upper Mesozoic and Cenozoic rocks of the Grand Banks, Atlantic Continental Margin; Geological Survey of Canada, Bulletin 236, 162p.
- Williams, G.L. and Bujak, J.P.  
1977: Cenozoic palynostratigraphy of offshore eastern Canada; *in* Contributions of Stratigraphic Palynology, v.1, Cenozoic Palynology, ed. W.C. Elsik; American Association of Stratigraphic Palynologists, Contribution Series 5A, p.14-47.
- Wodehouse, R.P.  
1933: Tertiary pollen, II; The oil shales of the Eocene Green River Formation; Torrey Botanical Club, Bulletin v.60, p.479-524.

## PISTON CORING ON CESAR

F. Jodrey<sup>1</sup> and D. Heffler<sup>1</sup>  
Geological Survey of Canada

Jodrey, F. and Heffler, D., *Piston coring on CESAR; in Initial Geological Report on CESAR — the Canadian Expedition to Study the Alpha Ridge, Arctic Ocean*, ed. H.R. Jackson, P.J. Mudie and S.M. Blasco; Geological Survey of Canada, Paper 84-22, p. 175-177, 1985.

### Abstract

*Coring on CESAR presented many problems because of inexperience in attempting 10m cores from an ice platform and because the heavy equipment had to be assembled in -45°C weather. The components used, how they were put together, and a step by step procedure for taking a core is described.*

### Résumé

*Le prélèvement des carottes au cours de l'expédition CESAR a présenté de nombreux problèmes vu le manque d'expérience dans le domaine de l'extraction de carottes de 10 m à partir d'une plate-forme de glace et à cause de l'équipement lourd qu'il a fallu assembler à -45 °C. Le présent rapport décrit les pièces utilisées, leur assemblage et la marche à suivre pour prélever une carotte.*

## EQUIPMENT

### Housing

The main building was a 12 × 16ft. (3.6 × 4.9m) plywood prefab made of 0.25 in. (.64cm) plywood panels separated by 2in. (5.1cm) of insulation. This was heated soon after it was erected. Holes 3 × 6ft. (0.9 × 1.8m) were cut in each end wall; a hole was cut in the floor near one end to expose the 6 × 4ft. (1.8 × 1.2m) hole in the 6ft. (1.8m) thick ice. The ice hole was cut first and the building assembled over it. A 6 × 4ft. (1.8 × 1.2m) hole was also cut in the roof directly over the ice hole (see Fig. 12.1).

The end holes were covered by butting 8 × 16ft. (2.4 × 4.9m) 'manigan' tents against each end.

### Gantry

The support structure was a gantry 14ft. (4.9m) wide, 13ft. (3.9m) high with a 8ft. (2.4m) spread at the base of the legs. It straddled the prefab with the eye beam centered over the hole in the roof. The eye beam and hole were enclosed with a custom built insulated tent.

The structure was back guyed by running cable from the ends of the eye beam to ice anchors<sup>1</sup>. A six ton shive was attached to the beam over the hole, with two ton chain blocks hanging from eye beam rollers on either side.

### Winch

The winch used was a Gearhart Owen with a four speed transmission driven by a hydraulic motor. A 14 HP gasoline engine drove the hydraulics. The engine was operated outside the tent with hydraulic lines connecting it to the winch. About half of the drum was filled with 8000ft (2454m) of 5/16in. (.8cm) cable. The pull of the winch was estimated at 5000lb. (2272kg) with a very slow line speed, less than 50ft. (15m) per minute.

The front of the winch was held down by placing a drilled 6 × 6in. (15 × 15cm) timber across the frame. A 18in. (0.46m) bolt wired to an ice anchor was put through the 6 × 6 (15 × 15cm) beam and tightened down. The back of the winch was also secured by running cables, with turn buckles, to ice anchors located outside the tent. The winch was located in a manigan tent with the drum 14ft. (4.3m) from the edge of the ice hole.

### Coring equipment

A 1200lb. (545 kg) Alpine head was used with an adapter to take the 10ft. (3.06m) Benthos core pipe. Special clamps<sup>2</sup> were used to hold the core pipes while they were tightened with 36in. (.9m) pipe wrenches. Two 4 × 4in. (10cm) timbers with notches were laid across the ice hole to take the weight of the core pipe while the corer was being assembled.

<sup>1</sup>Atlantic Geoscience Centre, Bedford Institute of Oceanography, Box 1006, Dartmouth, Nova Scotia, B2Y 4A2

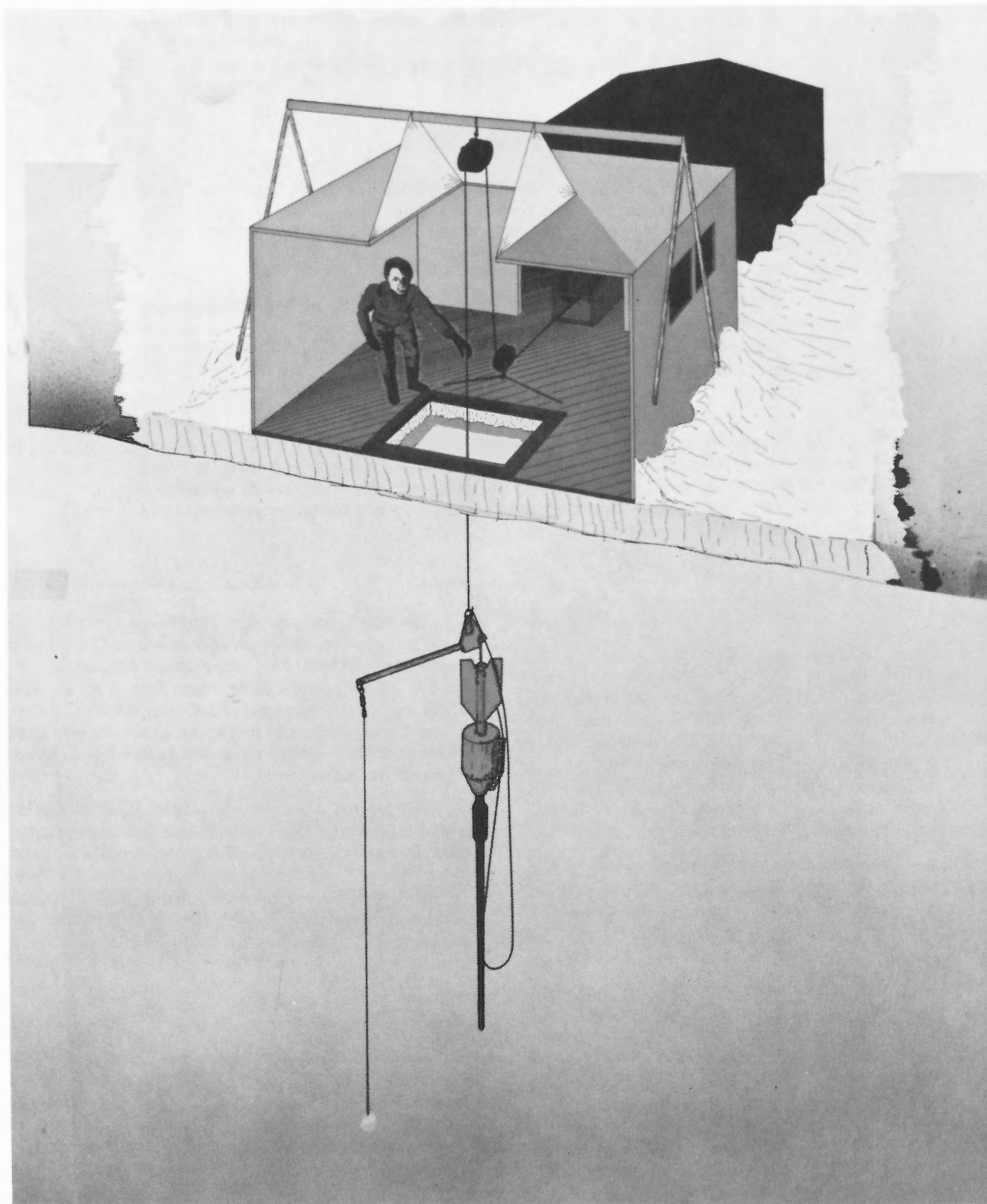


Figure 12.1 Housing set-up used for coring at CESAR main camp: cut-away of main building shows the hydrohole, winch and cable system. Drawn by Ken Hale.

## ***Coring Procedure***

The actual assembly of the corer in a vertical position involved a lot of juggling that could have been eliminated by increasing the gantry height by 2ft. (.6m) and adding 2ft. (.6m) to the throw of the chain block.

The first step was hauling enough cable from the drum to allow the various components to be moved and assembled.

The wire first passed through a 5 ton (4545kg) shive attached to an ice anchor 12 in. (30.5cm) from the edge of the ice hole and then through the 6 ton (5454kg) shive attached to the gantry. This allowed the pull from the winch to be transmitted almost vertically on the gantry legs, reducing tendency to tip the gantry or lift the front of the winch.

The core head and core pipe were laid parallel to each other. It should be noted that because of the order of assembly (opposite to that done on a ship), the core liners must be pre-cut carefully. This should be done before the cable is fed through the pipes. The core cutter and catcher were fitted on the bottom pipe and the liner inserted. This liner and each successive liner must be cut flush with the top of the pipe, the last liner being adjusted to meet the piston stop in the core head. The cutter was removed from the bottom pipe and the wire was run through the core head and each pipe from the top to the bottom of the last core pipe being used. The figi fitting on the end of the wire was attached to the split piston and the core catcher and cutter fitted to the bottom pipe.

A clamp was then put on the top of the bottom core pipe which was lifted with the chain block and lowered to rest in notches on 4 × 4 (10 × 10cm) timbers spanning the hydro hole. A second clamp was attached to the top of the next core pipe, lifted with the second chain block and lowered to fit the top of the first core pipe. The chain block was then disengaged, the top core pipe screwed in by hand and tightened with the pipe wrenches. The two core pipes were raised slightly with the chain block to remove the bottom clamp, then lowered until they were supported by the top clamp resting on the 4 × 4 timbers. The next pipe was fitted in the same manner and lowered.

The core pipes were now supported the 4 × 4 timbers while both chain blocks were used to manoeuvre the head into place. The first chain block lifted the core head from its cradle in a horizontal mode and moved it into position over the core pipes. The second chain block raised the top of the core head as the first was slackened. This put the head in the vertical position over the core pipe; at this point, 6 or 8 back spins were put in the core head and chain to eliminate a tangled mess as the core head was lowered down and screwed into the core pipe. The top chain block took the weight of the corer while the correct length of cable was coiled for the free fall. The trip arm was then attached to the cable and core head, and the trip weight was lowered down the ice hole. A pressure release prevented the corer from tripping while still near the surface. The winch could now take the weight of the corer, raising it slightly to allow the clamp chain block and 4 × 4 timbers to be removed.

The rest of the operation was the long wait down and back. Disassembly of the corer was the reverse of putting it together except the end of the cable was now retracted into the core head and was not a problem. On recovery of the corer, some care had to be taken as each pipe was lifted. The liner sometimes stuck in the pipe causing sediment to be lost or causing injury when it suddenly slid out. This was overcome by pushing down on the top of the liner as the pipe was lifted, exposing the liner resting on the next pipe. At this point the liner could be gripped, slid off and quickly capped. This had to be done carefully because it was heavy, cold and slippery.

## **NOTES**

<sup>1</sup>Ice anchor design: a 6in. hole was drilled through the ice and the guy cable was attached to the centre of either a 3ft. piece of pipe or to a 4 × 4in. wooden block; the pipe or wood was then pushed through the ice hole and brought up horizontally against the bottom of the ice.

<sup>2</sup>Special core pipe clamps: a piece of pipe 4in. long and slightly larger than the core barrel was cut length-wise and fitted over the core barrel; tips were welded to the edges of the 4in. cut pipe and drilled so it could be bolted tightly to the core barrel. A 1ft. long piece of 1.5in. pipe was then welded to the back of each 4in. section so they could rest in the notched 4 x 4in. timbers.



